Tadeusz Kościuszko Cracow University of Technology
Faculty of Civil Engineering
Wind Engineering Laboratory (L-14)

Piotr Krajewski MSc. Eng.

Using of vertical ventilation systems to improve the air quality of selected urban areas

Wykorzystanie pionowych układów wentylacyjnych do poprawy warunków aerosanitarnych wybranych obszarów zurbanizowanych

A dissertation submitted for the degree of doctor of philosophy

Supervisor: Andrzej Flaga, Prof., DSc, Eng.

Kraków, April 2023

I would like to thank my wife Joanna for support, patience and love during creating this work and all my life.

Abstract

This dissertation mainly concerns experimental model tests and the subject of active ventilation in urbanized areas. The main purpose of the work was to answer the question whether it is possible to model the inversion layer of the atmosphere with sufficient accuracy and the active ventilation system aimed at a quick improvement of air-sanitary conditions.

The progressing degradation of the natural environment of urbanized areas is an indicator of our times, our civilization. Improving the air-sanitary conditions of these areas should therefore be a primary and priority action undertaken by the relevant government and local government institutions, universities, and research and development institutions.

The basic action in this subject is and should be a radical reduction in the emission of municipal and transport pollutants. Taking into account the development of e.g. the Krakow agglomeration and the increase in its inhabitants, as well as the moderate achievements to date in improving air quality, actions taken only in the field of reducing pollutant emissions will certainly not be sufficient. They will have to be supported by other activities, especially dynamic ventilation carried out in horizontal ventilation ducts by series-parallel systems of special towers ventilation units cooperating with vertical ventilation chimneys.

The main author of the first concept of such solutions for active ventilation and smog reduction in urban areas, as well as the similarity criteria for these issues in model research, is prof. Andrzej Flaga.

Pioneering, preliminary model tests in this area were carried out in the Wind Engineering Laboratory of the Cracow University of Technology (LIW PK) by the team of: Prof. DSc Eng. Andrzej Flaga - team leader; MSc. Eng. Piotr Krajewski; MSc. Eng. Aleksander Pistol and Dr. Eng. Arch. Łukasz Flaga.

These issues were presented at 3 conferences:

1. 8th International Conference on Environmental Effects on Buildings and People: Actions, Influences, Interactions, Discomfort, (EEBP VIII), October 2018, Cracow-Tyniec, Poland
2. Dynamiczne przewietrzanie i redukcja smogu obszarów zurbanizowanych ze szczególnym uwzględnieniem miasta Krakowa, Politechnika Krakowska, September 2019, Cracow, Poland
3. Dynamiczne przewietrzanie i redukcja smogu obszarów zurbanizowanych, , Politechnika Krakowska, 2021, Cracow, Poland

The results of the work were published in the articles:

Krajewski P.: *Badania modelowe dynamicznego działania na warstwę przyziemną atmosfery*; Wpływy środowiskowe na budowle i ludzi; red. Ł. Flaga, R. Kłaput, Politechnika Krakowska, Kraków, 2022

Flaga Ł., Pistol A., Krajewski P., Flaga A.: *Model tests of dynamic action on the atmospheric boundary layer – linear configuration of ventilation towers on a rough terrain*; Environmental Effects on Buildings and People: Actions, Influences, Interactions, Discomfort, EEBP VIII, Cracow-Lublin 2018, Poland;

Krajewski P., Pistol A., Flaga Ł., Flaga A.: *Model tests of dynamic action on the atmospheric boundary layer – vertical ventilation towers of urban areas*; Environmental Effects on Buildings and People: Actions, Influences, Interactions, Discomfort, EEBP VIII, Cracow-Lublin 2018, Poland;

Pistol A., Krajewski P., Flaga Ł., Flaga A.: *Model tests of dynamic action on the atmospheric boundary layer – concentric configuration of ventilation towers witch central ventilation chimney*; Environmental Effects on Buildings and People: Actions, Influences, Interactions, Discomfort, EEBP VIII, Cracow-Lublin 2018, Poland;

Krajewski P., Pistol A., Flaga Ł., Flaga A.: *Badania modelowe dynamicznego działania na warstwę przyziemną atmosfery – efektywność różnych typów kominów wentylacyjnych*: Dynamiczne przewietrzanie i redukcja smogu obszarów zurbanizowanych, , Politechnika Krakowska, Kraków 2021.

The following monograph is also devoted to these issues:

„Wpływy środowiskowe na budowle i ludzi, Jubileusz 70-lecia Profesora Andrzeja Flagi i jego szkoła naukowa”; red. Ł. Flaga, R. Kłaput, Politechnika Krakowska, Kraków, 2022.

It is also worth noting that the solutions for active ventilation systems for urban areas developed by the LIW PK team have been covered by two patents:

1. WIPOST 10/C PL 424786: System do wymuszania ruchów mas powietrza nad otwartymi obszarami.
2. WIPOST 10/C PL 424785: System do wymuszania ruchów mas powietrza nad otwartymi obszarami, zwłaszcza wzbudzenia i podtrzymania strugi powietrza nad otwartymi obszarami zurbanizowanymi.

Four stages of unique, pioneering studies on the subject have been carried out. The first three stages of this research are presented in the research reports:

1. Report 1: Flaga A., Flaga Ł., Krajewski P., A. Pistol: *Badania wstępne możliwości dynamicznego oddziaływania na warstwę przyziemną. Etap 1: Pomiar pola prędkości przepływu i zasięgu strumienia powietrza generowanego przez modele wentylatorów/wież wentylacyjnych w różnych wariantach ich konfiguracji*; Research Report, Wind Engineering Laboratory, Cracow University of Technology, Cracow 2017;
2. Report 2: A. Flaga, Ł. Flaga, P. Krajewski, A. Pistol, *Badania wstępne możliwości dynamicznego oddziaływania na warstwę przyziemną. ETAP II – Badania w tunelu aerodynamicznym pola prędkości przepływu generowanego przez układ wentylatorów/wież wentylacyjnych w konfiguracji promienistej i specjalny membranowy komin wentylacyjny*; Research Report, Wind Engineering Laboratory, Cracow University of Technology, Cracow 2017;

3. Report 3: A. Flaga, Ł. Flaga, P. Krajewski, A. Pistol, *Badania wstępne możliwości dynamicznego oddziaływania na warstwę przyziemną. Etap III – Badania w tunelu aerodynamicznym wybranych zagadnień z Etapów I i II przy uwzględnieniu wpływu chropowatości podłoża (zabudowy miejskiej)*; Cracow University of Technology, Cracow 2018;

The fourth stage of this research was carried out experimentally by the author, and the theoretical foundations and similarity criteria for this research were developed mainly by prof. Andrzej Flaga.

This doctoral thesis describes all the research and issues covered by all four stages of this work.

Based on the results obtained at the time, the concept of further stages, initial assumptions, or directions of development changed in the course and was improved during the progress of the research. The work presents the next stages of research, initial assumptions, physical and theoretical models so that the reader can understand how the concept has changed and which factors influenced its development.

The phenomenon of smog formation is an urgent problem for most Polish cities, and only expensive, long-term solutions are proposed, which are primarily a burden on the budget of the residents. The construction of the examined city ventilation system would make it possible to temporarily, quickly, and significantly improve the air-sanitary conditions in many cities.

In the first chapter, theses of the doctoral dissertation were formulated:

1. It is possible to dynamically act on the ground level layer of air in urbanized areas by using vertical ventilation systems cooperating with the radial horizontal system of ventilation ducts that effectively improve the aerosanitary conditions of these areas.

2. The model of vertical ventilation systems cooperating with the radial horizontal system used in wind model tests imitates this phenomenon with sufficient accuracy for engineering practice.

The second chapter contains a description of the motivation for writing the following work and the initial concept that initiated the research. The main purpose of the research was to enable the construction of an active city ventilation system, which would be located in naturally occurring ventilation ducts and would serve for quick, ad hoc ventilation of the urban area in the event of wind calm or the phenomenon of atmospheric temperature inversion.

The third chapter is a study on the subject of smog. It describes three types of smog: - two commonly known, i.e. winter smog (acid, London) and summer smog (photochemical, Los Angeles type), and the third - Polish smog. Polish smog is characterized by high acidity, just like winter smog, but it contains much larger amounts of PM10, PM2.5 and PM1.

The fourth chapter describes the phenomenon of temperature inversion in the atmosphere. Temperature inversion is an anomaly that blocks natural convection and thus the ability to remove pollutants generated by an urbanized area (mainly the so-called low-emissions). The particular equilibrium states of the atmosphere and thus the conditions conducive to the formation of the blocking layer are described. Next, the focus was on the time frame of inversion occurrence - from a daily inversion to a multi-day inversion caused, for example, by a change in the atmospheric front. Further, the formation of inversion layers is described in detail in the example of the city of Krakow. The last point of the chapter focuses on the height of the inversion layer, its thickness and the time of its occurrence in a year.

The fifth chapter contains a description of the concept of an active ventilation system, a description of ventilation towers, chimneys, their potential location in natural ventilation ducts and cooperation in the series of ventilation towers. The similarity criteria for model studies, the adopted similarity scales and the theoretical model were also presented.

The sixth chapter focuses on the horizontal ventilation system aimed at creating an artificial air stream enabling the transport of pollutants outside the city along the existing natural ventilation channels. The first tests that were carried out for models of fans were also described to determine the velocity field of the stream generated by a single tower. Then, the tests carried out in the further stages of the tests were described, but also those related to horizontal ventilation, i.e. taking into account the influence of the substrate roughness. The research results and their analysis are presented at the end of the chapter.

The seventh chapter describes the concept of a vertical ventilation chimney designed to eject masses of polluted air above the inversion layer. A physical and theoretical model of the phenomenon and criteria and similarity scales were proposed.

The eighth chapter contains a description of research on vertical ventilation, the experimental model built, the adopted various shapes of the chimney shell, the method of covering the lower spaces, the effect of shortening the chimney jacket and changing the angles of the fans at the base of the chimney. Smoke visualization was also described. The chapter presents the results of the research and their analysis.

The ninth chapter concerns the possibility of modeling the inversion layer in laboratory conditions and checking at which parameters the system is able to penetrate the layer. The adopted theoretical model of the phenomenon and the physical model was also presented. It was proposed to replace the resistance of the inversion layer with a mesh system. Next, the influence of the external fan ring on the operation of the ventilation chimney was checked. Velocity distribution for the air stream generated by the chimney for various input parameters was determined. Based on the obtained results, an analyze and conclusions were carried out. The method of smoke visualization was also shown and described.

Chapter ten contains general conclusions from the entire doctoral thesis.

Chapter eleven describes further directions of development and the necessary research, development of the concept and the way to the final implementation of the project.

The last chapter contains the bibliography used in the work.

Keywords: wind engineering, model test research, active ventilation of cities, horizontal and vertical urban ventilation system, penetration of the inversion layer, smog

Szczegółowe streszczenie w języku polskim (Extended abstract in Polish)

Praca ma charakter przede wszystkim eksperymentalny i dotyczy tematyki aktywnego przewietrzania terenów zurbanizowanych. Podstawowym celem pracy było odpowiedzenie na pytanie czy możliwe jest zamodelowanie z wystarczającą dokładnością warstwy inwersyjnej atmosfery oraz aktywnego systemu wentylacyjnego mającego na celu szybką poprawę warunków aerosanitarnych.

Podczas badań nad kolejnymi etapami pracy, na podstawie otrzymanych wyników koncepcja co do dalszych etapów, przyjętych założeń początkowych czy kierunków rozwoju zmieniała się w trakcie i była udoskonalana w trakcie postępów badań. W pracy przedstawiono kolejne etapy badań zachowując ówczesne podejście, założenia początkowe, modele fizyczne i teoretyczne tak aby czytelnik mógł zrozumieć w jaki sposób koncepcja się zmieniała i, które czynniki miały wpływ na jej rozwój. Badania wykonywane w kolejnych etapach dotyczyły zarówno systemu wentylacji poziomej jak i pionowej. W celu lepszej czytelności i zrozumienia, badania z różnych etapów zostały rozdzielone tak, aby wentylację poziomą i pionową przedstawić w dwóch osobnych rozdziałach.

Zjawisko powstawania smogu jest naglącym problem większości polskich miast a proponowane są jedynie rozwiązania długofalowe, bardzo kosztowne i obciążające przede wszystkim mieszkańców. Budowa badanego systemu przewietrzania miast pozwoliłaby doraźnie, szybko i znacząco poprawić warunki aerosanitarne w wielu miastach, szczególnie tych, których topografia naturalnie stwarza warunki sprzyjające powstawaniu warstwy inwersji a co za tym idzie – smogu.

W rozdziale pierwszym sformułowane zostały tezy pracy doktorskiej:

1. Możliwe jest dynamiczne oddziaływanie na przyziemne warstwy powietrza na terenach zurbanizowanych poprzez zastosowanie systemów wentylacji pionowej współpracujących z promienistym poziomym układem kanałów wentylacyjnych, które skutecznie poprawiają warunki aerosanitarne tych terenów.

2. Model pionowych układów wentylacyjnych współpracujących z promienistym poziomym układem kanałów wentylacyjnych wykorzystanych w badaniach modelowych w tunelu aerodynamicznym odwzorowuje to zjawisko z wystarczającą dokładnością dla praktyki inżynierskiej.

Rozdział drugi zawiera opis motywacji napisania poniższej pracy oraz początkowej koncepcji, jaka zapoczątkowała badania. Głównym celem badań było umożliwienie budowy aktywnego systemu przewietrzania miast, który by był umiejscowiony w naturalnie występujących kanałach wentylacyjnych i służyłby szybkiej, doraźnej wentylacji terenu zurbanizowanego w przypadku wystąpienia ciszy wiatrowej czy zjawiska inwersji temperatury atmosfery. Ponieważ dalej wiele gospodarstw domowych w Polsce ogrzewanych jest za pomocą wysokoemisyjnych i niskowydajnych źródeł ciepła opalanych głównie węglem problem powstawania epizodów smogowych jest powszechny i nasila się w okresie jesienno-zimowym. Proponowane dotychczas rozwiązania skupiały

się przede wszystkim na działaniach długofalowych podczas gdy brak jest rozwiązań doraźnych. Rozpatrywany system mógłby z powodzeniem wypełnić tę lukę.

Rozdział trzeci to praca studialna dotycząca tematyki smogu. Opisano w niej trzy rodzaje smogu: - dwa powszechnie znane tj. smog zimowy (kwaśny, Londyński) oraz smog letni (fotochemiczny, typu Los Angeles) oraz trzeci – smog polski. Smog polski charakteryzuje się dużą kwasowością tak jak smog zimowy ale zawiera dużo większe ilości pyłów PM10, PM2.5 i PM1. Wspomniane pyły pochodzą głównie ze spalania węgla, co dla krajów Europy zachodniej nie jest powszechne tak jak w Polsce. Dalej krótko zarysowano wpływ zanieczyszczeń zawartych w smogu na zdrowie ludzi.

Rozdział czwarty opisuje zjawisko inwersji temperatury w warstwach atmosfery. Inwersja temperatury to anomalia powodująca blokadę naturalnej konwekcji a co za tym idzie możliwości usunięcia zanieczyszczeń generowanych przez obszar zurbanizowany (głównie tzw. niskiej emisji). Opisano poszczególne stany równowagi atmosfery a co za tym idzie warunki sprzyjające wytworzenia się warstwy blokującej. Następnie skupiono się na ramach czasowych występowania inwersji – od inwersji dziennej po inwersję kilkudniową spowodowaną np. zmianą frontu atmosferycznego. Dalej szczegółowo opisano tworzenie się warstw inwersyjnych na przykładzie miasta Krakowa. Ze względu na długą historię problemów smogowych (opisaną już w XIXw.) oraz specyficzne ukształtowanie terenu stwarzające korzystne warunki do zastojów powietrza i cisz wiatrowych temat inwersji w Krakowie jest poznany i opisany w badaniach i opracowaniach. Z tego względu w niniejszej pracy założono warunki wystąpienia warstwy inwersyjnej często występujące dla Krakowa. Ostatni podpunkt rozdziału skupia się na wysokości warstwy inwersyjnej oraz jej miąższości i czasie występowania w roku.

Rozdział piąty zawiera opis koncepcji systemu aktywnego przewietrzania, opis wież wentylacyjnych, kominów, ich potencjalnego umiejscowienia w naturalnych kanałach wentylacyjnych i współdziałania w ciągu wież wentylacyjnych. Przedstawione też zostały kryteria podobieństwa dla badań modelowych, przyjęte skale podobieństwa i model teoretyczny.

W rozdziale szóstym skupiono się na poziomym systemie wentylacji mającym na celu wytworzenie sztucznej strugi powietrza umożliwiającej transport poza miasto wzdłuż istniejących naturalnych kanałów wentylacyjnych. Opisano także pierwsze badania jakie wykonano dla wentylatorów zastępczych aby wyznaczyć pole prędkości strugi generowanej przez pojedynczą wieżę. Następnie opisano badania wykonane w dalszych etapach badań ale także dotyczące wentylacji poziomej tj. z uwzględnieniem wpływu chropowatości podłoża. Na końcu rozdziału zamieszczono wyniki badań oraz ich analizę.

W rozdziale siódmym opisano koncepcję pionowego komina wentylacyjnego mającego za zadanie wyrzucenie mas powietrza zanieczyszczonego ponad warstwę inwersyjną. Zaproponowano model fizyczny i teoretyczny zjawiska a także kryteria i skale podobieństwa.

Rozdział ósmy zawiera opis badań dotyczących wentylacji pionowej, zbudowanego modelu eksperymentalnego, przyjętych różnych kształtów powłoki komina, sposobu

zasłonięcia przestrzeni dolnych, wpływu skrócenia płaszcza komina oraz zmiany kątów wentylatorów u podstawy komina. Opisano, także przeprowadzoną wizualizację dymową. W rozdziale przedstawiono także wyniki z badań i ich analizę.

Rozdział dziewiąty dotyczy możliwości modelowania warstwy inwersyjnej w warunkach laboratoryjnych oraz sprawdzenia przy jakich parametrach rozpatrywany system aktywnej wentylacji jest w stanie przebić warstwę. Przedstawiono także przyjęty model teoretyczny zjawiska i model fizyczny. Zaproponowano zastąpienie oporu warstwy inwersyjnej za pomocą systemu siatek – obliczono zastępczy współczynnik oporu aerodynamicznego oraz wyznaczono współczynnik oporu dla użytych siatek. Następnie opisano przeprowadzone doświadczenie dla różnych wysokości komina, prędkości i ilości wentylatorów oraz wysokości podstawy komina. Dalej sprawdzono wpływ zewnętrznego pierścienia wentylatorów na pracę komina wentylacyjnego. Wyznaczono rozkład prędkości dla strugi powietrza generowanej przez komin dla różnych parametrów wejściowych. Na podstawie otrzymanych wyników dokonano ich analizy i wyciągnięto wnioski. Pokazano i opisano również zastosowaną metodę wizualizacji dymowej.

Rozdział dziesiąty zawiera generalne wnioski z całej pracy doktorskiej.

Rozdział jedenasty opisuje dalsze kierunki rozwoju oraz niezbędne badania, rozwinięcia koncepcji oraz drogę do ostatecznej realizacji przedsięwzięcia.

Ostatni rozdział zawiera bibliografię wykorzystaną w pracy.

Słowa kluczowe: inżynieria wiatrowa, badania w modelowe, aktywne przewietrzanie miast, system wentylacji poziomej i pionowej, przebicie warstwy inwersyjnej, smog

Acknowledgments

The stages I-III of the presented research were performed thanks to three internal dean's grants of the Faculty of Civil Engineering at Cracow University of Technology:

Stage I: internal grant of March 24, 2017;

Stage II: internal grant of July 19, 2017;

Stage III: internal grant of October 2, 2017.

The author would also like to express his gratitude to Dr. Eng. Renata Kłaput - head of LIW PK for help in organization, coordination, and support during all stages of the research.

Table of Contents

Abstract 1

Acknowledgments 8

Table of Contents 9

1. DOCTORAL THESES 11

2. INTRODUCTION 11

3. SMOG 13

3.1. Smog definition 13

3.2. Smog types 13

3.3. Health effects 15

4. INVERSION LAYER 16

4.1. Temperature Inversions 16

4.2. Equilibrium of the air 19

4.2.1. Unstable equilibrium of the air 20

4.2.2. Neutral equilibrium of the air 21

4.2.3. Stable equilibrium of the air 21

4.3. Time of inversion layer occurring 22

4.4. Inversion layer in Cracow 23

4.5. Height of the inversion layer 27

5. PROPOSED ACTIVE VENTILATION SYSTEM OF URBAN AREAS 30

5.1. The concept 30

5.2. The ventilation system 33

5.3. Work plan and similarity criteria 35

5.4. Horizontal ventilation system 37

5.4.1. Single ventilation tower with multiple parallel similar fans 37

5.4.2. Single ventilation tower with one substitutive fan 38

5.4.3. The array of substitutive ventilation towers 39

6. MODEL OF HORIZONTAL VENTILATION TOWERS SYSTEM 40

6.1. Aerodynamic tunnel of Wind Engineering Laboratory of Cracow University of Technology 40

6.2. Wind flow velocity measurements 43

6.3. The first stage experiment setup 44

6.4. Test results of the horizontal ventilation towers system 50

6.5. Conclusion for the results of the I stage 60

6.6. Model description and experiment setup of horizontal ventilation towers in stage III .. 60
6.7. The results of series I and II of stage III (the influence of terrain roughness) 62
6.8. The analysis and conclusion of series I and II of stage III (the influence of terrain roughness) 71
7. MODEL OF VENTILATION CHIMNEY AND SIMILARITY CRITERIA 72
8. TESTS OF VERTICAL VENTILATION CHIMNEYS 77
8.1. Model description and experiment setup of stage II 77
8.2. Test results of stage II 82
8.3. Conclusion for the results of the II stage 88
8.4. Model description and experiment setup of stage III - radial models of ventilation chimneys 89
8.5. Test results of the III stage (ventilation chimneys) 94
8.6. Analysis and conclusion for the results of the III stage (ventilation chimneys) 116
8.7. Fog visualization 118
8.8. Conclusion of fog visualization 123
9. TESTING THE POSSIBILITY OF PENETRATING THE INVERSION LAYER 124
9.1. Model of the inversion phenomenon 124
9.1.1. Physical parameters of the model 128
9.1.2. Model of the chimney 129
9.1.3. Estimation of the air velocities of the air stream 131
9.1.4. Estimation of the drag coefficient of the inversion layer 136
9.2. Model of the inversion layer 139
9.3. Tests of the mesh 141
9.4. Inversion layer tests 143
9.5. Smoke Visualization of stage IV 145
9.6. Test results and analysis 146
9.7. Analysis and conclusion for stage IV 194
9.8. Power of the system and economic assessment 194
10. GENERAL CONCLUSION 196
11. DIRECTIONS FOR FURTHER RESEARCH 197
12. Literature 198

1. DOCTORAL THESES

1. It is possible to dynamically act on the ground level layer of air in urbanized areas by using vertical ventilation systems cooperating with the radial horizontal system of ventilation ducts that effectively improve the aerosanitary conditions of these areas.

2. The model of vertical ventilation systems cooperating with the radial horizontal system used in wind model tests imitates this phenomenon with sufficient accuracy for engineering practice.

2. INTRODUCTION

The presented work is the result of a series of experimental studies carried out at the Laboratory of Wind Engineering of the Cracow University of Technology in the years 2017-2023. The research was aimed at checking the possibility of building an innovative system of active ventilation of urban areas. The idea of building the system resulted from the notoriously repeated smog episodes in Krakow and many smaller cities, especially in the south of Poland. Most of them are located in valleys surrounded by hills or mountains, and they have low emissions of pollutants, in particular PM1-10 dust, wind calms and long-term temperature inversions are frequent. The obvious solution is to remove the cause of the problem, i.e. low emissions and pollution sources, however, due to the high costs of changing the heating method and, consequently, high social resistance, solutions to improving air quality are introduced slowly. Krakow was the first city which introduces a large-scale program of replacing old stoves and legally banned solid fuel stoves from 1 st September 2019. Other cities followed his example by introducing programs encouraging and forcing the replacement of heat sources with more efficient, cleaner and not generating large amounts of dust.

The proposed active ventilation system is an ad hoc solution that does not eliminate the problem at the source, but eliminates the factors contributing to the occurrence of smog and can quickly and effectively improve air quality during the smog episodes.

Partial results from the research have been presented at several conferences: „Dynamiczne przewietrzanie i redukcja smogu obszarów zurbanizowanych ze szczególnym uwzględnieniem miasta Krakowa", Cracow, 2019, „Wpływy środowiskowe na budowle i ludzi" Kraków 2022, 8th International conference on environmental effects on buildings and people: actions, influences, interactions, discomfort, Cracow, 2018 and scientific papers.

The Cracow University of Technology has obtained two patents for the described system - for a horizontal and vertical ventilation system, patent No P.424785 [WIPO ST 10/C PL424785] and patent No P.424786 [WIPO ST 10/C PL424786].

Based on the results obtained at the time, the concept of further stages, initial assumptions or directions of development changed in the course and was improved during the progress of research. The thesis presents the next stages of research, initial assumptions, physical

and theoretical models so that the reader can understand how the concept has changed and which factors influenced its development. The tests carried out in subsequent stages concerned both the horizontal and vertical ventilation systems. For better readability and understanding, the tests from different stages have been separated so that horizontal and vertical ventilation are presented in two separate chapters.

3. SMOG

3.1. Smog definition

According to (wikipedia.org) smog, or smoke fog, is a type of intense air pollution that reduces air visibility. The word "smog" was coined in the early 20th century, and is a contraction of the words smoke and fog to refer to smoky fog due to its opacity, and odor. This kind of visible air pollution is composed of nitrogen oxides, sulfur oxide, ozone, smoke and other particulates. Man-made smog is derived from coal combustion emissions, vehicular emissions, industrial emissions, forest and agricultural fires and photochemical reactions of these emissions. Smog was common in industrial areas and remains a problem in some cities today.

3.2. Smog types

Wikipedia.org divides smog into only two categories: “Smog is often categorized as being either summer smog (Los Angeles type smog, photochemical smog), or winter smog (London type smog).

Summer smog is primarily associated with the photochemical formation of ozone. During the summer season when the temperatures are warmer and there is more sunlight present, photochemical smog is the dominant type of smog formation. Photochemical smog, as found for example in Los Angeles, is a type of air pollution derived from vehicular emission from internal combustion engines and industrial fumes. These pollutants react in the atmosphere with sunlight to form secondary pollutants that also combine with the primary emissions to form photochemical smog. In certain other cities, such as Delhi, smog severity is often aggravated by stubble burning in neighboring agricultural areas since 2002. The atmospheric pollution levels of Los Angeles, Beijing, Delhi, Lahore, Mexico City, Tehran and other cities are often increased by an inversion that traps pollution close to the ground. The developing smog is usually toxic to humans and can cause severe sickness, a shortened life span, or premature death.

Winter smog

During the winter months when the temperatures are colder, and atmospheric inversions are common, there is an increase in coal and other fossil fuel usage to heat homes and buildings. These combustion emissions, together with the lack of pollutant dispersion under inversions, characterize winter smog formation. Smog formation in general relies on both primary and secondary pollutants. Primary pollutants are emitted directly from a source, such as emissions of sulfur dioxide from coal combustion. Secondary pollutants, such as ozone, are formed when primary pollutants undergo chemical reactions in the atmosphere.

The book “Smog - causes - effects – countermeasures” (S. Godzik, S. Hławiczka, P. Poborski, 1995) reports that winter smog can form throughout the year, it is not limited

by temperature, humidity or intensity of solar radiation. Summer smog has a high ozone content and this is what distinguishes it, and its formation of summer smog (Los Angeles) is favored by high temperatures and low humidity. Conditions for the formation of smog: there must be pollution, appropriate meteorological conditions and a long duration - several hours.

Polish smog

In the book “Technologie i procesy ochrony powietrza” (G. Wielgosiński, R. Zarzycki, 2018) it is noted that: “…recently we also have a new term "Polish smog", which was created to distinguish smog phenomena appearing in Polish cities that differ from the described winter and summer smog. Polish smog differs primarily in its composition - it is mainly composed of PM10, PM2.5 and PM1 dust particles as well as numerous polycyclic aromatic hydrocarbons, including benzo(a)pyrene. So you can also use another term "dust smog" here. These are pollutants typical for the process of burning solid fuels in low-efficiency furnaces, in the absence of an exhaust gas purification system, i.e. simply put: home furnaces. Using a wider term, the basic cause of poor air quality in Polish cities is low emissions, i.e. emissions from home heating systems fired with solid fuels and car traffic, in particular worn-out vehicles, without catalytic converters. In the book, he notes that recently we also have a new term "Polish smog", which was created to distinguish smog phenomena appearing in Polish cities that differ from the described winter and summer smog. Polish smog differs primarily in its composition - it is mainly composed of PM10, PM2.5 and PM1 dust particles as well as numerous polycyclic aromatic hydrocarbons, including benzo(a)pyrene. So you can also use another term "dust smog" here. These are pollutants typical for the process of burning solid fuels in low-efficiency furnaces, in the absence of flue gas treatment systems, i.e. in simpler terms: home furnaces. Using a broader term, the basic cause of poor air quality in Polish cities is low emissions, i.e. emissions from home heating systems fired with solid fuels and car traffic, in particular worn-out vehicles, without catalytic converters. If we add to this the relatively frequent inversion phenomena in Poland in winter (e.g. after a period of frost and eastern circulation, the influx of warmer polar sea masses from the west, or periods of high-pressure weather with high pressure, lack of cloud cover and weak wind), it turns out that In many areas of the country, perfect conditions are created for the formation of smog, primarily "dust", but also sometimes acidic (winter). A characteristic feature of "Polish smog" is its formation in high-pressure weather and negative air temperatures. In winter, this is often associated with cloudless weather, which results in significant night temperature drops and the formation of inversions. In addition, at low temperatures, the demand for heat increases, hence, at the same time, higher emissions of pollutants from individual heating systems. The result is the concentration of dust in the ground-level part of the atmosphere many times exceeding the permissible levels, i.e. "dust smog". An interesting fact is that it is usually not accompanied by exceeding the permissible concentrations of SO_2 or CO, so typical for acid (winter) smog.

On the other hand, in the summer, with temperatures often exceeding 30°C, in the areas of many Polish cities, especially those heavily loaded with car traffic, perfect conditions are created for the formation of photochemical smog.

3.3. Health effects

On (wikipedia.org) we can easily find a whole list of health problems caused by smog: “Smog is a serious problem in many cities and continues to harm human health (Watson, Traci, 2004), (Marziali, Carl, 2015). Ground-level ozone, sulfur dioxide, nitrogen dioxide and carbon monoxide are especially harmful to senior citizens, children, and people with heart and lung conditions such as emphysema, bronchitis, and asthma (Smog — Who Does It Hurt? What You Need to Know About Ozone and Your Health, 1999), It can inflame breathing passages, decrease the lungs' working capacity, cause shortness of breath, pain when inhaling deeply, wheezing, and coughing. It can cause eye and nose irritation and it dries out the protective membranes of the nose and throat and interferes with the body's ability to fight infection, increasing susceptibility to illness (Kurt OK, Zhang J, Pinkerton KE, March 2016). Hospital admissions and respiratory deaths often increase during periods when ozone levels are high ("Ozone Pollution". Clean Water Action Council of Northeast Wisconsin), (Health Effects of Ozone in the General Population, 2013).

There is a lack of knowledge on the long-term effects of air pollution exposure and the origin of asthma. An experiment was carried out using intense air pollution similar to that of the 1952 Great Smog of London. The results from this experiment concluded that there is a link between early-life pollution exposure that leads to the development of asthma, proposing the ongoing effect of the Great Smog (Bharadwaj, Graff, Mullins, Neidelllast, 2016). Modern studies continue to find links between mortality and the presence of smog. One study, published in Nature magazine, found that smog episodes in the city of Jinan, a large city in eastern China, during 2011–15, were associated with a 5.87% (95% CI 0.16–11.58%) increase in the rate of overall mortality. This study highlights the effect of exposure to air pollution on the rate of mortality in China (Zhang, Liu, Cui, Liu, Yin, Li, 2017). A similar study in X'ian found an association between ambient air pollution and increased mortality associated with respiratory diseases (Mokoena, Ethan, Yu, Shale, Liu, 2019).”

4. INVERSION LAYER

4.1. Temperature Inversions

“Temperature inversions are meteorological phenomena which can occur over busy cities under particular environmental conditions see Fig. 4.1 and Fig. 4.2.

Fig. 4.1. This photograph shows an episode of a temperature inversion that occurred over the city of Glasgow in Scotland. Source: Understoryweather.

Above the clouds, the Sun is shining, and the air feels unseasonably warm. At ground level, however, the weather conditions are very different. The sky is obstructed by a very dense freezing fog.

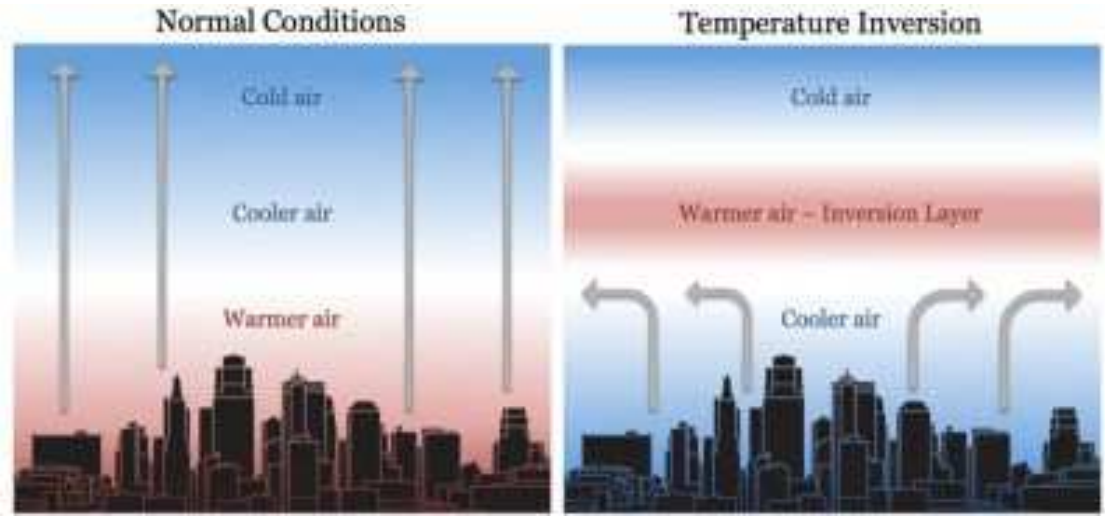

Fig. 4.2. Arrows show air flow in normal conditions on the left and during temperature inversion on the right. In normal conditions, warm air rises and normal convective patterns persist. During a temperature inversion, the warm air acts as a cap, effectively shutting down convection and trapping smog over the city. Source: thoughtco.com.

Thermal inversion layers or temperature inversions are areas where the normal decrease in air temperature with increasing altitude is reversed and the air above the ground is warmer than the air below it.

Temperature inversions can occur anywhere from close to ground level up to thousands of meters up into the Earth's atmosphere." (www.naturphilosophie.co.uk)

Normally, air temperature decreases at a rate of 6.4°C for every kilometer (roughly 3.5°F for every 1000 feet) you climb up into the atmosphere. When this normal cycle is present, it is considered an unstable air mass and air constantly flows between the warm and cool areas. As such, the air is better able to mix and spread around pollutants.

At times of temperature inversions, temperatures increase with increasing altitude. The warm inversion layer then acts as a cap and stops atmospheric mixing.

This is the reason why inversion layers are called stable air masses.

"By a thermal inhibiting layer we mean a layer of air in which the temperature increases with increasing altitude (the so-called thermal inversion), the temperature does not change, or the temperature decreases by less than 0.2°C for every 100m. The formation of such a layer hinders the vertical movements of the air mass, and therefore also significantly reduces the possibility of spreading pollutants. Depending on the height of appearing the inversion, we can distinguish between lower and upper inversions. The upper inversion occurs at an altitude of several hundred to over a thousand meters above sea level. Its height determines the thickness of the so-called mixing layer, i.e. the volume of the atmosphere in which pollutants are spread. The lower inversion layer appears directly in the ground layer, significantly limiting the diffusion of pollutants (Fig. 3.5). Thermal inversions are layers with an extremely strong state of stable equilibrium. Therefore, they prevent the development of processes favored by vertical air movements

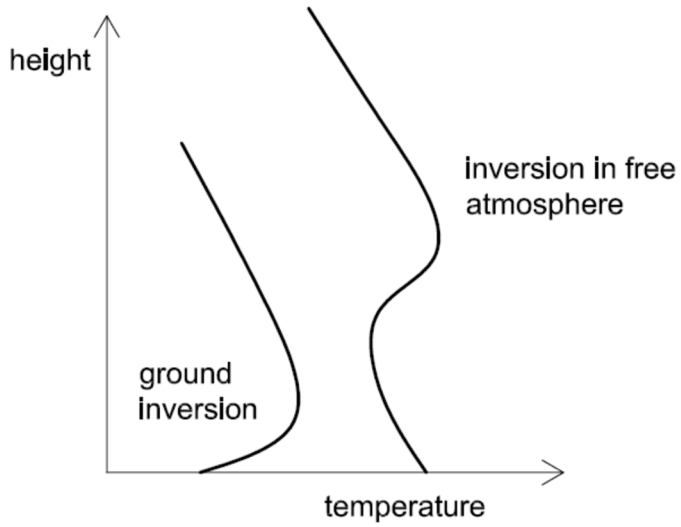

(Kożuchowski, 2005).

Fig. 4.3. Ground inversion and inversion in a free atmosphere.

In addition to the vertical and horizontal movement of air, which we call wind, there is a disorderly, randomly changing movement in the atmosphere called turbulence. It accompanies both vertical and horizontal air currents and is always a more or less

significant component of the actual velocities of the moving portions of air. Turbulent disturbances arise in the movement of fluids (gases and liquids) at a certain critical velocity, which causes changing the laminar movement into turbulent movement. The mechanical cause of turbulence is the internal viscosity of the fluid, which causes that neighboring particles moving relative to each other have the ability to exchange momentum (Kożuchowski, 2005)"

Impact of Inversion Layers on Micro-Climates and Smog (www.thoughtco.com)

Temperature inversion layers are significant to meteorology because they block the atmospheric flow which in turn causes the air over an area experiencing an inversion to become stable. This can result in various types of weather patterns.

More importantly, areas with heavy pollution are prone to unhealthy air and an increase in smog when an inversion is present, as they trap pollutants at ground level, instead of letting them circulate away.

Although freezing rain, thunderstorms, and tornadoes are significant weather events, one of the most important things to be impacted by temperature inversions is smog – the brownish gray haze that covers many of the World's largest cities as a result of dust, auto exhaust, and industrial manufacturing.

Smog is impacted by the inversion layer because it is in essence, capped when the warm air mass moves over an area. This happens because the warmer air layer sits over a city and prevents the normal mixing of cooler, denser air. Instead, the air becomes still and over time the lack of mixing causes pollutants to become trapped under the inversion, developing significant amounts of smog.

During severe inversions that last over long periods, smog can cover entire metropolitan areas and cause respiratory problems for the local inhabitants and urban air pollution is rising. The inversion layer blocks the natural vertical propagation of pollutions trapping it over a buildings comp. Fig. 4.2.

Smog occurring

Also, the height of the inversion layer base is significant. In higher levels of the base polluted air is trapped under the layer but when the base level is below the emitter, pollutants are not blocked and can dissipate freely as shown in Fig. 4.4.

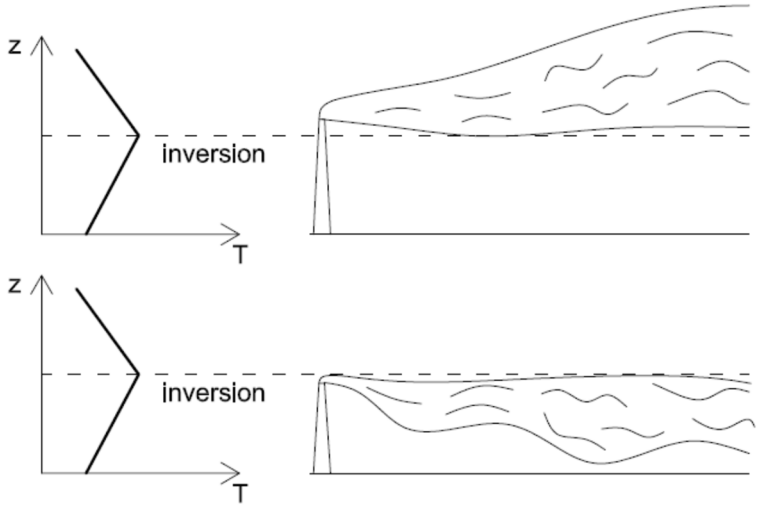

Fig. 4.4. The propagation of pollutants emitted from the emitter depending on the position of the inversion layer. (Szczygłowski, 2007).

4.2. Equilibrium of the air

The equilibrium of the air in the atmosphere was well described in (Szczygłowski, 2007: ”The basic parameter characterizing the state of the atmosphere is its temperature. Its value depends on the speed of heat exchange (due to radiation, conduction, or mixing of air masses) between the surface of the Earth, the layers of the atmosphere and space. The temperature change can also occur in the case of expansion or compression of air masses during vertical movements. When a fixed volume of air begins to rise, its pressure decreases, adiabatic expansion takes place and with it a decrease in temperature. The reverse movement of the air causes an increase in pressure and with it an increase in temperature (adiabatic compression).

The concept characterizing the above changes (for air in which water vapor does not occur or is present in small amounts) is the dry adiabatic gradient (γ_s). It is equal to $\gamma_s =$ 1°C for every 100 m of height. In the case of air saturated with water vapor, we are talking about a humid-adiabatic gradient γ_s, which is $\gamma_s = 0{,}6° \frac{\mathrm{C}}{100\mathrm{m}}$. This difference is explained by the release of heat contained in water vapor, which is used to heat the environment.”

In the book (Godzik et al., 1995) one defines that thermal inhibiting layers are those air layers in which the vertical temperature drop is small, not exceeding 0.2 C per 100 meters of the air layer. In these layers, the temperature may not change with increasing altitude.

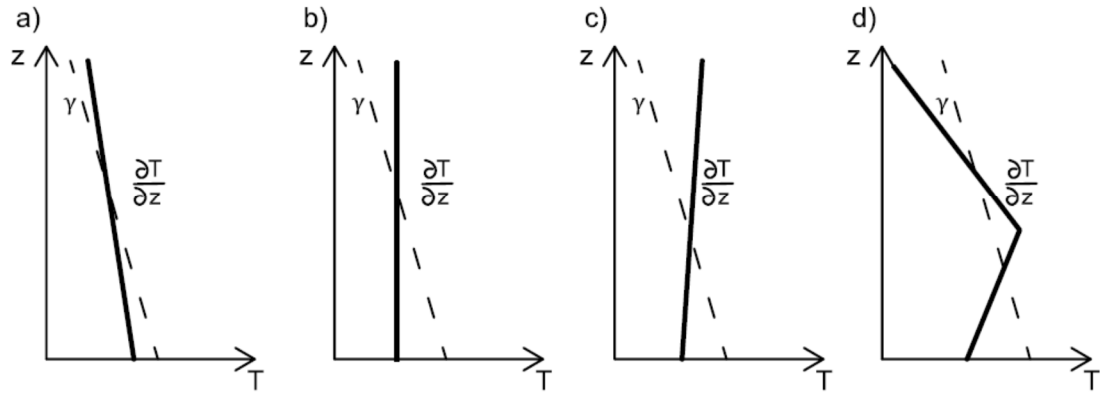

Fig. 4.5. Temperature gradient during the occurrence of different types of inhibiting layers. (Szczygłowski, 2007).

4.2.1. Unstable equilibrium of the air

To determine in which thermal-dynamic equilibrium a given part of the atmosphere is, it is necessary to determine the actual vertical gradient of temperature (γ). Depending on the ratio of the dry or wet adiabatic gradient to the real gradient, we distinguish the following possibilities (Olszewski, 1991): - the real gradient is greater than the adiabatic gradient, – real gradient equal to the adiabatic gradient, - the real gradient is smaller than the adiabatic gradient. When the change in temperature for every 100 m of altitude exceeds the adiabatic gradient, a certain volume of air rising adiabatically will be at a higher temperature than its surroundings. With the increased temperature, this volume will be lighter, and therefore it will be intensively lifted. Similarly, in the case of falling, the separated volume of air will always be at a lower temperature than the surroundings, which will make it heavier and accelerate its settling. Any vertical movements will be greatly facilitated. This state is called unstable equilibrium, causing the formation of vertical ascending air currents. The above behavior is shown in Fig. 4.6 (assuming a dry adiabatic gradient).

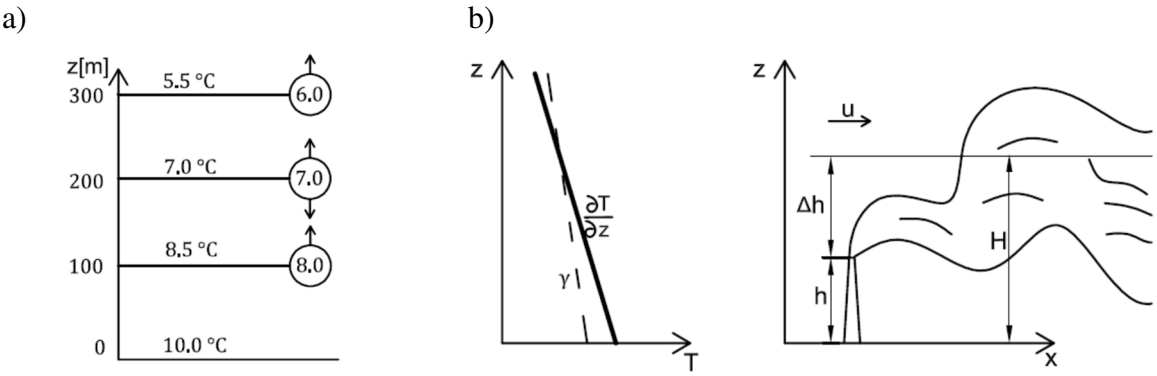

Fig. 4.6. Unsteady equilibrium $\gamma_s = 1.5\frac{^\circ C}{100m}$, $\gamma_s = 1.0\frac{^\circ C}{100m}$ *(Szczygłowski, 2007).*

4.2.2. Neutral equilibrium of the air

When the change in temperature for every 100 m of altitude is equal to the adiabatic gradient, a certain volume of air rising adiabatically will have the same temperature as its surroundings. Thus, this volume does not tend to rise or fall. This state shown in Figure 4.7 (assuming a dry adiabatic gradient) is called neutral equilibrium.

a) b)

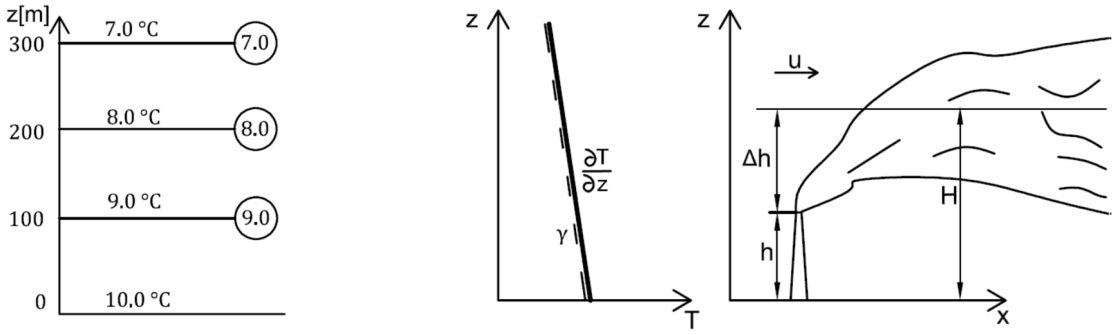

Fig. 4.7. Neutral equilibrium $\gamma_s = 1.0\frac{^\circ C}{100m}$, $\gamma_s = 1.0\frac{^\circ C}{100m}$ *(Szczygłowski, 2007).*

4.2.3. Stable equilibrium of the air

When the change in temperature for every 100m of altitude exceeds the adiabatic gradient, a certain volume of air rising adiabatically will have a lower temperature than its surroundings. Colder air will have difficulty continuing to rise. Similarly, in the case of descending, the isolated volume of air will always be at a higher temperature than its surroundings, which will make it lighter, so it will occur settling slowdown. Any vertical movements will be much more difficult. This state, called constant equilibrium, is shown in Figure 4.8 (assuming a dry adiabatic gradient).

a) b)

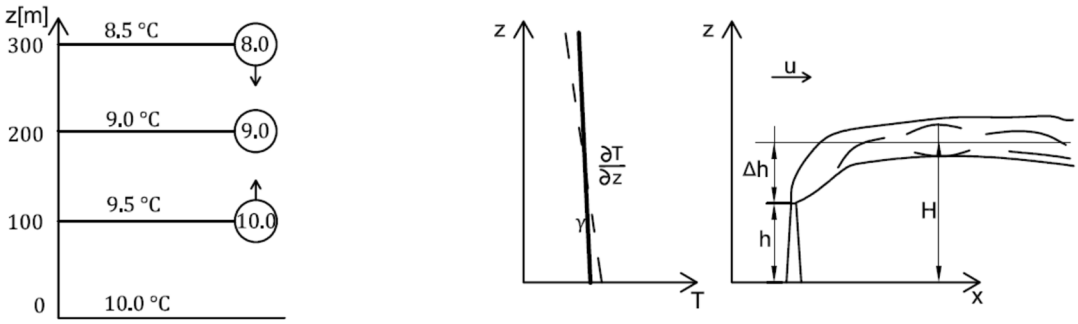

Fig. 4.8. Constant equilibrium $\gamma_s = 0.5\frac{^\circ C}{100m}$, $\gamma_s = 1.0\frac{^\circ C}{100m}$ *(Szczygłowski, 2007).*

4.3. Time of inversion layer occurring

The equilibrium states of the atmosphere are formed under certain meteorological conditions. Unsteady equilibrium occurs most often during sunny weather, winds are characterized by low speed, and there is also increased pressure. In such conditions, the surface of the land is quickly heated, and then the accumulated energy is transferred to the air layer. This causes significant temperature differences between successive layers of air (increased vertical temperature gradient). Therefore, such an equilibrium very rarely occurs at night (from 10 to 20% of all observations) (Parczewski, 1972).

Permanent equilibrium is observed primarily in the evening and night when heat is radiated from the ground and the difference between the individual layers of the atmosphere decreases. It is also formed when warm air masses flow onto a cooled surface (advection). The proper classification of atmospheric equilibrium states can be determined based on various data sets (Pasquill 1961):

- wind speed, intensity of solar radiation and degree of sky cloudiness,

- measurements of wind direction fluctuations,

- vertical temperature gradient,

- gradient Richardson number,

- bulk Richardson number,

- Monin-Obukhov length scale and terrain roughness coefficient,

- the ratio of wind speeds at two heights.

The most popular classification based on indirect measurements and observations was given by Pasquill (Pasquill 1961) and (Zwoździak J., Zwoździak A., Szczurek, 1998). Table 4.1 presents the 6 equilibrium states proposed by (Pasquill 1961).

Table 4.1. Classification of equilibrium states (Pasquill 1961):

Wind velocity [m/s]	Day			Night	
	Solar radiation intensity			Cloudiness	
	Strong	Medium	Weak	≥4/8	≤3/8
<2	A	A-B	B	F	F
2-3	A-B	B	C	E	F
3-5	B	B-C	C	D	E
5-6	C	C-D	D	D	D
>6	C	D	D	D	D

Where:

A – strongly unstable equilibrium,

B - unstable equilibrium,

C – slightly unstable equilibrium,

D - neutral equilibrium,

E - slightly stable equilibrium,

F – constant equilibrium.

Sometimes an additional category G is also assumed, denoting a strongly constant equilibrium atmosphere.

The inversion layer occurring is a cyclical phenomenon. The shortest period encloses in a one day cycle. During the night the ground radiates heat and forms a layer of colder air right on the ground. With the lack of receiving the heat from the Sun radiation, the cold ground layer gets bigger and higher until the morning when the first Sun rays start to heat the ground. Then thanks to the radiation the air right on the ground become warmer and creates a new layer of warmer air enlarging upwards till the inversion layer will disappear. The process is shown in Fig. 4.9.

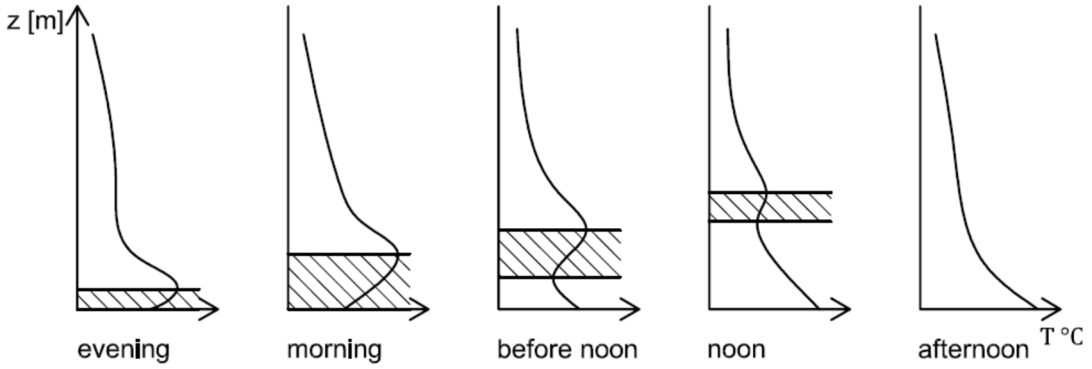

Fig. 4.9. Typical daily change of temperature inversion.

It is necessary also to mention Low Level Jet (LLJ) phenomena occurring sometimes below the inversion layer. LLJ forms in warmer months during the night (during the day also but not so strongly). On a layer height of 50-170 m the wind speed increase from 2 m/s to 5 m/s, up to about 250m level and slightly decreases below the inversion layer (Godłowska, 2019).

4.4. Inversion layer in Cracow

In further consideration author focused mainly on Cracow urban area due to the most probable placing of a potential test polygon on a larger scale, Cracow's big problem with the smog and good knowledge of the local area. The lesser Poland region has many towns lying in valleys and having many smog episodes during the year. Cracow is the capital of the region and also good represents the problem of the entire region being the most extensive of them all.

Cracow is the second largest city in Poland with about 750 thousand citizens, forming a typical agglomeration with satellite cities inhabited by 1 mln to 1,639 mln citizens (depending on the counting method). The most important in terms of smog is the city's location in the valley – surrounded by hills, low emission of pollutants and low average annual wind speed resulting now wind weather for many days.

A good description of the anemological conditions in Krakow is in (Ośródka, 2010):

"General characteristics of the ventilation conditions of the city of Krakow air flow in the surface layer of the atmosphere in the area of the city of Krakow is conditioned primarily by the general circulation of the Earth's atmosphere. The location of Kraków in the Vistula River valley running W-E (west-east), surrounded from the north and south by hills, determines the shape of the observed wind rose (i.e. shares of directions from which the wind blows). In the area including the city of Krakow, winds from the west dominate, and winds from the east occur with high frequency. The terrain relief (concave form) determines the main ventilation axis of Kraków, while the existing buildings (roughness of the ground) are responsible for weakening the wind speed in the city in comparison to non-urban areas. Urban and industrial buildings also cause modifications to the wind direction. A characteristic feature of Kraków is also a significant frequency of wind calm during the year (approx. 20-30%), as well as the prevailing share (approx. 40%) of wind with a speed of less than 2 m/s, i.e. very weak."

The anemological conditions in Cracow are also strongly determined by terrain topography (see Fig. 4.10.) (Godłowska, 2019).

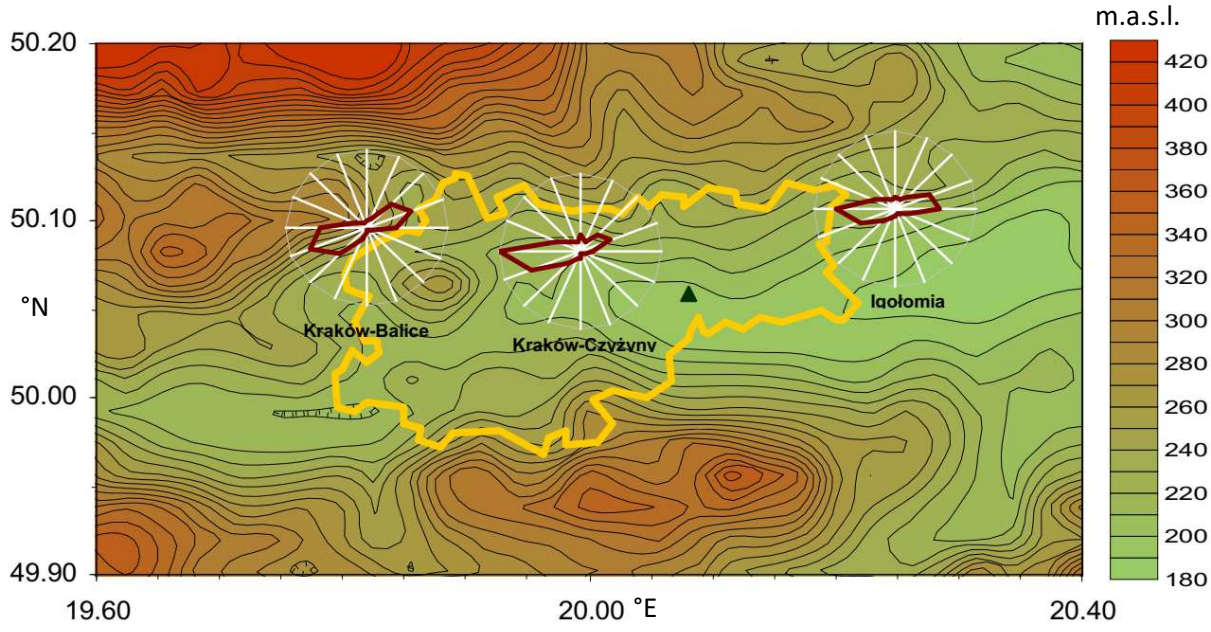

Fig. 4.10. Hypsometric map (isolines every 10 m) height m.a.s.l., of the area covering the city of Kraków (marked administrative border) with wind roses marked at the points of meteorological stations (Kraków-Balice, Kraków-Czyżyny, Igołomia). A triangle marks

the planned location of the Thermal Waste Processing Plant in Krakow at Giedroyc street. (Ośródka, Kraków 2010)

"From the point of view of anemological conditions, the topography for the majority of the city area forces the air to move along the east-west axis, along the Vistula valley trough. However, the Sowiniec massif dominant in the central part of the riverside depression in the west of the town modifies this flow. Topography affects not only anemological conditions but also favors the occurrence of temperature inversions, determining the constant type of atmospheric balance within them. In the neutral equilibrium of the atmosphere, it is natural for the air temperature to drop slightly with height, following an adiabatic gradient, of about 0.6 to 1.0°C per 100 m. In such equilibrium, vertical air movements are neither damped nor enhanced. The occurrence of a temperature inversion changes the situation. Air layers lying at a lower height are cooler and therefore heavier than those located higher, and the vertical movement of air is damped. Inversions are observed more often in valleys than in flat terrain and hills. The process of creating inversions in the valleys is favored by the downward movement of cold air along the slopes of the valley. In the case of Krakow, the presence of the river is also important. Water has a high heat capacity, which means that much more energy needs to be supplied to achieve the same heating effect as on the surface of the earth. In addition, because it is a liquid, it has a better ability than a solid body to transport heat from the surface to the lower layers. The surface temperature of the water is also lowered by evaporation responsible for transporting energy from the water to the air by the latent heat flux. Evaporation is a process that helps to limit the access of short-wave radiation to the water's surface. Absorption of this radiation by water vapor additionally increases the amount of available energy in the air, affecting its heating. The effect of all these processes is much slower heating of the water surface than in the case of the earth's surface, and faster heating of the air, which weakens the ability to create an unstable equilibrium above the water.

"Anemological conditions in Kraków, depending on the synoptic situation, are described in the literature by (Niedźwiedź 1981, 2013) and (Ustrnul,1997). The synoptic situation is described using various classification systems, most often based on the analysis of atmospheric pressure distribution over a large area. Knowledge of this distribution enables the location of low and high pressure systems and also allows us to determine the direction of air advection in a given location. Circulation conditions are a factor that strongly determines the local anemological situation.

The analysis of Niedźwiedz circulation types for the decade 1966-1975 (Niedźwiedz, 1981) showed the presence of a clear seasonality in the circulation phenomena, manifested by the predominance of the western circulation in the period from October to January, a large share of advection from the north in the period from April to July, and an increase in high-pressure activity in from August to October. Analyzing synoptic maps at the level of 700 hPa, Niedźwiedz also noticed a significant increase in the frequency of advection from the west at an altitude of about 3000 m at the expense of advection from eastern directions. Clear seasonal variability of circulation conditions in the upper Vistula basin has been confirmed on data from the period 1901-2000 (Ustrnul, 2007). Analyzes of the annual variability of circulation types for both classification systems indicate that

in the autumn and winter periods, flow from the west is most common. In autumn, non-advective high-pressure situations (Ca, Ka types according to Niedźwiedź classification and Ba according to Ustrnul types) also have a large share, they are also frequent in summer. In spring, high-pressure situations with advection from the east have a relatively large share. Non-advective situations are particularly important for the spread of air pollution, especially those occurring in the presence of high-pressure systems (about 15% of them per year). They are responsible not only for low wind speeds or wind calms in Krakow but also suppress the ability to spread pollutants vertically through the presence of large-scale subsidence in high-pressure systems - which keeps the emitted pollutants close to the earth's surface" (Godłowska 2019, p. 31-33)

In urban areas, an important role in forming a wind near ground level has an orography i.e. buildings, trees, and obstacles. It is assumed that the layer with high turbulency (the friction layer) is forming from 1.5 H where H is the average height of the obstacles – roofs in cities. Due to this fact, using data from a weather station located in high density urban areas should be taken very carefully. (Godłowska 2019)

Most of the data on the behavior of the downwind in Krakow comes from the development of a relatively short series of measurements. An exhaustive review of historical works on this parameter and an analysis of the available measurement data were presented by Kowanetz in the monograph "Klimat Krakowa w XXwieku" (Matuszko 2007). In the context of the impact on air quality, the most important conclusion of his study is the characteristics of wind speed in the city center, based on data from the years 1961-1980 from the Botanical Garden in Krakow, namely the high share of very weak winds (57.5%, v <2 m/s) and weak (30.4%, 2 < v<4 m/s) and a high share of wind calms (25.1% per year, autumn - 32%, winter - 26.3%). The reason for this state of affairs is not only urbanization processes, as evidenced by the work of (Karliński,1877), who, analyzing data from the same location, then located on the outskirts of Krakow, wrote already in the 19th century about the poor natural ventilation conditions of the Vistula valley. The strong influence of the terrain in Krakow is evidenced by the comparison of data from the years 1954-1960 from several meteorological stations located in the city and its vicinity (Matuszko, 2007). The highest average wind speeds were recorded on hills (Garlica Murowana station), and the lowest – on concave landforms (Tyniec station). It was also found that the relief modifies the wind direction. In the 1970s, on the basis of two-year wind measurements in ten points located within the city and six outside it, Lewińska's team described the horizontal differentiation of the directions and speeds of the lower winds (Lewińska et al., 1982)." (Godłowska 2019, p. 34)

For most stations, the largest share of wind calms is observed in autumn. Such a result is consistent with the conclusion resulting from the analysis of circulation types, indicating the largest share of the occurrence of non-advective circulation types at this time of the year. Data on the frequency of wind calms in different periods of the day confirm the well-known picture of daily variability of wind speed, with the wind intensifying around noon and calming down at night. For most road stations, the percentage of silence at night is several times higher than during the day. The smallest share of silences and their lowest daily variability was recorded in the Vistula valley. The analysis of the frequency of wind calms indicates that autumn and night hours are the periods when we are most likely to

deal with anemological conditions unfavorable from the point of view of the spread of pollutants. The results at the stations located in the Vistula valley seem to prove that, at least the Vistula valley from the very center of the city to the east, is a well-ventilated area." (Godłowska, 2019 p. 48)

Based on the available literature, it can be seen that the authors of the publications are in agreement as to the conditions conducive to the formation of smog. In the study "Meteorological determinants of air quality in Krakow" (Oleniacz et al. 2014), **it was found that even 60-70% of the time in Krakow there is wind calm or wind speed below 2m/s**. The influence of wind on pollutant concentration levels was also shown. It was also found that the appearance of the wind above 2 m/s and the increase of the mixing layer facilitate the ventilation of the city, and the most unfavorable conditions occur in combination with high pressure, a small horizontal pressure gradient, and an inverse temperature distribution.

The work "Some data on the occurrence of all-day inversion layers in the atmosphere of Krakow and the conditions of this phenomenon", (Walczewski, 2009) reports that **the number of inversion days varied depending on the year, 34% to 45% during the year, and the maximum number of inversion days is in winter. Correlation of meteorological types with inversions was also found - anticyclone center, anticyclone wedge**, etc. In the work "Czynniki meteorologiczne wpływające na koncentrację aerozoli w Krakowie oraz analiza cząstek aerozoli" (Pietras, 2013), an analysis of dust in the air of Krakow was made, a strong dependence on the anticyclonic situation was found. The conclusion stated that the main factor influencing the high concentration of particulate matter in Kraków is the deterioration of the conditions conducive to the dispersion of pollutants, i.e. the high-pressure situation - a small horizontal pressure gradient and temperature inversion.

(Godłowska 2010) **notes that distant sources of pollution affect the situation in Krakow**, e.g. pollution from the **Benelux countries, the Ruhr region, and the vicinity of Dresden and Leipzig also reach Krakow**. In the work (Stefan, Necula, Georgescu, 2010) it was found that **the average time that aerosols spend in the air is from one to six days, and rain removes 70-80% of the mass of the aerosols** (Falkowska and Lewandowska 2009).

In a book which is an extensive study of the issue of smog (Godzik et al., 1995) we find information **that after 5-6 days of silence the concentration of smog increases several times** and that the wind speed is a parameter shaping the equilibrium of the atmosphere.

4.5. Height of the inversion layer

The height of the base of the inversion layer is variable and different sources describe different ranges. The work of (Oleniacz et al. 2014) describes **the height of the mixing layer, i.e. the layer below the inversion layer, from several dozen to 1000 m**, and that in 2012 **the mixing layer was below 100m for Krakow for about 31-33% of the time (see Fig. 4.11)**. In (Oleniacz et al. 2016) describes **a high concentration of PM10 dust up to about 220-270m and that the mixing layer can be from 10m high in the case of**

temperature inversion at night to 1000m in the case of strong thermodynamic convection. The influence of the mixing layer on the concentration of impurities was noted in the work. It was also described how the low height of the mixing layer limits the vertical movement, which results in the concentration of pollutants, and a strong dependence of the lack of wind on the concentration of pollutants was noted. In (Godzik et al., 1995) is information that the height of **the mixing layer depends on the season, lower in winter, and higher in summer**. (Parczewski, 1971) defines, however, that the lower thermal inhibiting layers are those that start directly from the earth's surface, while the upper thermal inhibiting layers are those that lie at a certain distance from the ground, but not higher than 1000 m above sea level.

In this thesis, the author, based on the available data**, assumed the height of the base of the inversion layer to be 200m and the limiting wind speed to be 2m/s**. This is the speed that provides the minimum ventilation necessary to reduce the concentration of pollutants.

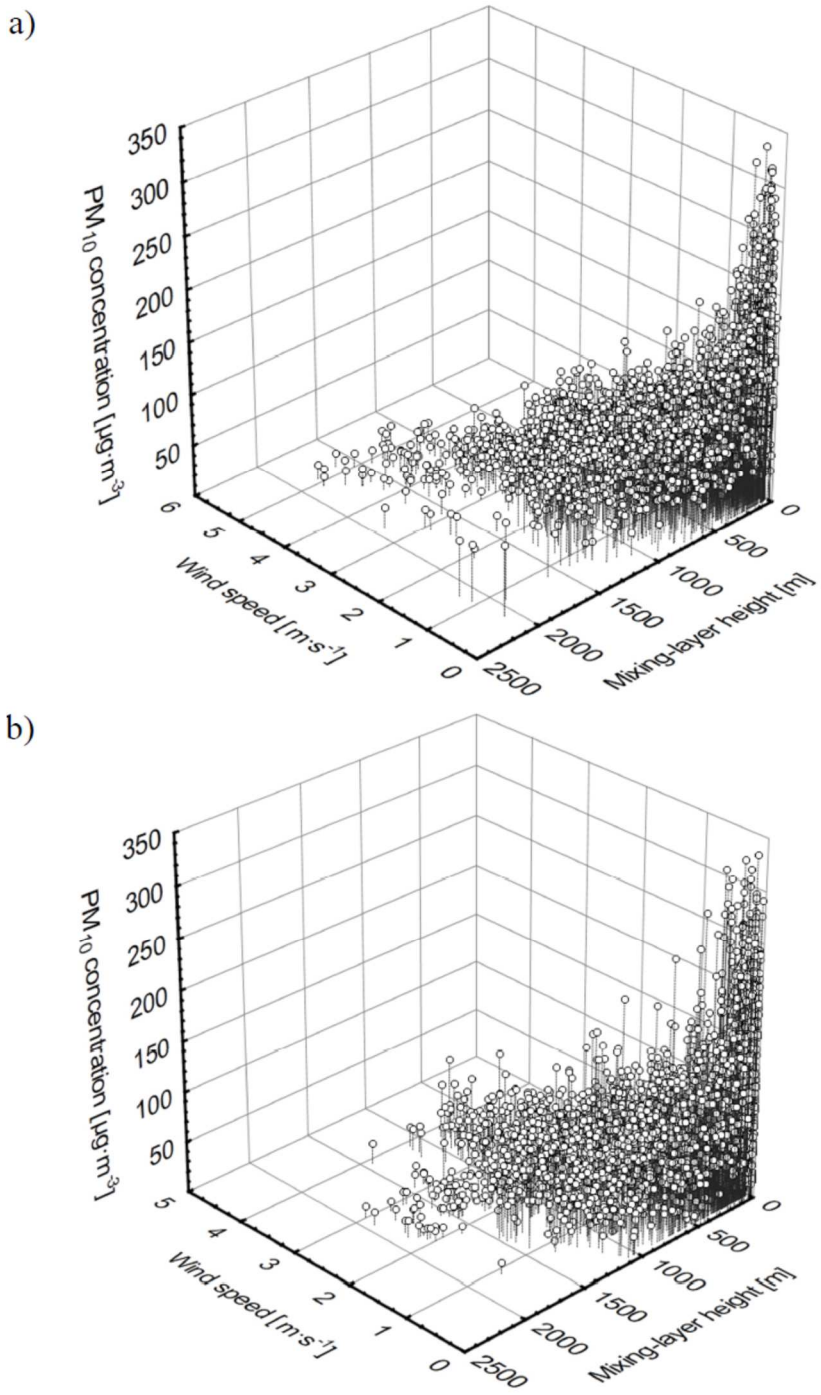

Fig. 4.11. The cumulative impact of wind speed and mixing-layer height on the PM10 levels in the air recorded during the heating season at the analyzed stations: a) Nowa Huta, b) Kurdwanow (1-hour averaged data from 2014)(Oleniacz et al., 2016)

5. PROPOSED ACTIVE VENTILATION SYSTEM OF URBAN AREAS

5.1. The concept[1]

The concept of the ventilation system was first developed in Wind Engineering Laboratory at the Cracow University of Technology by a team of prof. Andrzej Flaga, Piotr Krajewski, Aleksander Pistol and Łukasz Flaga. After the first stage of the project, the test was continued by the author.

On 14th May 2016, the World Health Organization issued a report (www.who.int, 2017) on air pollution in urban areas. According to this report, 33 out of 50 most polluted cities in the European Union are located in Poland. This illustrates the problem of smog and decreasing level of ventilation conditions faced by modern cities and urban areas in Poland, but also cities all over the world. Deterioration of air quality is caused not only by the growth of industry, communication, or population but also by the blocking of natural ventilation channels.

Hence, an idea came up to improve the conditions of urban areas ventilation by forcing dynamically the movement of air mass in urban areas. However, for this purpose, it is crucial to examine the phenomenon of dynamic action on the atmospheric boundary layer as well as to determine whether such action is feasible and effective. Therefore, the main scientific aim of this thesis is to investigate the phenomenon of dynamic action on the atmospheric boundary layer, assuming the following ways of moving the air mass:

1) Mechanical generation of additional horizontal air streams in parallel configurations of stream generation points (Fig. 5.1a) as well as additional horizontal vortex air streams in circulating configurations of stream generation points (Fig. 5.1b). The configurations are presented for the Cracow topography case. Currently, in the Kraków agglomeration, on average, about 150 days a year are affected by the smog phenomenon.

[1] This chapter was written based on:

Flaga A.: *Działanie dynamiczne na warstwę przyziemną powietrza jako efektywna metoda poprawy przewietrzania i redukcji smogu obszarów zurbanizowanych*: Dynamiczne przewietrzanie i redukcja smogu obszarów zurbanizowanych ze szczególnym uwzględnieniem miasta Krakowa, Politechnika Krakowska, Kraków 2019

Report 1: Flaga A., Flaga Ł., Krajewski P., Pistol A.: *Badania wstępne możliwości dynamicznego oddziaływania na warstwę przyziemną. Etap 1: Pomiar pola prędkości przepływu i zasięgu strumienia powietrza generowanego przez modele wentylatorów/wież wentylacyjnych w różnych wariantach ich konfiguracji*; Research Report, Wind Engineering Laboratory, Cracow University of Technology, Cracow 2017;

a)

b)

*Fig.5.1. Concept sketch of additional air streams generated mechanically on the example of air exchange and regeneration system for Cracow (*Błażejczyk, 2013*): a) horizontal air streams in the parallel configuration of stream generation points; b) horizontal vortex air streams in circulating configurations of stream generation points (Flaga A. 2019).*

2) Mechanical generation of additional horizontal radial air streams in concentric configurations of stream generation points cooperating with central ventilation vertical exhaust system (Fig. 5.2).

a)

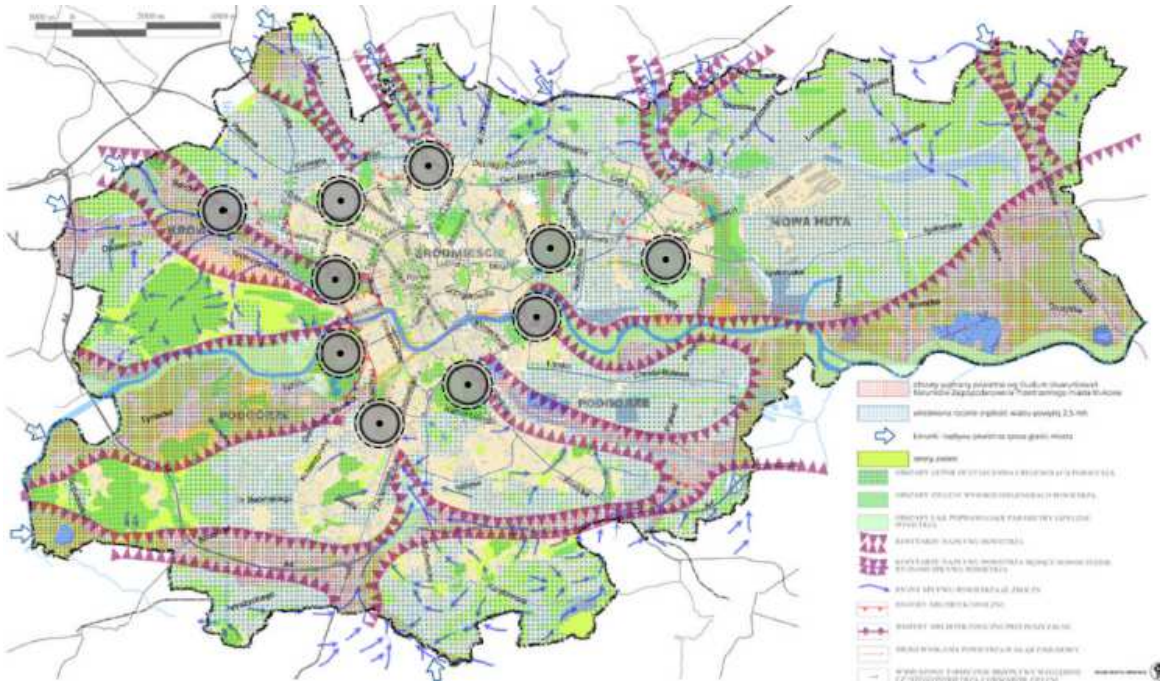

b)

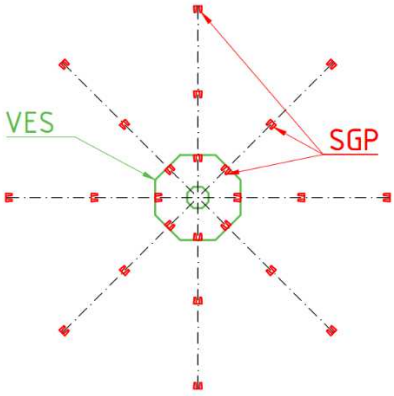

*Fig.5.2. Concept sketch for: a) locating the areas for horizontal radial air streams generation and the central ventilation vertical exhaust systems – on the example of air exchange and regeneration system for Cracow (*Błażejczyk, 2013*); b) single radial system of stream generation points (SGP) cooperating with central ventilation vertical exhaust system (VES), (Flaga A. 2019).*

To investigate the phenomenon of dynamic action on the atmospheric boundary layer one should analyze some individual items that affect the final result, especially:

- a method of horizontal and vertical air streams generation;

- forming air streams (turbulence reduction, flow rate control, elimination of local losses);

- aerodynamic interference between generated air streams;

- parameters that affect the movement of air streams, i.e. terrain roughness, flow resistance, distribution of pressure, temperature and density of the air in the atmospheric boundary layer.

To verify the possibility of the project's success, preliminary model studies were carried out in Wind Engineering Laboratory at Tadeusz Kościuszko Cracow University of Technology. The results were very encouraging, hence the following research hypothesis has been set up:

Proposed solutions (S1 and S2) of dynamic action on air boundary layer as a method of improving the ventilation of cities and urban areas are effective, feasible and economically reasonable.

It was claimed that it is worth continuing this research in a wider range: in a small model scale in the wind tunnel and afterward in a large model scale in an enclosed space of suitable dimensions, as well as by using numerical simulations. The scope of this thesis scopes only the small model wind tunnel tests.

5.2. The ventilation system[2]

Current solutions used to improve the ventilation conditions in urban areas mainly relate to the application of preventive measures such as:

- reduction of pollution sources (Godzik et al. 1995), (Shi et al., 2016) based on air quality monitoring (New Directions, 2016);

- urban planning to ensure adequate ventilation conditions (Ng, 2009), (] Buccolieri et al. 2011).

These actions are passive in nature, i.e. they are only suitable for the prevention of unfavorable ventilation conditions in urban areas. This is certainly the best way to act against bad ventilation conditions, but not always sufficient.

The ventilation system sometimes requires some support. For this purpose, active actions are required, which may improve the existing conditions. The use of air purifiers may be such an active solution (Błażejczyk et al. 2013), (US 20090308244 A1), (WO

[2] This chapter was written based on:

Report 1: Flaga A., Flaga Ł., Krajewski P., Pistol A.: *Badania wstępne możliwości dynamicznego oddziaływania na warstwę przyziemną. Etap 1: Pomiar pola prędkości przepływu i zasięgu strumienia powietrza generowanego przez modele wentylatorów/wież wentylacyjnych w różnych wariantach ich konfiguracji*; Research Report, Wind Engineering Laboratory, Cracow University of Technology, Cracow 2017;

Report 4: Flaga A.: *Podstawowe zależności stosowanej mechaniki płynów dla komina wentylacyjnego*; Research Report, Wind Engineering Laboratory, Cracow University of Technology, Cracow 2017;

Flaga Ł., Pistol A., Krajewski P., Flaga A.: *Model tests of dynamic action on the atmospheric boundary layer – linear configuration of ventilation towers on a rough terrain*; Environmental Effects on Buildings and People: Actions, Influences, Interactions, Discomfort, EEBP VIII, Cracow-Lublin 2018, Poland

2010084385 A1). There is also the idea to create barriers in the form of water walls to block the flow of pollution from industrial areas (CN 101991999 A). Nevertheless, the territorial range of all these actions is rather local. Therefore, the paper (CN 203620447) suggests using an air exchange and regeneration system as a global active measure against bad aero-sanitary conditions in urban areas. Hitherto, such a system has not been created and applied. What is more, it has not been investigated whether it would be physically possible to create such a system as well as whether the system would be economically justified.

The research covers the study of the phenomenon of dynamic action on the atmospheric boundary layer. The aim was to investigate whether it is possible to force the movement of air mass on such a large scale. The study also includes an analysis of this phenomenon's effectiveness. To emphasize the pioneering nature of this type of research, it is worthwhile to analyze the current state of knowledge in the field of urban ventilation as well as the phenomenon of forced air mass movement. Thus, these are some relevant studies that have been conducted and described so far:

- studies of natural ventilation channels in the urban areas: CFD simulations of air pollution dispersion in urban areas (Chu et al., 2005),(Wingstedt et al., 2017) wind tunnel tests of wind conditions in urban areas (Carpentieri et al. 2009), comparisons of CFD results with wind tunnel measurements (Wingstedt et al., 2017), the influence of the terrain (buildings, roughness, etc.) on natural ventilation channels (Buccolieri et al. 2010), (Ramponi, 2015), (Oke, 1978), (Sorbjan, 1983);
- influence of wind conditions on the transport of air pollution outside the urban areas as well as on changes in urban microclimatic conditions (Hang, Sandberg, 2009);
- study on the phenomenon of forced air movement on a small scale (home ventilation) (Jiang et al., 2003), (Omrani et al. 2017);
- study of natural vertical air movement: impact of cities thermal conditions on their ventilation (Yang et al. 2016), (Yang, Li, 2011), (Lewińska, 1991);
- study of forced vertical air movement: increasing the efficiency of small-scale ventilation by creating a tornado-like artificial vortex (Cao, 2017); patent for the cooling tower with forced ventilation and natural draft (US 4164256 A) or cooling tower discharging the polluted air after breaking through the inversion layer (US 5425413 A), (Spurr 1959); study of the process for reducing smog by the chimney inversion/injector effect – sucking warmer and cleaner air from the higher layers towards the ground by pipelines (DE 3503138 A1);
- aerodynamic interference test: mainly aerodynamic interference study of buildings, and objects (Blackman et al., 2015); investigation of generated air streams interference only in a vertical direction and on a small scale (Zhai, Brannon, 2016);
- similarity criteria for the phenomenon of dynamic action on atmospheric boundary layer: only own works discussed in the pre-test section.

Summing up the above literature review, it is evident that there are many gaps in the state of knowledge about the phenomenon of dynamic action on the atmospheric boundary layer. First of all, no one has ever thoroughly investigated the mechanical movement of air mass on such a large scale. Perchance, this phenomenon – in a large scale – is ruled by some other factors or a new phenomenon that affects this movement will be discovered. Moreover, the effectiveness of such a dynamic action is not known. So far, there is also little information about the aerodynamic interference of the generated air streams. This phenomenon is particularly important since, as a result of air streams

interference, the efficiency of the system can be dramatically improved or deteriorated. Another issue that requires extensive research is penetration through the inversion layer and throwing the previously sucked air (for example polluted air) over this layer. It is necessary to answer the question of whether such action is physically feasible and economically justified.

All of the aforementioned shortcomings and doubts are the subject of the research presented in this thesis. Hence, it is clear that the planned study is reasoned and pioneering. The detailed analysis of the phenomenon of dynamic action on the atmospheric boundary layer makes it possible to fully describe all factors that may affect the feasibility and effectiveness of such a dynamic action. Autor hopes in the longer term, this phenomenon could be used to improve the aero-sanitary conditions of many urban areas if their natural ventilation is insufficient.

5.3. Work plan and similarity criteria

To plan all the research tasks, several preliminary studies were required. Only their results allowed them to determine the stages of the main research plan. Hence, first, the scope and results of preliminary experimental works will be presented.

In the beginning, it was necessary to adopt a model of stream generation points (SGP) and vertical exhaust system (VES) for all conducted tests. It was assumed that SGP would be modeled in the form of a ventilation tower equipped with several single fans. The assumed dimensions of such a tower in a real scale are shown in Fig. 5.3a. Furthermore, a vertical exhaust system was modeled as a chimney assisted by ventilation towers. The dimensions and position of the chimney were related to the thickness and height of the inversion layer (Fig. 5.3b).

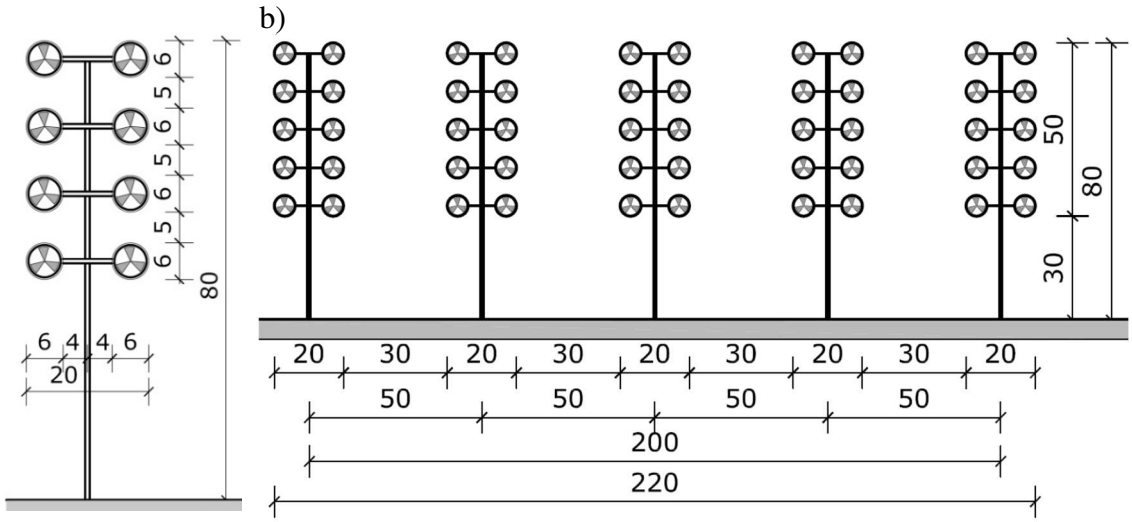

c)

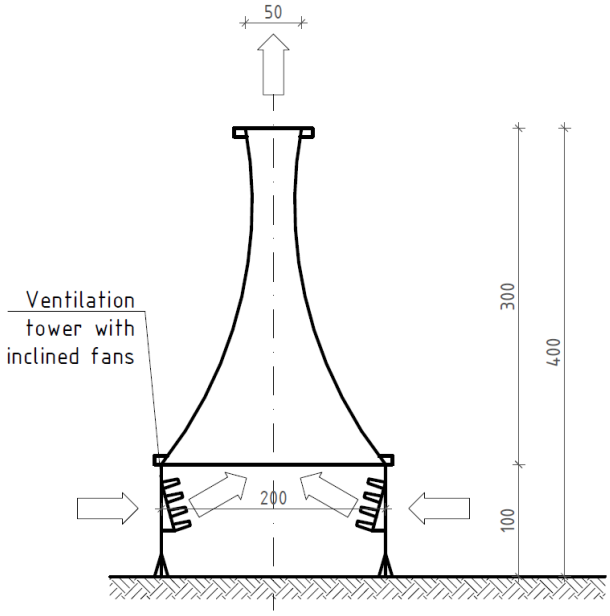

Fig. 5.3. Sketch and dimensions in [m] of assumed system elements in real scale: a) stream generation points as a tower equipped with several fans; b) a system of 5 towers arranged in a 200m wide strip c) vertical exhaust system as a chimney supported by ventilation towers (Flaga Ł. et al. 2018).

At the beginning of the research, the following assumptions were made:

• A forcing air movement in a layer with a height of approx. 100 m by 2 million m3/h is sufficient.

• For this purpose, approx. 1000 axial fans with a diameter of 6 m are needed to be used in approx. 100 towers (see Fig. 5.3)

• Two concepts of dynamic impact on the air layer with a height of approx. 100 m will be taken into account in the tests: mechanical excitation of additional streams (see Fig. 5.1) and air vortices (see Fig. 5.2).

• Structure of the towers - truss, removable/temporary (multiple assemblies).

• The exchange of the above-mentioned volume of air would take place during approx. 3 hours a day for approx. 150 days a year.

• The total cost of electricity for fan operation, with the current 1kWh tariff, is estimated at approx. 1-2 million PLN per year.

• The estimated total cost of the project of building a system of ventilation towers will amount to approx. 100 million PLN.

It was assumed that most of the tests would be conducted in scale models. Model tests reflect reality with satisfactory accuracy if the basic relations in the analyzed phenomenon are preserved. Hence, the first key step in the initial test was to define these relations, i.e. similarity criteria, which must be fulfilled during investigations. The

following elements of the system were analyzed, from the most basic to the more complex sets.

5.4. Horizontal ventilation system

5.4.1. Single ventilation tower with multiple parallel similar fans

At first, a ventilation tower equipped with multiple parallel similar fans was studied. Its concept scheme showing the relevant parameters is shown in Fig. 5.4.

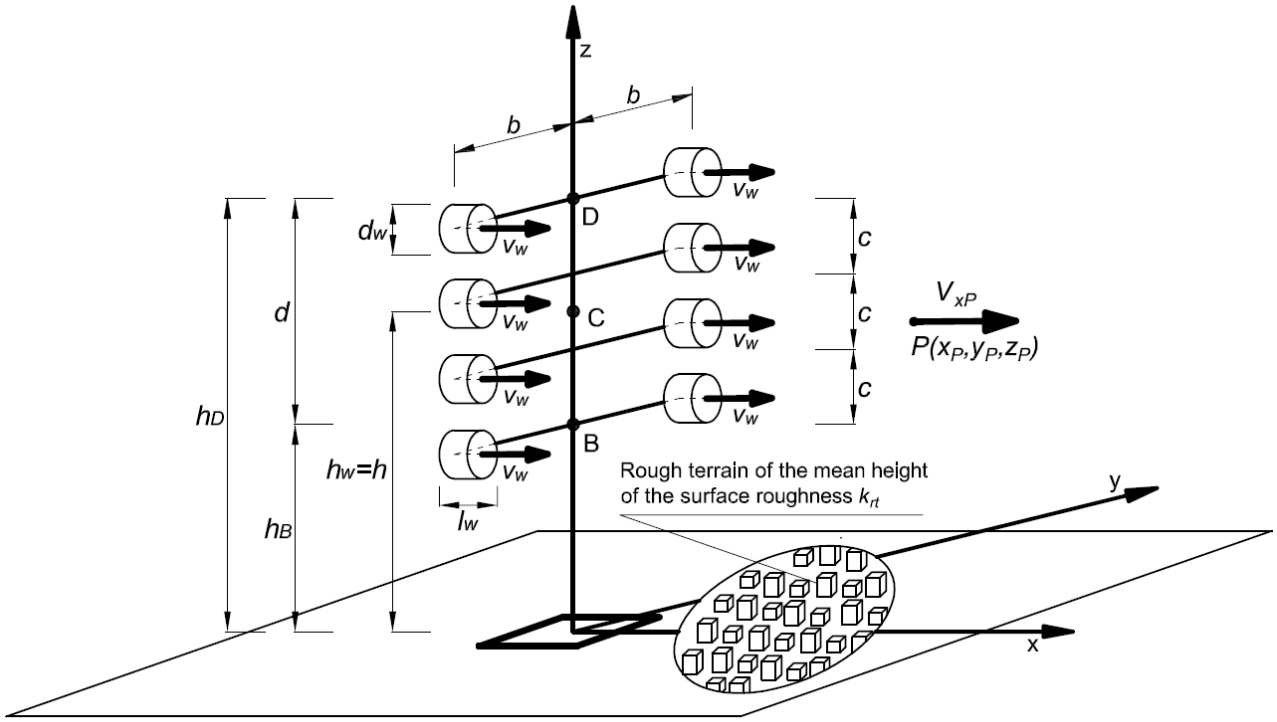

Fig.5.4. Sketch of ventilation tower equipped with eight fans; each fan generates an air stream of mean outlet velocity v_w (Flaga Ł. et al. 2018).

The x-component of the mean air stream velocity at point P $(x_P,\ y_P,\ z_P)$ marked as V_{xP} is a function dependent on the following factors: geometric parameters of a ventilation tower $(h_B,\ d,\ h,\ h_D,\ c,\ b)$, geometric parameters of a single fan $(d_w,\ l_w,\ \ldots) = (g_w)$, mean outlet air velocity (v_w), coordinates of point P: $(x_P,\ y_P,\ z_P)$, physical characteristics of air (ρ - mass density, μ - dynamic viscosity, $\nu = \frac{\mu}{\rho}$ - kinematic viscosity), terrain roughness parameters (k_{rt} – the mean height of the surface irregularity – assuming quite uniformly rough terrain). Based on all the above parameters, the undermentioned functional relationship can be stated:

$$V_{xP} = F[h_B, d, h, h_D, c, b; (g_w); (x_P, y_P, z_P); v_w, \rho, \mu; k_{rt}]. \tag{5.1}$$

Assuming the dimensional base of the problem as $(\rho,\ v_w,\ h)$ and using the Π (Buckingham) theorem that concerns the dimensional analysis, the following dimensionless function is defined:

$$\check{V} = \frac{V_{xP}}{v_w} = \check{F}\left[\frac{h_B}{h}, \frac{d}{h}, \frac{h}{h}, \frac{h_D}{h}, \frac{c}{h}, \frac{b}{h}; (\check{g}_w); \left(\frac{x_P}{h}, \frac{y_P}{h}, \frac{z_P}{h}\right); Re; \check{k}_{rt}\right], \tag{5.2}$$

Where $Re = \frac{v_w h \rho}{\mu} = \frac{v_w h}{\nu}$ is a Reynolds number, $\check{k}_{rt} = \frac{k_{rt}}{h}$ is a dimensionless roughness of the surface.

From the above relations, it follows that at given dimensionless geometric parameters of ventilation tower and fans, dimensionless velocity $\check{V}$ depends on: the dimensionless coordinates of point P $\left(\frac{x_P}{h}, \frac{y_P}{h}, \frac{z_P}{h}\right)$, Reynolds number *Re* and dimensionless roughness of the surface $\check{k}_{rt}$. The easiest method of achieving the individual values of the function $\check{F}$ is conducting a series of model tests.

5.4.2. Single ventilation tower with one substitutive fan

Stream generation point can be modeled in a simpler way as a single ventilation tower with one substitutive fan (Fig.5.5) generating air stream of a mass flow rate Q_w equal to the sum of mass flow rates $\sum q_w$ of eight (or, in general, n_w) fans mounted on the ventilation tower presented in Fig.5.6.

In this case:

$$Q_w = \rho A_w V_w = \rho \frac{\pi D_w^2}{4} V_w, \qquad q_w = \rho a_w v_w = \rho \frac{\pi d_w^2}{4} v_w, \qquad Q_w = n_w q_w = 8 q_w, \tag{5.3-5}$$

where A_w is an area of substitutive fan, a_w is an area of every single fan and V_w is a mean outlet velocity of a substitutive fan. Therefore:

$$A_w V_w = 8 a_w v_w \text{ or } D_w^2 V_w = 8 d_w^2 v_w, \tag{5.6}$$

$$V_w = 8 \frac{a_w}{A_w} v_w \text{ or } V_w = 8 \left(\frac{d_w}{D_w}\right)^2 v_w. \tag{5.7}$$

Assuming $V_w = v_w$, we obtain that: $A_w = 8 a_w$ or $D_w = \sqrt{8} d_w$. Dimensionless functional relationship for ventilation tower with one substitutive fan can be defined as follows:

$$\check{V}^* = \frac{V_{xP}{}^*}{V_w} = \check{F}^* \left[\frac{D}{H}; \left(\check{G}_w\right); \left(\frac{x_P}{H}, \frac{y_P}{H}, \frac{z_P}{H}\right); Re; \check{k}_{rt}\right], \tag{5.8}$$

where: $Re = \frac{V_w H}{\nu}$.

For comparable parameters of both functions $\check{F}$ and $\check{F}^*$ it can be stated that $\check{V}^* = \check{V}$. For further considerations of similarity criteria for different set-ups of stream generation points, it was assumed that they are modeled as a ventilation tower with one substitutive fan.

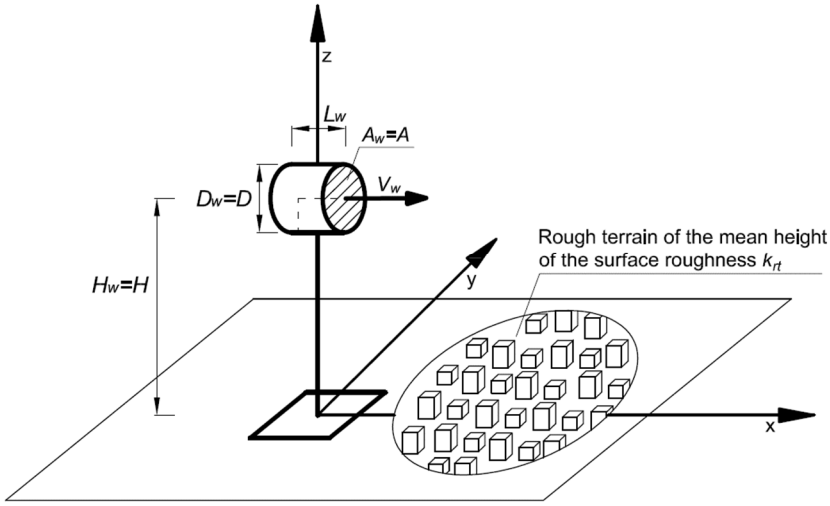

Fig.5.5. Sketch of a single ventilation tower with one substitutive fan (Flaga Ł. et al. 2018).

5.4.3. The array of substitutive ventilation towers

Now, consider a general case for a system of multiple substitutive ventilation towers located at the nodes of a regular mesh where towers are located side-by-side in rows in the *y*-direction and one-by-one in lines in the *x*-direction as shown in Fig. 5.6. Additional parameters of this issue are: distances between rows L; distances between the lines B; the number of rows n_y; the number of lines n_x.

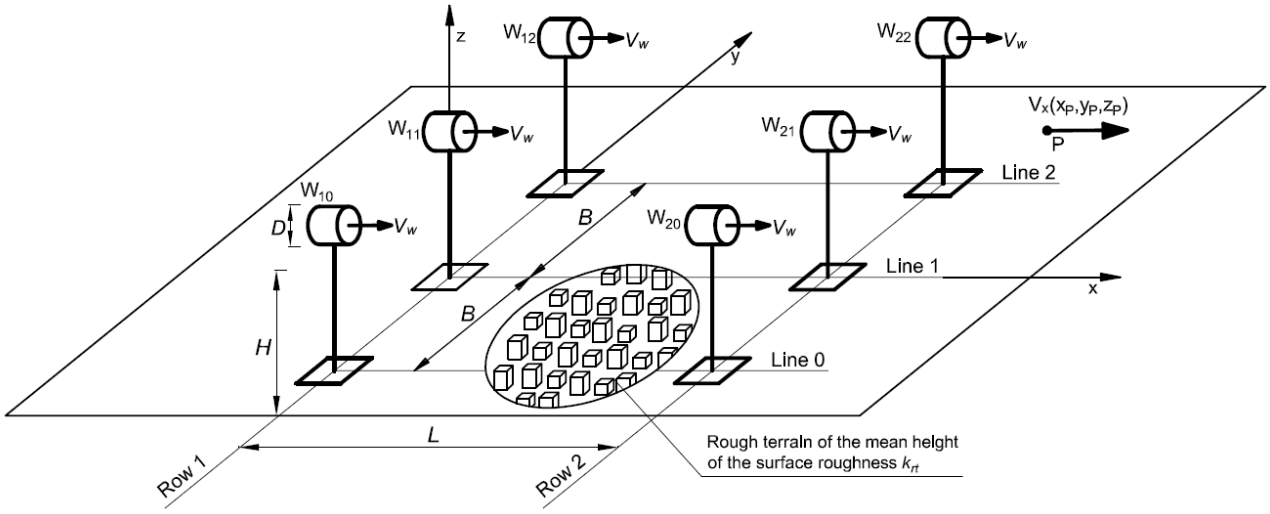

Fig.5.6. Six substitutive ventilation towers on a meshed system of two rows and three lines (Flaga Ł. et al. 2018).

By conducting a dimensional analysis as above, the resulting functional relationship is (Flaga, 2017):

$$\check{V}^{**} = \frac{V_{xP}{}^{**}}{V_w} = \check{F}^{**}\left[\frac{D}{H}, \frac{L}{H}, \frac{B}{H}; (\check{G}_w); \left(\frac{x_P}{H}, \frac{y_P}{H}, \frac{z_P}{H}\right); Re; \check{k}_{rt}\right]. \tag{5.9}$$

6. MODEL OF HORIZONTAL VENTILATION TOWERS SYSTEM[3]

6.1. Aerodynamic tunnel of Wind Engineering Laboratory of Cracow University of Technology

The wind tunnel of a mixed circuit: closed (at closed throttles) when the air flowing out from the tunnel tube through the outlet returns to the tunnel tube through the return channel above the beginning part of the working section; open (at open throttles) when the air flowing into the inflow comes from outside the building by an air scoop located above the inflow on the building roof and is exhausted also outside the building by an air launcher located behind the fan. The open air circuit in the wind tunnel is applied mainly in the case of visualization investigations.

The basic geometric dimensions of the working section are: width – 2.20 m; height – from 1.40 m at the beginning and 1.60 m at the end of the working section; length – 10 m. Formation of the mean wind velocity profile and atmospheric turbulence takes place in the first part of the working section at the length of 6 m by use of respective turbulence networks, barriers, spires, and blocks of respective geometry and an automatically controlled height.

Four characteristic segments each 2.5 m long can be distinguished in the working section. The side walls of the front segment are full (with windows) 2.20 m apart. The other segments have slotted side walls (with horizontal controlled slots aiming at diminution of the so called blockage effect) 2.20 m apart and full side walls with windows 3.40 m apart. In the third and fourth segments of the working section, there are two round rotational tables 2 m in diameter. The first one is designed mainly for the examination of flow

[3] This chapter was written based on:

Flaga Ł., Pistol A., Krajewski P., Flaga A.: *Model tests of dynamic action on the atmospheric boundary layer – linear configuration of ventilation towers on a rough terrain*; Environmental Effects on Buildings and People: Actions, Influences, Interactions, Discomfort, EEBP VIII, Cracow-Lublin 2018, Poland

Krajewski P.: *Badania modelowe dynamicznego działania na warstwę przyziemną atmosfery*; Wpływy środowiskowe na budowle i ludzi; red. Ł. Flaga, R. Kłaput, Politechnika Krakowska, Kraków, 2022

Report 1: Flaga A., Flaga Ł., Krajewski P., Pistol A.: *Badania wstępne możliwości dynamicznego oddziaływania na warstwę przyziemną. Etap 1: Pomiar pola prędkości przepływu i zasięgu strumienia powietrza generowanego przez modele wentylatorów/wież wentylacyjnych w różnych wariantach ich konfiguracji*; Research Report, Wind Engineering Laboratory, Cracow University of Technology, Cracow 2017;

Report 2: Flaga A., Flaga Ł., Krajewski P., Pistol A.: *Badania wstępne możliwości dynamicznego oddziaływania na warstwę przyziemną. ETAP II – Badania w tunelu aerodynamicznym pola prędkości przepływu generowanego przez układ wentylatorów/wież wentylacyjnych w konfiguracji promienistej i specjalny membranowy komin wentylacyjny*; Research Report, Laboratorium Inżynierii Wiatrowej Politechniki Krakowskiej, Kraków 2017;

Report 3: Flaga A., Flaga Ł., Krajewski P., Pistol A.: *Badania wstępne możliwości dynamicznego oddziaływania na warstwę przyziemną. Etap III – Badania w tunelu aerodynamicznym wybranych zagadnień z Etapów I i II przy uwzględnieniu wpływu chropowatości podłoża (zabudowy miejskiej)*; , Laboratorium Inżynierii Wiatrowej Politechniki Krakowskiej, Kraków 2018;

around phenomena and their visualization and examination of snow precipitation and snow redistribution phenomena. The other rotational table is designed mainly for aerodynamic and aeroelastic tests of buildings and structures.

In the upper part of the working section, there is equipment for fixing all kinds of measurement probes and their controlled movements at the whole working section in directions *x*, *y*, *z*. The roof of the working section may change its position in the direction up and down; this permits control of the gradient of static pressure in the working section. In the back part of the working section, there are two aerodynamic balances for measurements of aerodynamic forces and moments: one of the six-components for vertical models, and the other of three-components for horizontal models.

The working section is ended with a cascade of horizontal airfoil profiles that reduces the influence of vortices generated by the fan on an air flow in the area of the rotational table. Guide vanes, inlet, beehive frame, stabilization chamber, and confusor are the elements designed to take over the stream either returning through the return channel or taken from above the building roof by external air scoop and direct it respectively, making the stream homogeneous and of very low turbulence before the inflow to the working section. The diffuser which is behind the working section is rectangular at the beginning part and of a circular shape at the end part (cross-section of the fan) and its length is equal to 5 m.

The axial fan, single-stage of efficiency 0.8 – 0.9, the outer diameter 2.72 m, and the velocity of the end of the fan blade up to 100 m/s, is located on the suction side of the wind tunnel. The engine of the alternate current, shorted, driving the fan with a power of 200 kW, of nominal revolutions 750 rpm and supply voltage 220 V, controlled by inverter. The maximum mean flow velocity in the working section is $V_{max} = 40 \frac{m}{s}$. A scheme of the most important dimensions and elements of the wind tunnel is shown in Fig. 6.1 and Fig. 6.2.

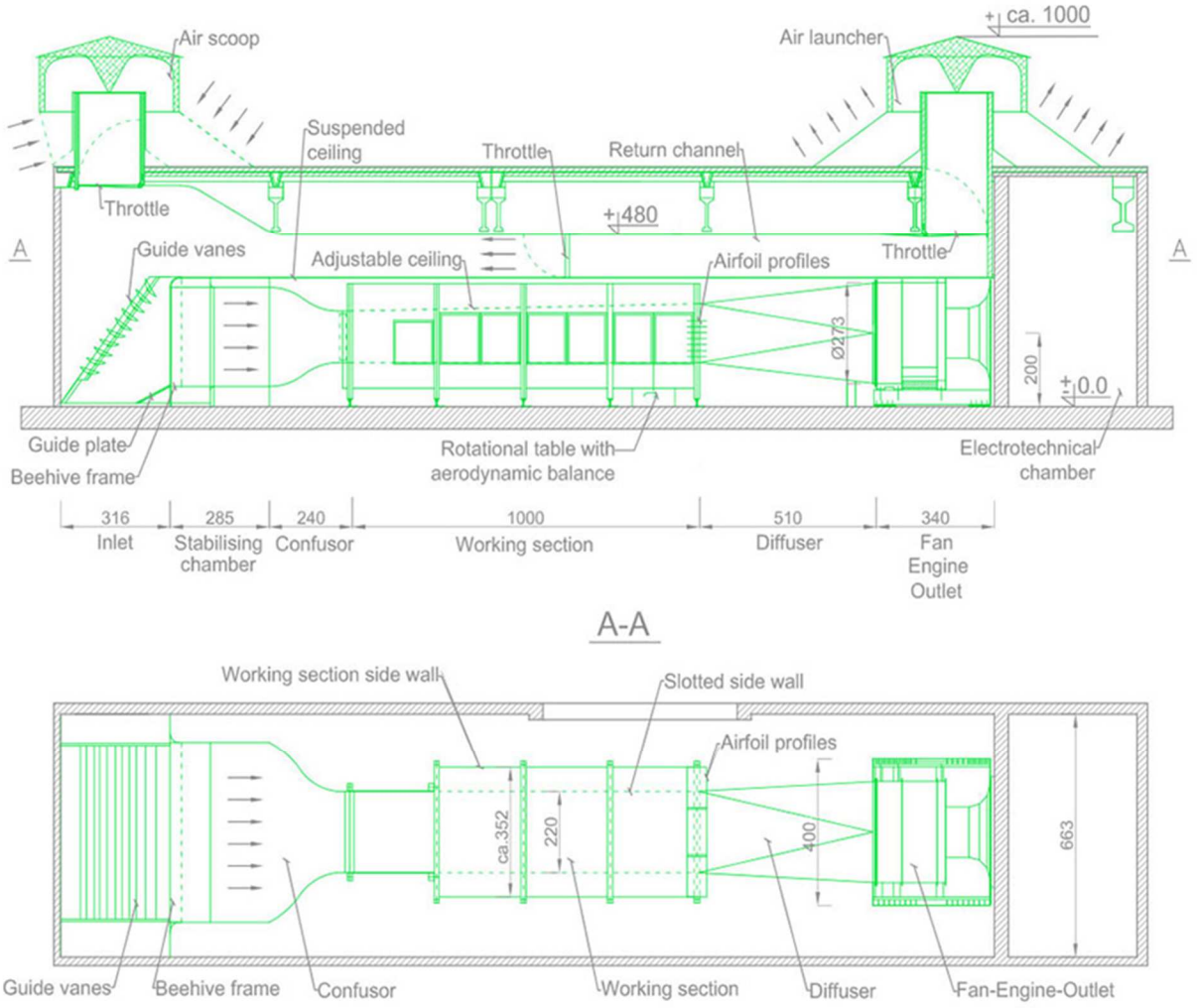

Fig. 6.1. Top and side views of the wind tunnel (dimensions in [cm])(Flaga Ł. et al. 2018).

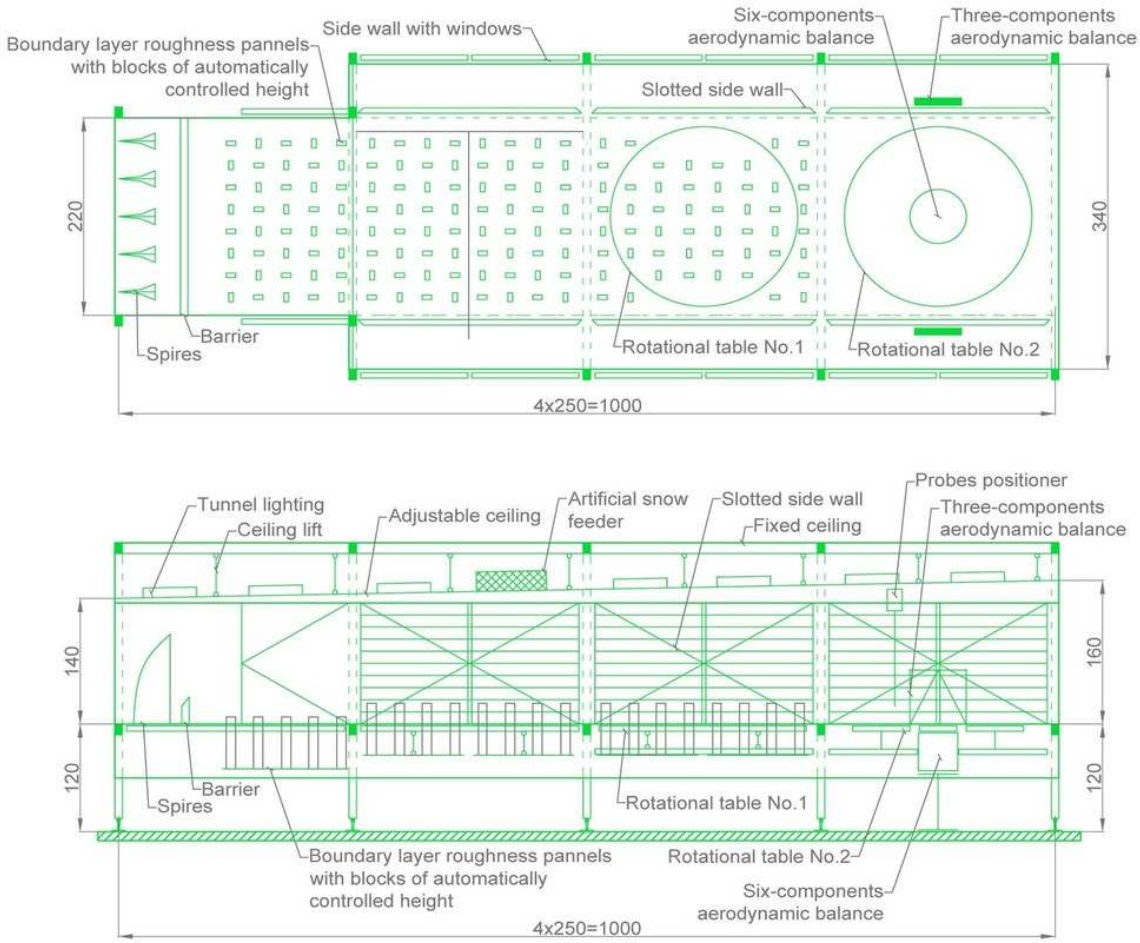

Fig. 6.2. Top and side views of the wind tunnel working section (dimensions in [cm]) (Flaga Ł. et al. 2018).

6.2. Wind flow velocity measurements

Wind flow velocity measurements are conducted with hot-wire anemometric system (Fig. 6.3 and 6.4), which is used for the acquisition and visualization of measurement data from ATU2001 hot-wire anemometers connected with multipurpose data acquisition module National Instruments NI-USB 6009. The cooperation between this module and hot-wire anemometers is executed by 4 analog inputs in a differential configuration.

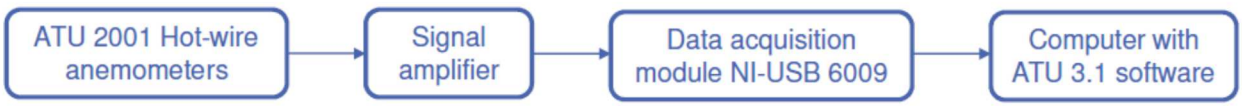

Fig. 6.3. Scheme of measurement path for wind flow velocity (Report 1)

4-channel hot-wire anemometric module is designed for velocity and temperature measurement in air flows. The set consists of complete mono- and double-filament probes, holders that connect probes with the module, data acquisition module and external power supply. The module acts as a converter of signals from probes on voltage output

signals proportional to air flow velocity and temperature. It consists of four channels, each equipped with a DC thermometer and DC hot-wire anemometer.

Module technical data:

Thermometer characteristics:

- measuring range – 0÷100°C,
- output filter – low-pass,
- maximum output voltage – up to +12 V.

Hot-wire anemometer characteristics:

- measuring range – 0÷100 m/s,
- output filter – low-pass,
- maximum output voltage – up to +12 V.

In Fig. 6.4. a 4-channel hot-wire anemometric module ATU2001 is shown along with the probe holders.

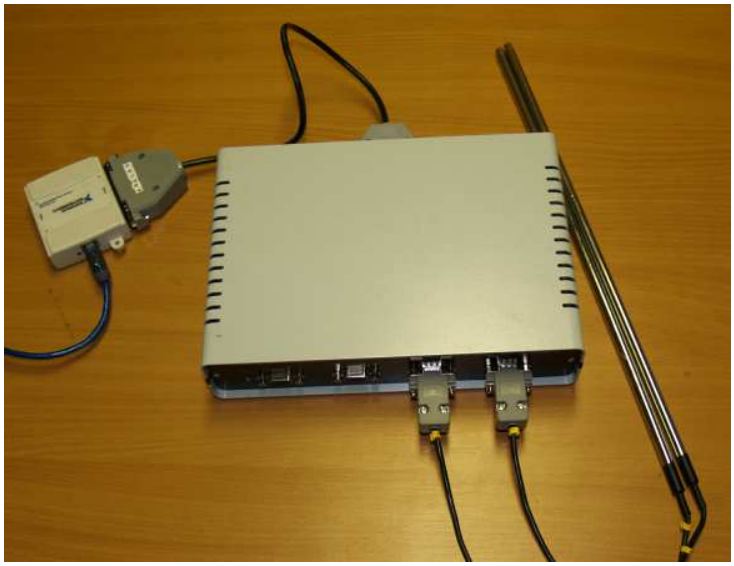

Fig. 6.4. ATU 2001 module with probe holders (Fot. R. Kłaput)

6.3. The first stage experiment setup

The objectives of the first stage of the study were: development of a practical model of air flow in urban areas along with elaborating similarity criteria for the analyzed issue; preparing work station for measurement of air flow velocity field generated by ventilation towers in chosen variants of their parallel configuration; conducting model tests to measure air flow velocity field in the proximity of ventilation towers in parallel configuration with different fan rotation speeds, number and location of the fans; smoke visualization of the phenomena.

Test series I-V were carried out in a model scale of 1:833. The model scale was determined by the dimensions of the available fans (see Fig. 6.5) and the measurement space of the wind tunnel. Due to the different proportions of the fans used (60x60mm) to the proportions of the target ventilation tower (80x20m), only the vertical dimension of the tower was kept in the tests (series I-V). Air stream flow measurements were made using 4 hot-wire anemometric probes, spaced every 20 mm, each time located in the middle plane of the fan (see Fig. 6.5).

It was decided that the series of model tests would differ in the number of rows and lines in which the fans are arranged. The distances between fan rows resulting in generation of the air stream (i.e. keeping the air flow velocity at a specified level) were specified empirically during preliminary model tests. Characteristics of the model test series are as follows:

- Series I: single fan with voltages of 5.6 V, 7.7 V, 9.5 V, 11.4 V, 13.6 V, scale 1:833;
- Series II: 2 fans in single line distanced by 250 cm and 280 cm, voltage 13.6 V, scale 1:833;
- Series III: a row of 3 fans spaced by 1.5 D (D – fan diameter), voltage 13.6 V, scale 1:833 (Fig.6.6a);
- Series IV: a row of 3 fans spaced by 3 D, voltage 13.6 V, scale 1:833;
- Series V: 2 rows of fans distanced by 370 cm in 3 lines spaced by 3 D, 13.6 V, scale 1:833;
- Series VI: single ventilation tower, voltage 13.6 V, scale 1:100 (Fig.6.6b).

a)  b) 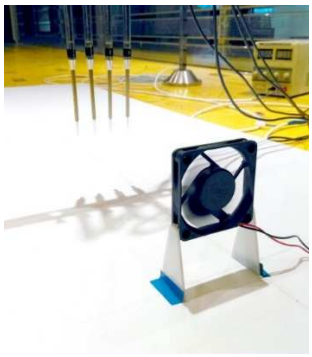

Fig.6.5. Models of ventilation towers used in model tests: a) set of 3 fans – substitutive ventilation towers, scale 1:833; b) single substitutive ventilation towers with thermoanemometric probes.

Fig.6.6. single ventilation tower, scale 1:100

The fans used in experiments are CPU cooling fans measuring 60x60x10 mm in size and nominal voltage DC 12 V, 0.22 A. Rotation speed was controlled by adjusting the voltage. The air flow was measured by four hot-wire anemometers spaced by 20 mm located in the central plain of the fan. The case was different in series VI where the complete ventilation tower was modeled in the scale of 1:100. Measurement for this series was conducted on three horizontal plains at different heights.

a)

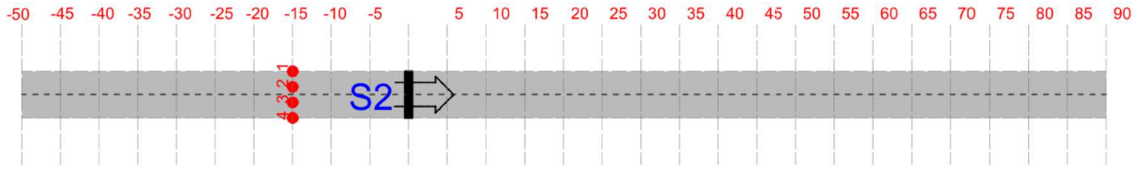

b)

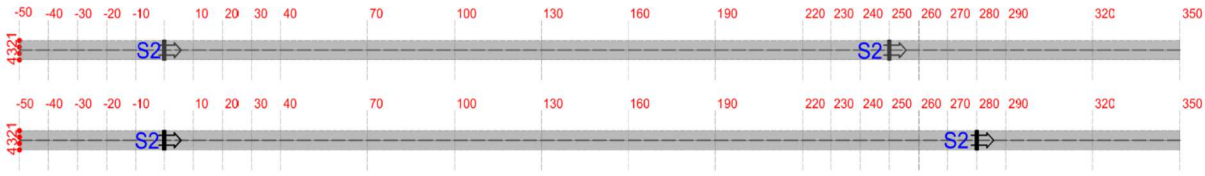

c)

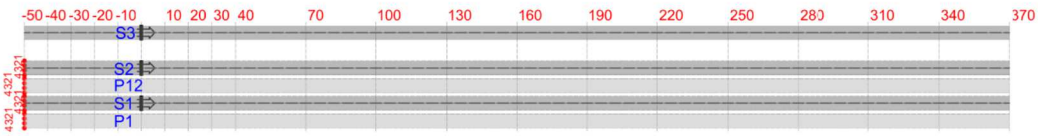

d)

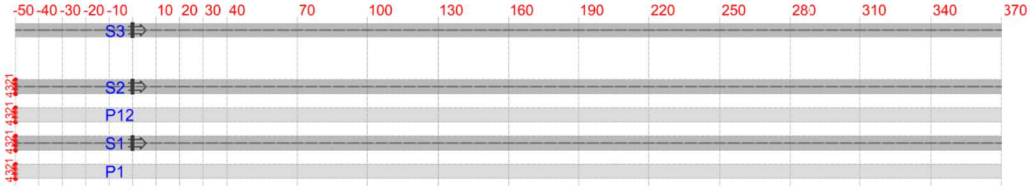

e)

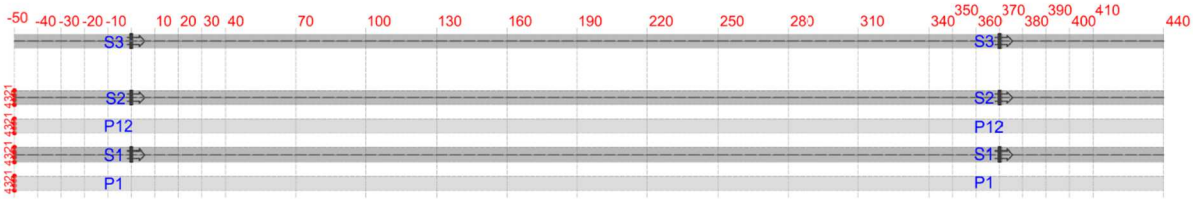

f)

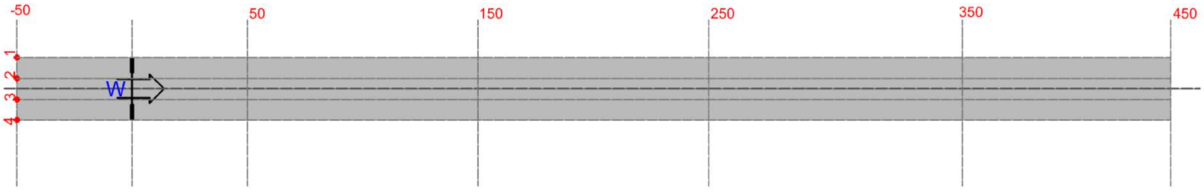

Fig. 6.7. Schematic view showing the distance between the planes where the measurements were made and the fans for: a) series I, b) series II, c) series III, d) series IV, e) series V and f) series VI (Flaga Ł. et al. 2018).

a)

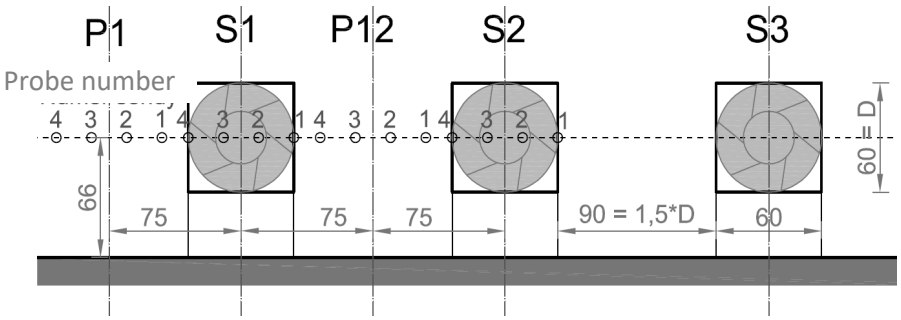

b)

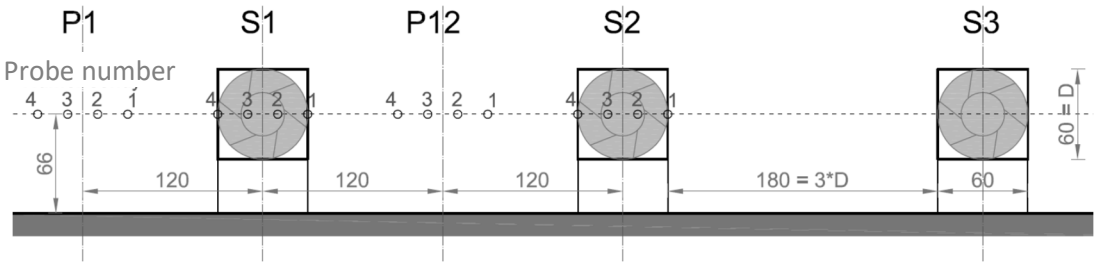

Fig. 6.8. Schematic cross-section with marking of planes in which measurements were made for: a) series III and b) series IV and V (Flaga Ł. et al. 2018).

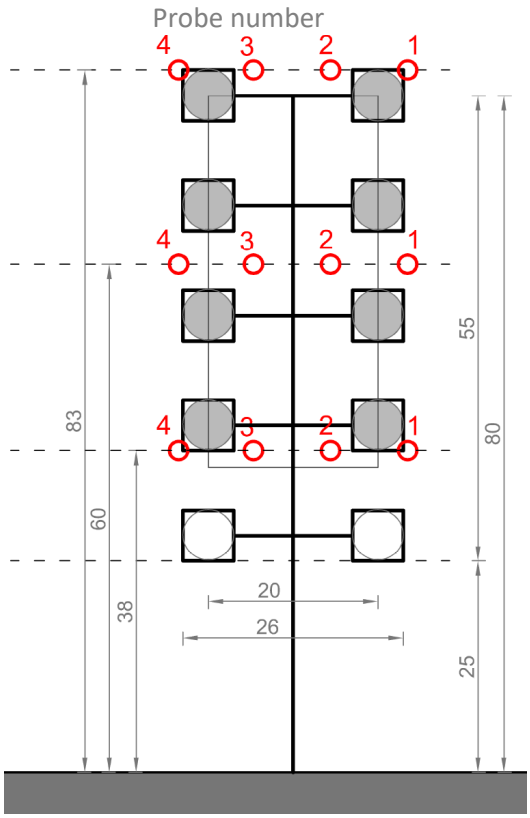

Fig. 6.9. Schematic cross-section with marking of planes in which measurements were made for series VI (Flaga Ł. et al. 2018).

Model similarity criteria The dimensional basis of the conducted tests are physical quantities (ρ, V, D) (see Fig. 5.1.) where: ρ – air density, V – air outlet velocity, D – fan diameter.

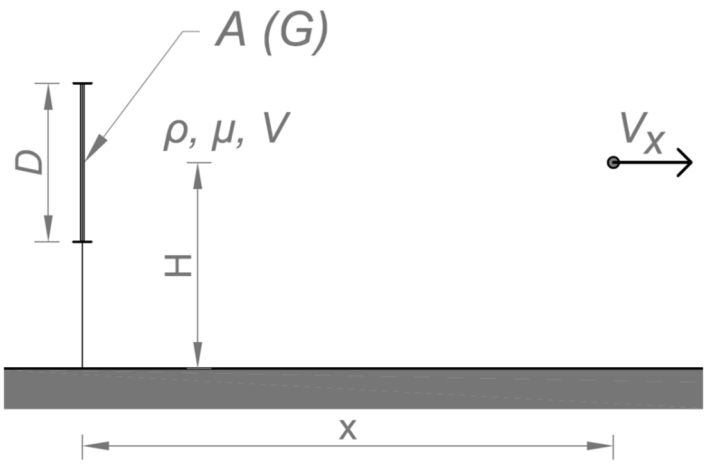

Fig. 6.10 Geometric and physical parameters of the analyzed problem (Flaga Ł. et al. 2018).

The function of air velocity V_x at a distance x from the fan depends on the following parameters:

$$V_x = F\left(\rho, \mu, V, H, x, D, \left(\check{G}\right)\right) \tag{6.1}$$

where: μ – dynamic viscosity of the air, H – the height of the fan axis above the terrain, x – distance from the fan, $\check{G}$ – set of dimensionless geometric parameters.

Dimensionless quantities have been defined as:

$$\frac{V_x}{V} = \Pi_V = \check{V} \tag{6.2}$$

$$\frac{VD}{\nu} = \Pi_\nu = Re \tag{6.3}$$

$$\frac{H}{D} = \Pi_H \tag{6.4}$$

$$\frac{x}{H} = \Pi_x = \check{x} \tag{6.5}$$

$$\frac{V_x}{V} = \check{F}\left(\frac{Va}{\nu}, \frac{H}{D}, \frac{x}{H}, \left(\check{G}\right)\right) = \check{V} \tag{6.6}$$

hence:

$$V_x = V \cdot \check{F}\left(Re, \frac{H}{D}, \frac{x}{H}, \left(\check{G}\right)\right) \tag{6.7}$$

where: ν – kinematic viscosity of air, Re – Reynolds number.

Based on (7), it can be seen that the air velocity in the considered problem depends on the Reynolds number and the distance from the fan, other geometrical parameters remain unchanged. To find the variability of air velocity depending on the Reynolds number, the first series of tests was carried out.

6.4. Test results of the horizontal ventilation towers system

All presented test results were corrected taking into account the air velocity with the fans off, defined as the background velocity. This value reached values at the level of 0.15-0.20 m/s.

In fig.6.11. the results for a series of tests I - one fan at different rotational speeds (5.6V, 7.7V, 9.5V, 11.4V, 13.6V) are presented. The vertical axis shows the dimensionless value of the quotient of velocity at a distance of x = 10cm to velocity $v_{x.}$ - at distance x.

a)

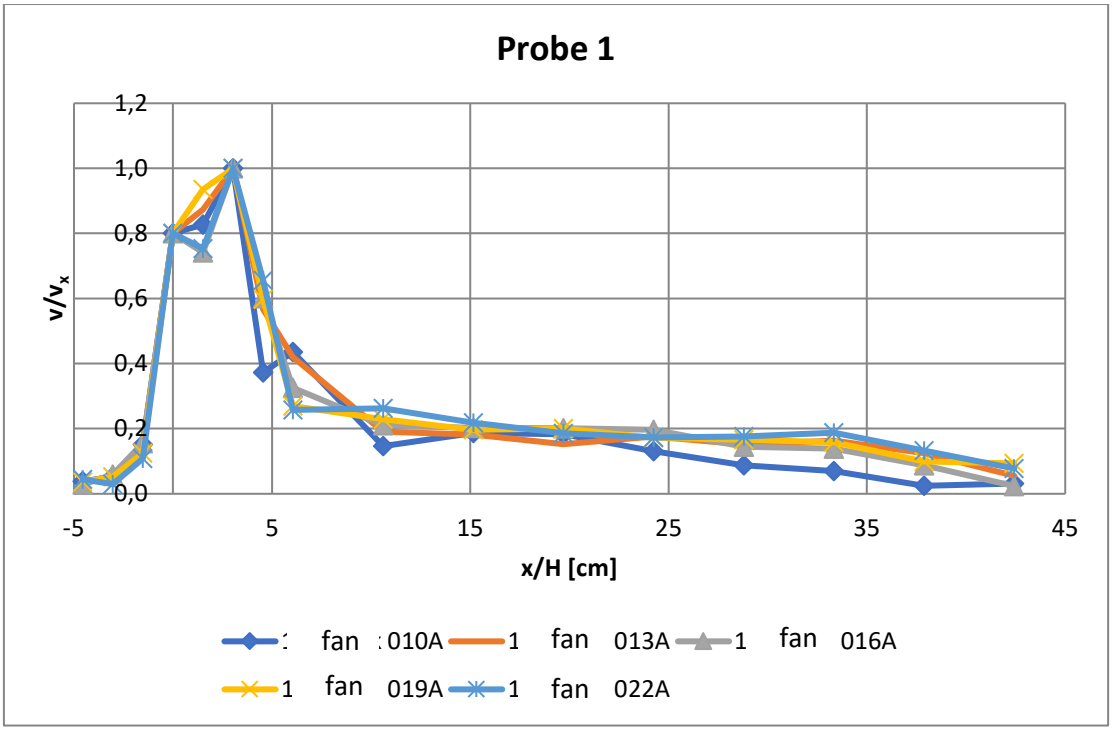
Probe 1
1,2
1,0
0,8
0,6
0,4
0,2
0,0
v/v_x
-5
5
15
25
35
45
x/H [cm]
1 fan 010A
1 fan 013A
1 fan 016A
1 fan 019A
1 fan 022A

b)

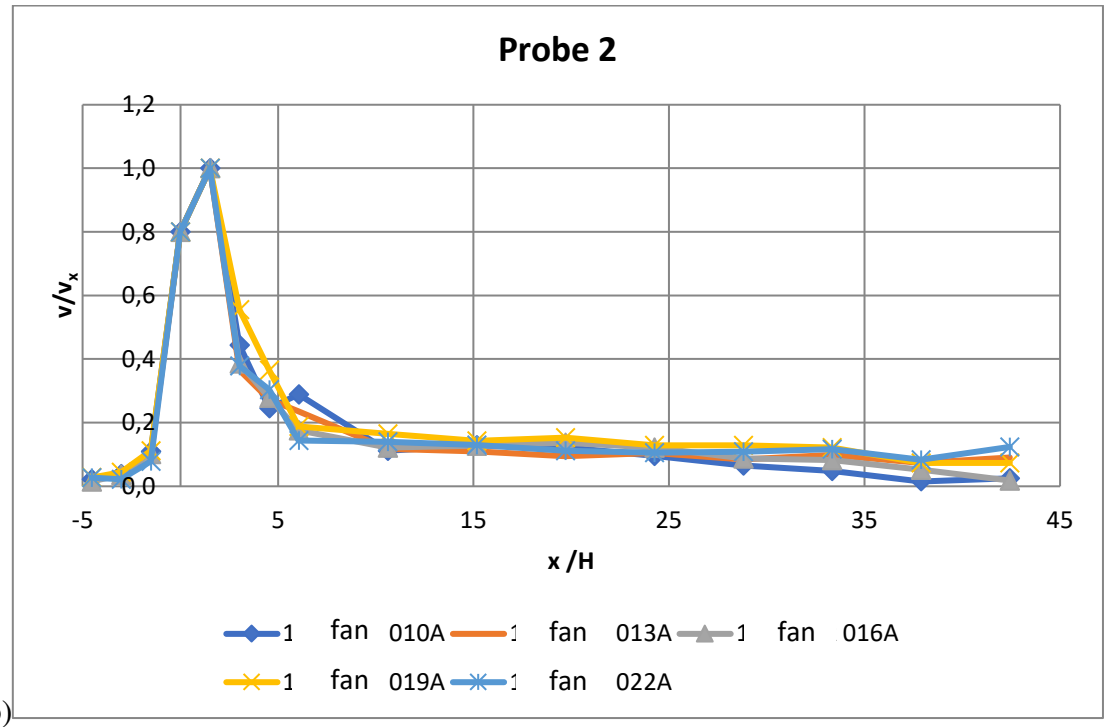
Probe 2
1,2
1,0
0,8
0,6
0,4
0,2
0,0
v/v_x
-5
5
15
25
35
45
x /H
1 fan 010A
1 fan 013A
1 fan 016A
1 fan 019A
1 fan 022A

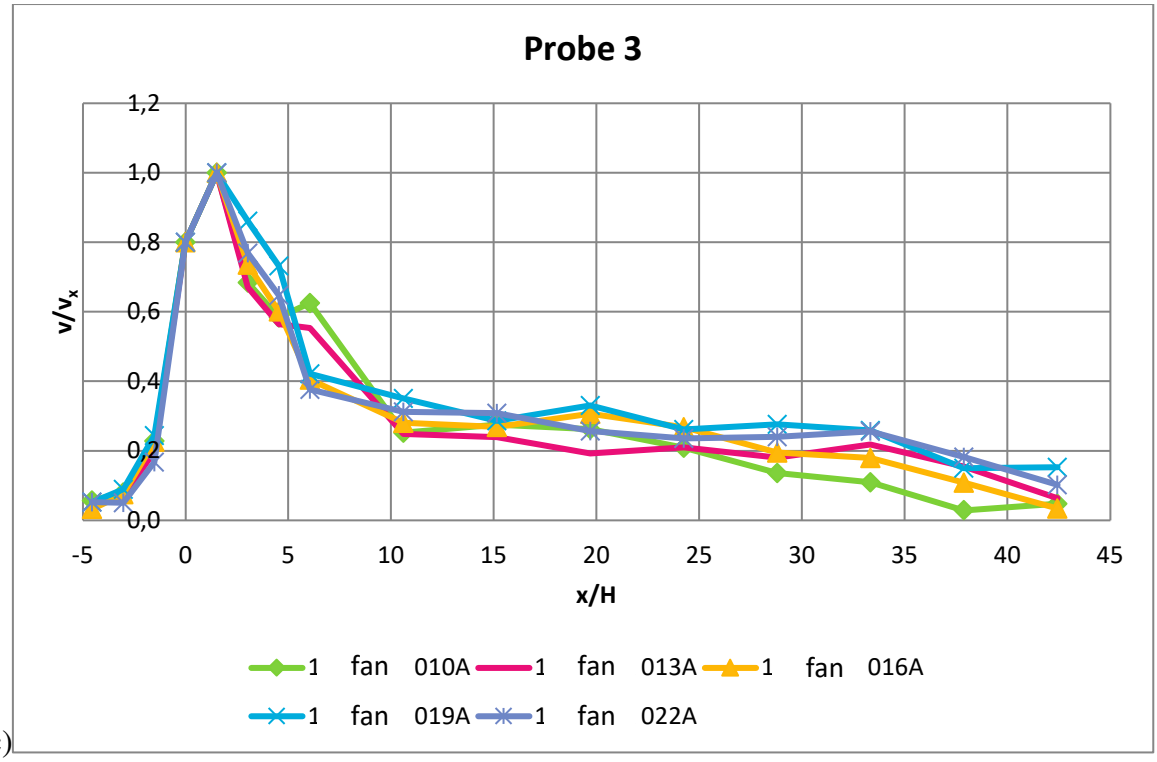

c)

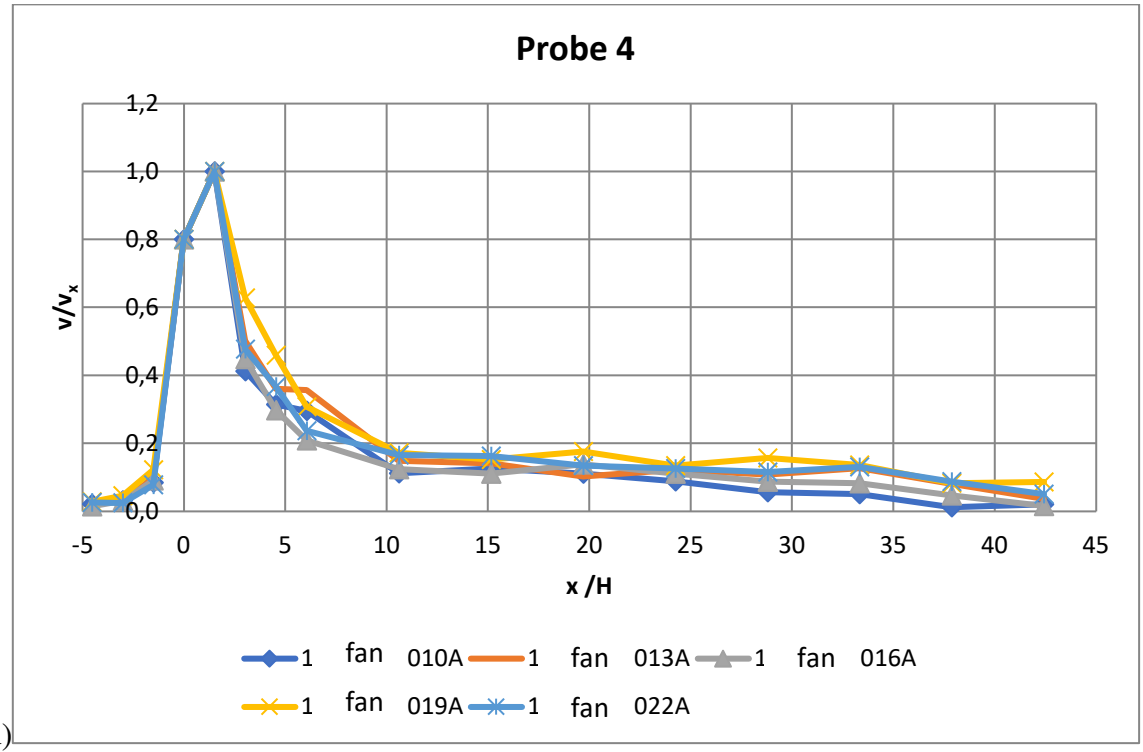

d)

Fig. 6.11. Air velocity for individual rotational speeds in series I for: probe 1 a), probe 2 b), probe 3 c) and probe 4 d).

In Fig. 6.12. the results for the test series II are presented: 1 row of fans in two planes spaced from each other at a distance of 250 cm and 280 cm

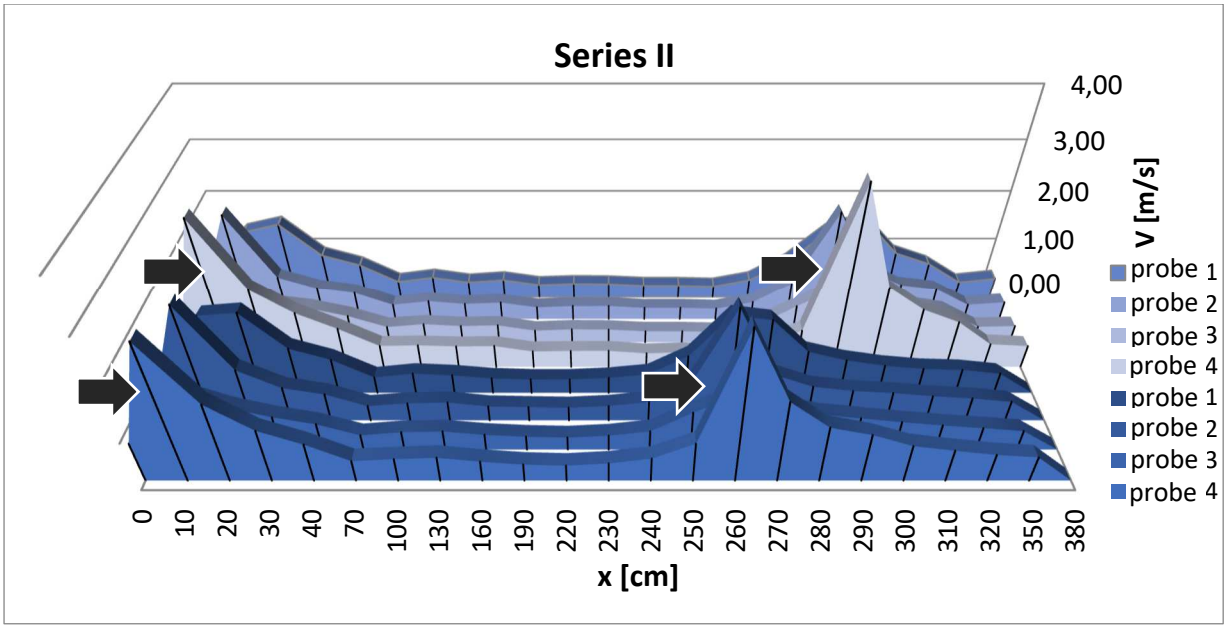

Fig. 6.12. Comparison of air velocity for series II and voltage on 13.6V fans for 250cm and 280cm fan distances.

In Fig. 6.13. the results for the test series III are presented: a row of 3 fans spaced 1.5 D

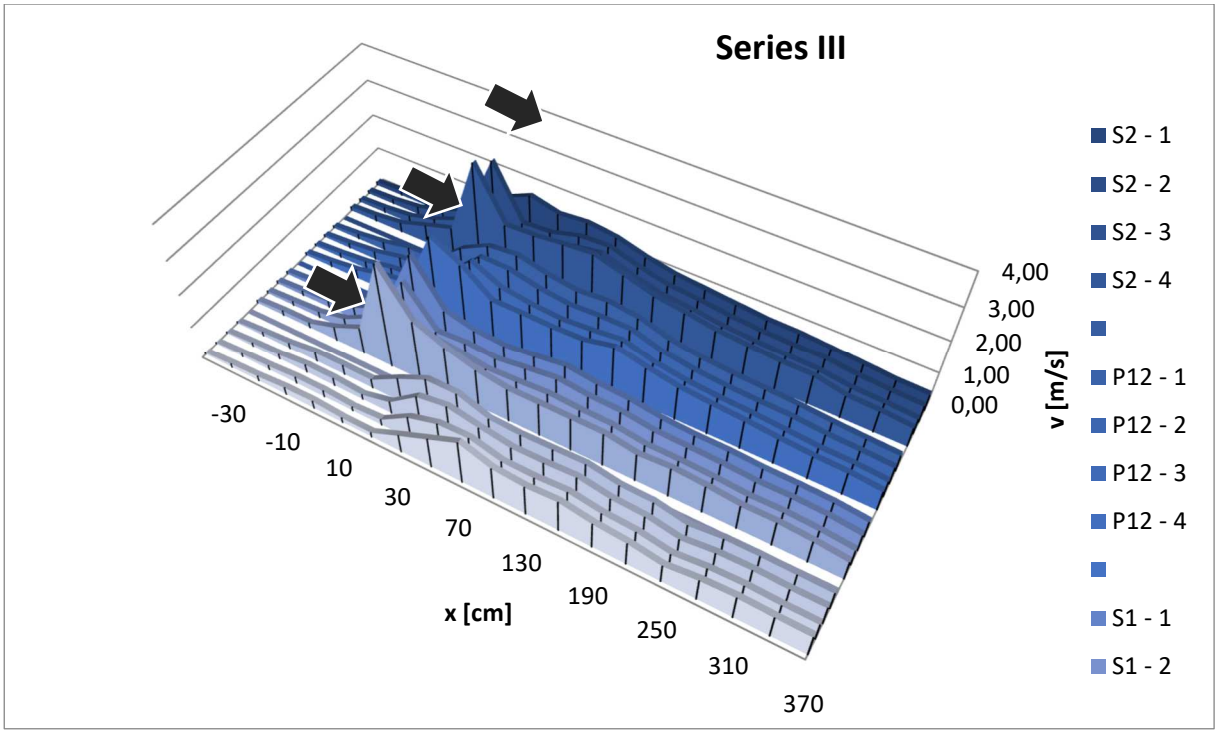

Fig. 6.13. Comparison of air velocity for series III and voltage on 13.6V fans for 3 fans spaced 1.5D

In Fig. 6.14. the results for the IV test series are presented: a row of 3 fans spaced 3 D

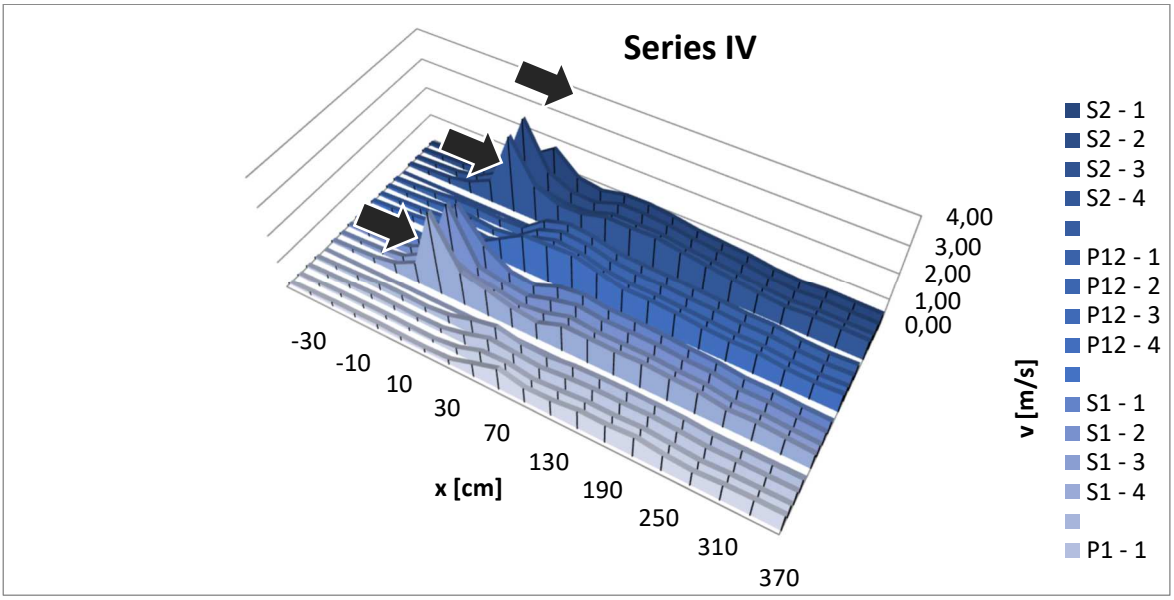

Fig. 6.14. Comparison of air velocity for the IV series and the voltage on the fans 13.6V for 3 fans in 3D spacing

In Fig. 6.15. the results for the V test series are presented: a row of 3 fans spaced 3 D in the configuration of planes spaced apart by a distance of 370 cm

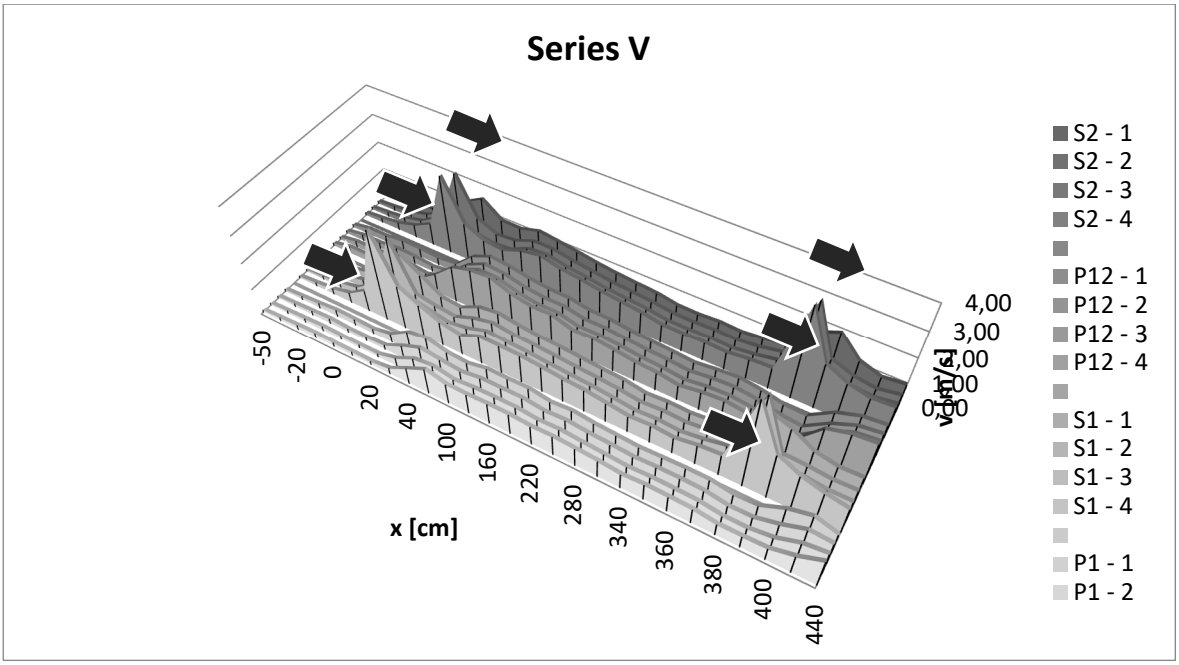

Fig. 6.15. Comparison of the air velocity for the V series and the voltage on the 13.6V fans for 3 fans in 3D spacing in the configuration of planes spaced apart by a distance of 370cm, fan distance 370cm.

In Fig. 6.16. the results for the test series VI are presented: Single ventilation tower - vertical cross-sectional plan

a)

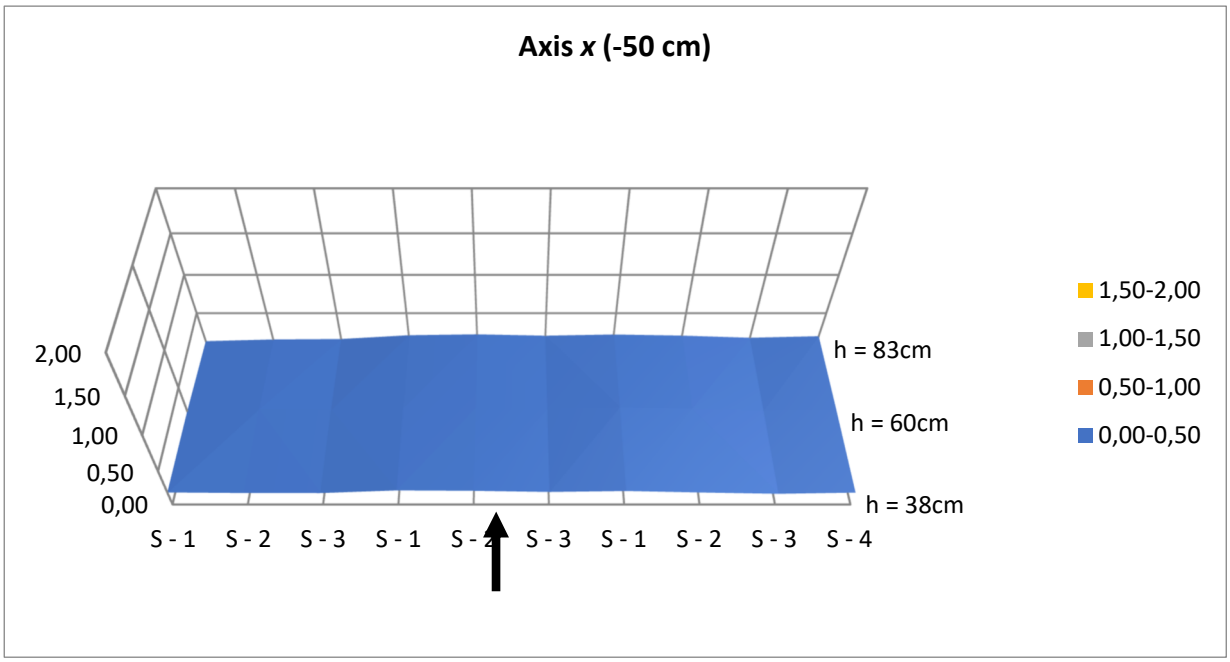

b)

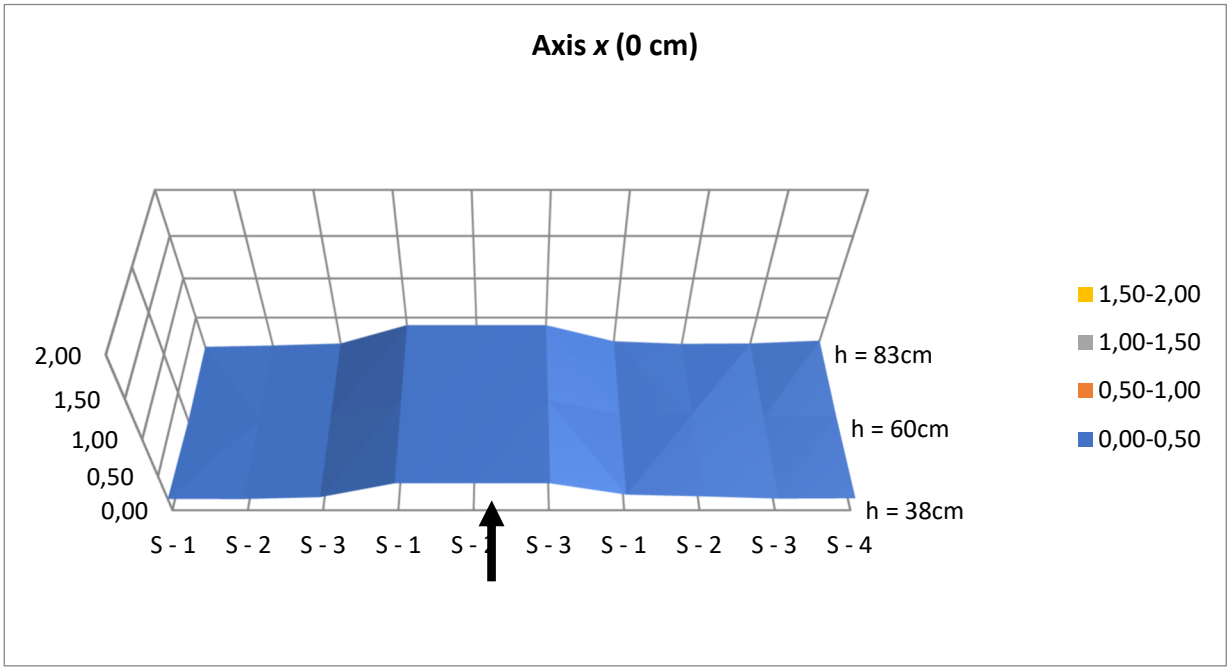

c)

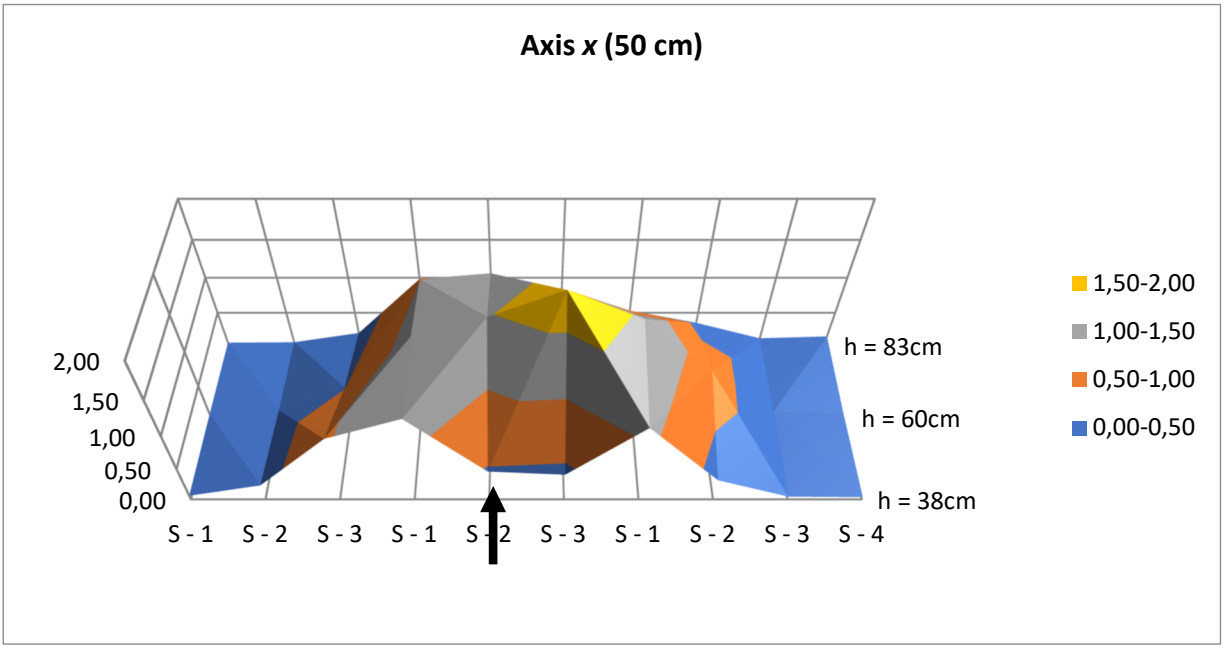
Axis x (50 cm)
2,00
1,50
1,00
0,50
0,00
S - 1
S - 2
S - 3
S - 1
S - 2
S - 3
S - 1
S - 2
S - 3
S - 4
h = 83cm
h = 60cm
h = 38cm
1,50-2,00
1,00-1,50
0,50-1,00
0,00-0,50

d)

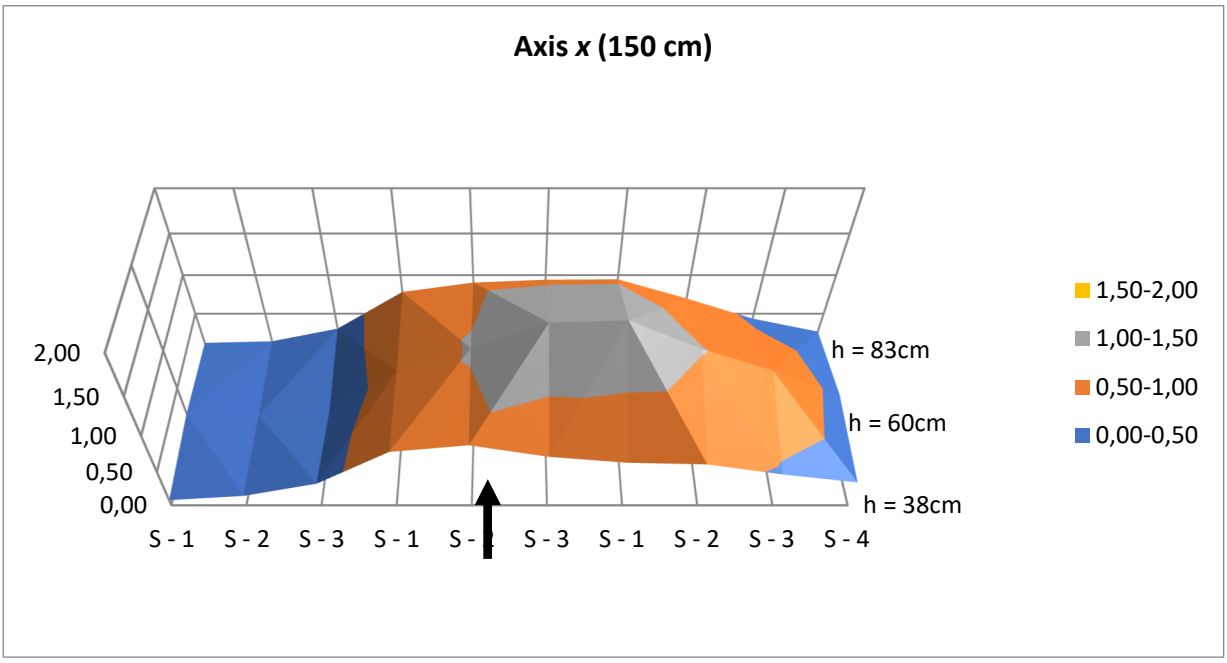
Axis x (150 cm)
2,00
1,50
1,00
0,50
0,00
S - 1
S - 2
S - 3
S - 1
S - 2
S - 3
S - 1
S - 2
S - 3
S - 4
h = 83cm
h = 60cm
h = 38cm
1,50-2,00
1,00-1,50
0,50-1,00
0,00-0,50

e)

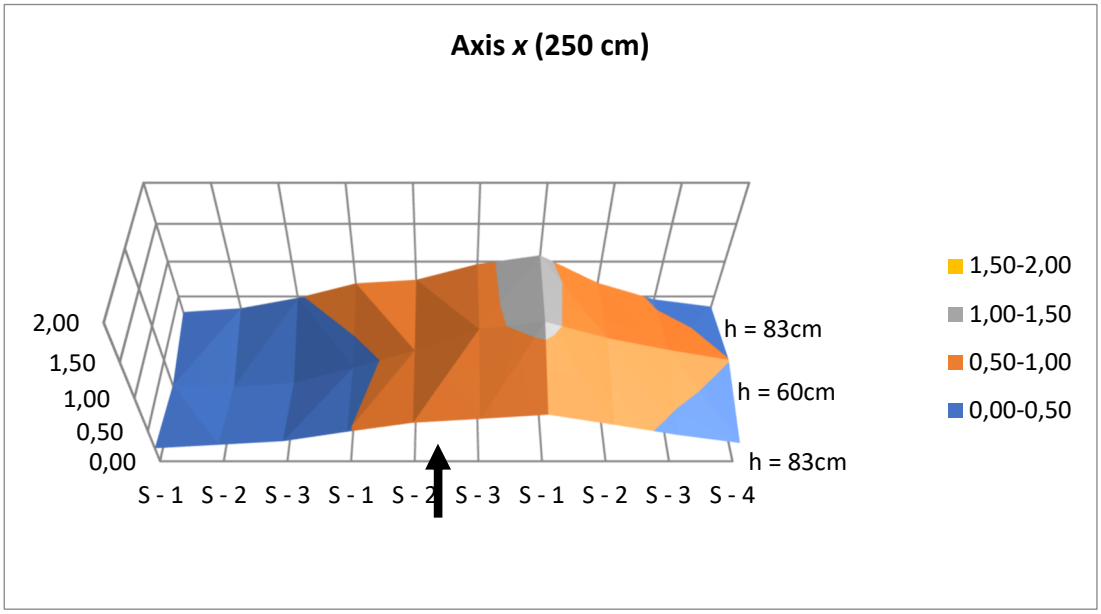
Axis x (250 cm)
2,00
1,50
1,00
0,50
0,00
S - 1 S - 2 S - 3 S - 1 S - 2 S - 3 S - 1 S - 2 S - 3 S - 4
h = 83cm
h = 60cm
h = 83cm
1,50-2,00
1,00-1,50
0,50-1,00
0,00-0,50

f)

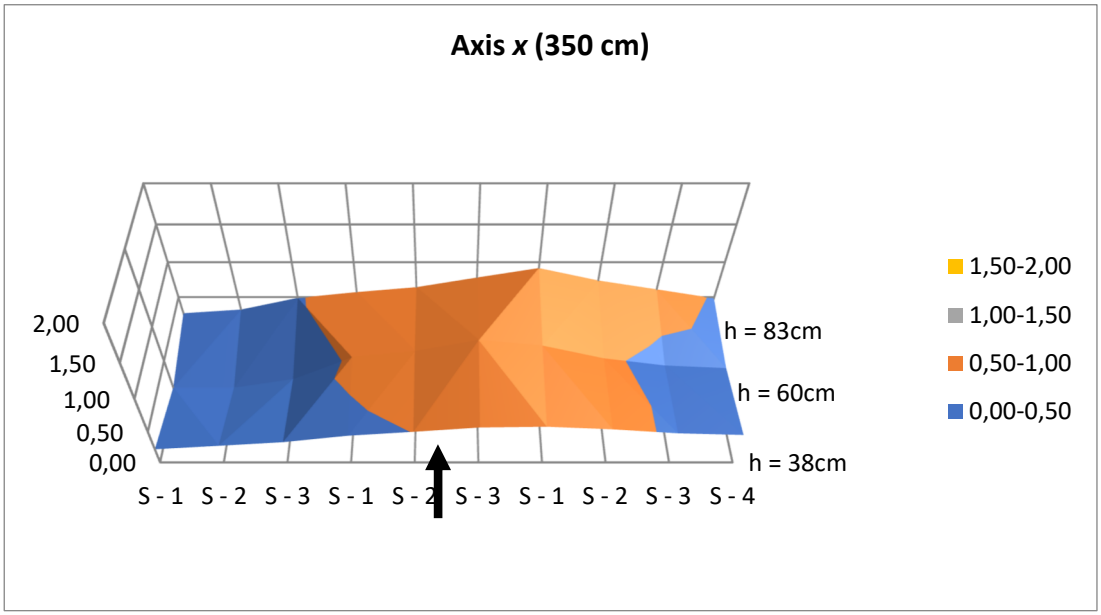
Axis x (350 cm)
2,00
1,50
1,00
0,50
0,00
S - 1 S - 2 S - 3 S - 1 S - 2 S - 3 S - 1 S - 2 S - 3 S - 4
h = 83cm
h = 60cm
h = 38cm
1,50-2,00
1,00-1,50
0,50-1,00
0,00-0,50

g)

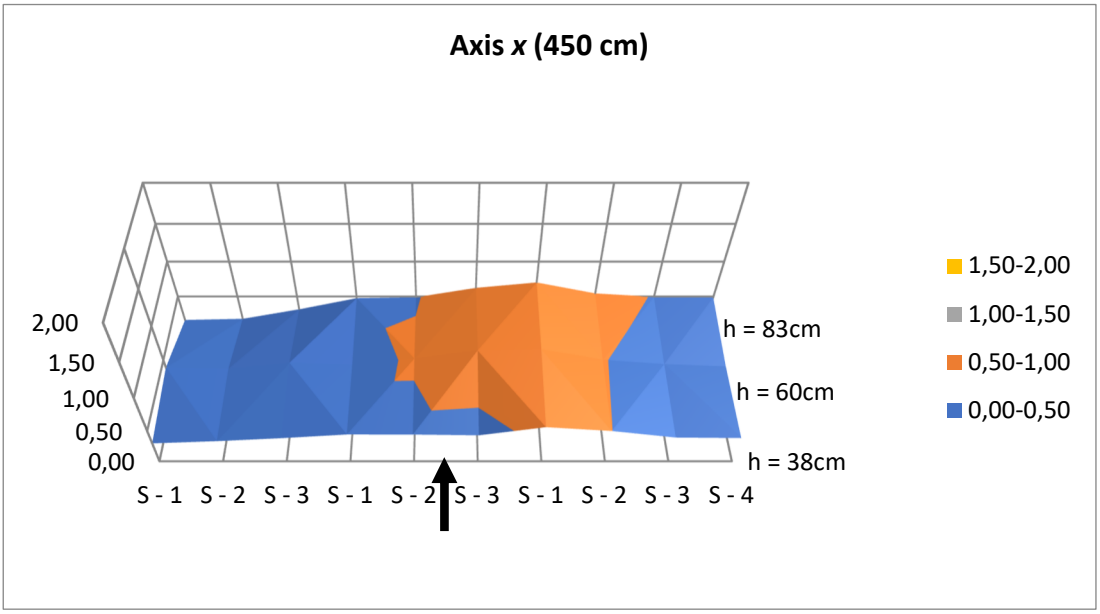

Fig. 6.16. Comparison of the air velocity for the VI series and the voltage on the 13.6V fans for the ventilation tower and the planes x = -50cm a), x = 0cm b), x = 50cm c), x = 150cm d), x = 250cm e), x = 350cmf), x = 450cmg)

In Fig. 6.17. the results for the test series VI are presented: Single ventilation tower - horizontal cross-sectional planes

a)

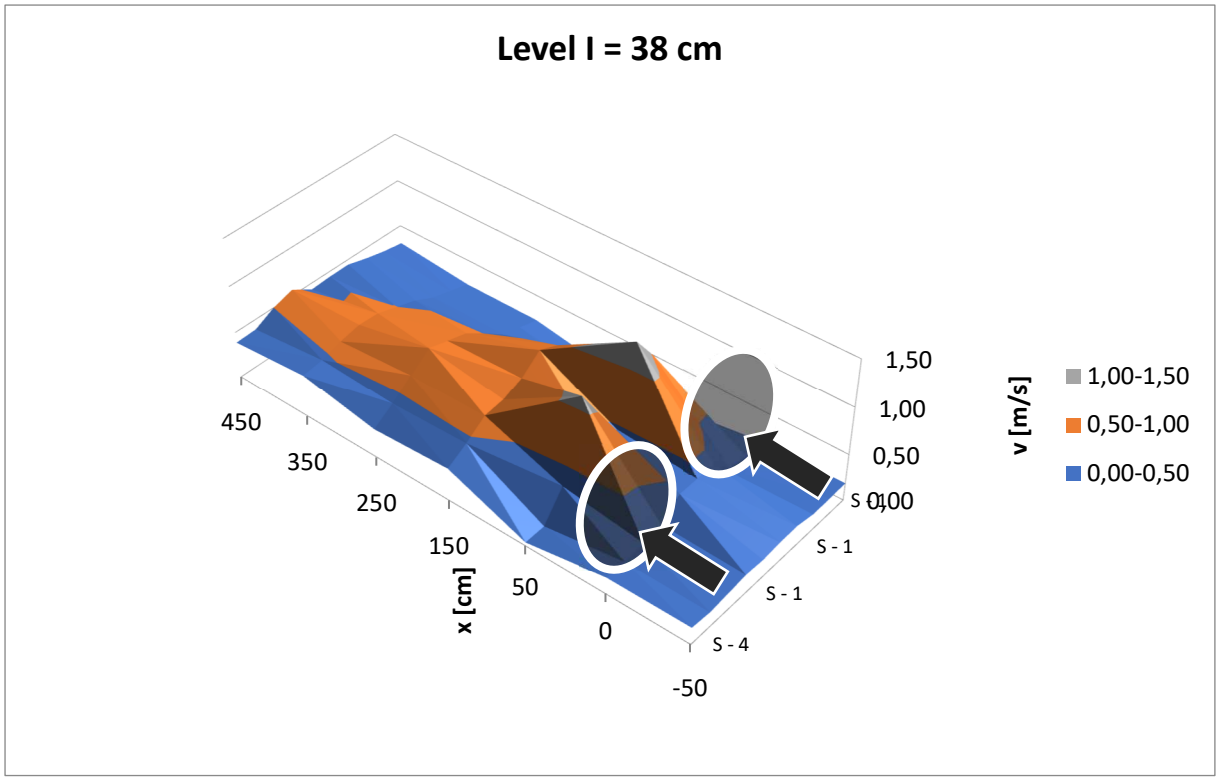

b)

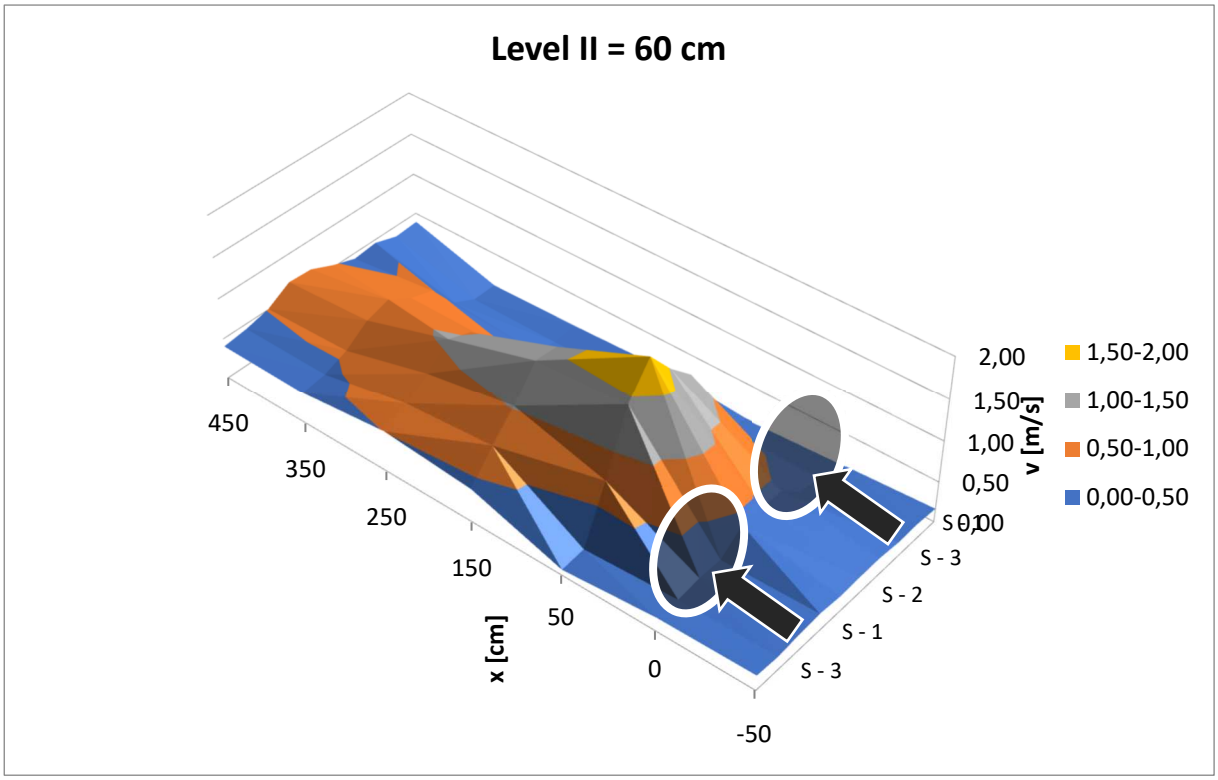

c)

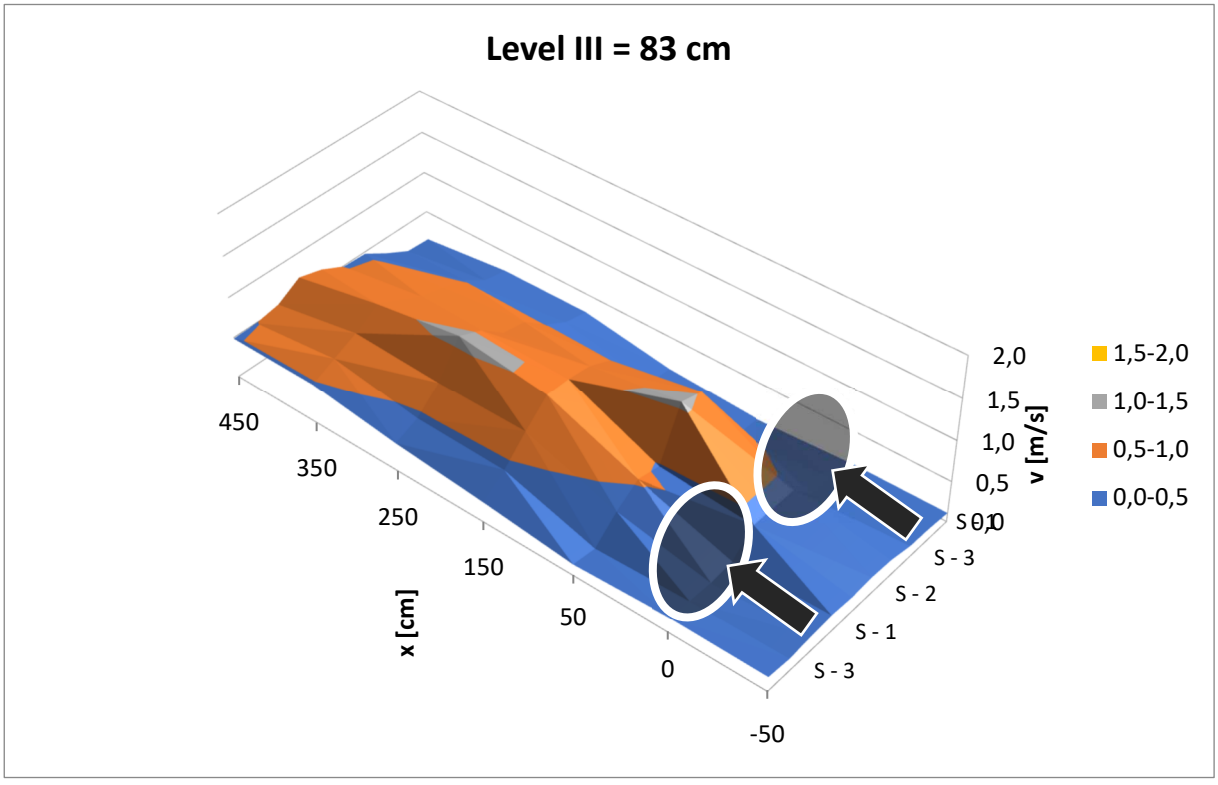

Fig. 6.17. Comparison of the air velocity for the VI series and the voltage on the 13.6V fans for the ventilation tower on the planes h = 38cm a), h = 60cm b), h = 83cm c).

The results of the stage I study gave the following conclusions:

1). Relative wind velocity at a distance of more than 30 cm is kept on a similar level for every tested rotation speeds. It means that the Reynolds number is not a significant factor influencing the results in the small scale experiments;

2). The range of air suction in front of the fan is limited to no more than 10-20 cm. Thus, it is economically reasonable to place the second row of fans at a distance where the air stream is fading away. For the case of the study, the distance was x = 280 cm. Placing the rows of fans closer to each other has an insignificant influence on increasing the air flow velocity, so there is no reason for it;

3). The spread of fans in a single row was adjusted between 1.5 D (series III) and 3 D (series IV). The air flow velocity at the end of the stream (i.e. at a distance x = 370 cm) reached similar values for both cases, although at the spacing of 3 D the total width of the stream, so also the area of action of the fans, was two times larger than at 1.5 D and the same number of fans. Therefore, it was decided to increase the spread of the fans on the ventilation tower to 3 D and continue the tests with this spacing;

4). The wide stream generated with 3 fans spaced in 3 D can be successfully kept by adding another row of fans at a distance of x = 370 cm. No significant difference in air flow velocity was observed in close ranges ahead of the 2nd row (i.e. 340-360 cm); hence it was concluded that the location of the 2nd row was correct. Increasing the distance further could result in decreasing the air flow velocity or even interrupting the continuity of the stream;

5). Despite the change of the number of fans from 1 to 8 and the change of scale from 1:833 to 1:100, the shape of the airstream was similar to the previous series. This confirms the thesis that in model tests a group of fans cooperating close to each other can be replaced by a single fan in a larger scale.

6.5. Conclusion for the results of the I stage

The conducted research confirmed that the previous assumptions of the general concept of dynamic impact on the boundary layer are correct and possible to perform; what's more - the results obtained are often more favorable than initially estimated. It is advisable to continue these studies as part of Stage II and Stage III, mentioned earlier.

6.6. Model description and experiment setup of horizontal ventilation towers in stage III

It was necessary to investigate the influence of terrain roughness and the Reynolds numbers, so in the stage III some series of tests with the horizontal ventilation towers were also performed:

1. Type of terrain roughness depending on the standard terrain category:
   • category 0 - sea, coastal area open to the sea - flat area, without roughness - tests carried out during the first stage,

• category III - areas regularly covered with vegetation or buildings or single obstacles separated by no more than 20 of their height (such as villages, suburban areas, permanent forests) (see Fig. 6.19),
• category IV – areas where at least 15% of the area is covered by buildings with an average height exceeding 15 m (see Fig. 6.20);

2. Number and configuration of fans:
   • series I - one fan at different speeds,
   • series II – two fans arranged in a line at a distance of 250 cm at a fixed rotational speed by applying a voltage of 13.6 V;
3. The rotational speed of the fans working in the system, depending on the power supply and expressed in the voltage of the current supplied to the system:
   • speed 1 - 4 V power supply,
   • speed 2 - 5.6 V power supply,
   • speed 3 - 9.5 V power supply,
   • speed 4 - 13.6 V power supply.

All series of tests were carried out in a model scale of 1:833 (see Fig. 6.18). In Tab. 6.1. the completed series of tests of fans in a linear configuration are summarized.

Table 6.1. List of completed research cases - ventilation towers in a parallel configuration in rough terrain conditions

Series	**Fans configuration**	**Terrain category**	**Fan speeds (voltage)**
Series I	1 fan	(0), III, IV	4 V, 5.6 V, 9.5 V, 13.6 V
Series II	2 fans in spacing of 250 cm	(0), III, IV	13.6 V

a) b)

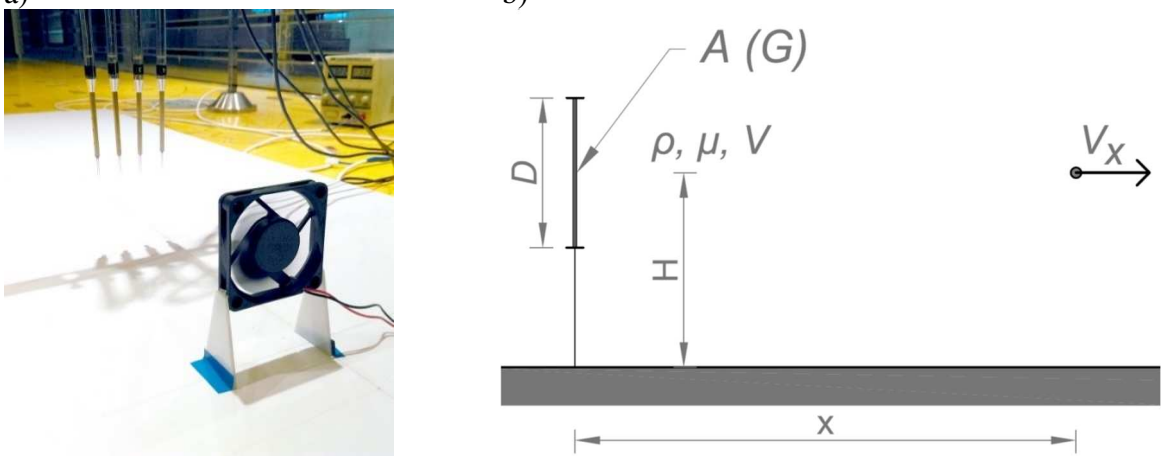

Fig. 6.18: Equivalent fan representing a ventilation tower in a model scale: a) view of the fan with hot-wire probes in the measurement space of the tunnel, b) schematic drawing with fan dimensions, where: where: ρ, μ, V – density, dynamic viscosity and velocity of the generated air stream, D – the height of the fan, H=6,6 cm – the height of the fan axis above the terrain, x – distance from the fan, V_x – air stream velocity at a distance x, G ˇ – set of dimensionless geometric parameters

a) b)

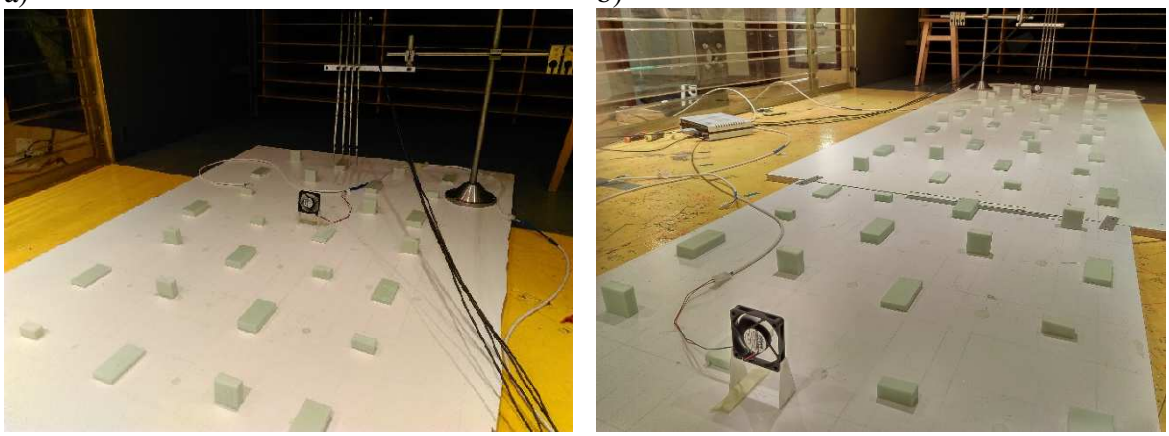

Fig. 6.19: The roughness model used in the tests - terrain category III: a) a single fan, b) two fans spaced 250 cm (Fot. Ł. Flaga)

a) b)

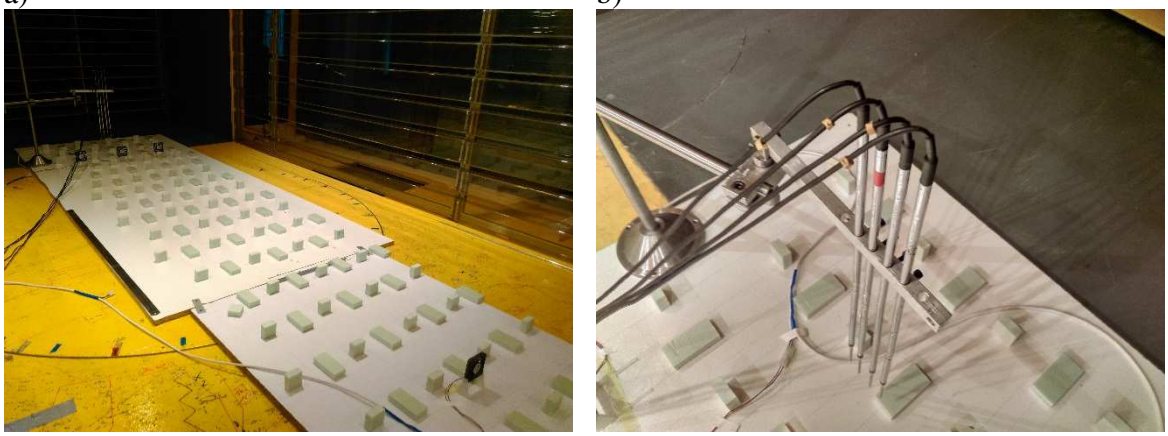

Fig. 6.20: Terrain roughness model used in the research - terrain category IV: a) general view, b) detail of the arrangement of measuring probes (Fot. Ł. Flaga)

6.7. The results of series I and II of stage III (the influence of terrain roughness)

For the first series of tests - one fan in rough terrain conditions (terrain category III and IV in accordance with PN-EN 1991-1-4 code) - Fig. 6.21-6.28 presents dimensionless air stream velocities related to the reference velocity (set at a distance of 10 cm in front of the fan) along the length (the length was related to the equivalent height of the ventilation tower H=66 mm). These graphs compare the dimensionless velocities for each probe obtained at a given roughness for different fan voltages. This allows us to determine the influence of the Reynolds number criterion on the studied phenomenon.

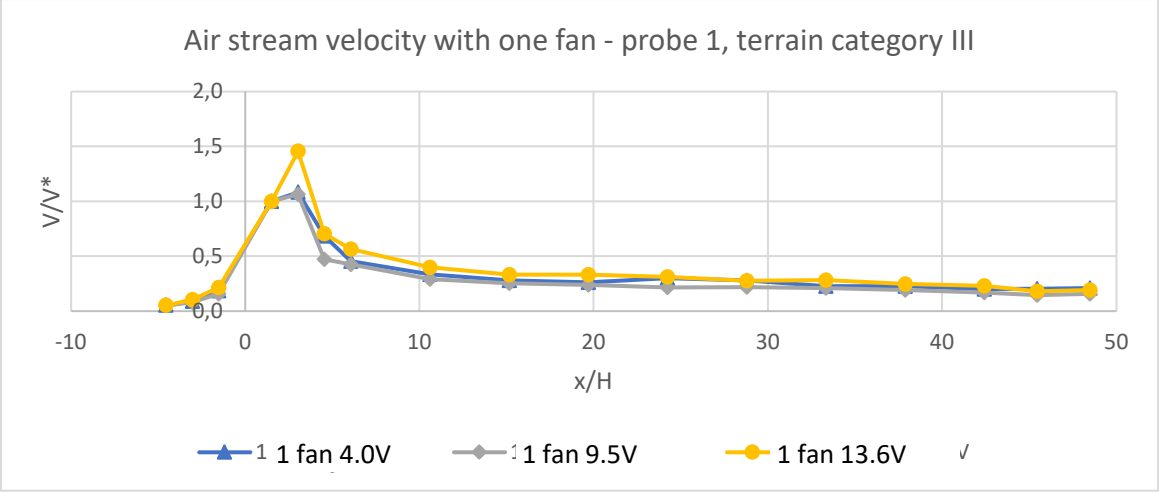

Fig. 6.21: Stream speed vs. reference speed and distance - series I (single fan), probe 1, terrain category III

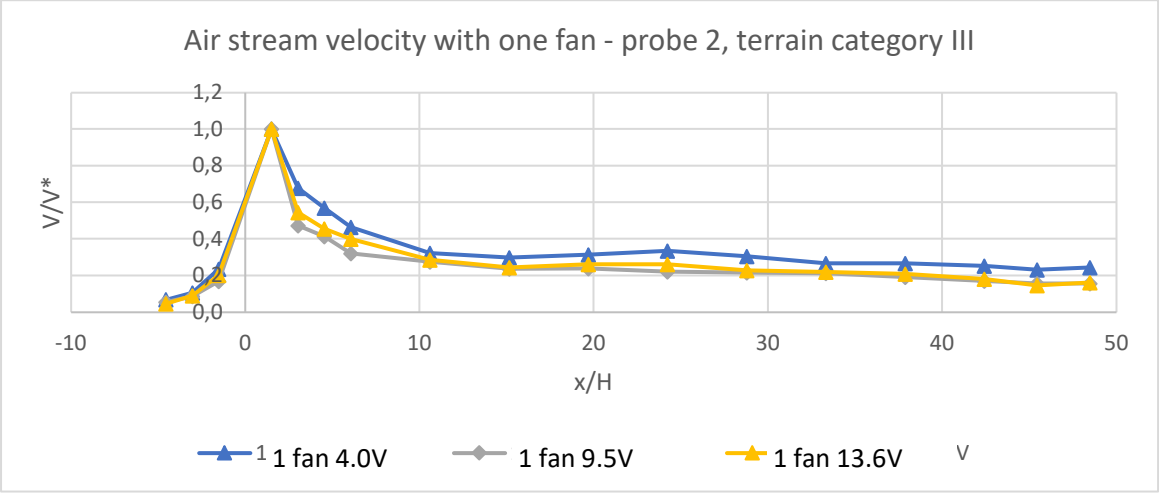

Fig. 6.22: Stream speed vs. reference speed and distance - series I (single fan), probe 2, terrain category III

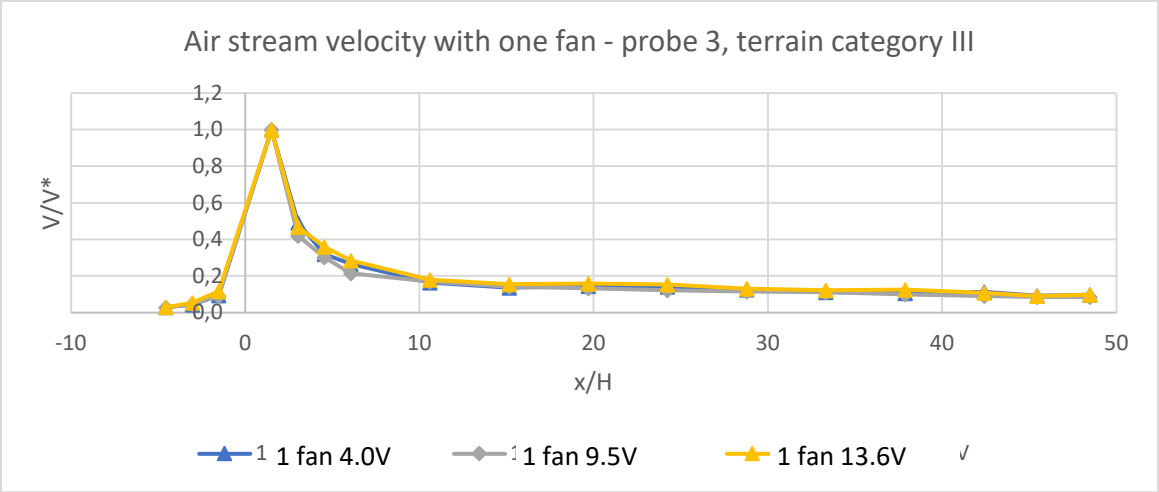

Fig. 6.23: Stream speed vs. reference speed and distance - series I (single fan), probe 3, terrain category III

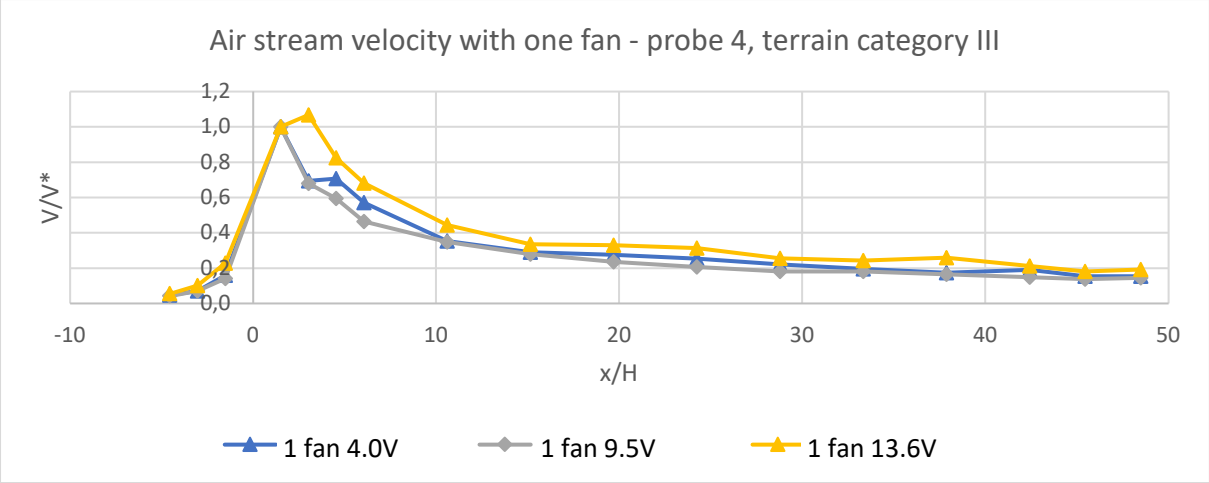

Fig. 6.24: Stream speed vs. reference speed and distance - series I (single fan), probe 4, terrain category III

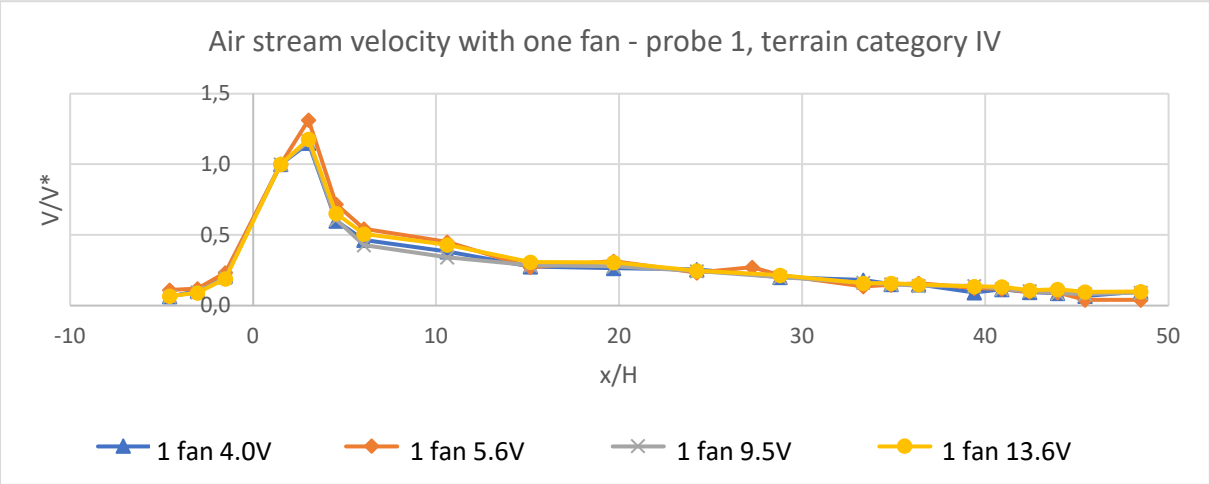

Fig. 6.25: Stream speed vs. reference speed and distance - series I (single fan), probe 1, terrain category IV

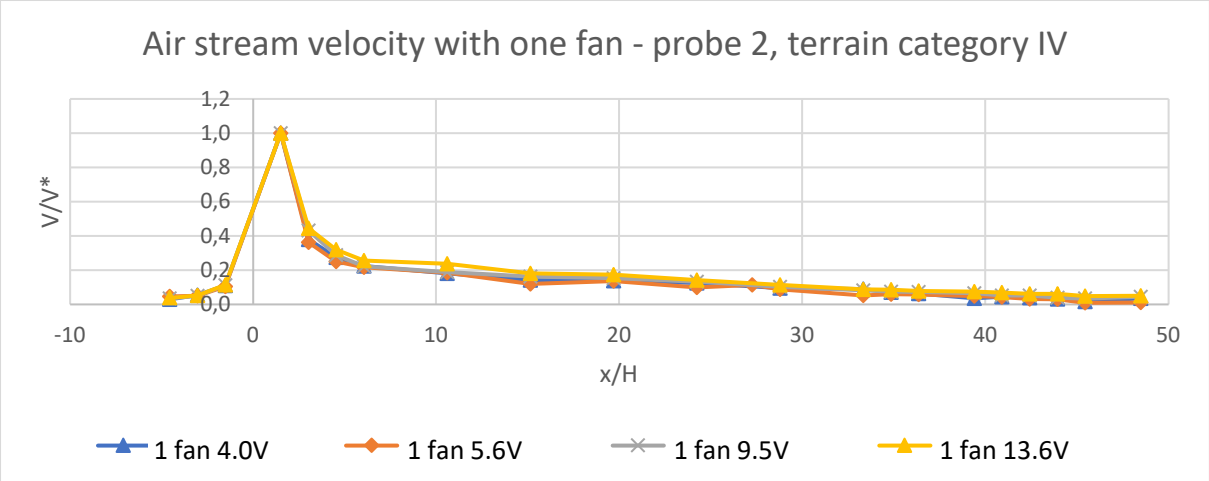

Fig. 6.26: Stream speed vs. reference speed and distance - series I (single fan), probe 2, terrain category IV

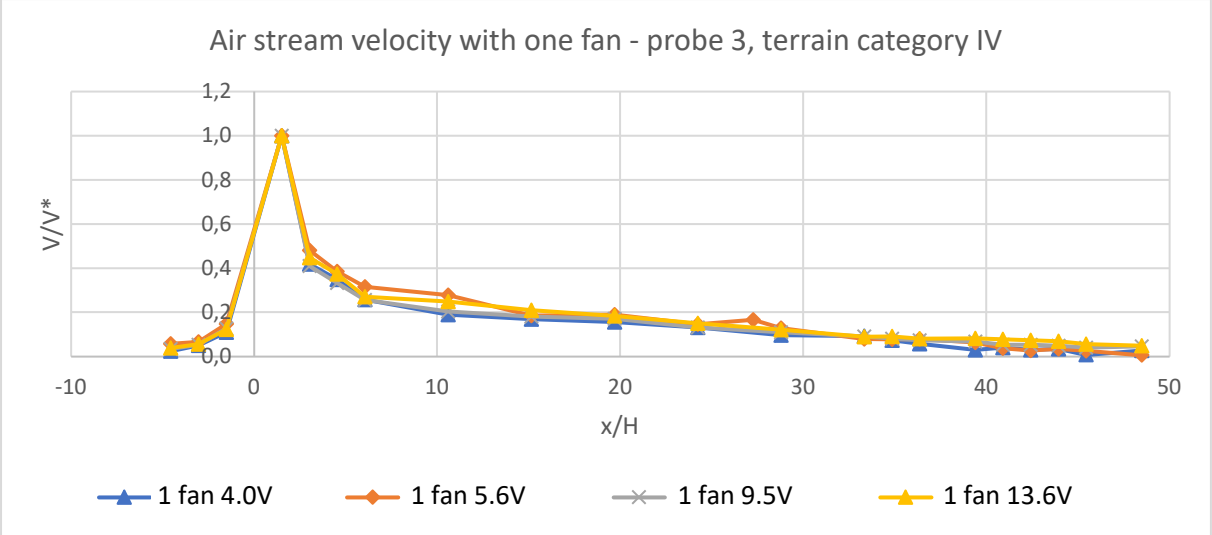

Fig. 6.27: Stream speed vs. reference speed and distance - series I (single fan), probe 3, terrain category IV

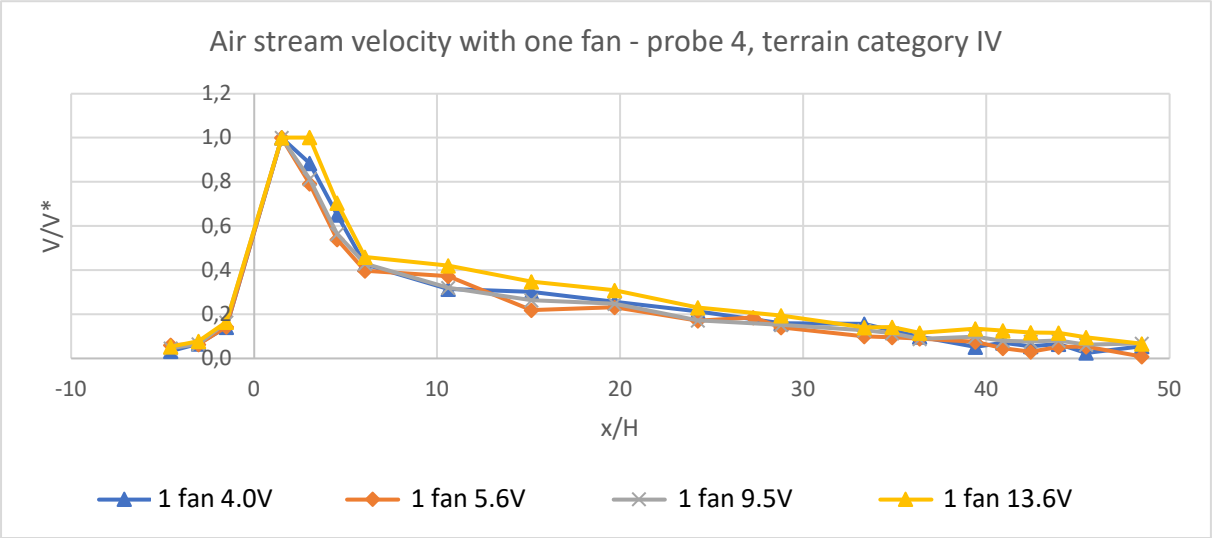

Fig. 6.28: Stream speed vs. reference speed and distance - series I (single fan), probe 4, terrain category IV

Fig. 6.29-6.32 shows the dimensionless velocity for each probe for three different terrain categories (category 0 - no roughness, and categories III and IV) at the voltage applied on the fans with a value of 13.6 V for the first series of tests.

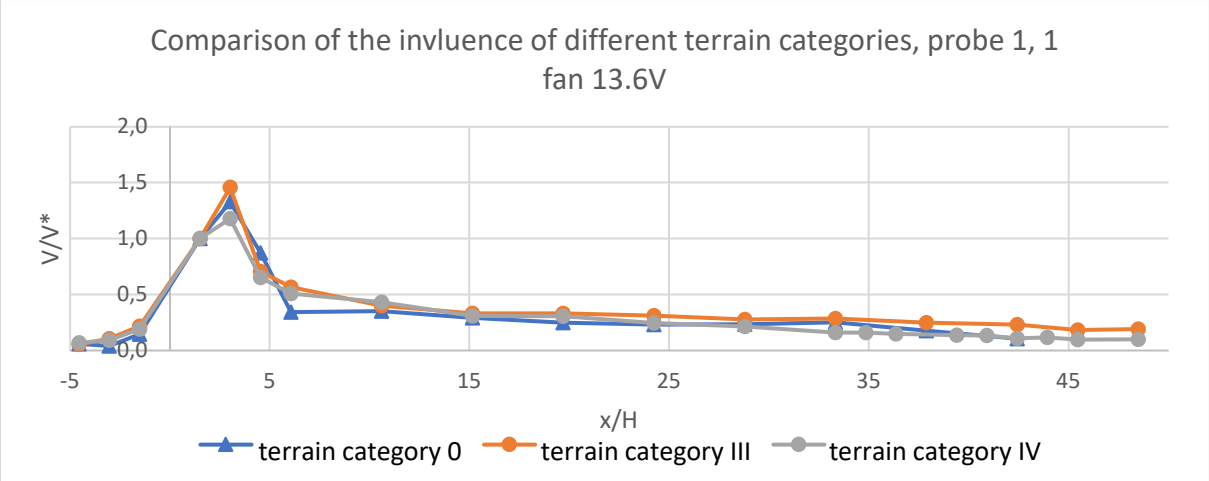

Fig. 6.29: Stream speed vs. reference speed and distance - Comparison of the effects of different terrain categories (surface roughness types) - Series I (single fan), Probe 1

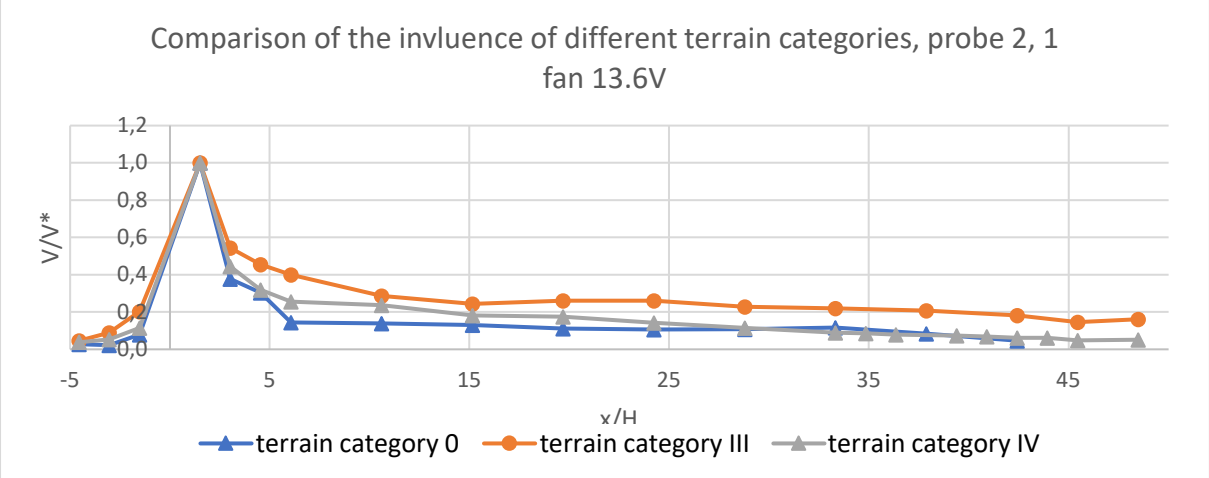

Fig. 6.30: Stream speed vs. reference speed and distance - comparison of the effects of different terrain categories (surface roughness types) - series I (single fan), probe 2

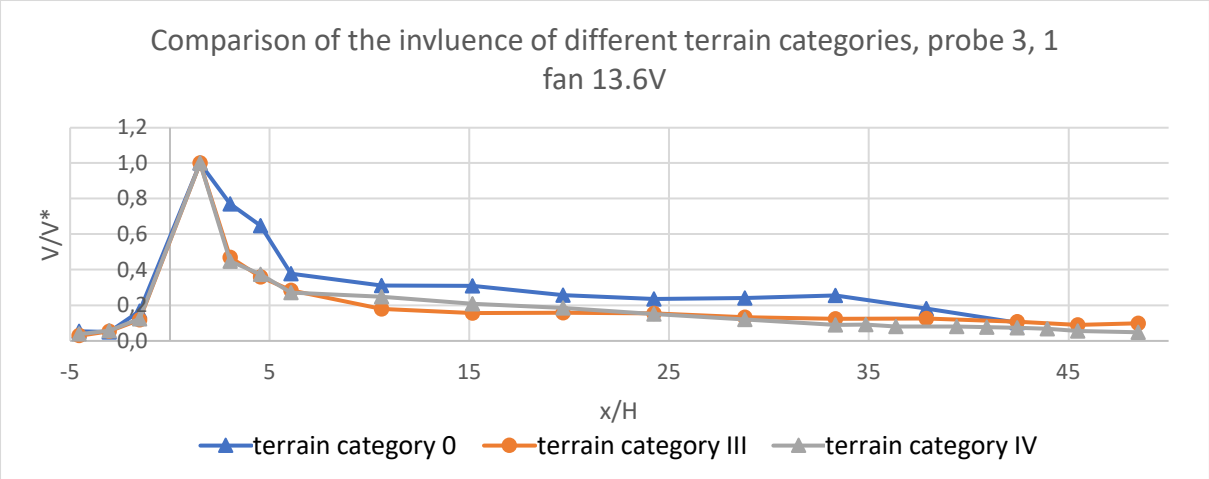

Fig. 6.31: Stream speed vs. reference speed and distance - comparison of the effects of different terrain categories (surface roughness types) - series I (single fan), probe 3

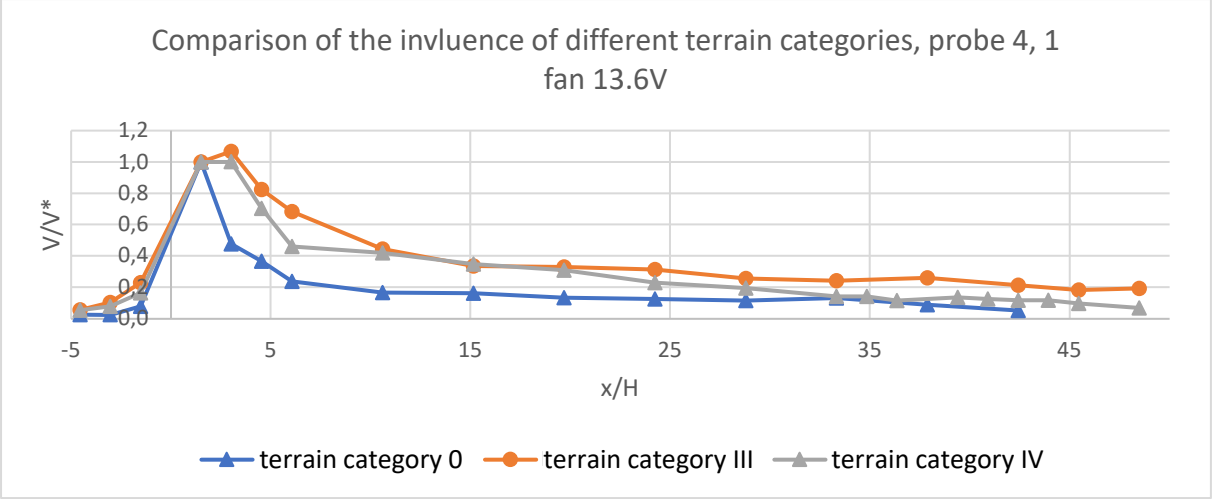

Fig. 6.32: Stream speed vs. reference speed and distance - comparison of the effects of different terrain categories (surface roughness types) - series I (single fan), probe 4

Fig. 6.33-6.35 show graphs of dimensionless velocity values simultaneously for all probes for each roughness category during series II (two fans positioned 250 cm apart).

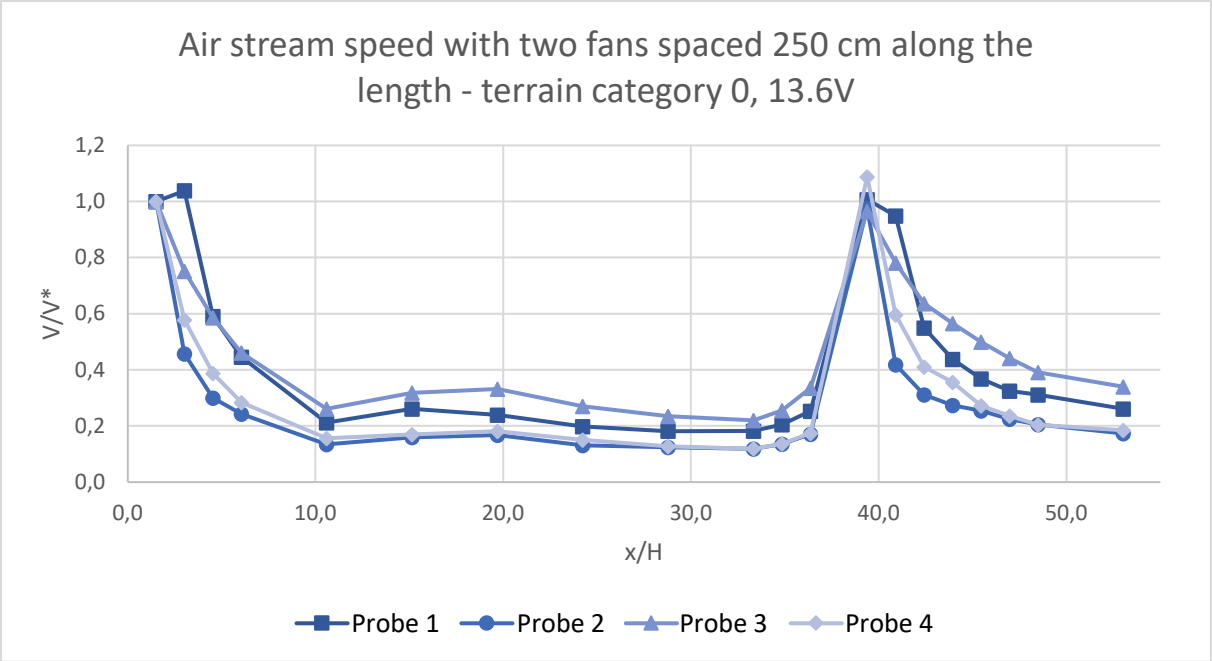

Fig. 6.33: Stream speed in relation to the reference speed depending on the distance - series II (two fans at a distance of 250 cm from each other), terrain category 0

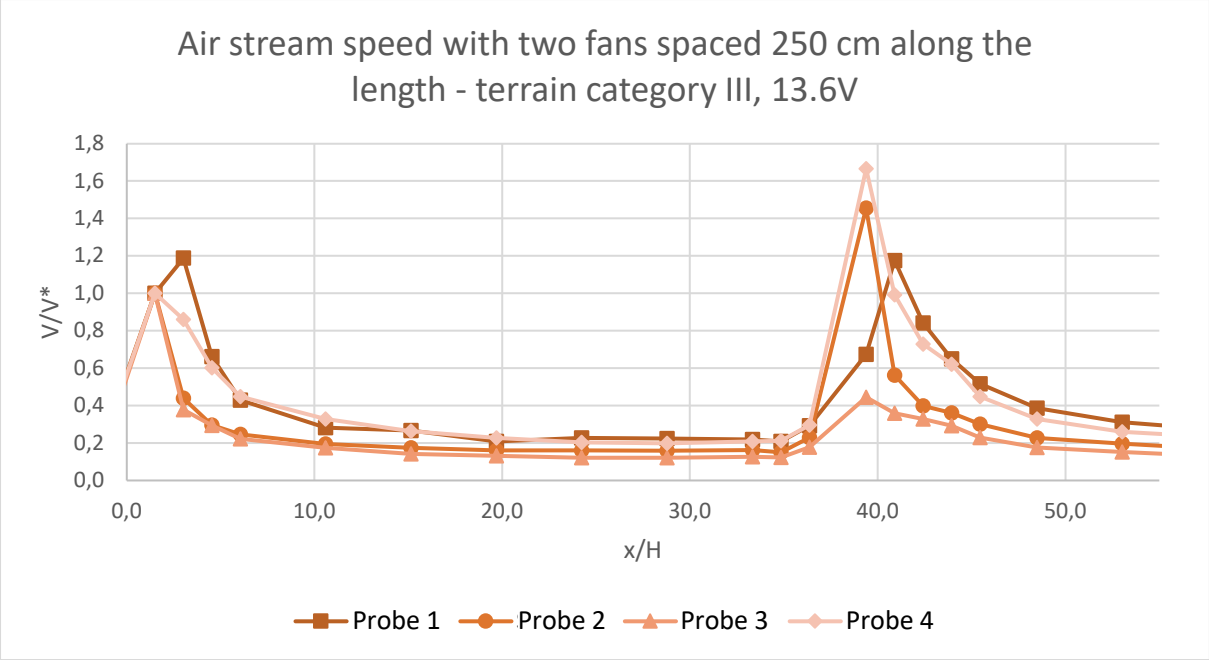

Fig. 6.34: Stream speed in relation to the reference speed depending on the distance - series II (two fans at a distance of 250 cm from each other), terrain category III

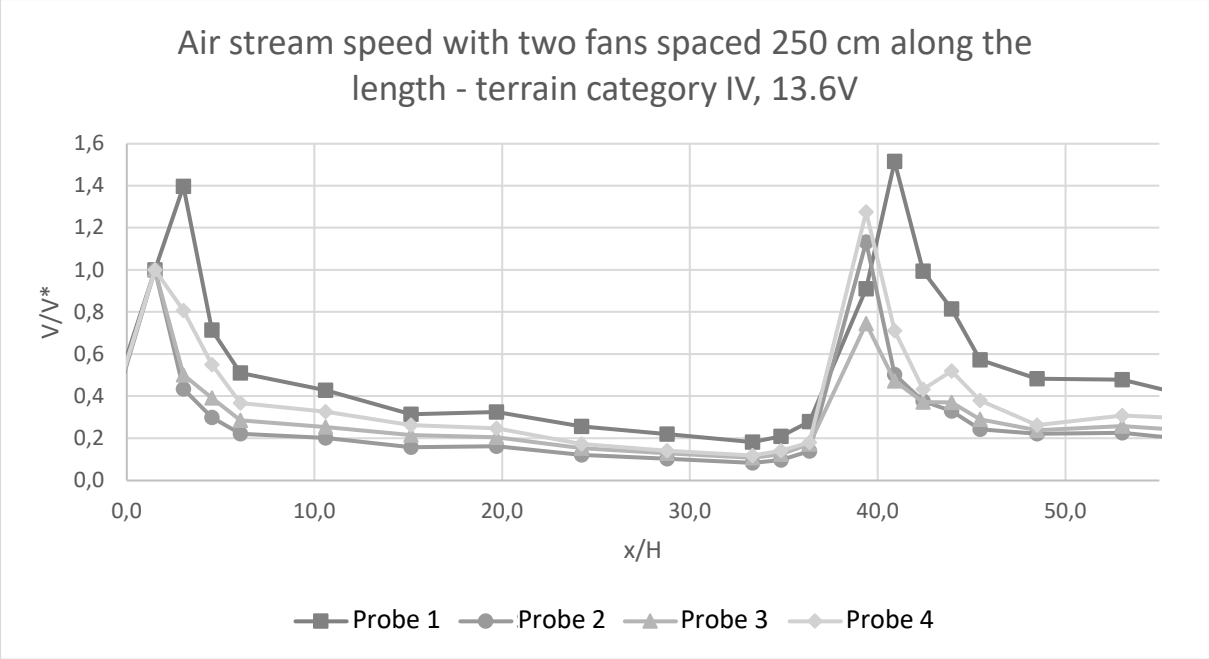

Fig. 6.35: Stream speed in relation to the reference speed depending on the distance - series II (two fans at a distance of 250 cm from each other), terrain category IV

Fig. 6.36-6.39 shows a comparison of the dimensionless velocity values for each of the probes for different terrain categories. This comparison allows us to determine the influence of the terrain roughness on the studied phenomenon.

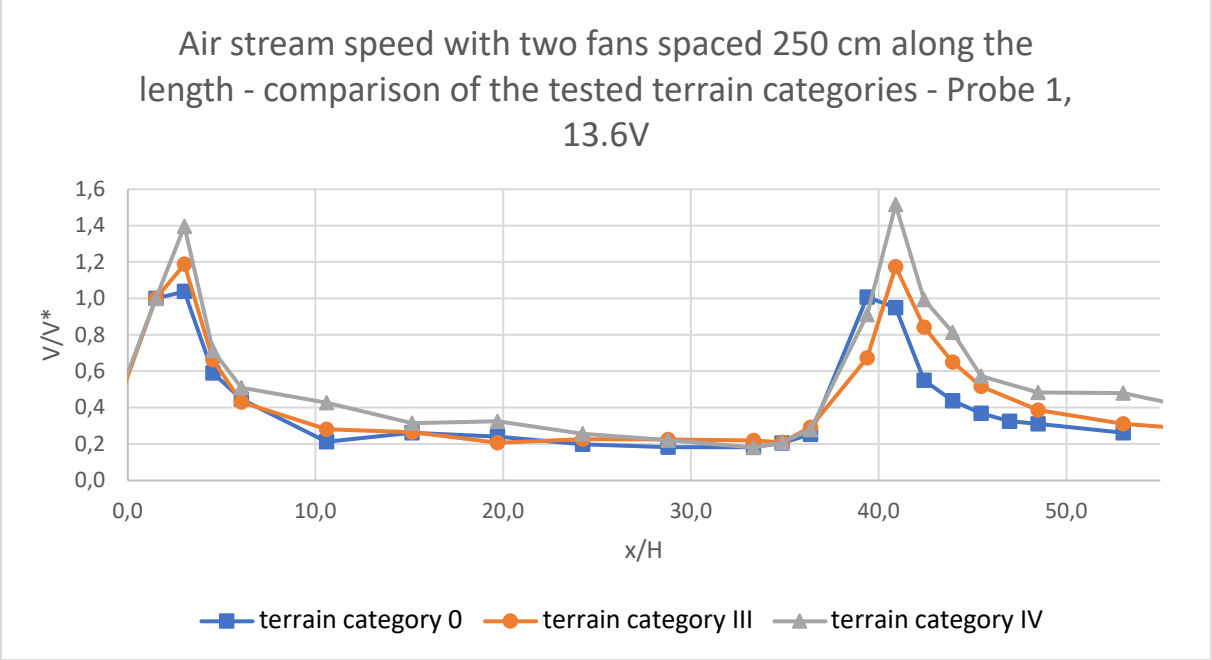

Fig. 6.36: Stream speed in relation to the reference speed depending on the distance - comparison of the influence of different terrain categories (surface roughness types) - series II (two fans 250 cm apart), probe 1

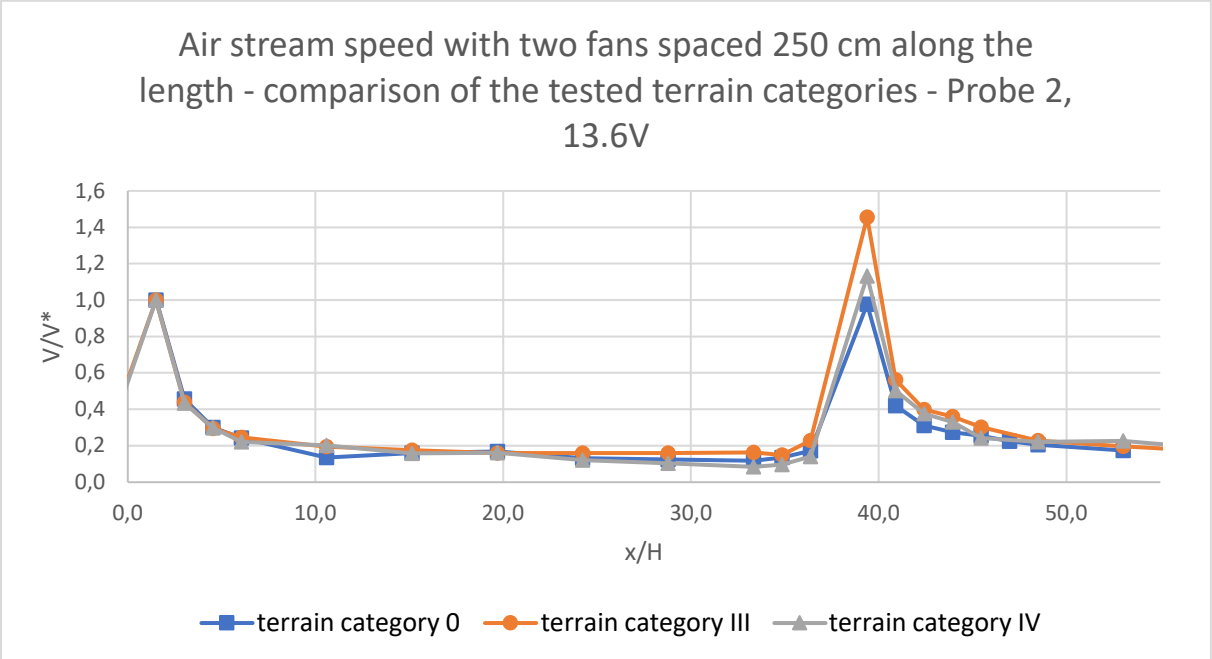

Fig. 6.37: Stream speed in relation to the reference speed depending on the distance - comparison of the influence of different terrain categories (surface roughness types) - series II (two fans 250 cm apart), probe 2

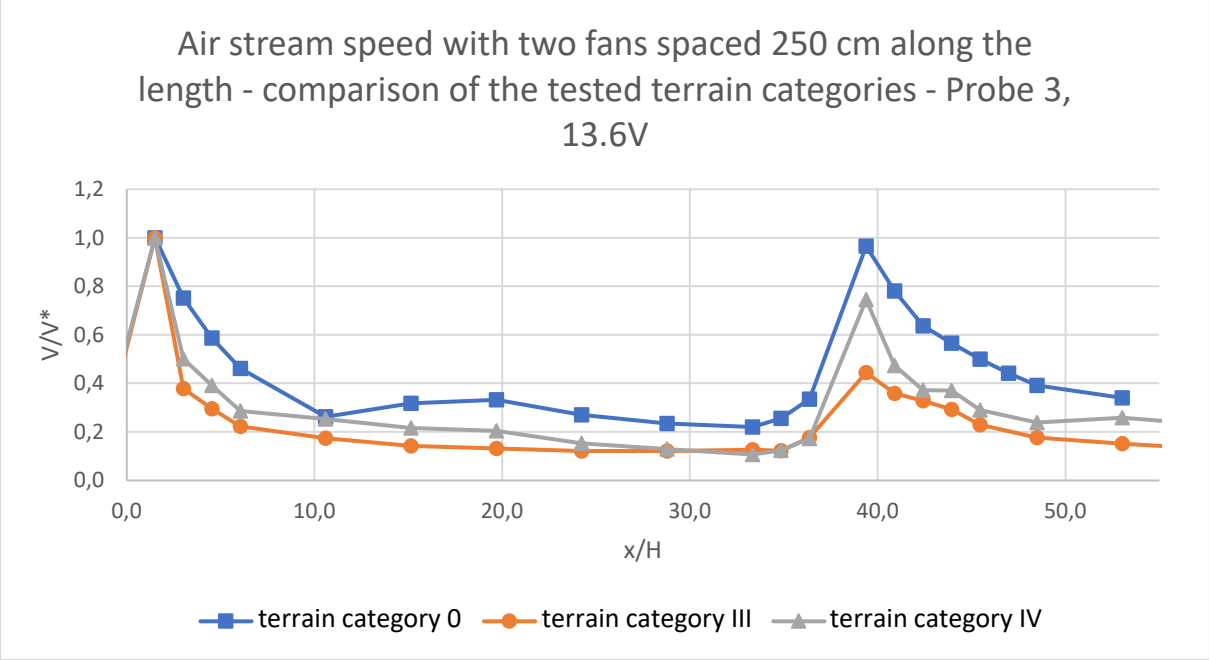

Fig. 6.38: Stream speed in relation to the reference speed depending on the distance - comparison of the influence of different terrain categories (surface roughness types) - series II (two fans 250 cm apart), probe 3

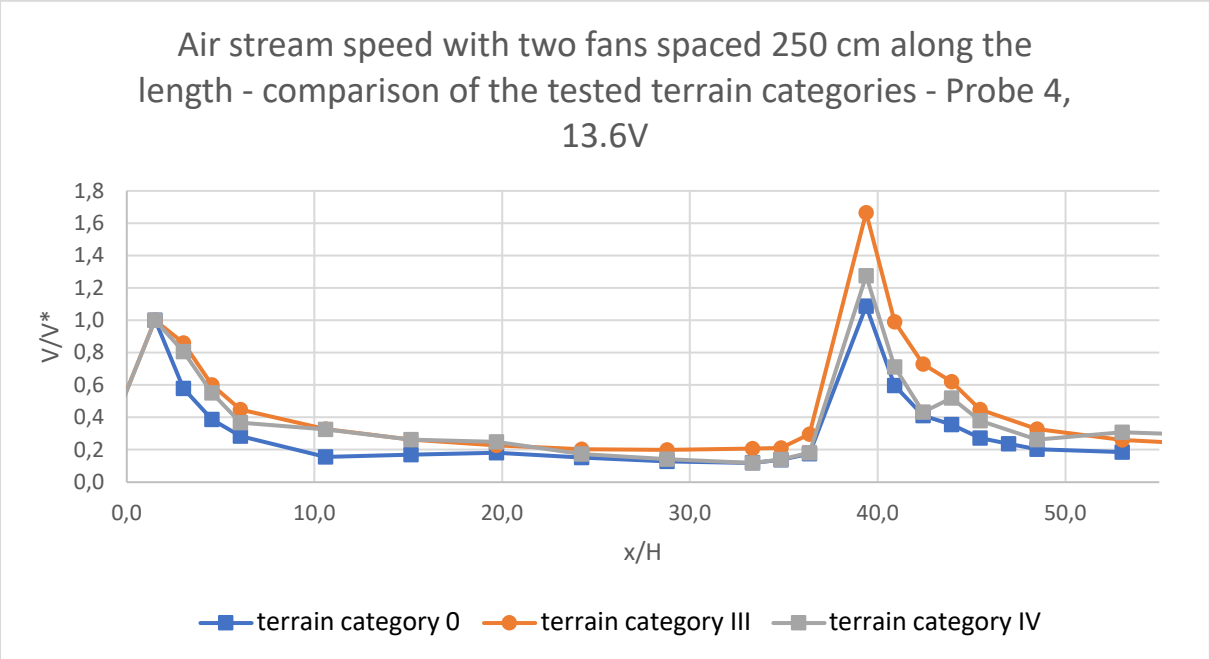

Fig. 6.39: Stream speed in relation to the reference speed depending on the distance - comparison of the influence of different terrain categories (surface roughness types) - series II (two fans 250 cm apart), probe 4

6.8. The analysis and conclusion of series I and II of stage III (the influence of terrain roughness)

Series I

The graphs presented in Fig. 6.11-6.18 indicate that the values of the dimensionless velocities generated by the fan along the length slightly differs from each other depending on the voltage applied to the fans, and thus - due to differences in the stream velocity. The greatest differences can be observed in the zone just in front of the fan, at a distance of about 30 cm, where there may be strong disturbances related to the movement of the fan itself.

Differences between dimensionless stream velocities depending on the type of terrain roughness are shown in Fig. 6.29-6.32. The main purpose of the conducted research was to determine whether the launch of the system over an area with a specific roughness - which better imitates the urban, urbanized area - will not drastically reduce the parameters of the air stream. The graphs show that the roughness causes a slight decrease in speed, while in the case of probes 2 and 4, the speed on smooth terrain is relatively lower than on rough terrain. The reason for this is probably a local increase in the air velocity caused by the measuring probe placed in the narrowing of modeling blocks.

Series II

Also in the case of a system consisting of two fans arranged in a line with a spacing of 250 cm, there was no significant decrease in the stream speed due to the roughness of the terrain. This is shown in Fig. 6.37-6.39. As in the case of the single fan, a local increase in velocity under rough terrain conditions is also observed here, possibly as a result of local flow restriction. For a detailed determination of the impact of the terrain roughness on the stream, it seems advisable to carry out a smoke visualization, which will allow us to observe the locally formed vortices and disturbances at the elements modeling the rough terrain.

7. MODEL OF VENTILATION CHIMNEY AND SIMILARITY CRITERIA[4]

Ventilation chimney with a concentric configuration of substitutive ventilation towers

The last element of the examined system is a ventilation chimney. For similarity analysis, it was considered a set consisting of a chimney, two rows of substitutive ventilation towers arranged concentrically around the chimney as well as a relevant section of the atmospheric boundary layer. Fig.7.1 shows the most important dimensional and dimensionless parameters of this set in its vertical plane. The whole set, marked as V, is divided into four subsystems I – IV. In addition, in Fig.7.1 there are marked vertical distributions of static pressure p, mass density ρ and absolute temperature T throughout the analyzed atmospheric boundary layer.

Ventilation towers which are a part of the set are arranged regularly around the chimney once every β angle. Towers located in the inlet row – round about the chimney – generate an air stream of velocity V_{wo}, whilst towers in the first row generate an air stream of velocity V_w.

[4] This chapter was written based on:

Report 4: Flaga A.: *Podstawowe zależności stosowanej mechaniki płynów dla komina wentylacyjnego*; Research Report, Wind Engineering Laboratory, Cracow University of Technology, Cracow 2017;

Flaga A.: *Dynamic action on atmospheric boundary layer as an effective method of improving the urban areas ventilation with similarity criteria of the problem*; Environmental Effects on Buildings and People: Actions, Influences, Interactions, Discomfort, EEBP VIII, Cracow-Lublin 2018, Poland

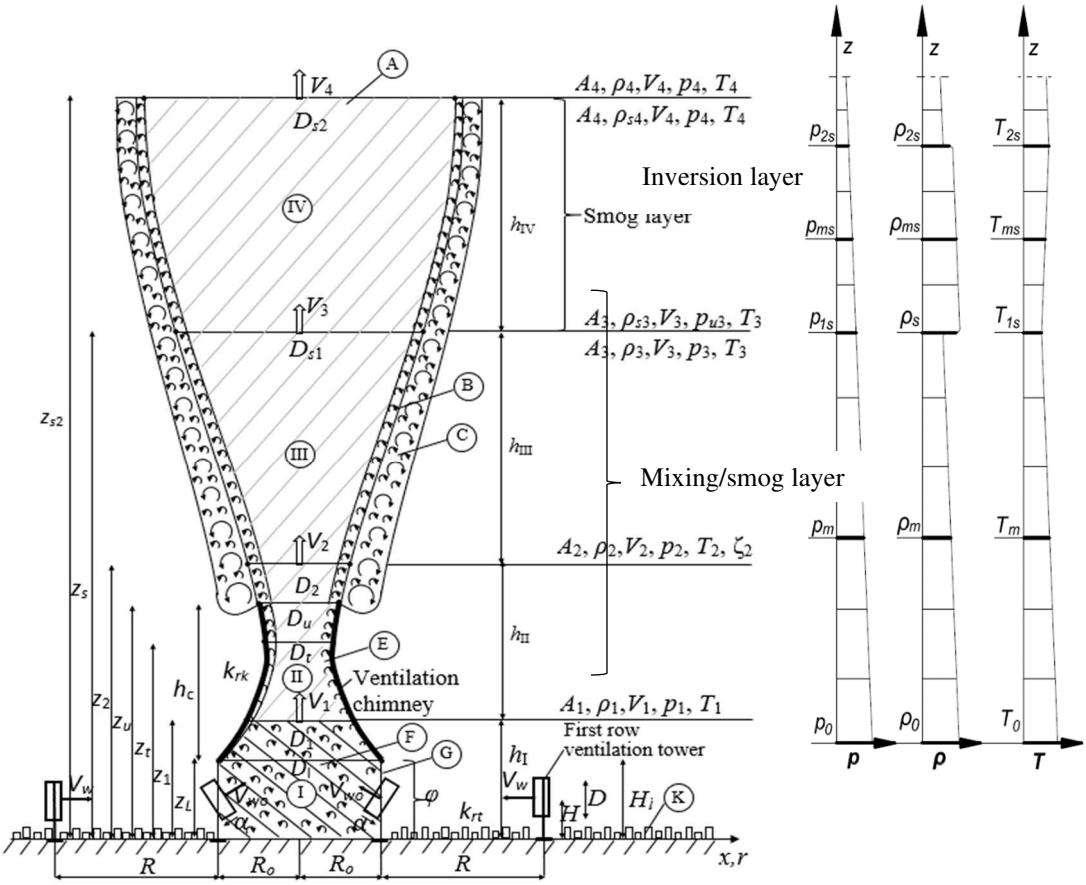

Fig.7.1. Sketch of a set consisting of a ventilation chimney, substitutive ventilation towers as well as a relevant section of the atmospheric boundary layer with marked vertical distribution of static pressure p, mass density ρ and absolute temperature T; A – core of air stream with dominant component V of flow velocity; B – contact boundary/shear layer of stream core (area of turbulent flow with small scale vortexes); C – strongly turbulent mixing area with vortexes of smaller and larger scale; E – ventilation chimney boundary/shear layer of the mean height of inner surface roughness k_{rc}; F – a strongly turbulent inlet of mixing area with vortexes of smaller and larger scale; G – inlet wall of ventilation chimney with permeability coefficient φ; K – rough terrain with a mean height of surface roughness k_{rt} (Flaga 2018).

Now, taking into account the most important geometric, kinematic and physical quantities of the presented set, let us carry out the analysis of similarity criteria for the particular subsystems I-IV and the whole system V (Flaga, 2017).

Subsystem I:

$$V_1 = F_I\left(V_w, V_{w0}, \rho_H, p_H, C_p, T_H, \nu_H; H, D, H_w, z_1, D_1, R, R_0, \alpha, \beta; \varphi, \zeta_2; k_{rt}\right), \tag{7.1}$$

where: V_1 – mean velocity of air stream in the ventilation chimney on the level z_1 (i.e. near the ventilation chimney inlet); V_w – mean air velocity on the outlet of each first order ventilators; V_{w0} – mean air velocity on the inlet of each inlet ventilators (i.e. zero row

ventilators); ρ_H – air mass density (on the H level) ($\rho_H \cong 1{,}225$ kg/m^3 at $p_H = 1013$ Pa and $T = 289$ K); p_H – atmospheric static pressure; C_p – specific heat at constant pressure; T_H – absolute temperature; ν_H – air kinematic viscosity; H, D, H_w – geometric parameters of the substitutive ventilation towers (respective heights); α – inclination angle of the substitutive inlet ventilators (in radians); $R, R_0, \beta = \frac{2\pi}{n_\beta}$ – geometric parameters of the radial locations of the substitutive ventilation towers (n_β – number of towers in a row); φ – permeability of the inlet wall corresponding to the substitutive inlet ventilation towers defined as: $\varphi = \frac{A_{free,inlet}}{A_{total,inlet}}$ (where: $A_{free,inlet}$ and $A_{total,inlet}$ are respective inlet wall areas); k_{rt} – mean irregularities height of the terrain roughness; ζ_2 – coefficient of local losses due to the end of the ventilation chimney.

Assuming the dimensional base for the subsystem I as (V_w, ρ_H, H) and using the Π theorem of the dimensional analysis, the following dimensionless functional relationship can be written:

$$\frac{V_1}{V_w} = \breve{F}_I\left(\frac{V_{w0}}{V_w}, \pi_{pI}, \pi_{T,I}, Re_I; \frac{D}{H}, \frac{H_w}{H}, \frac{z_1}{H}, \frac{D_1}{H}, \frac{R}{H}, \frac{R_0}{H}, \alpha, \beta; \varphi, \zeta_2; \frac{k_{rt}}{H}\right), \tag{7.2}$$

where: $\pi_{pI} = \frac{p_H}{\rho_H V_w^2}$; $\pi_{T,I} = \frac{C_p T_H}{V_w^2}$; $Re_I = \frac{V_w H}{\nu_H}$ (Reynolds number). All dimensionless quantities appearing in the above relationship are the similarity numbers of the subsystem I. Fulfillment of these similarity criteria in model tests – excluding Reynolds number Re_I – is possible and simple. Reynolds number Re_I influences vortexes dimensions in mixing area F (comp. Fig.7.1) in subsystem I and hence the size of this area. It indirectly affects D_1 parameter of the area I. From the continuity equation of air flow in the area I it results that the change in mean velocity V_1 at the outlet of this area depends on the change in D_1 parameter. So, the hypothesis can be assumed, that influence of Reynolds number Re_I on V_1 is a secondary issue. However, validation in this matter is needed based on measurement results which should be conducted in two different model scales differing at least in one order of magnitude.

Subsystem II:

$$V_2 = F_{II}(V_1, \rho_1, p_1, e_1, \Delta e_{II}, \nu_{II}; D_1, D_t, D_u, D_e, z_1, z_t, h_c, z_e; k_{rc}), \tag{7.3}$$

where: V_2 – mean air stream velocity corresponding to the width D_e at the height z_e; $V_1, \rho_1, p_1, \nu_{II}$ – similarly as before; $D_1, D_t, D_u, D_e, z_1, z_t, h_c, z_e$ – geometric parameters of the ventilation chimney; k_{rc} – mean irregularities height of the chimney roughness; $e_1, \Delta e_{II}$ – quantities connected with respective pressures, gravitational energies and inner energies (per unit mass of air) defined as follows:

$$e_1 = \frac{p_1}{\rho_1} + gz_1 + C_\Omega T_1 = RT_1 + gz_1 + C_\Omega T_1 = C_p T_1 + gz_1 \cong C_p T_1, \tag{7.4}$$

$$\Delta e_{II} = e_1 - e_2 = \left(\frac{p_1}{\rho_1} - \frac{p_2}{\rho_2}\right) + g(z_2 - z_1) + C_p(T_1 - T_2) \cong C_p(T_1 - T_2). \tag{7.5}$$

Assuming in this case the dimensional base as (V_1, ρ_1, h_c), one can write:

$$\frac{V_2}{V_1} = \breve{F}_{II}\left(\pi_{p1}, \pi_{T1}, \pi_{\Delta T,II}, Re_{II}; \frac{D_1}{h_c}, \frac{D_t}{h_c}, \frac{D_u}{h_c}, \frac{D_e}{h_c}, \frac{z_1}{h_c}, \frac{z_t}{h_c}, \frac{z_e}{h_c}; \frac{k_{rc}}{h_c}\right), \tag{7.6}$$

where: $\pi_{p1} = \frac{p_1}{\rho_1 V_1^2}$; $\pi_{T1} \cong \frac{C_p T_1}{V_1^2}$; $\pi_{\Delta T,II} \cong \frac{C_p(T_1 - T_2)}{V_1^2}$ $Re_{II} = \frac{V_1 h_c}{\nu_{II}}$.

Comparing similarity numbers for model test in smaller scale (subscript M) with these in natural scale (subscript P) and taking into account that atmospheric air is in usual conditions, it is obtained that: $(T_1 - T_2)_P \neq 0 = (T_1 - T_2)_M$; $(h_c)_P \neq (h_c)_M$. Thus, two similarity numbers – $\pi_{\Delta T,II}$ and Re_{II} – will not be fulfilled. It was shown in (Flaga, 2017) that Reynolds number Re_{II} has negligible importance, however, it is also necessary to prove it experimentally. Fulfillment of the number $\pi_{\Delta TII}$ (the number of significant importance) is artificially possible with quite good approximation if the air layer h_{II} will be divided into smaller layers of thicknesses Δh_i, density ρ and temperature differences ΔT_i and grid with orthogonal wires electrically heated will be added for every layer, according to the relationship: $C_p \Delta T_i = \frac{\Delta \dot{q}_i}{\rho \Delta h_i}$, where: $\Delta \dot{q}_i$ – density of heat stream generated by one mesh net. The grids should be placed one above one both inside the ventilation chimney and in contact air area outside the chimney.

Subsystem III:

$$V_3 = F_{III}(V_2, \rho_2, p_2, e_2, \Delta e_{III}, \nu_{III}; D_2, h_{III}), \tag{7.7}$$

Assuming dimensional base as (V_2, ρ_2, h_{III}) the following dimensionless quantities will be obtained:

$$\frac{V_3}{V_2} = \breve{F}_{III}\left(\pi_{p2}, \pi_{T2}, \pi_{\Delta T,III}, Re_{III}; \frac{D_2}{h_{III}}\right) \tag{7.8}$$

Definitions of criterial numbers and problems with their fulfillment in layer of thickness h_{III} are similar to these in layer of thickness h_{II}. However, it is necessary to validate experimentally the influence of Reynolds number Re_{III} on the velocities ratio $\frac{V_3}{V_2}$. Reynolds number Re_{III} has an influence on vortexes dimensions in the mixing area C (comp. Fig.7.1) and hence, on the size of this area. Then, it has an indirect effect on the width of the stream core, which is characterized by the parameter D_2. Based on the continuity equation, a change in the parameter D_2 influence the value of mean velocity V_3. It is assessed that the influence of Reynolds number Re_{III} on velocities ratio $\frac{V_3}{V_2}$ will be of secondary importance.

Subsystem IV:

$$\frac{V_4}{V_3} = \breve{F}_{IV}\left(\pi_{p3}, \pi_{T3}, \pi_{\Delta T,IV}, Re_{IV}; \frac{D_3}{h_{IV}}\right), \tag{7.9}$$

where: $\pi_{p3} = \frac{p_3}{\rho_{s1} V_3^2}$; $\pi_{T3} \cong \frac{C_{ps} T_3}{V_3^2}$; $\pi_{\Delta T,IV} \cong \frac{C_{ps}(T_3 - T_4)}{V_3^2}$ $Re_{IV} = \frac{V_3 h_{IV}}{\nu_s}$ as well as it is assumed that: $\rho_s \neq \rho$, $\nu_s \neq \nu$ and $C_{ps} \neq C_p$.

Remark concerning unfulfillment of Reynolds number Re_{IV} is similar to before (in the case of Re_{III}). In terms of the other criterial numbers, in (Flaga, 2017) it was shown the way of artificially substituting the smog layer by the system of additional multiple grids/ beehive frames placed one above the other. This results in dimensionless pressure losses in model tests in such a way that they are equivalent to dimensionless pressure losses generated by the smog layer in nature.

Whole system V:

$$\frac{V_4}{V_w} = \breve{F}_V(\dots, \pi_i, \dots) \tag{7.10}$$

where: $(\dots, \pi_i, \dots)$ – the set of similarity numbers π_i from all subsystems I-IV.

8. TESTS OF VERTICAL VENTILATION CHIMNEYS

8.1. Model description and experiment setup of stage II

Stage II

The purpose of the second stage of model tests was to measure the air flow velocity field in the proximity of the system of ventilation towers in the concentric configuration with a central ventilation chimney and specify the effective range of the vertical air flow generated by the system of ventilation towers and the chimney. The model tests in the scale of 1:833 included 8 series that differ by: the shape of the ventilation chimney, the inclination of the fans that model the ventilation towers (perpendicular to the bottom of the chimney or inclined 47 degrees from vertical direction), and permeability of the inlet wall (i.e. different types of closure of the space between ventilation towers: no fence, fences between the base construction of fans, full fences between the ventilation towers). These variants are presented in Fig.8.1. and Tab. 8.1.

Table 8.1. List of completed research cases

Series	Shape	Location of the fans	Aeration
S1	A	I	1
S2	B	I	1
S3	A	II	1
S4	B	II	1
S5	A	II	2
S6	B	II	2
S7	A	II	3
S8	B	II	3

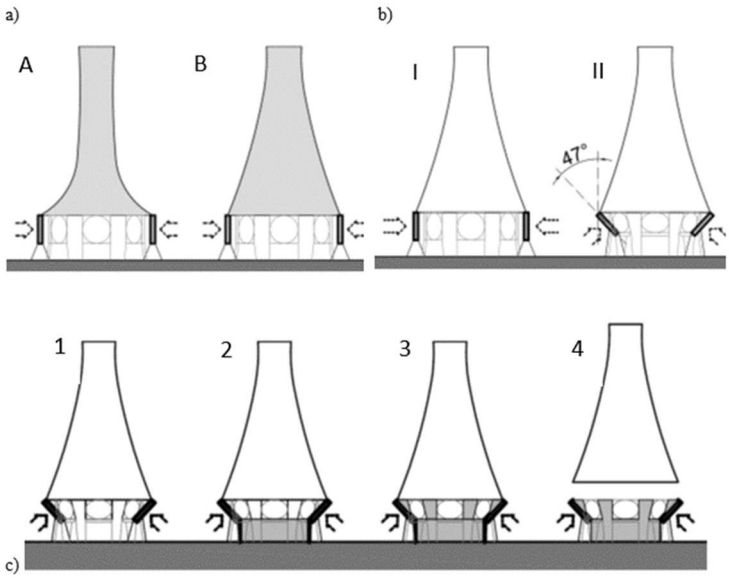

Fig. 8.1. Variants of the system used in tests (stage II): a) shapes of the ventilation chimney, type A and B; b) angle set-up of the fans, type I and II; c) permeability of the system type 1, 2, 3 and 4

The shape of the ventilation chimneys was adopted based on a study of the literature. The basic dimensions of the chimney-fan ring ventilation system are shown in Fig. 8.2, and their view in Fig. 8.3.

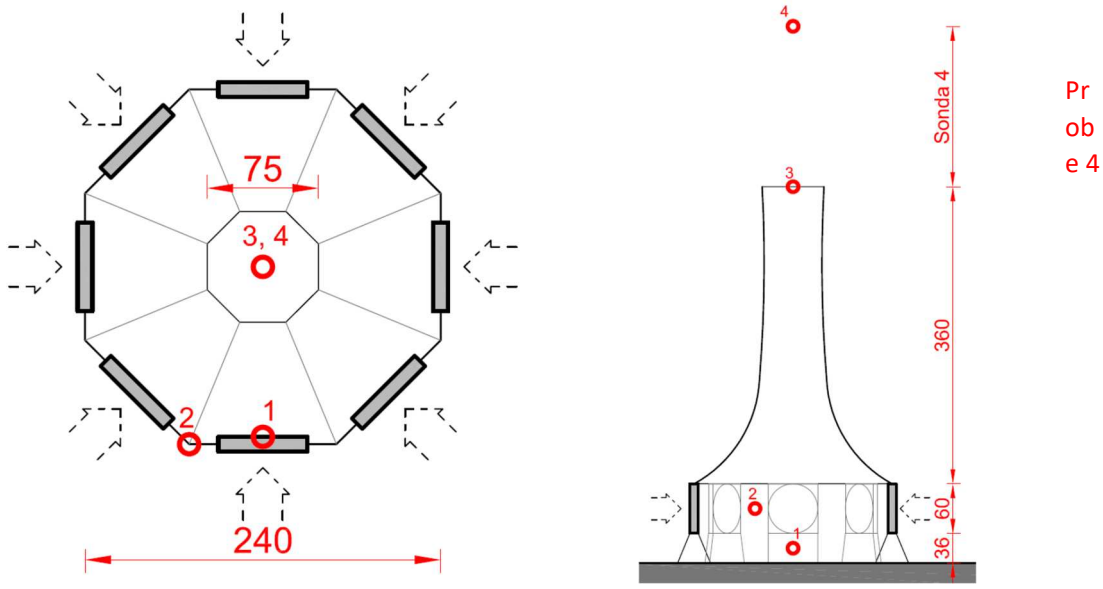

Fig. 8.2. Schematic drawing presenting the basic dimensions of the chimney-fan ring ventilation system.

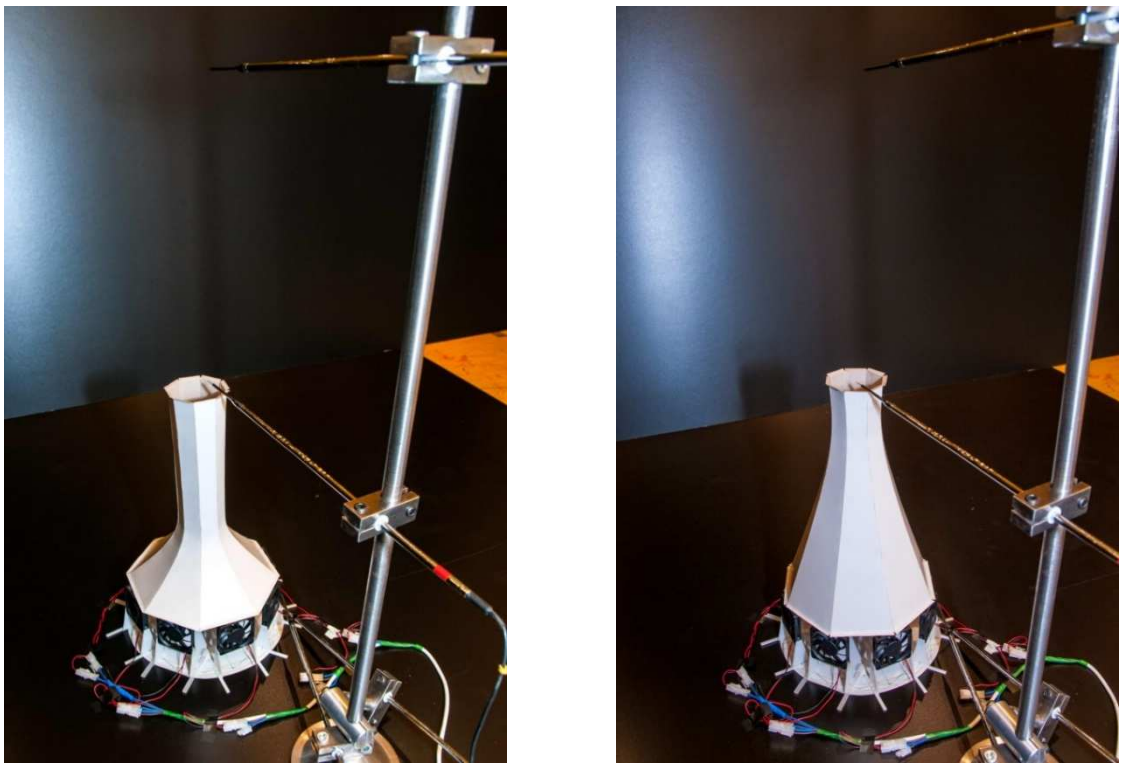

Fig. 8.3. View of ventilation chimneys during tests in the measuring space of the wind tunnel; type A and type B respectively.

In all research stages (I-III) the same fans were used. The fans were powered by a stabilized DC power supply. Speed regulation was carried out by voltage regulation.

In Fig. 8.5. and 8.6. the realized configurations of fans and various aeration of the ring fan arrangement are shown.

a) b)

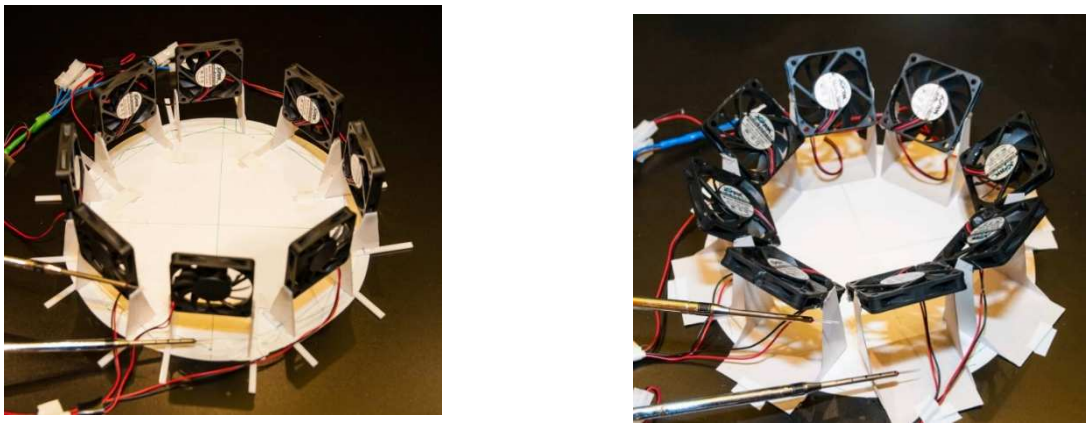

Fig. 8.5. View of the fan configuration at the base of the ventilation chimneys, configuration I and II respectively (description in the text) (Fot. Ł. Flaga)

a) b)

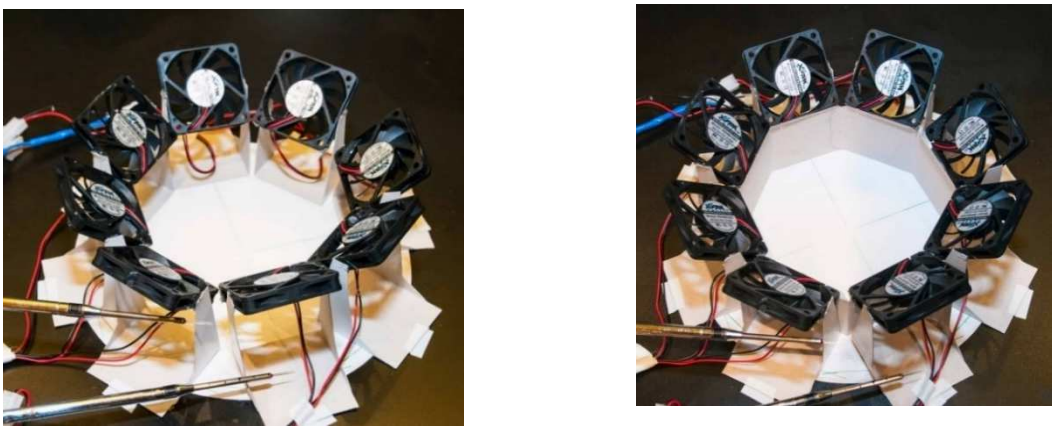

c)

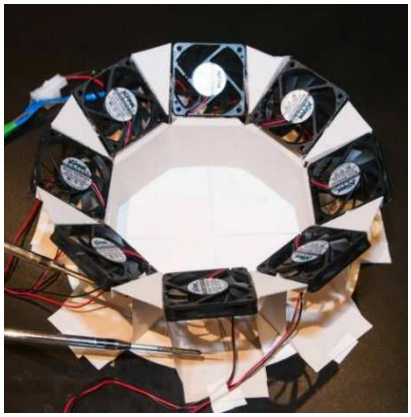

Fig. 8.6. View of the airflow of the ring fan system at the base of the ventilation chimney, type 1, 2 and 3, respectively (description in the text) (Fot. Ł. Flaga)

During the model tests, it was recognized that adding the ventilation chimney vastly increases the efficiency of the generated stream. It is especially observed for outlet velocity of air above the ventilation chimney that is in the range of effect of the system (i.e. over the chimney by 10 times the diameter of the chimney in the widest part). It is important that the kinetic energy of moving air flow is meant to break the resistance of the smog layer and move above it.

In Fig. 8.7. Selected sources of the ventilation signal obtained as part of smoke visualization studies were obtained.

a) b) c)

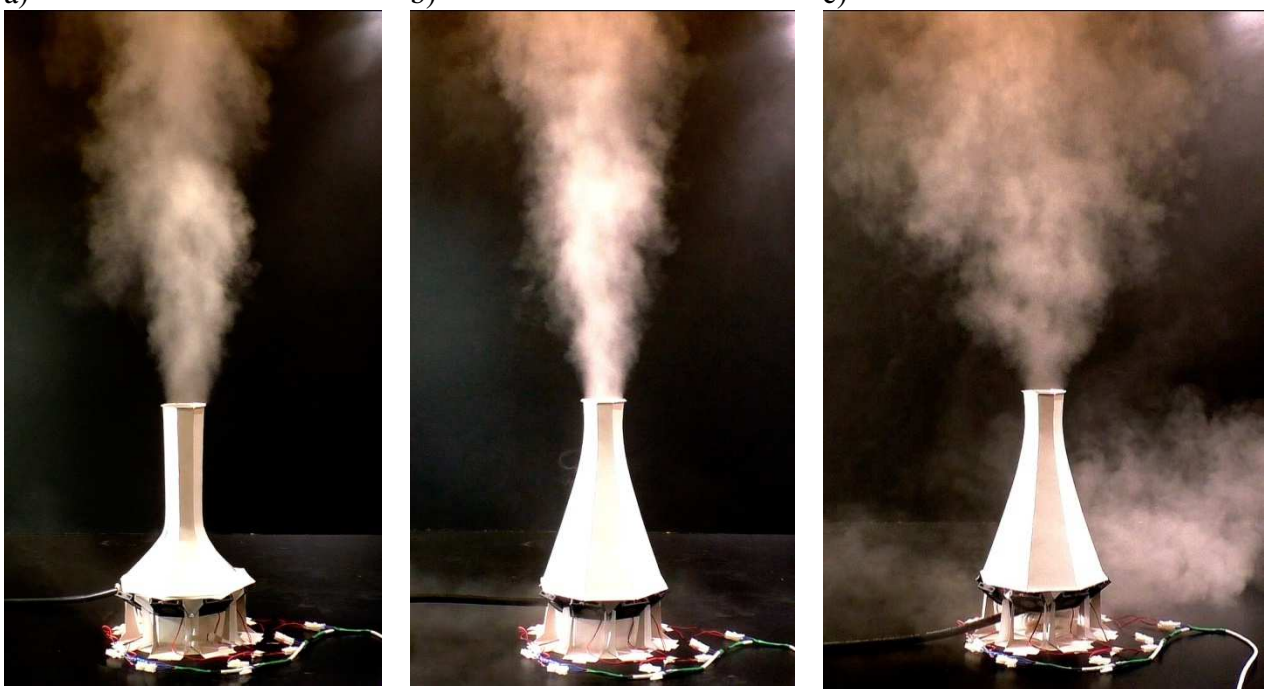

Fig. 8.7. Smoke visualization of chosen system set-ups used in tests showing the efficiency of the proposed solution: a) chimney shape A, closed space between fans -series S7; b) chimney shape B, closed space between fans where the optimal smoke cone is generated above the chimney – series S8; c) chimney shape B, open space between fans, a large spread of the smoke at the outside of the chimney – series S6

It was also determined that the chosen configuration of ventilation towers (shape B, inclination II, permeability 3) generates a relatively strong and wide stream. Based on this observation it was decided that the following stages of model tests should include additional configurations (different angles of inclination) of inlet fans allowing to achieve the velocity and range of the vertical stream at a satisfactory level even without the ventilation chimney or with ventilation chimneys of different shape, height and level of elevation above the ventilation towers. Smoke visualization, showing the efficiency of selected solutions is presented in Fig.10. What is important, such an effect of generating a high air stream can be achieved also in nature which confirms the photo shown in Fig.8.9.

Fig. 8.9. Photo of the flow field velocity above the cooling tower and chimney - power plant in Cracow (Fot. R. Kłaput).

8.2. Test results of stage II

Fig. 8.10-8.15. shows a comparison of dimensionless air velocities obtained in tests depending on the voltage (4V, 6V, 9V, 12V, and 13.6V) applied to the fans for the S1-S8 test series. The reference point was taken at the location of probe No. 3.

a)

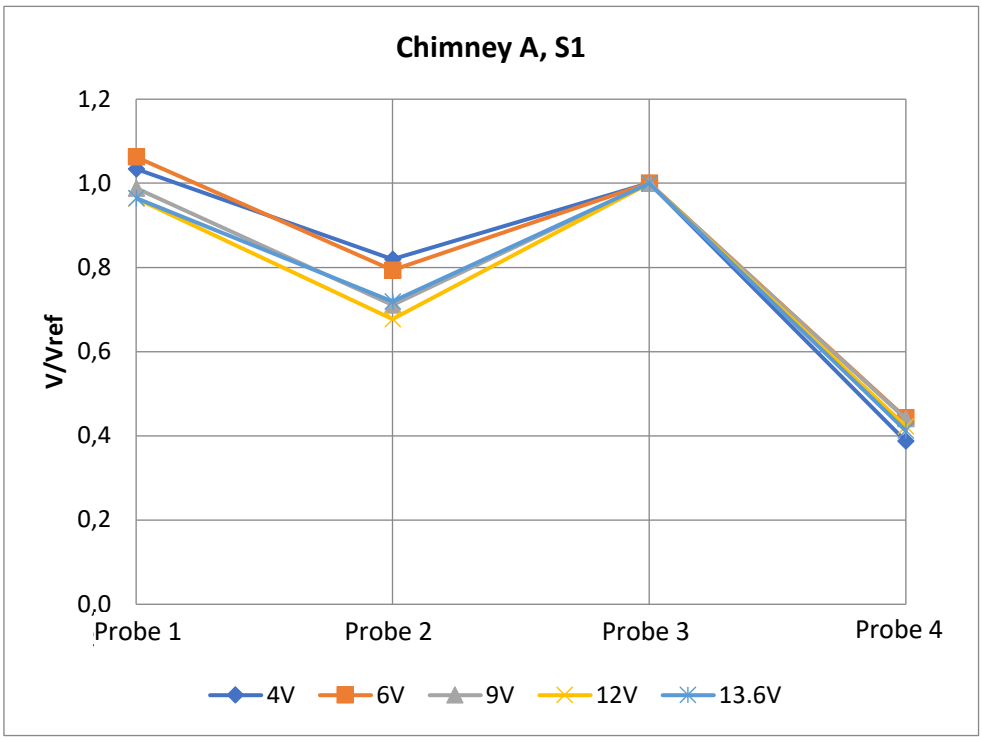

b)

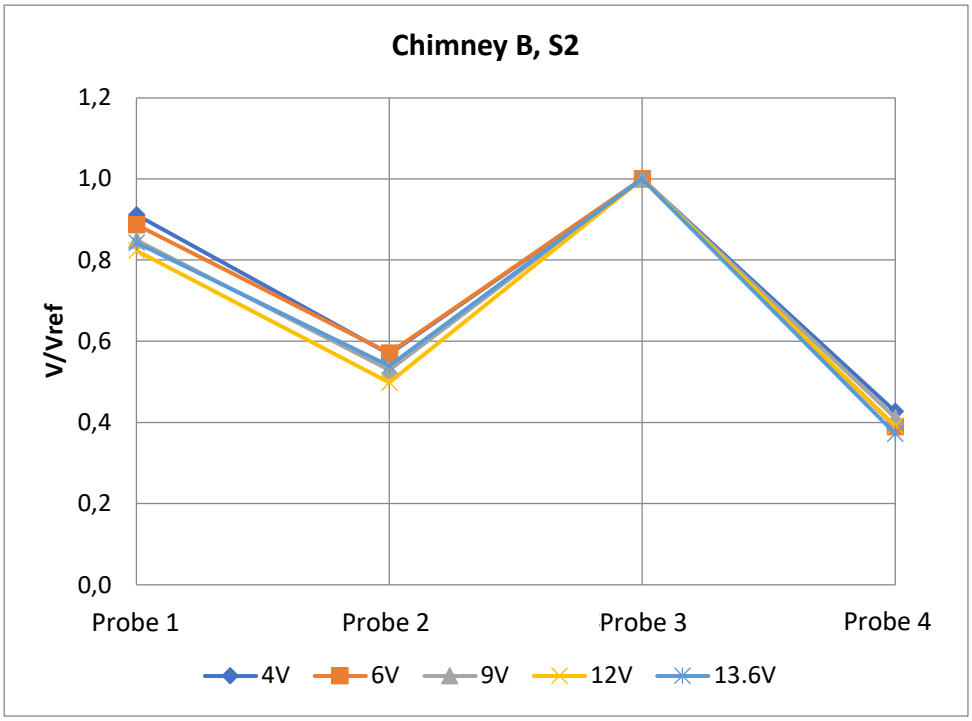

Fig. 8.10. Air velocity for individual rotational speeds in: S1 a) and S2 b) series.

a)

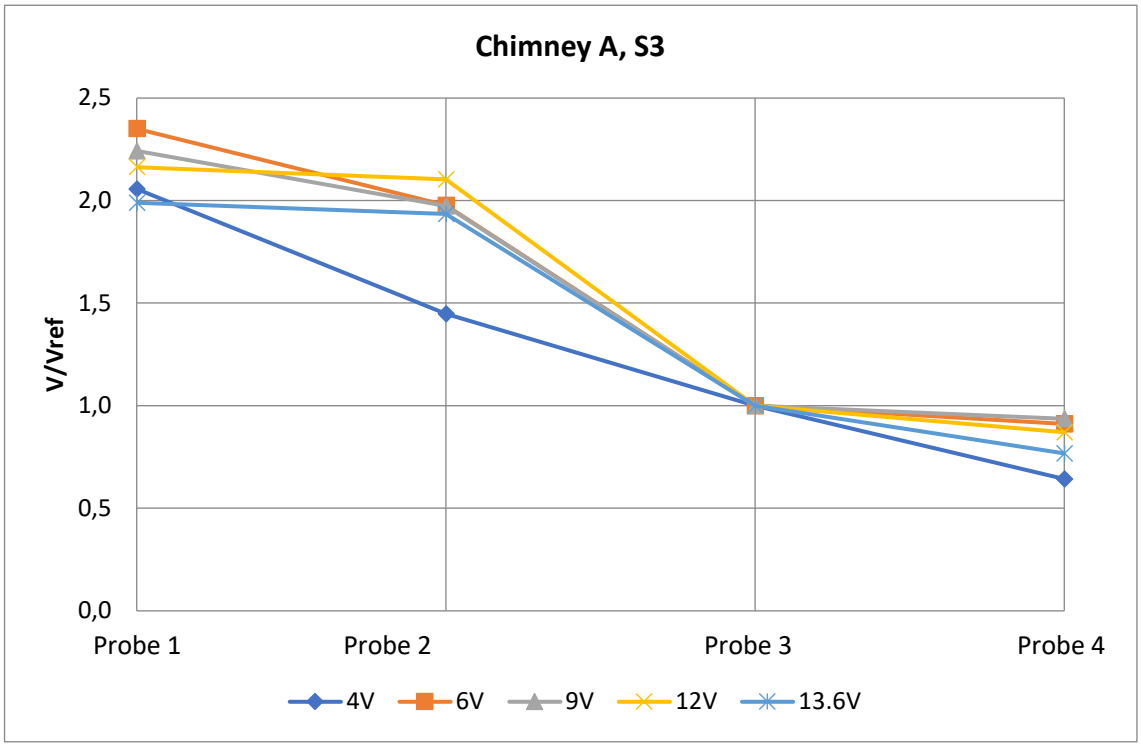

b)

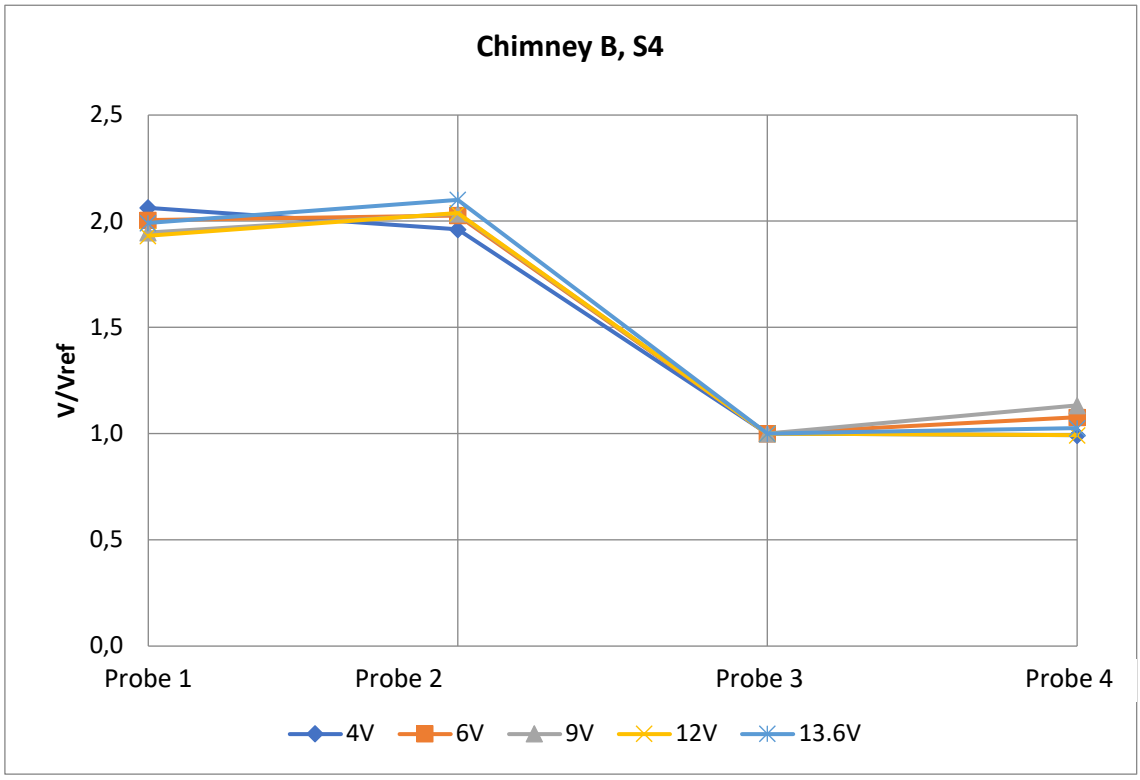

Fig. 8.11. Air velocity for individual rotational speeds in: S3 series a) and S4 series b).

a)

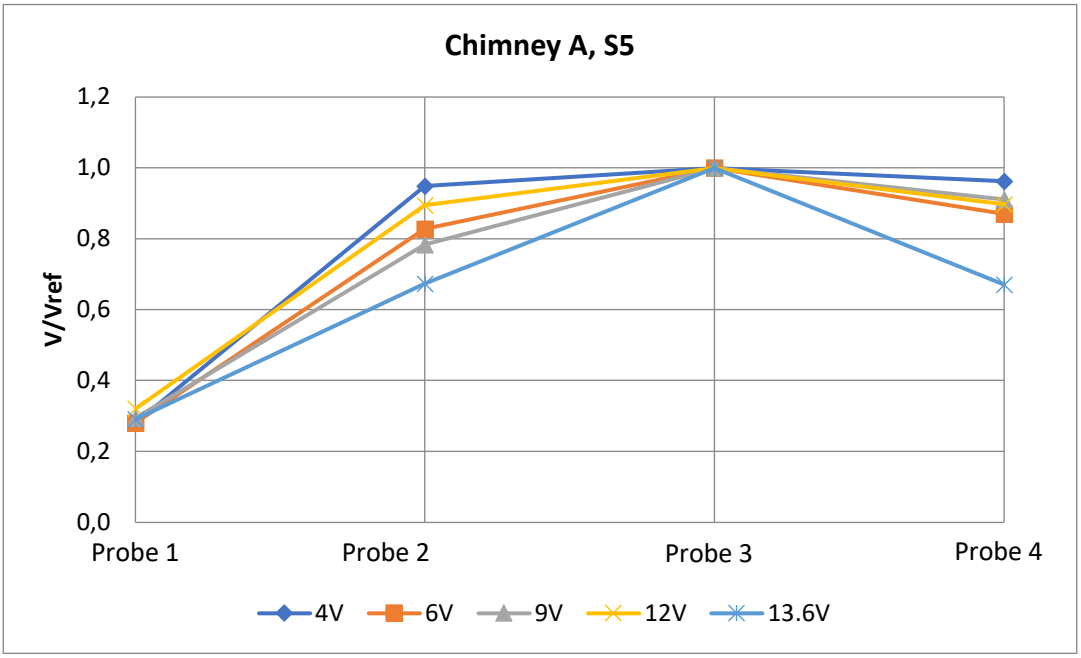

b)

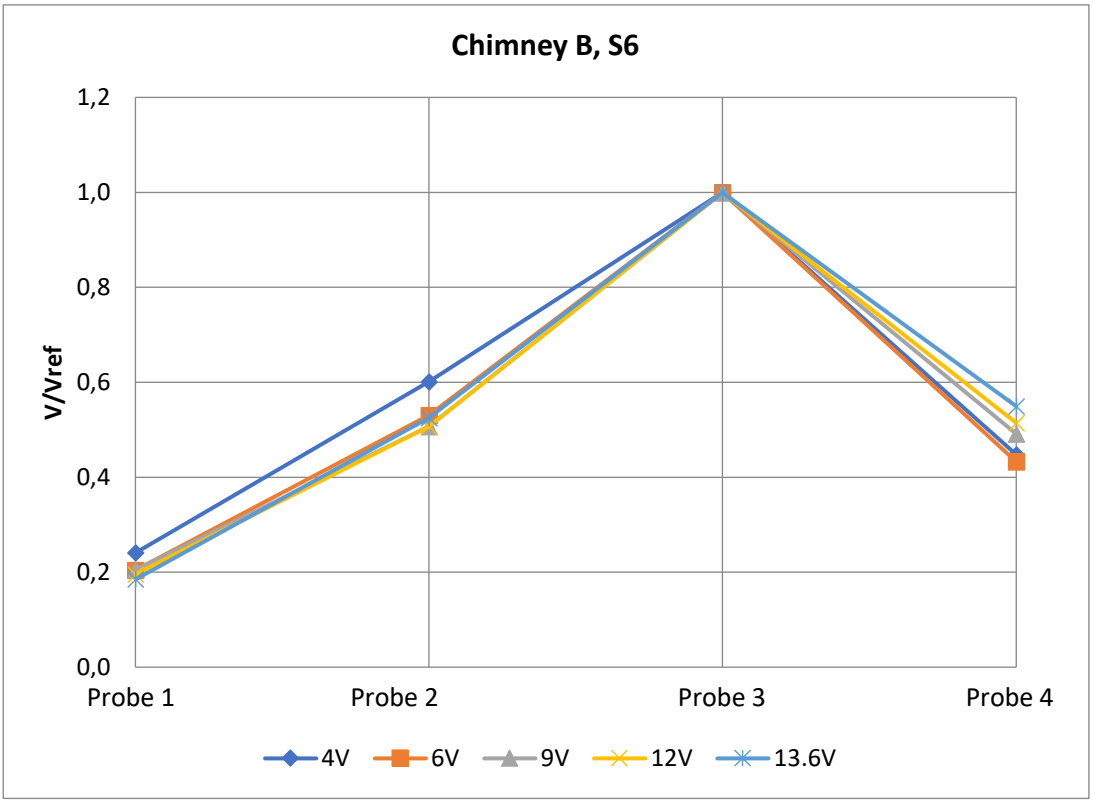

Fig. 8.12. Air velocity for individual rotational speeds in: S5 series a) and S6 series b).

a)

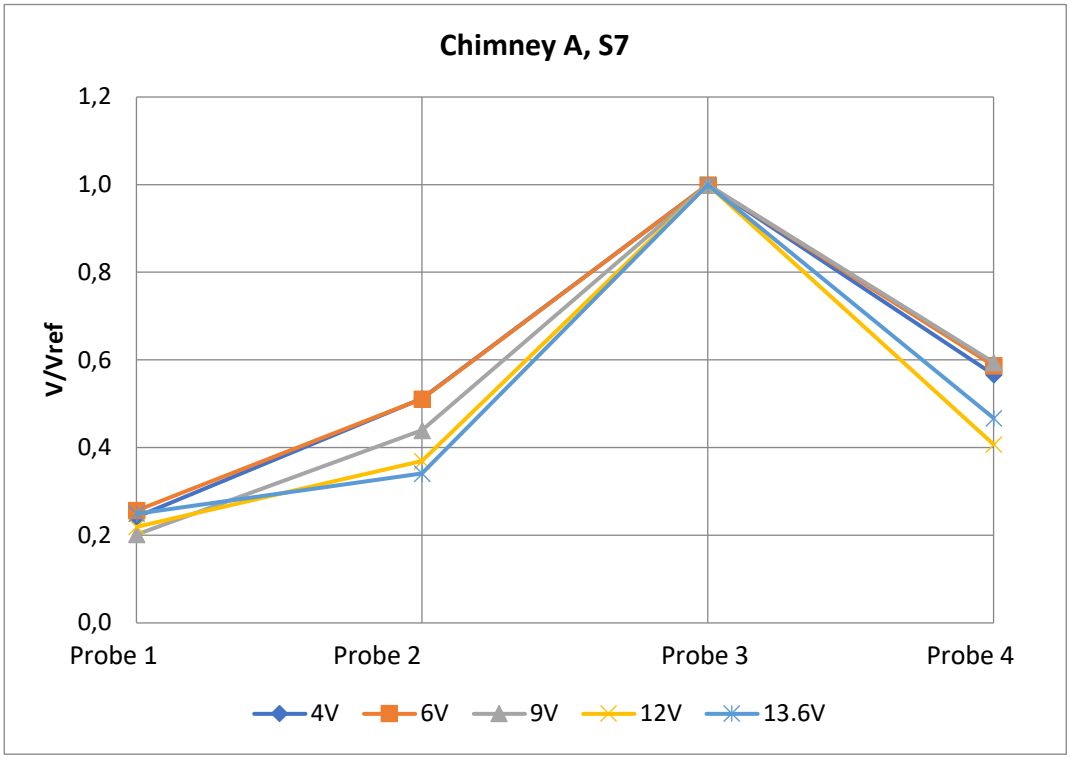

b)

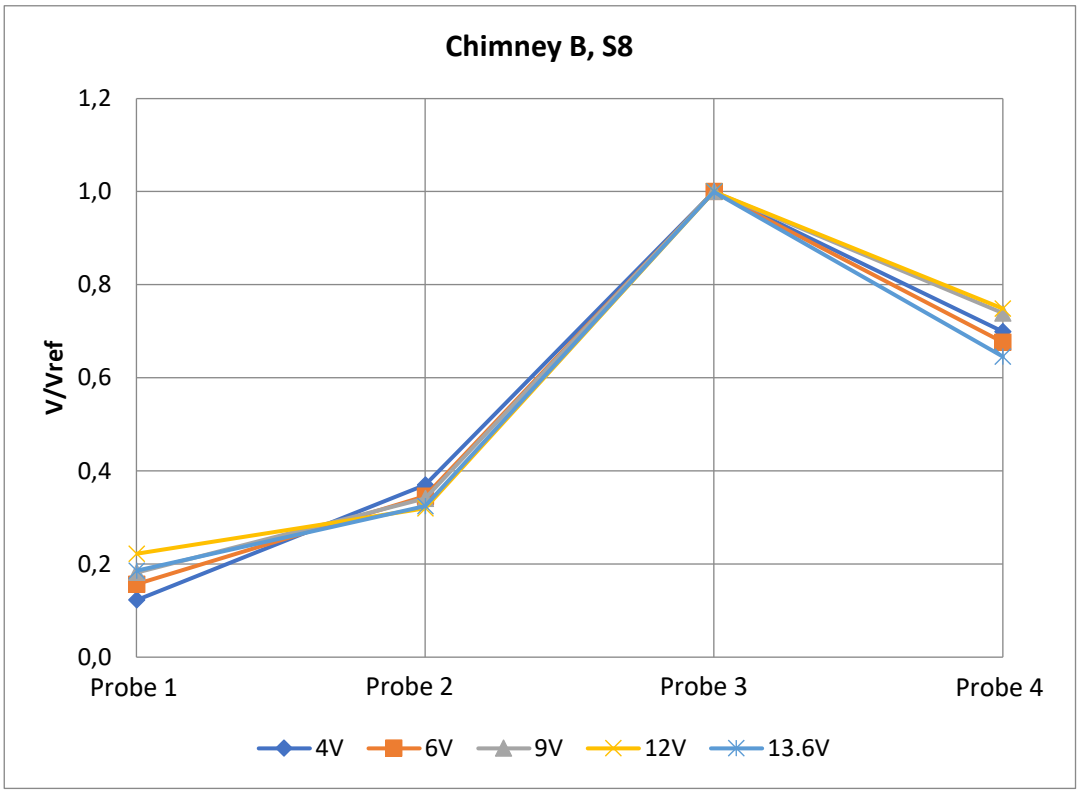

Fig. 8.13. Air velocity for individual rotational speeds in: S7 series a) and S8 series b).

Fig. 8.14. presents a comparison of the actual air velocities obtained in tests for 12V voltage on fans in each series.

a)

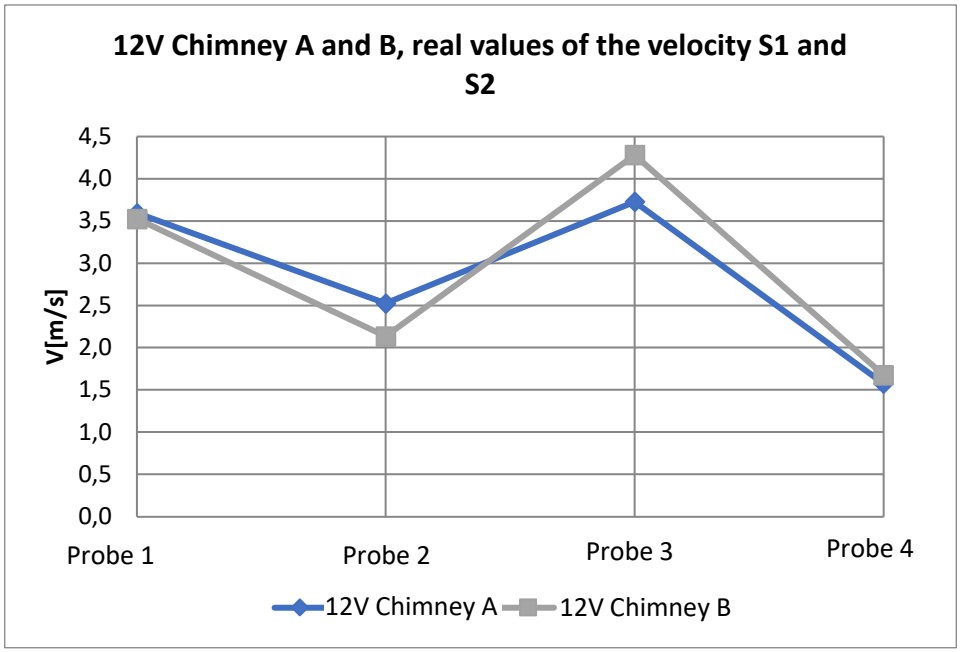

b)

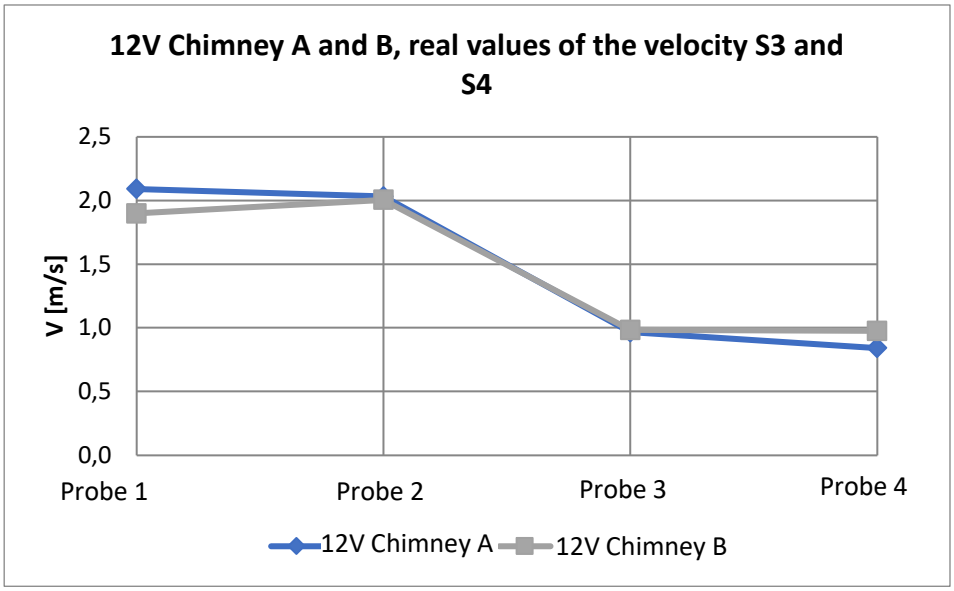

c)

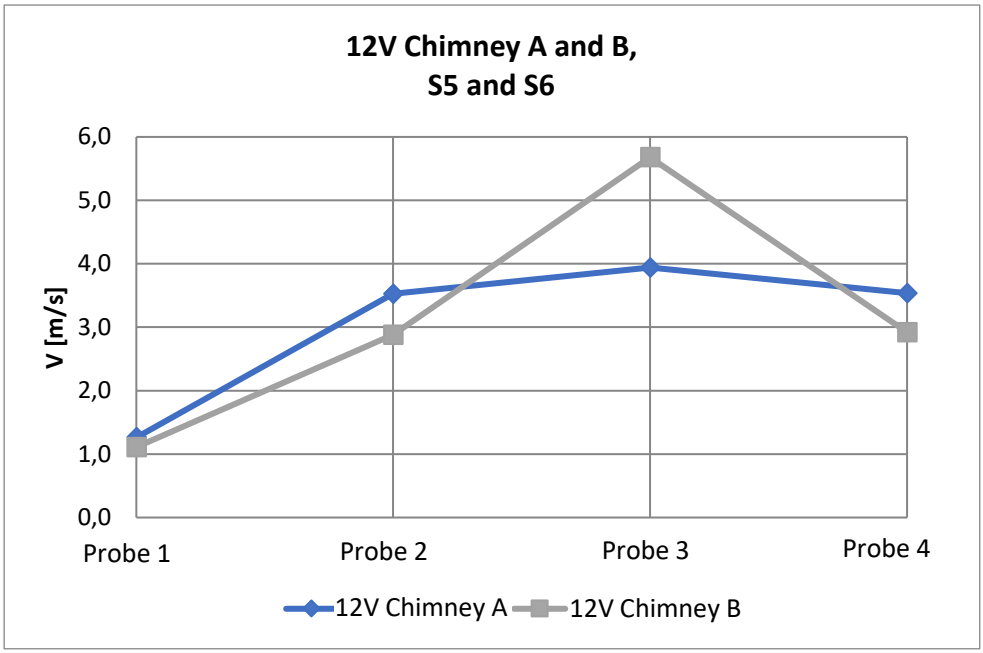

d)

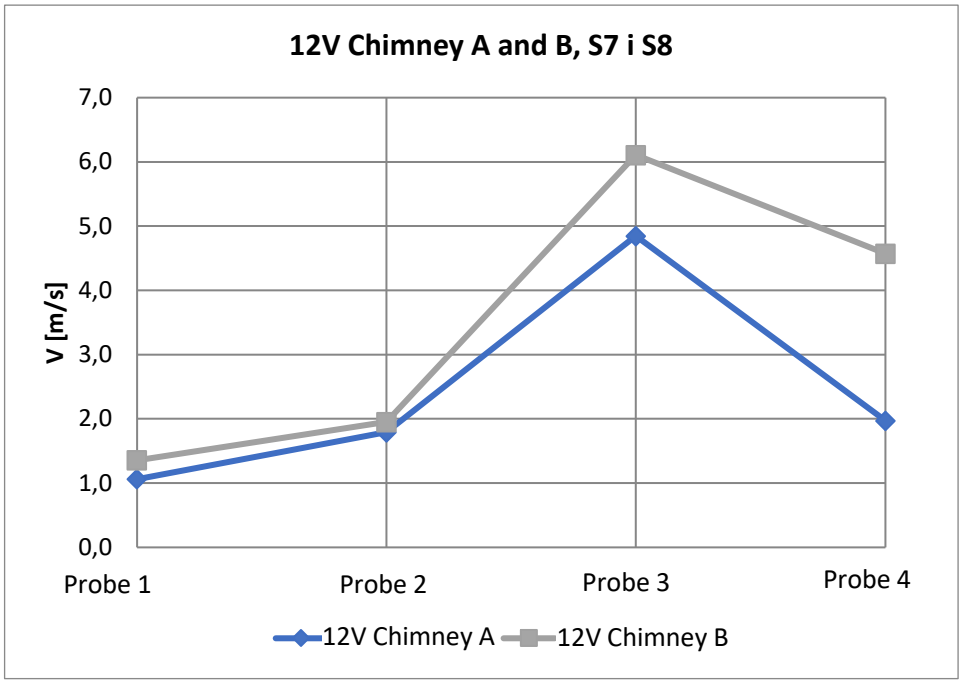

Fig. 8.15. Comparison of actual air velocities for 12V voltage on fans for various measurement situations: S1 and S2 series a), S3 and S4 series b) , S5 and S6 series c) , S7 and S8 series d)

Due to the location of the measurement points, the high velocity values obtained in points 3 and 4 are a positive and desirable phenomenon, while in points 1 and 2 they mean losses resulting from the escape of air streams under the tested structure. High values in points 1 and 2 in situations S1, S2, S3, and S4 indicate large losses of the stream compression and the occurrence of the blockage effect. In the subsequent stages of the S5-S8 tests, the lower spaces (S5 and S6) were covered and all free spaces (S7 and S8) were completely covered, which allowed to significantly reduce the air stream causing losses. Considering the arrangement of measurement points 3 and 4, the most favorable

situation in terms of the geometry of the chimney is when the velocity values at point 3 assume the maximum values, while at point 4 these values decrease slightly. Comparing the results of the tests carried out, such a situation occurred in the series of tests S3 and S4, but after comparing the actual values obtained with the same fan power (see Fig. 8.14-8.15), it can be seen that the values of air velocity in points 3 and 4 reached the level of respectively 1m/s and 1m/s, while in the S8 series they reached the level of 6m/s and 4.6m/s. This phenomenon can be explained by very large losses of air streams escaping under the tested structure, which resulted in the creation of a greater circulation within the chimney surroundings.

In all tested series, the speed charts for individual voltages on the fans do not differ significantly within a given series. It can therefore be assumed that the influence of the Reynolds number in the research is negligible. The highest actual air velocities at measurement point 3 were obtained in series S6 and S8 for chimney B, while at measurement point 4 a much higher value was obtained in series S8 for chimney B. Therefore, the S8 series is the most advantageous case, of course it is more complicated in terms of construction because it requires complete construction of the space between the fans, however, the economic benefits resulting from the better shape of the stream and greater efficiency of the entire system are significant. Fig. 8.13b shows that the air velocity at point 4 is lower by only about 30% of the velocity at point 3. Due to the planned use of the tested chimney system to break up the smog layer, is a very favorable result and encourages further research.

8.3. Conclusion for the results of the II stage

During the tests, it was found that the presence of a ventilation chimney in the S8 series significantly improves the efficiency of the generated air stream and positively affects the movement of air masses above the chimney. In particular, this applies to air masses located in the upper parts of the volume affected by the ventilation system (i.e. at a distance greater than 10 D) and the shape of the stream itself. This is important because the kinetic energy of the moving air masses must overcome the aerodynamic resistance of the smog layer to "break through" this layer. During the tests, it was also found that the adopted fan configuration (case II-3) generates a relatively strong stream with a wide cone. On this basis, it was decided that stage III of the preliminary tests should include additional tests of the configuration (different angles of inclination) of the fan plane enabling to obtain a satisfactory level of speed and range of the air stream without additional ventilation chimneys, such as optional ones and ventilation chimneys of various shapes, total height and the height of the base of the chimneys supporting the overall system.

The results of the model tests obtained in the two stages are very promising and were continued in stage III. In the third stage, the following cases were examined: with a cylindrical chimney - shape C and without a ventilation chimney - shape D (see Fig. 8.16) in various positions of the fans and ventilation. The list of research cases suggested in stage III of the preliminary research is given in Tab. 8.2.

Table 8.2. List of research cases suggested in stage III of the preliminary research

Series	Shape	Location of the fans	Aeration
S9	A	II	4
10	B	II	4
S11	C	II	2
S12	C	II	3
S13	C	III	3
S14	C	IV	3
S15	D	II	3
S16	D	III	3
S17	D	IV	3

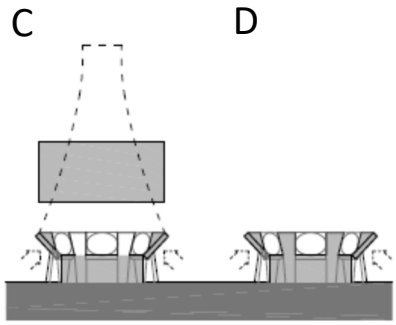

Fig. 8.16. The shapes of the ventilation system suggested in further studies (Krajewski 2021)

8.4. Model description and experiment setup of stage III - radial models of ventilation chimneys

Proper preparations for experimenting were preceded by a study of the thematic literature. On this basis, it was concluded that the conditions for conducting the experiment related to the radial configuration of ventilation chimneys as part of stage III of the preliminary tests should take into account test series that differ from each other:

4. The shape and variants of the shapes of ventilation chimneys (shapes A, B, C, and D, see Fig. 8.17 and 8.18);

5. Location of the first row fans:

• configuration I - a distance of the fan ring from the chimney of 150 cm,

• configuration II - a distance of the fan ring from the chimney of 120 cm;

6. The speed of the fans in the system, depending on the power supply and expressed by the voltage applied to the system:

• speed 1 - 4 V power supply,

• speed 2 - 9.5 V power supply,

• speed 3 - 13.6 V power supply.

The remaining parameters of the system such as the angle of inclination of the inlet fans and the ventilation of the inlet fan system, were determined as the most effective solutions obtained in stage II, i.e.:

• ventilation of the system configuration 3 (full coverage of the space between the fans on both levels),

• angle of inclination of the fans relative to the vertical 47º. All series of tests were carried out in a model scale of 1:833 (Fig. 8.19). Measurements were carried out separately for each shape of the chimney at different distances and voltages supplying the system. In Tab. 8.3. the completed series of tests of ventilation chimneys are presented.

Table 8.3. List of performed research cases - ventilation chimneys in a radial configuration

Series	**Distance of the fan ring**	**Chimney shape**	**Shape variant**
Series III	150 cm	A, B, C, D	1
Series IV	120 cm	A, B, C, D	1
Series V	120 cm	A, B	1, 2, 3

-

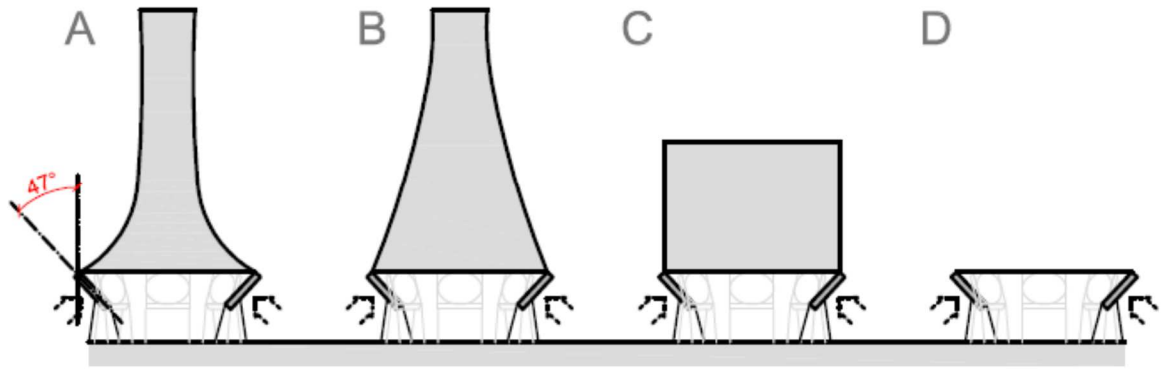

Fig. 8.17: Tested shapes of chimneys with inlet fans and closed space between them (Krajewski 2021).

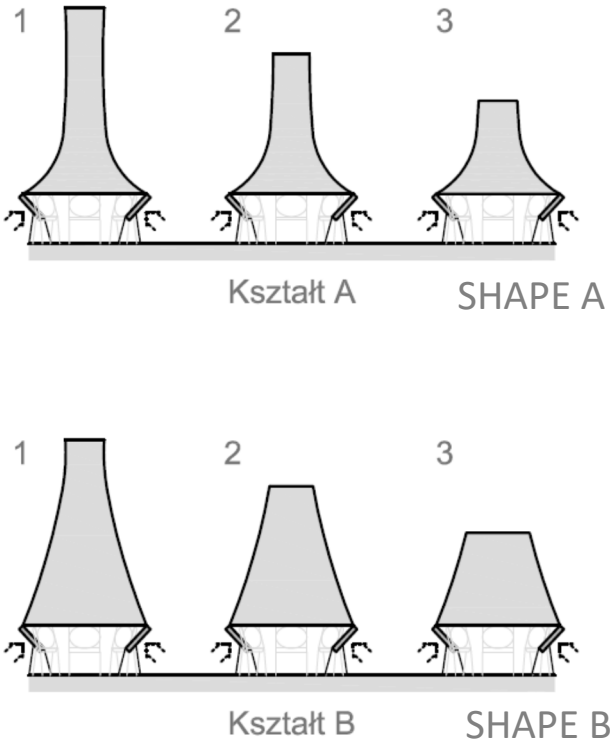

Fig. 8.18: Different variants of chimney shapes A and B: 1 - full chimney 360 mm high, 2 - chimney cut to 3/4 height (270 mm), 3 - chimney cut to half height (180 mm) (Krajewski 2021).

a) b)

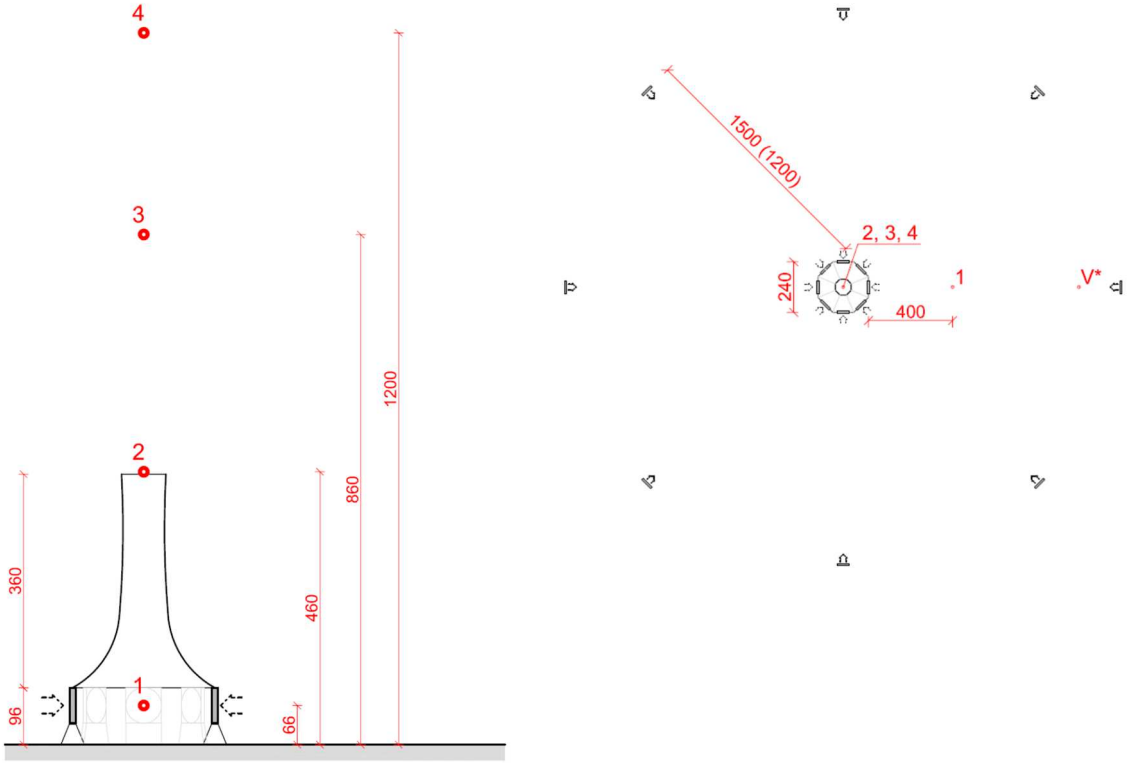

Fig. 8.19: Scheme of arrangement of hot-wire anemometric sensors on the system model: a) side view b) top view (Krajewski 2021).

Fig. 8.20-8.22 presents photos of models with instrumentation in the used measuring space.

Fig. 8.20: Chimney model (shape A) with inlet fans visible at the base, fan outer ring at a distance of 120 cm from the chimney, and stands with measuring probes 1 and 2

a) b)

Fig. 8.21: View of the arrangement of hot-wire anemometric sensors on the system model: a) shape A, variant 1 b) shape B, variant 3

Fig. 8.22: Model of the chimney (shape C) with the position of the inlet fans visible from the inside

8.5. Test results of the III stage (ventilation chimneys)

Series of test numbers III, IV, and V were performed to examine cooperation between the horizontal system (outer ring) and the vertical system (ventilation chimney). Fig. 8.23-8.25 shows a comparison of the dimensionless velocities obtained in tests for individual shapes of the chimney depending on the voltage (4 V, 9.5 V, and 13.6 V) applied to the fans for the 3rd series of tests. The reference speed V* was each time taken as the speed measured 20 cm in front of the outer ring fan (Fig. 8.19b). All results were corrected for the values of the measured background velocities (with fans off) for the individual probes.

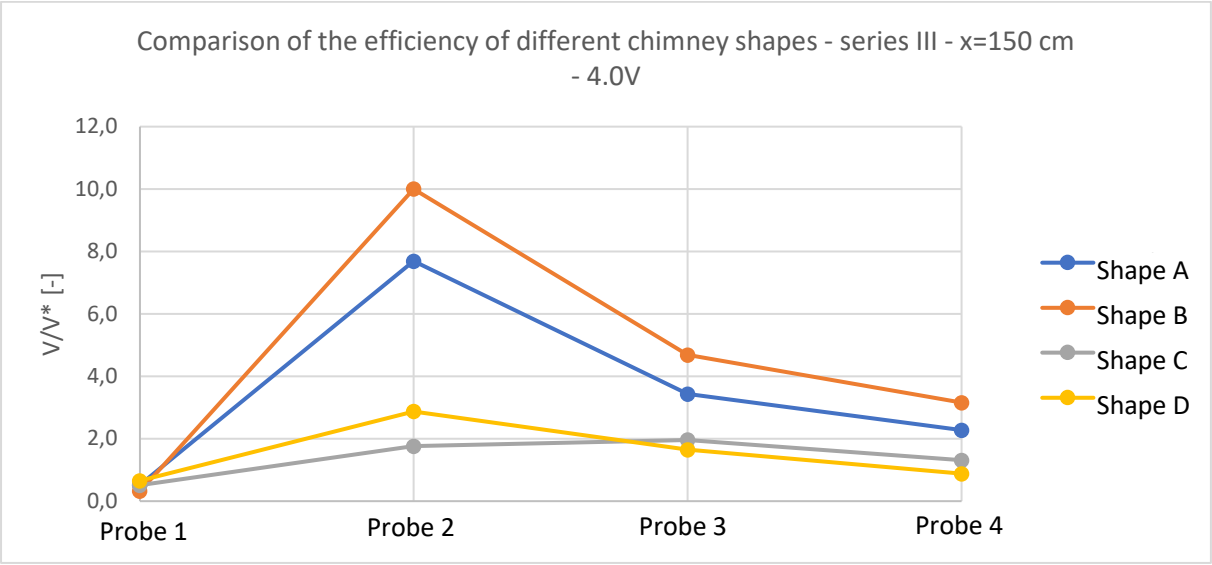

Fig. 8.23: Comparison of the efficiency of different chimney shapes - series III, voltage 4.0 V

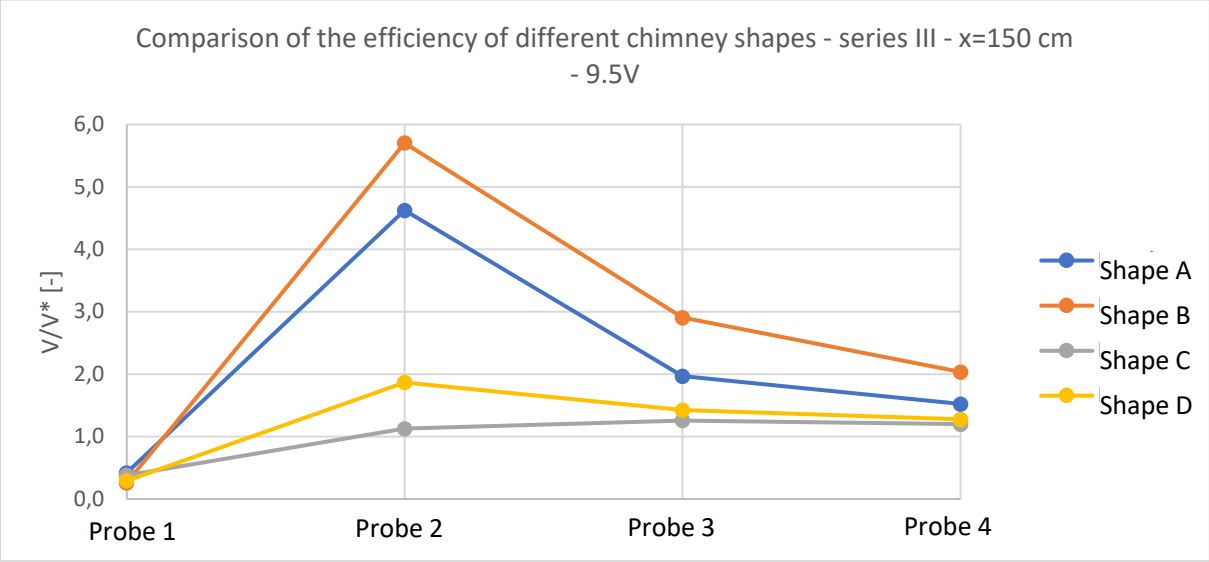

Fig. 8.24: Comparison of the efficiency of different chimney shapes - series III, voltage 9.5 V

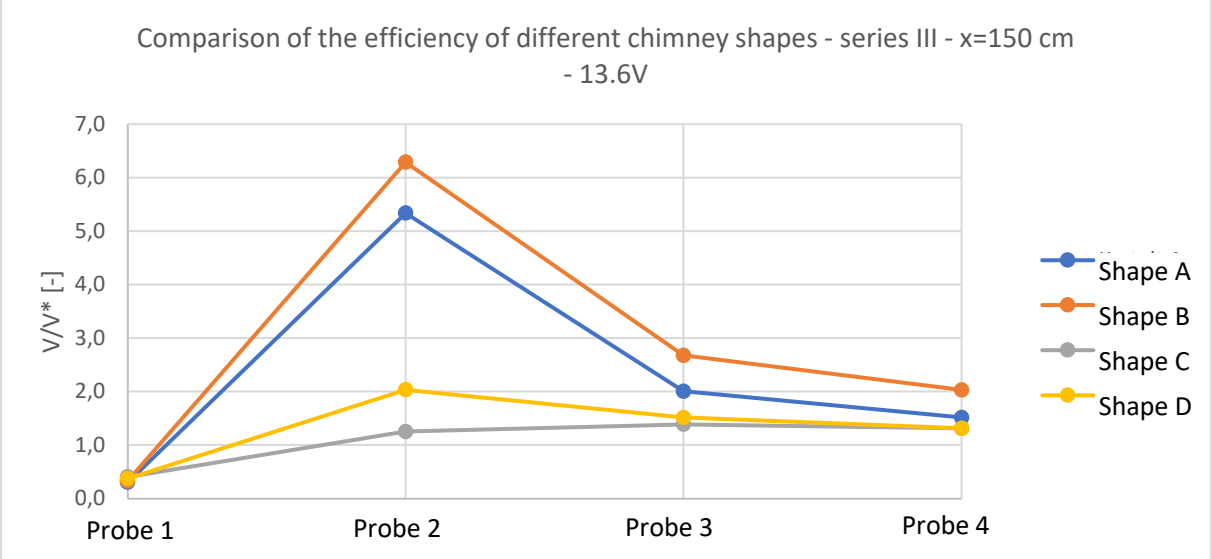

Fig. 8.25: Comparison of the efficiency of different chimney shapes - series III, voltage 13.6 V

Fig. 8.26-8.29 lists the dimensionless velocities obtained at different voltages applied to the fans for series III for each shape of the chimney. This allows us to determine the influence of the Reynolds number criterion on the studied phenomenon.

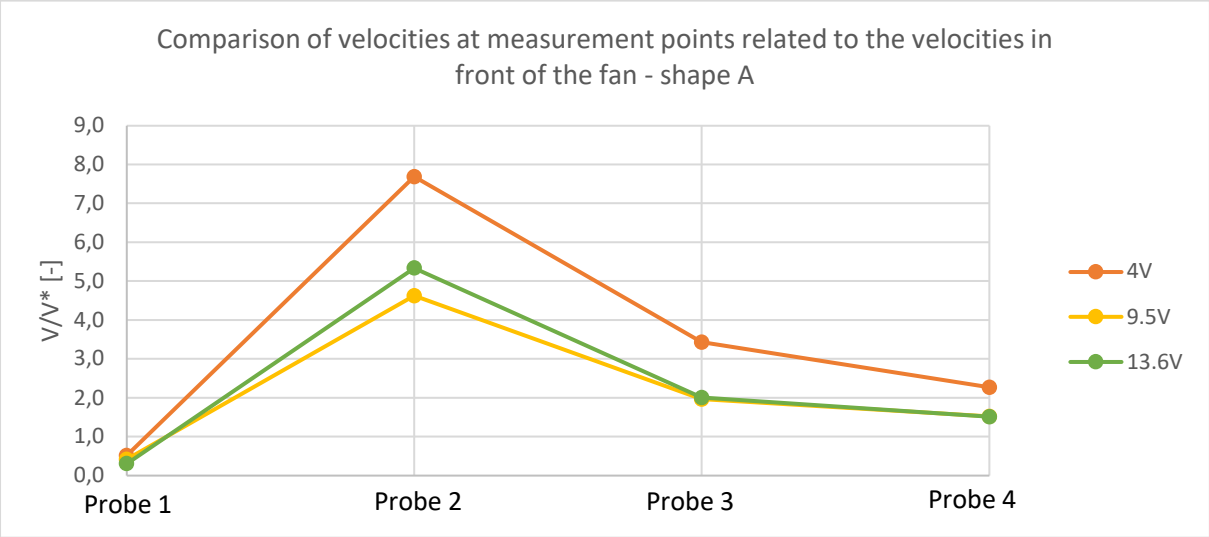

Fig. 8.26: Comparison of the stream velocity at various measurement points related to the velocity in front of the fan for various voltages supplying the system - series III, shape A

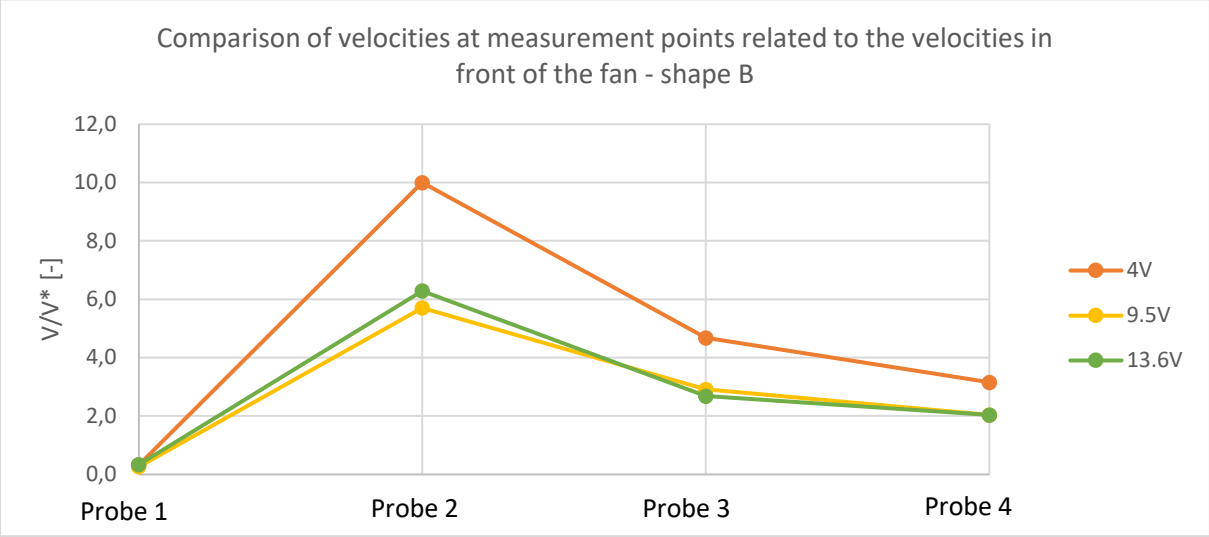

Fig. 8.27: Comparison of the stream velocity at various measurement points related to the velocity in front of the fan for various voltages supplying the system - series III, shape B

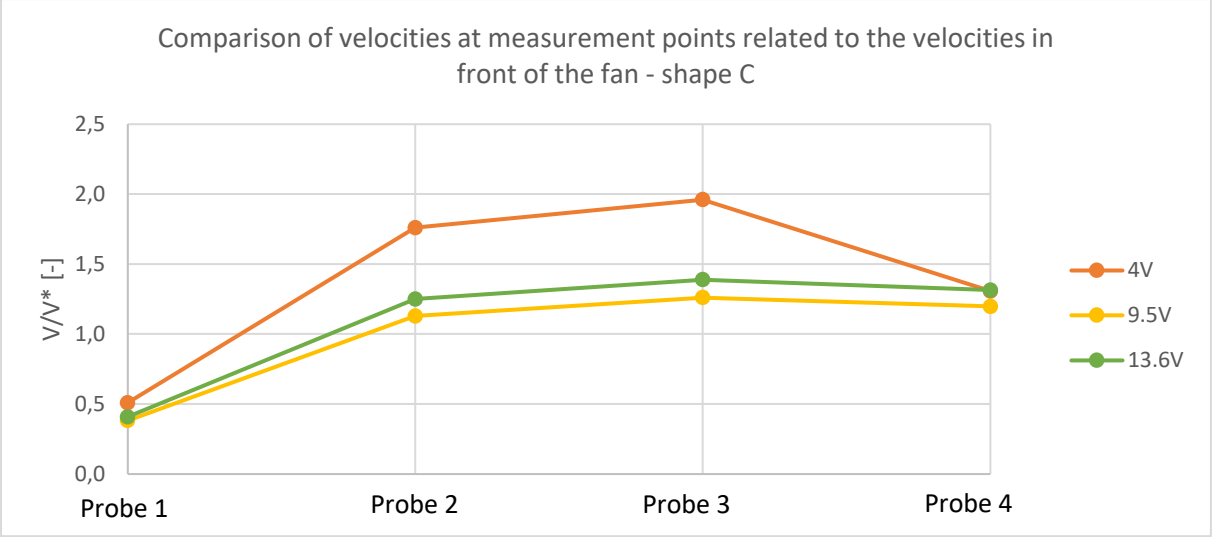

Fig. 8.28: Comparison of the stream velocity at various measurement points to the velocity in front of the fan for various voltages supplying the system - series III, shape C

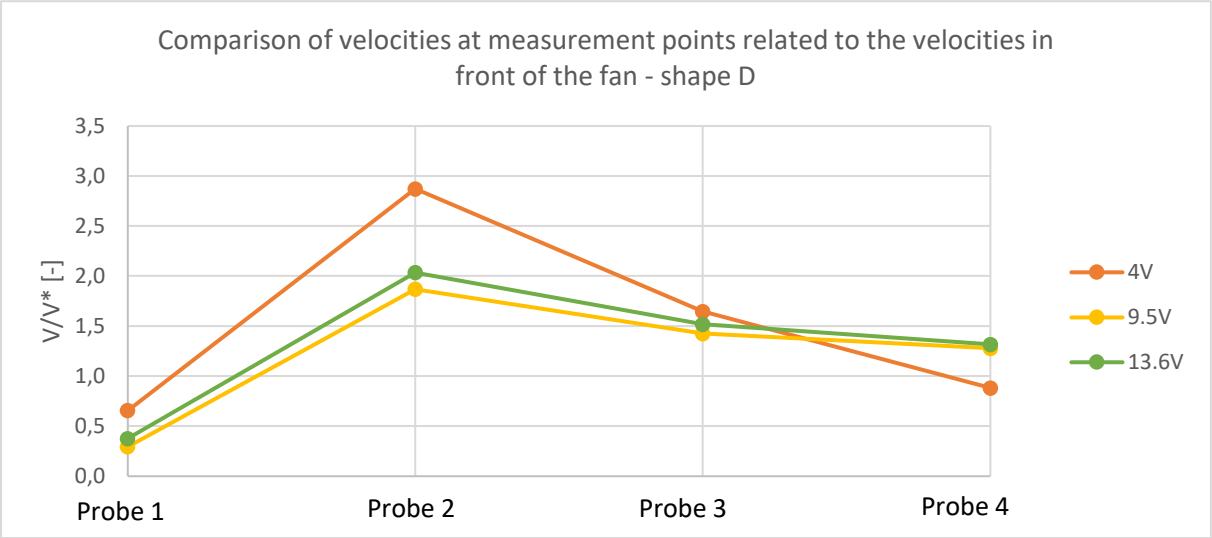

Fig. 8.29: Comparison of the stream velocity at various measurement points to the velocity in front of the fan for various voltages supplying the system - series III, shape D

Fig. 8.30-8.32 shows a comparison of dimensionless velocities obtained in tests for individual shapes of the chimney depending on the voltage (4 V, 9.5 V and 13.6 V) applied to the fans for the 4th series of tests.

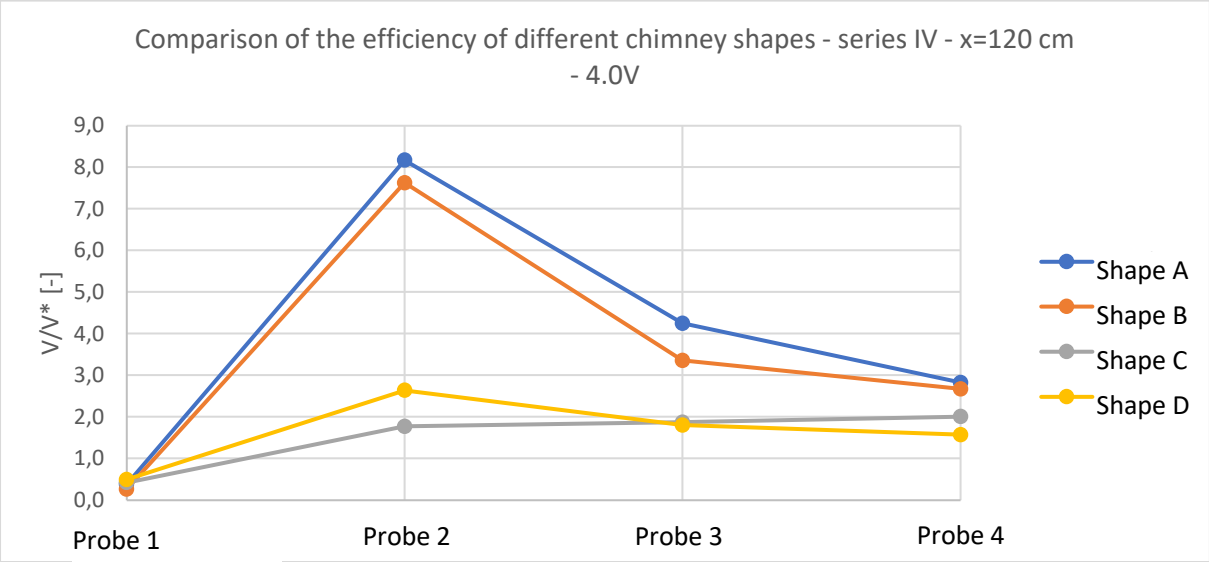

Fig. 8.30: Comparison of the efficiency of different chimney shapes - series IV, voltage 4.0 V

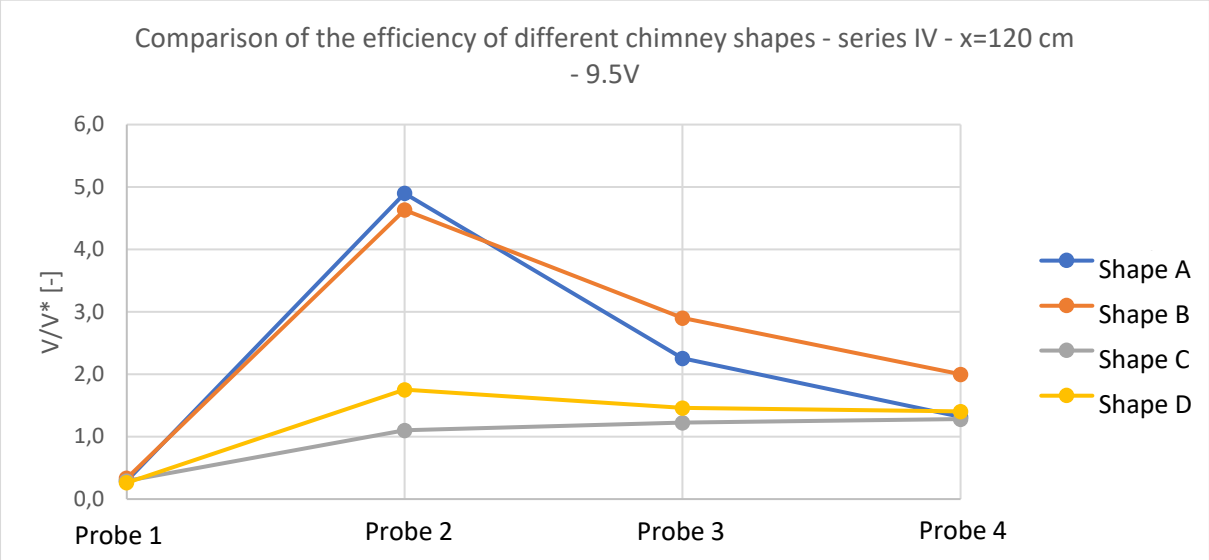

Fig. 8.31: Comparison of the efficiency of different chimney shapes - series IV, voltage 9.5 V

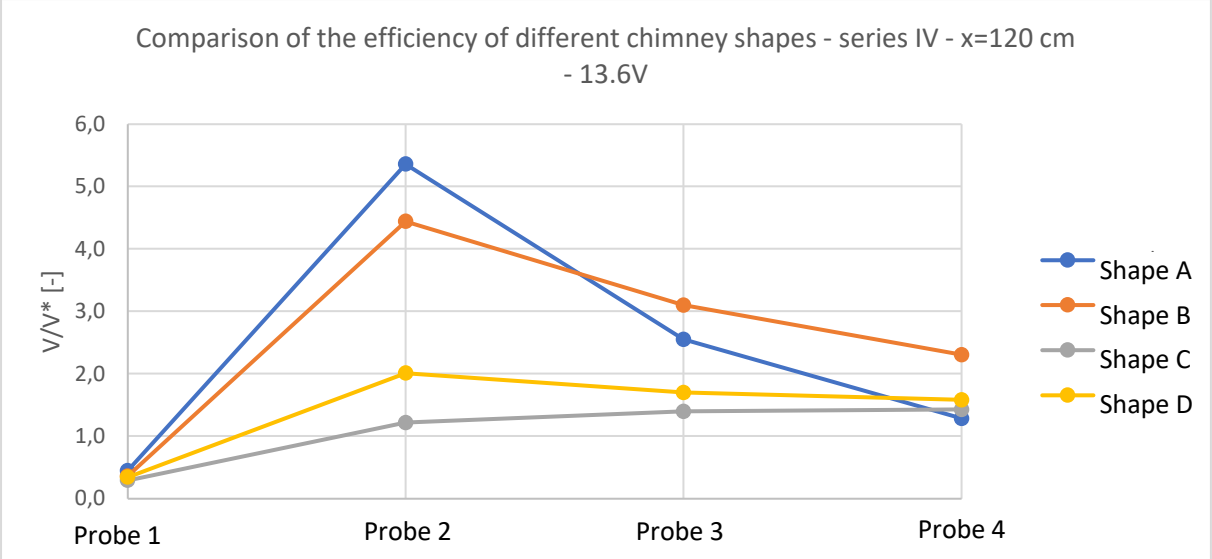

Fig. 8.32: Comparison of the efficiency of different chimney shapes - series IV, voltage 13.6 V

Fig. 8.33-8.36 lists the dimensionless velocities for each shape of the chimney obtained at different voltages applied to the fans for series IV. Performed tests allow us to determine the influence of the Reynolds number criterion on the studied phenomenon.

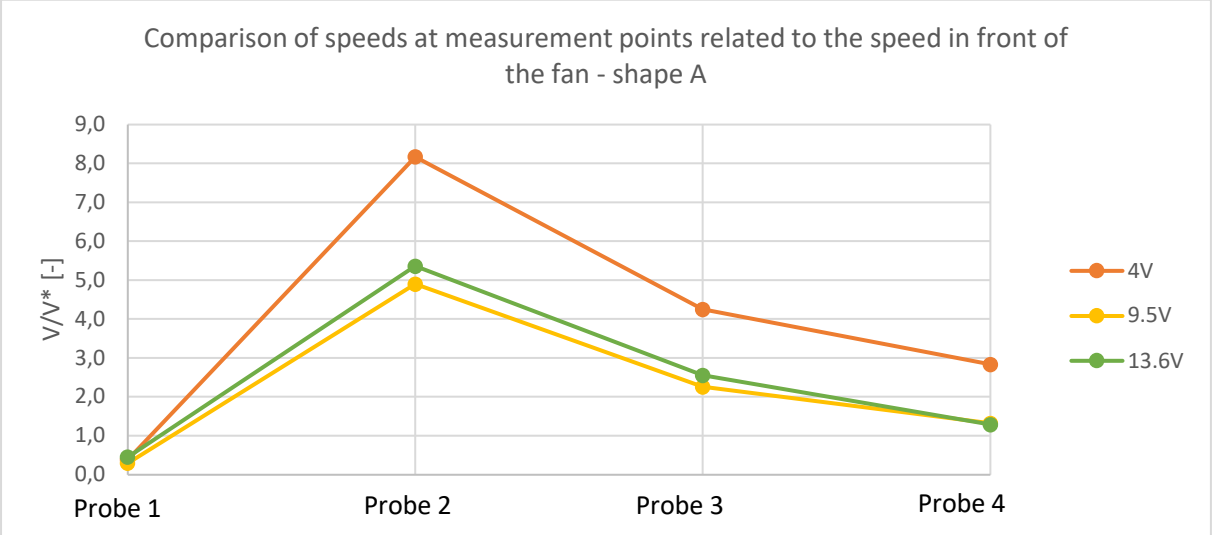

Fig. 8.33: Comparison of the stream velocity at various measurement points related to the velocity in front of the fan for various voltages supplying the system - series IV, shape A

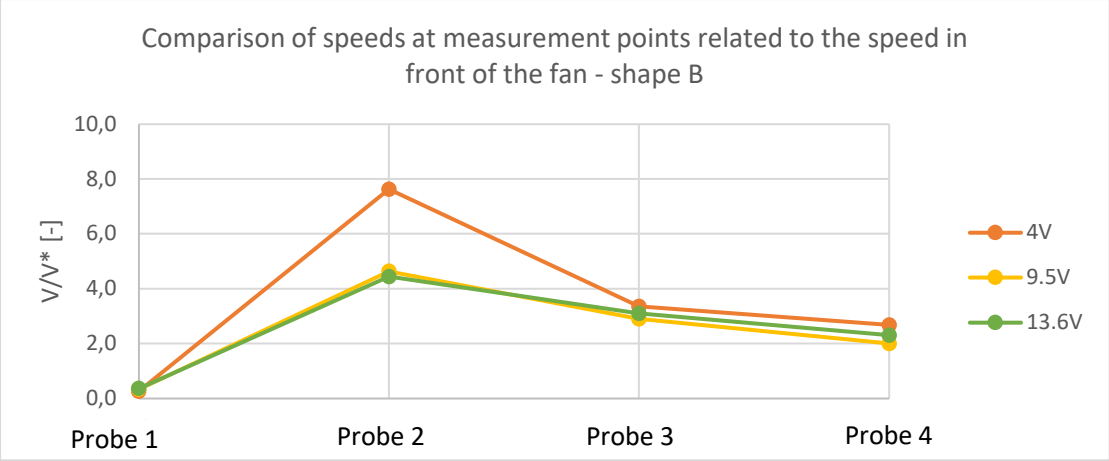

Fig. 8.34: Comparison of the stream velocity at various measurement points related to the velocity in front of the fan for various voltages supplying the system - series IV, shape B

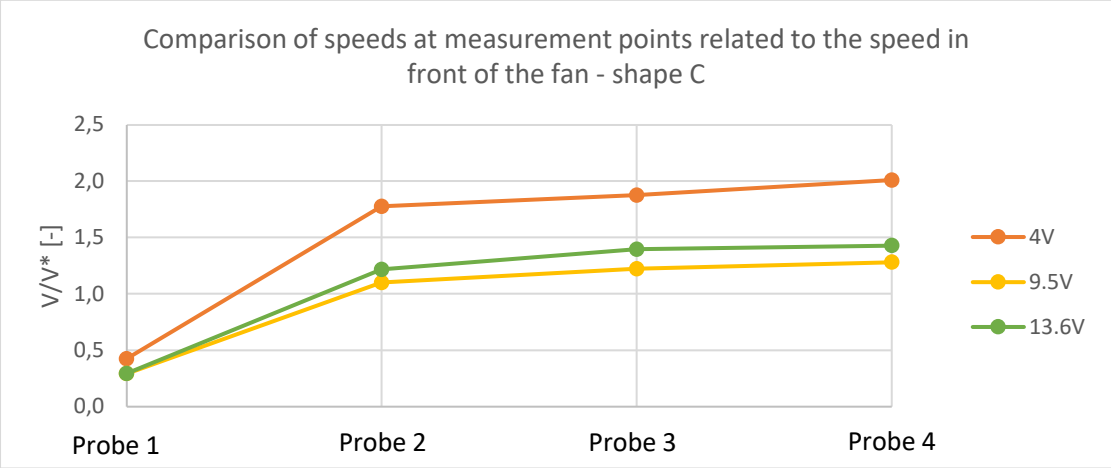

Fig. 8.35: Comparison of the stream velocity at various measurement points related to the velocity in front of the fan for various voltages supplying the system - series IV, shape C

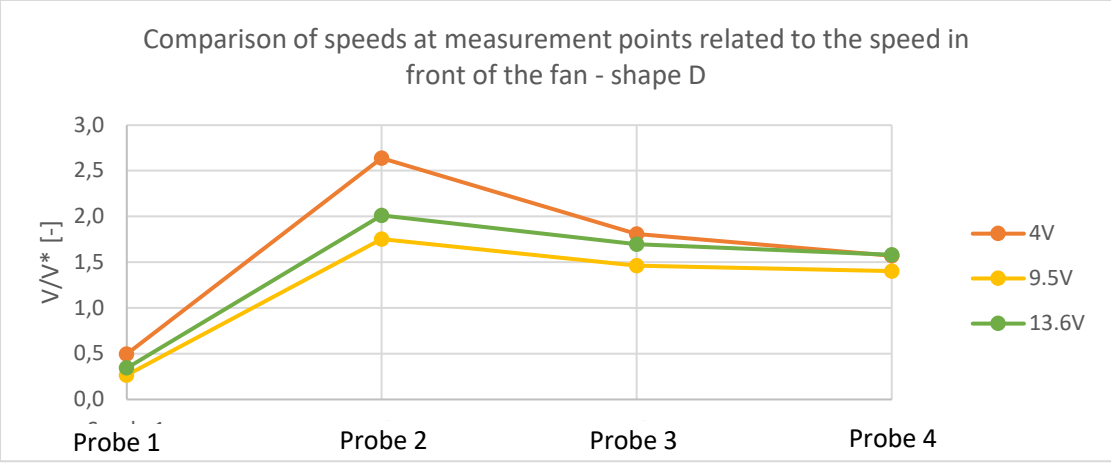

Fig. 8.36: Comparison of the stream velocity at various measurement points related to the velocity in front of the fan for various system supply voltages - series IV, shape D

To assess the impact of the positioning of the outer ring of fans to the central ventilation chimney, graphs comparing the results obtained for the two tested distances in series III and IV are presented in Fig. 8.37-8.48.

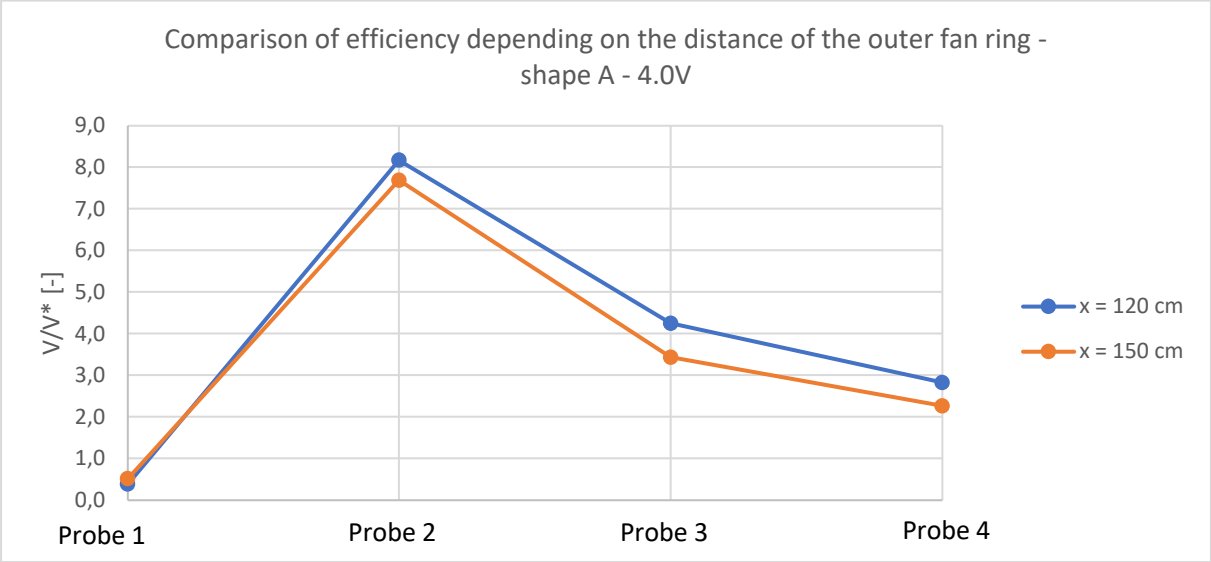

Fig. 8.37: Comparison of the stream velocity at various measurement points to the velocity in front of the fan depending on the distance of the outer ring of the fans - series III and IV, shape A, 4.0 V

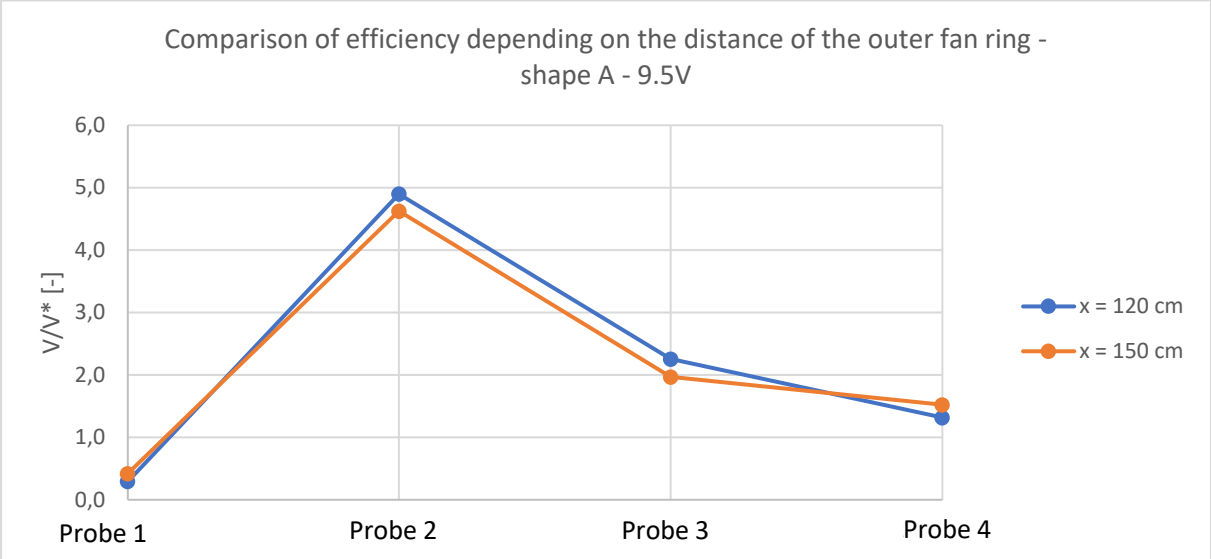

Fig. 8.38: Comparison of the stream velocity at various measuring points to the velocity in front of the fan depending on the distance of the outer ring of the fans - series III and IV, shape A, 9.5 V

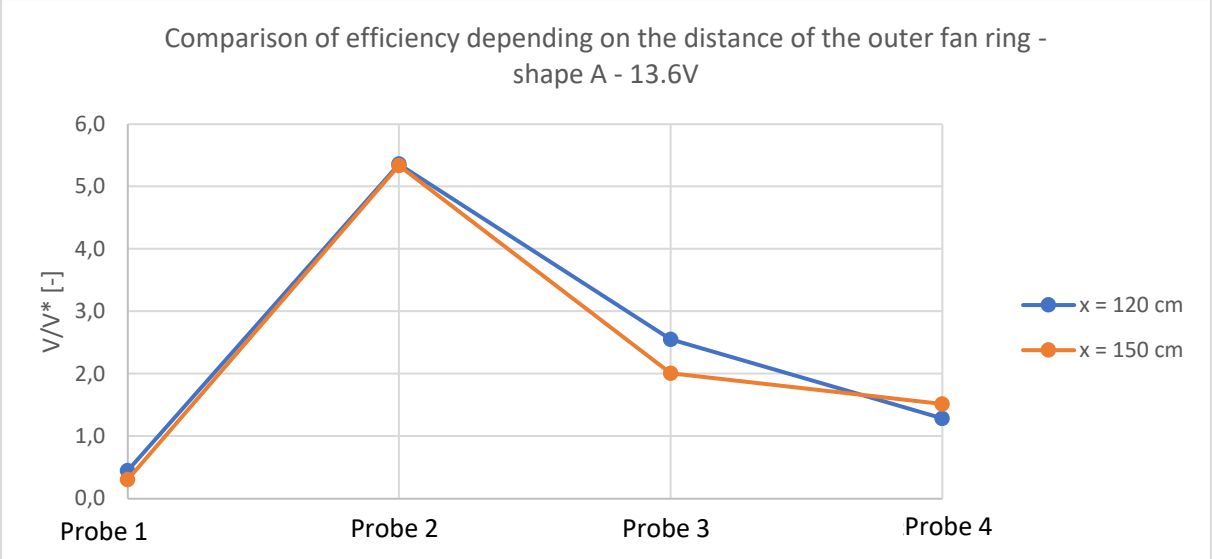

Fig. 8.39: Comparison of the stream velocity at various measurement points to the velocity in front of the fan depending on the distance of the outer ring of the fans - series III and IV, shape A, 13.6 V

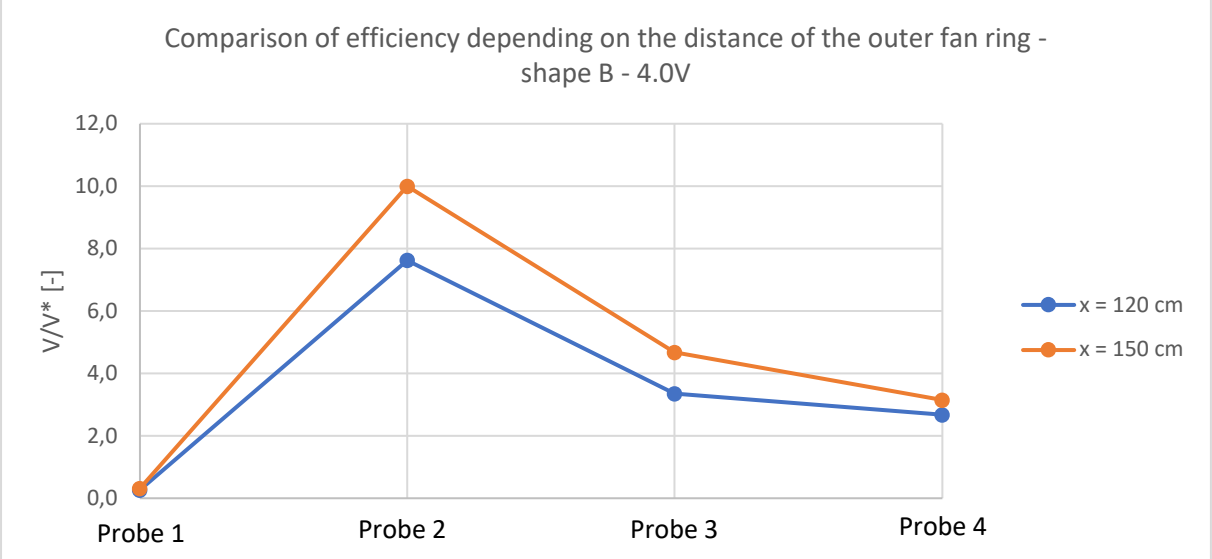

Fig. 8.40: Comparison of the stream velocity at various measurement points to the velocity in front of the fan depending on the distance of the outer ring of the fans - series III and IV, shape B, 4.0 V

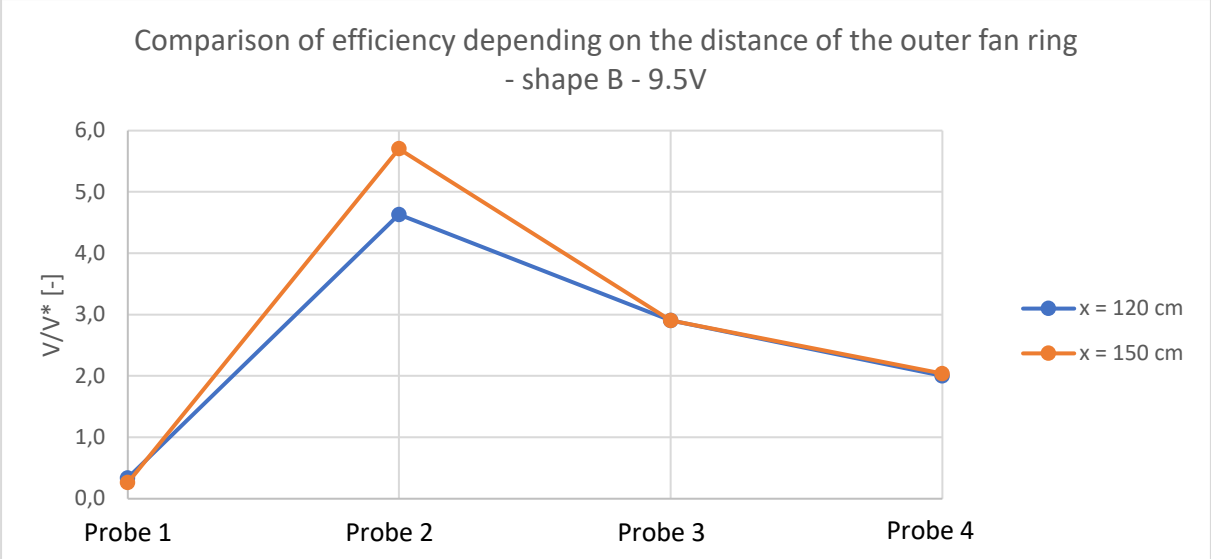

Fig. 8.41: Comparison of the stream velocity at various measurement points to the velocity in front of the fan depending on the distance of the outer ring of the fans - series III and IV, shape B, 9.5 V

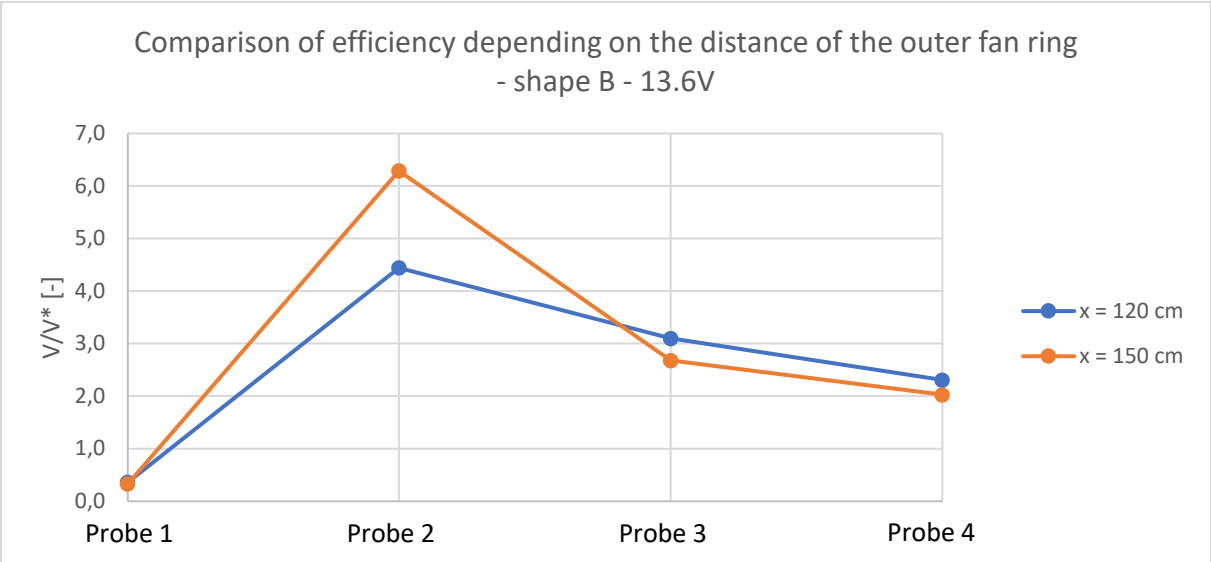

Fig. 8.42: Comparison of the stream velocity at various measuring points to the velocity in front of the fan depending on the distance of the outer ring of the fans - series III and IV, shape B, 13.6 V

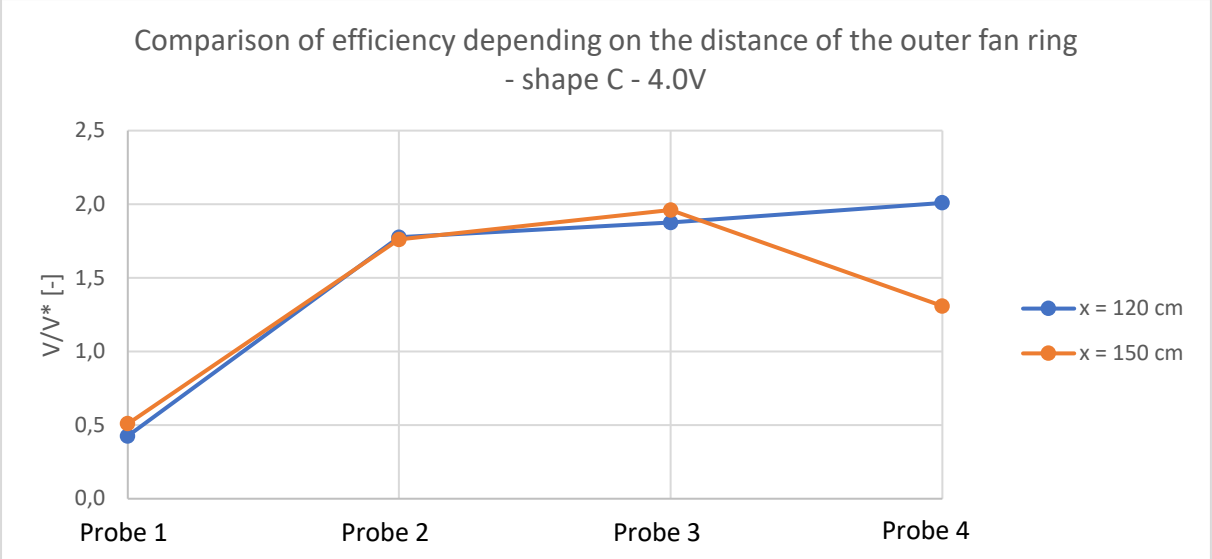

Fig. 8.43: Comparison of the stream velocity at various measurement points to the velocity in front of the fan depending on the distance of the outer ring of the fans - series III and IV, shape C, 4.0 V

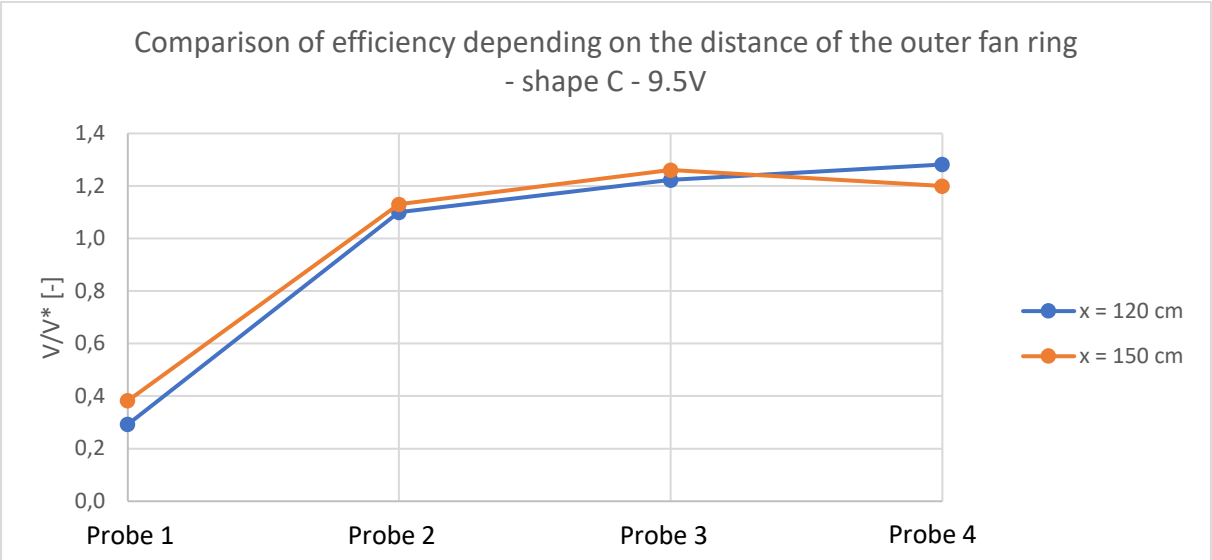

Fig. 8.44: Comparison of the stream velocity at various measuring points to the velocity in front of the fan depending on the distance of the outer ring of the fans - series III and IV, shape C, 9.5 V

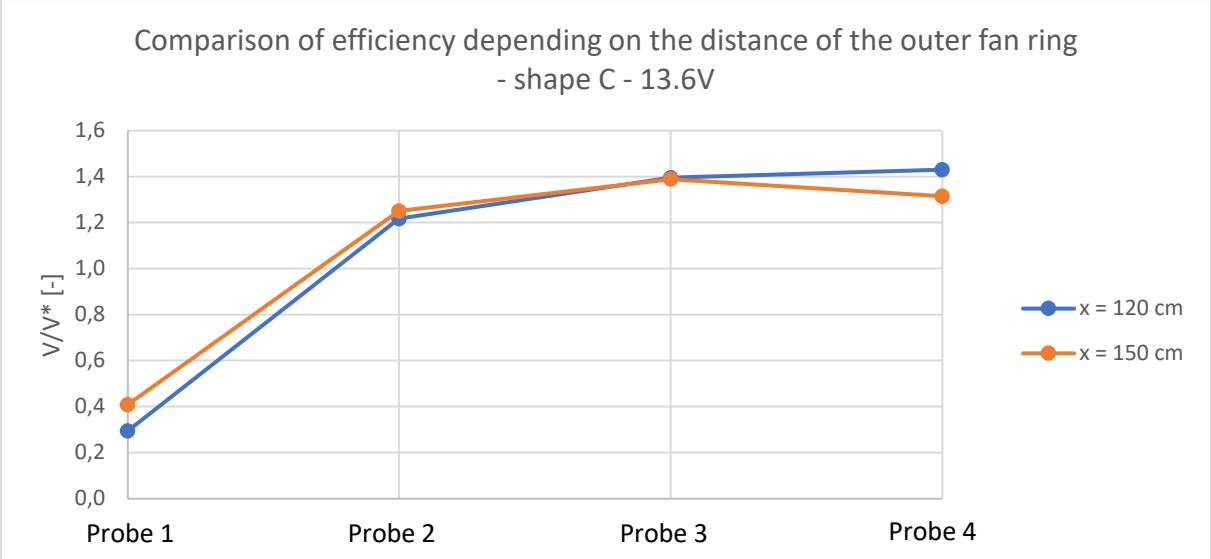

Fig. 8.45: Comparison of the stream velocity at various measuring points to the velocity in front of the fan depending on the distance of the outer ring of the fans - series III and IV, shape C, 13.6 V

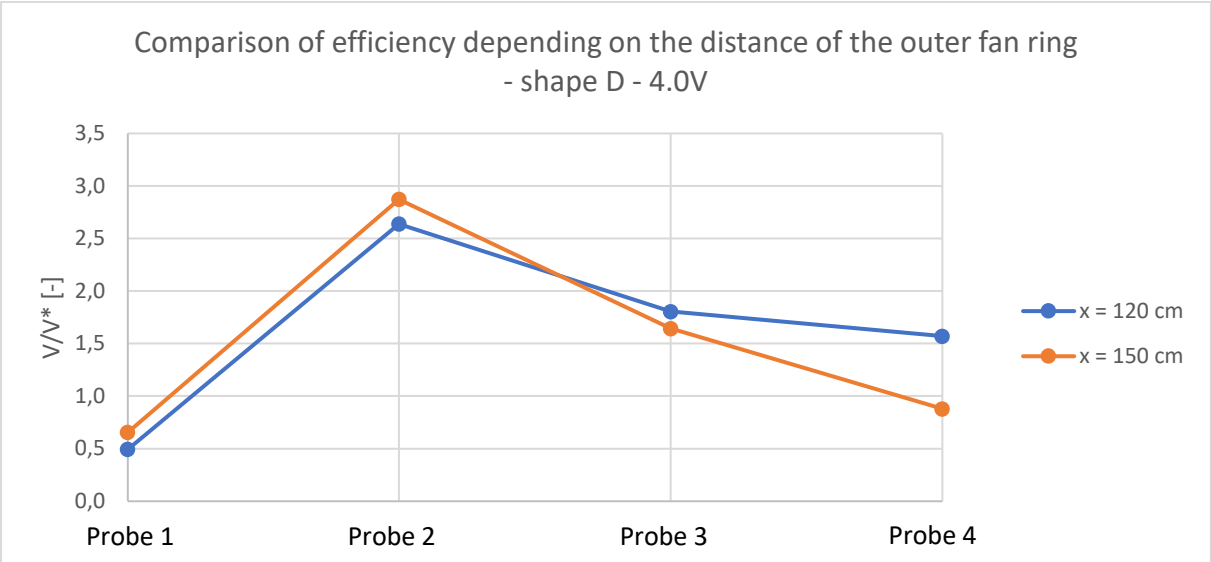

Fig. 8.46: Comparison of the stream velocity at various measuring points to the velocity in front of the fan depending on the distance of the outer ring of the fans - series III and IV, shape D, 4.0 V

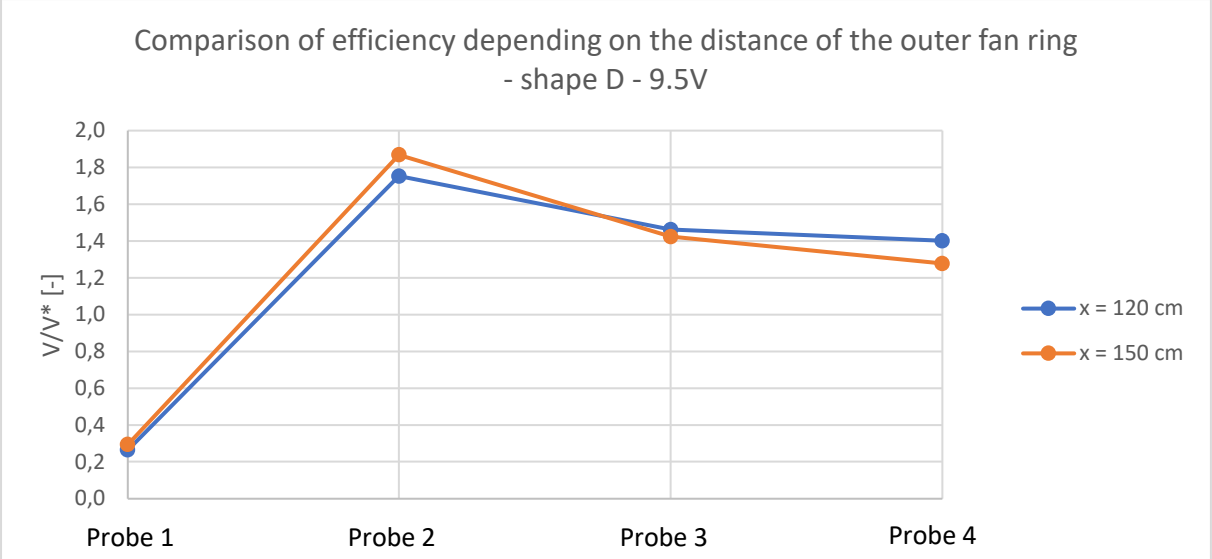

Fig. 8.47: Comparison of the stream velocity at various measurement points to the velocity in front of the fan depending on the distance of the outer ring of the fans - series III and IV, shape D, 9.5 V

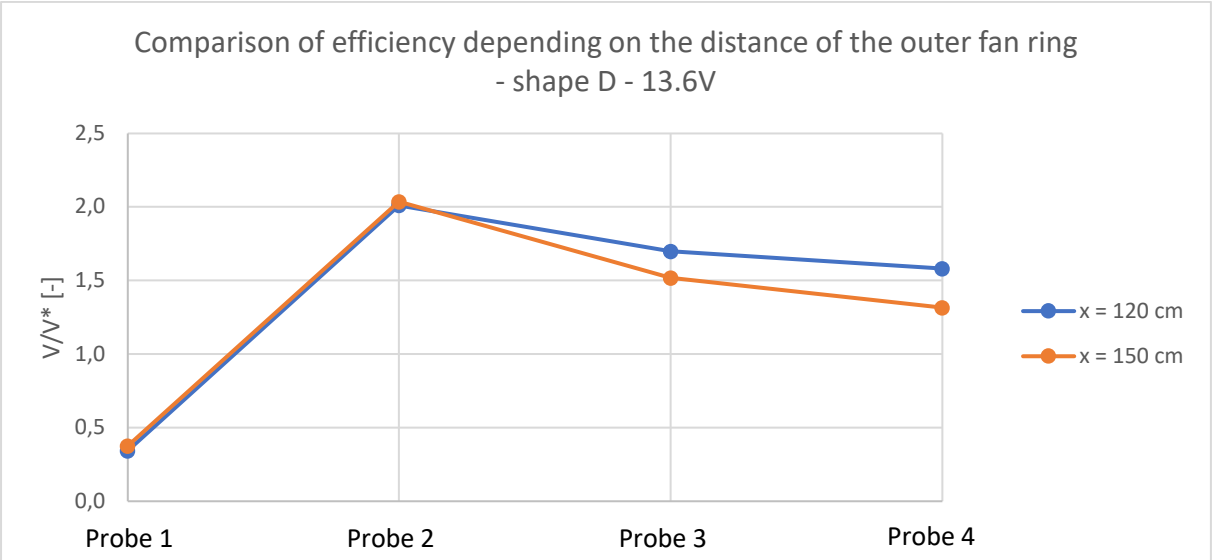

Fig. 8.48: Comparison of the stream velocity at various measuring points to the velocity in front of the fan depending on the distance of the outer ring of the fans - series III and IV, shape D, 13.6 V

Fig. 8.49-54 shows a comparison of dimensionless velocities obtained in tests for different variants of chimney shapes A and B depending on the voltage (4 V, 9.5 V, and 13.6 V) applied to the fans for the 5th series of tests.

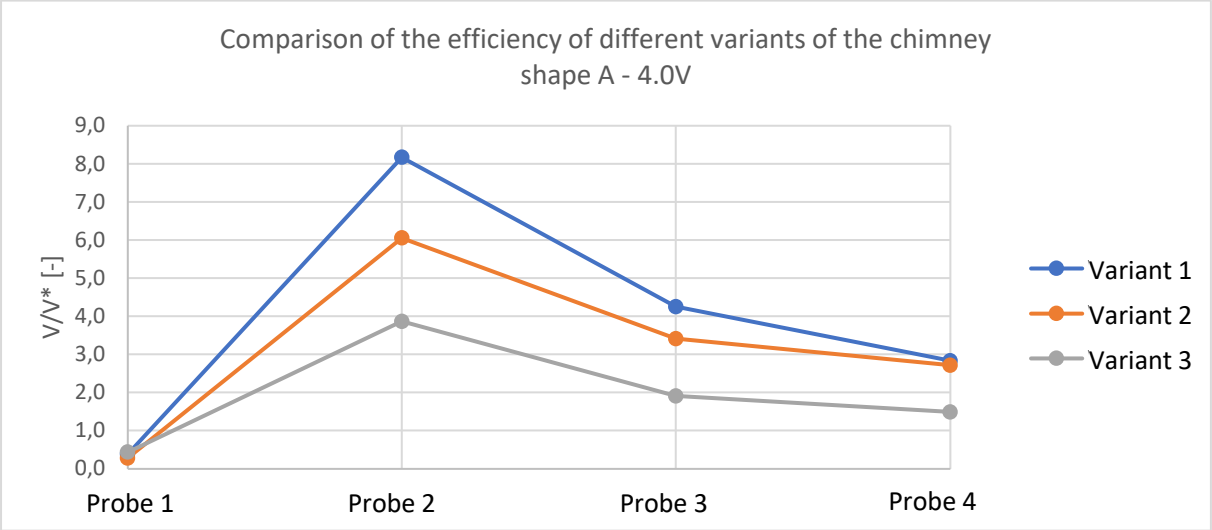

Fig. 8.49: Comparison of the efficiency of different variants of the shape A of the chimney - V series, voltage 4.0 V

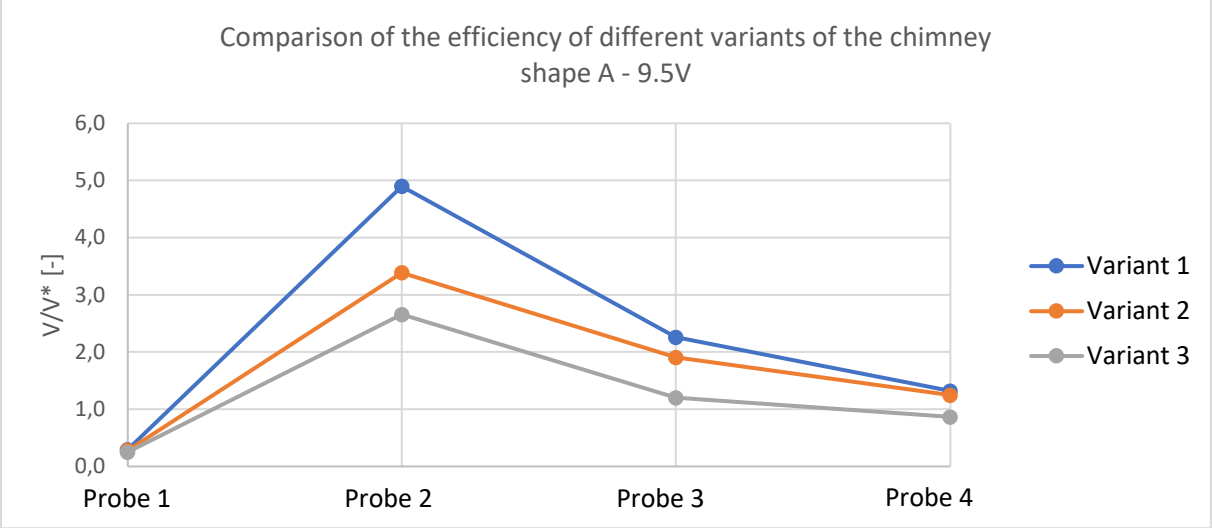

Fig. 8.50: Comparison of the efficiency of different variants of the shape A of the chimney - V series, voltage 9.5 V

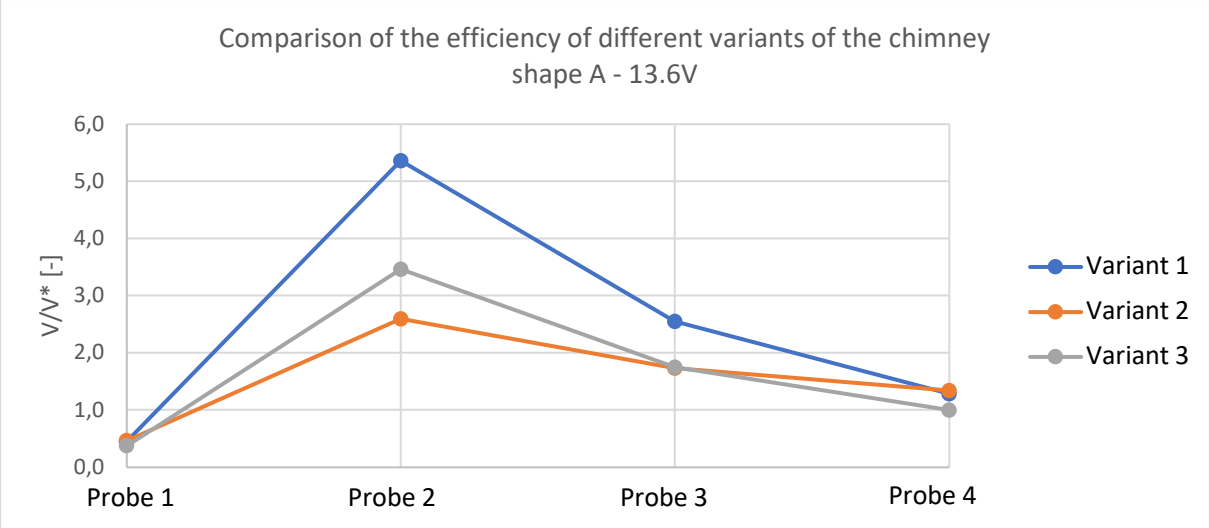

Fig. 8.51: Comparison of the efficiency of different variants of shape A of the chimney - V series, voltage 13.6 V

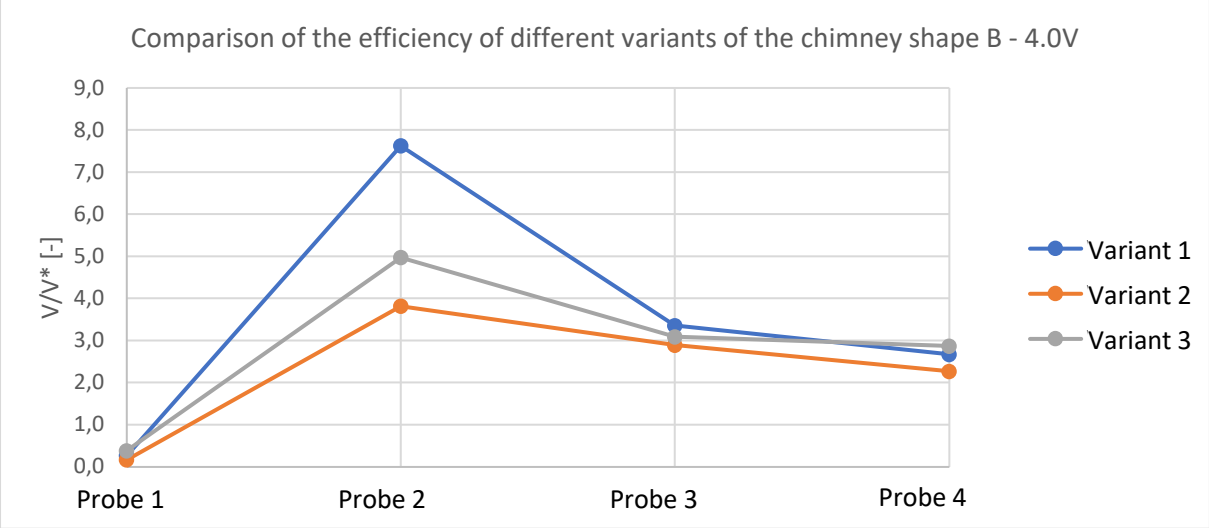

Fig. 8.52: Comparison of the efficiency of different variants of the B shape of the chimney - V series, voltage 4.0 V

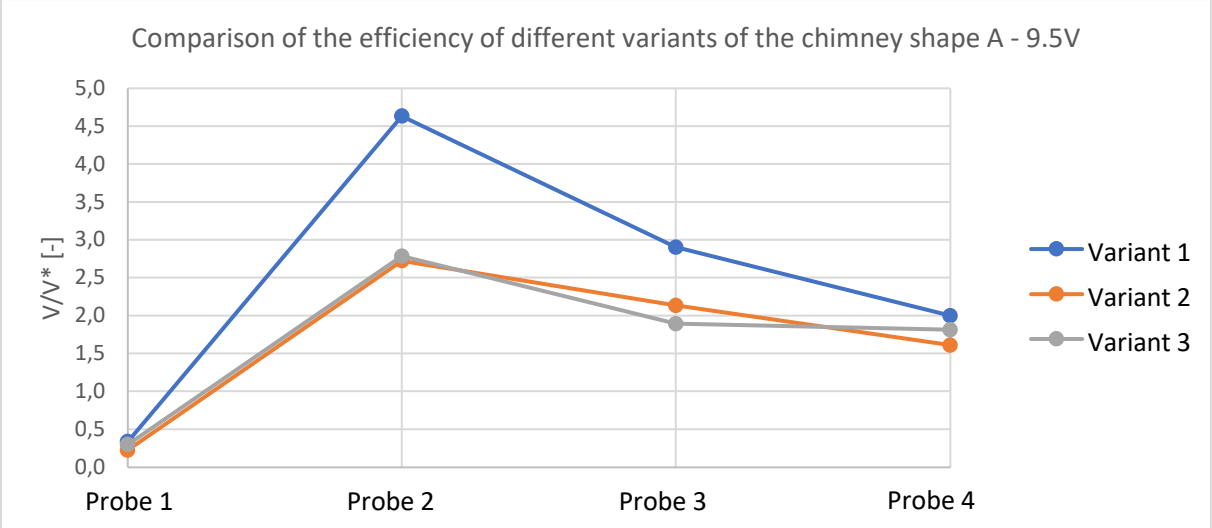

Fig. 8.53: Comparison of the efficiency of different variants of the B shape of the chimney - V series, voltage 9.5 V

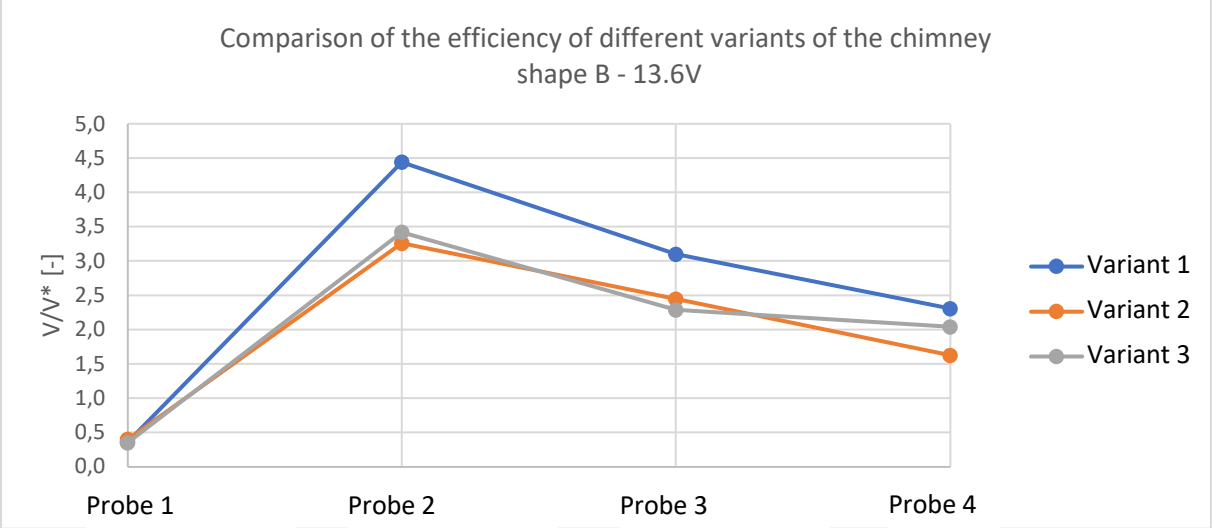

Fig. 8.54: Comparison of the efficiency of different variants of the B shape of the chimney - V series, voltage 13.6 V

Fig. 8.55-8.63 show a comparison of dimensionless velocities obtained in tests for similar variants of chimneys A and B depending on the voltage (4 V, 9.5 V, and 13.6 V) applied to the fans for the 5th test series.

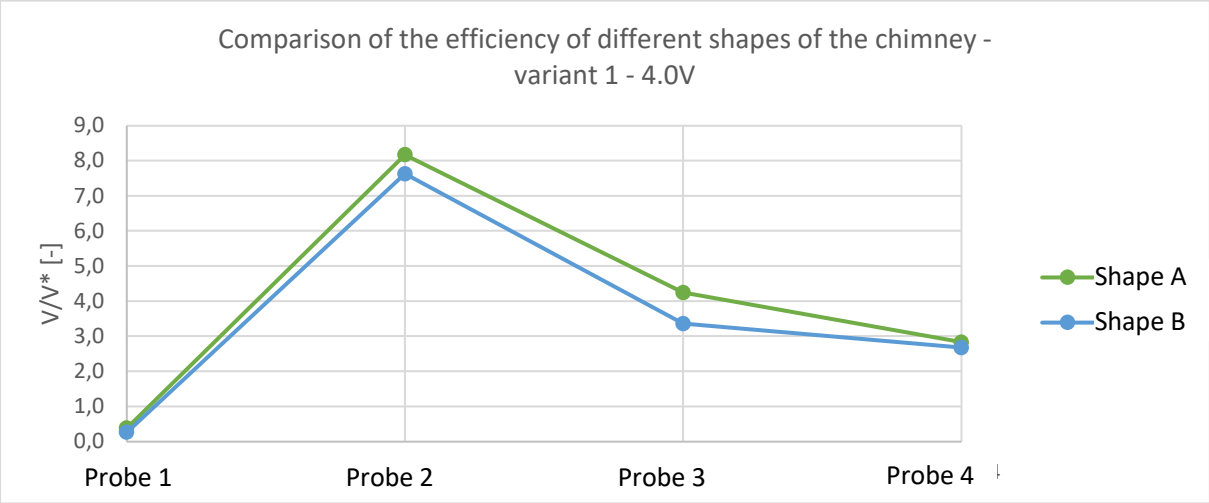

Fig. 8.55: Comparison of the efficiency of similar chimney variants for shape A and B - series V, variant 1, voltage 4.0 V

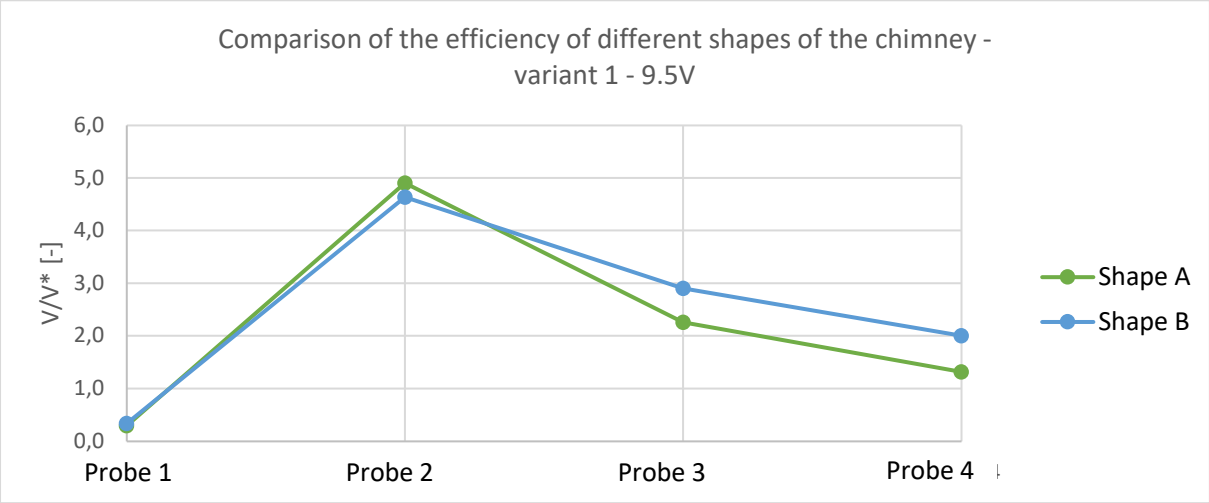

Fig. 8.56: Comparison of the efficiency of similar chimney variants for shape A and B - series V, variant 1, voltage 9.5 V

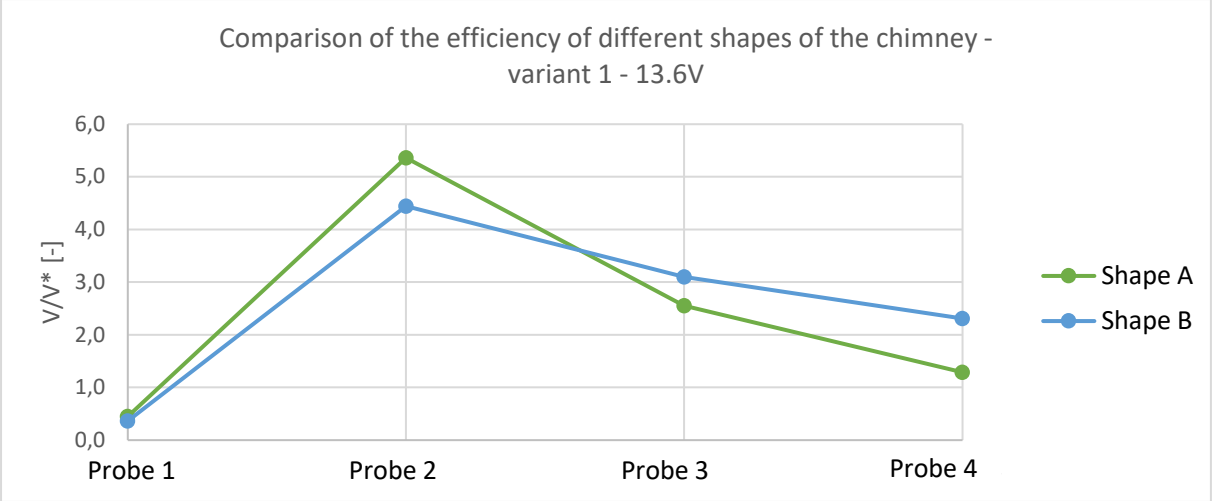

Fig. 8.57: Comparison of the efficiency of similar chimney variants for shape A and B - series V, variant 1, voltage 13.6 V

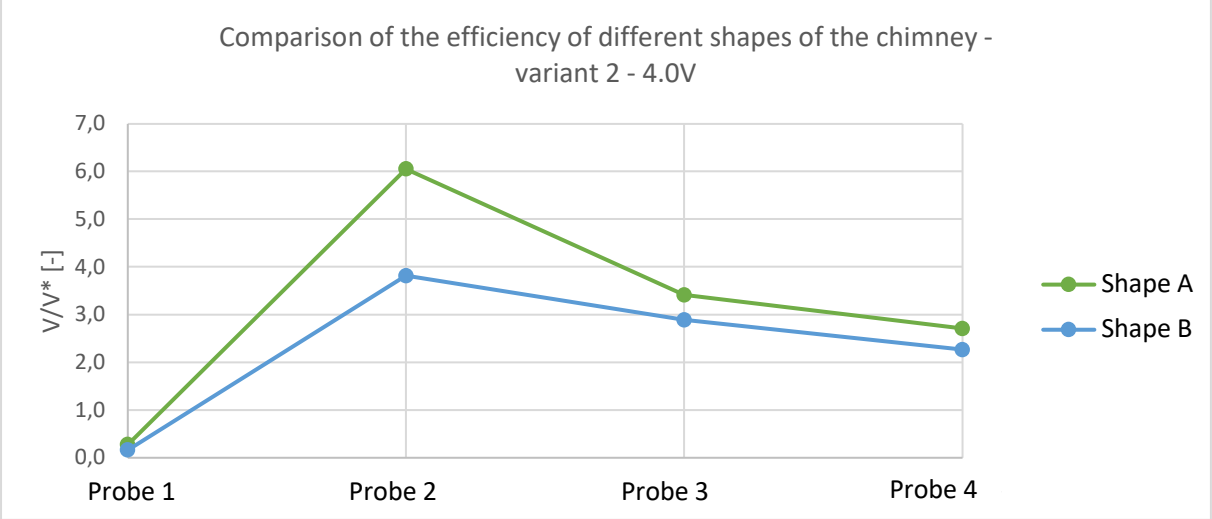

Fig. 8.58: Comparison of the efficiency of similar chimney variants for shape A and B - series V, variant 2, voltage 4.0 V

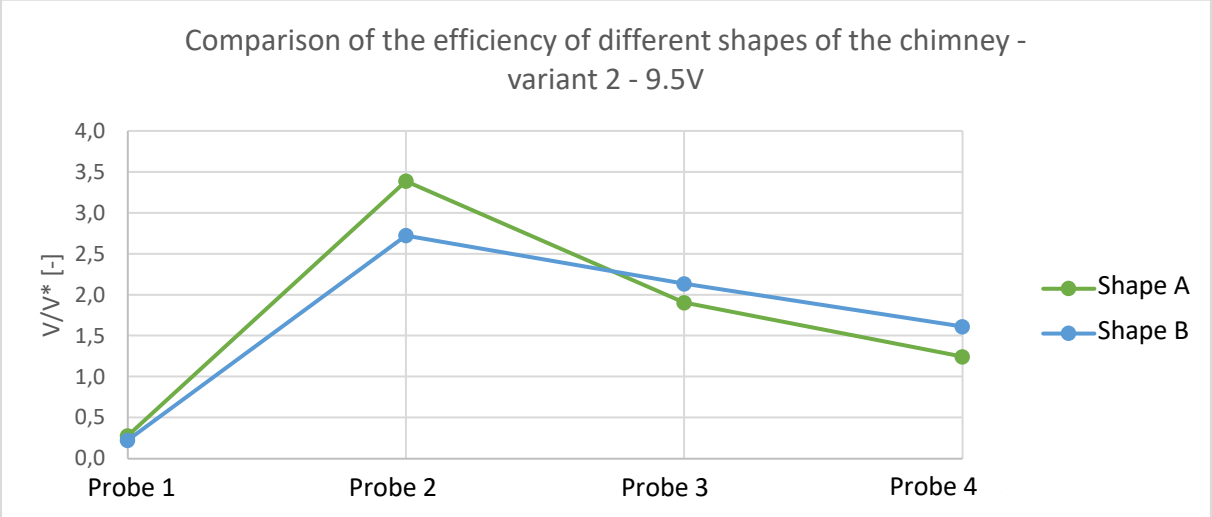

Fig. 8.59: Comparison of the efficiency of similar chimney variants for shape A and B - series V, variant 2, voltage 9.5 V

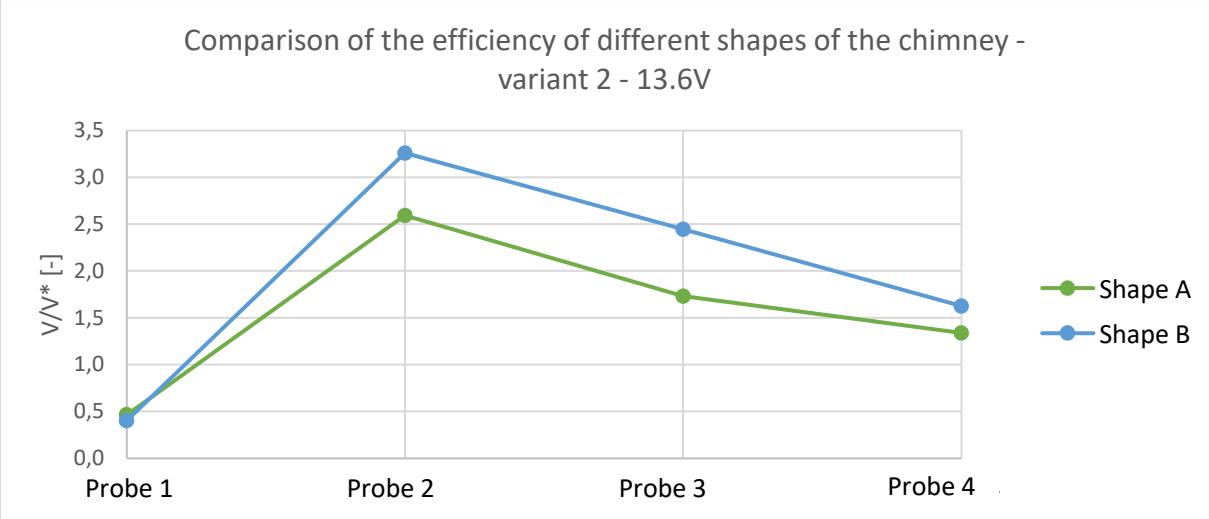

Fig. 8.60: Comparison of the efficiency of similar chimney variants for shape A and B - series V, variant 2, voltage 13.6 V

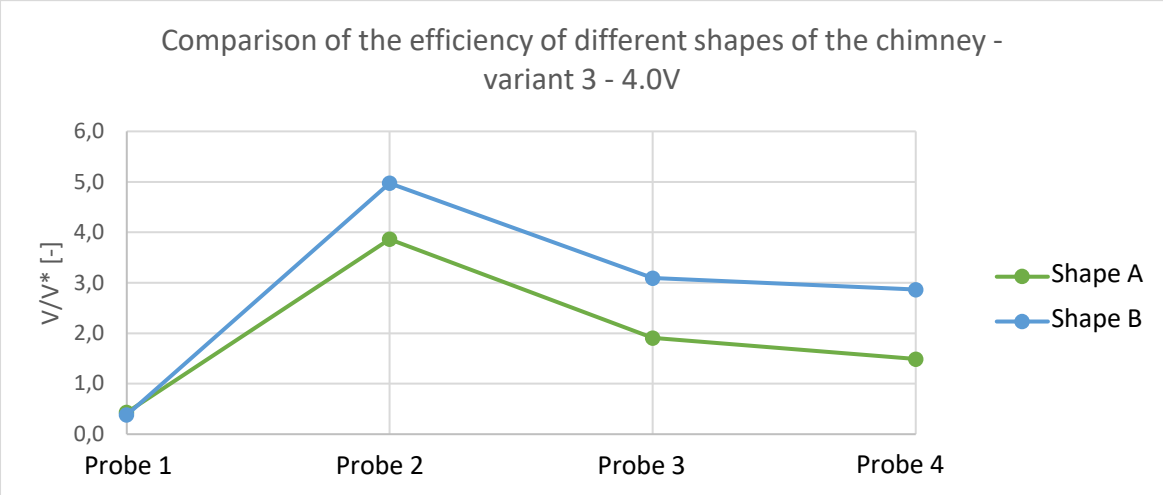

Fig. 8.61: Comparison of the efficiency of similar chimney variants for shape A and B - series V, variant 3, voltage 4.0 V

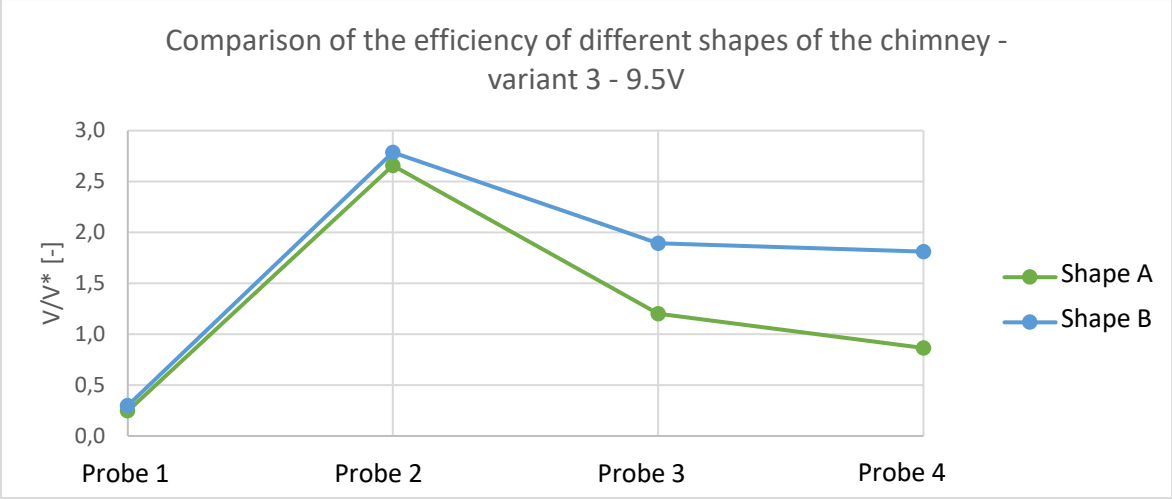

Fig. 8.62: Comparison of the efficiency of similar chimney variants for shape A and B - series V, variant 3, voltage 9.5 V

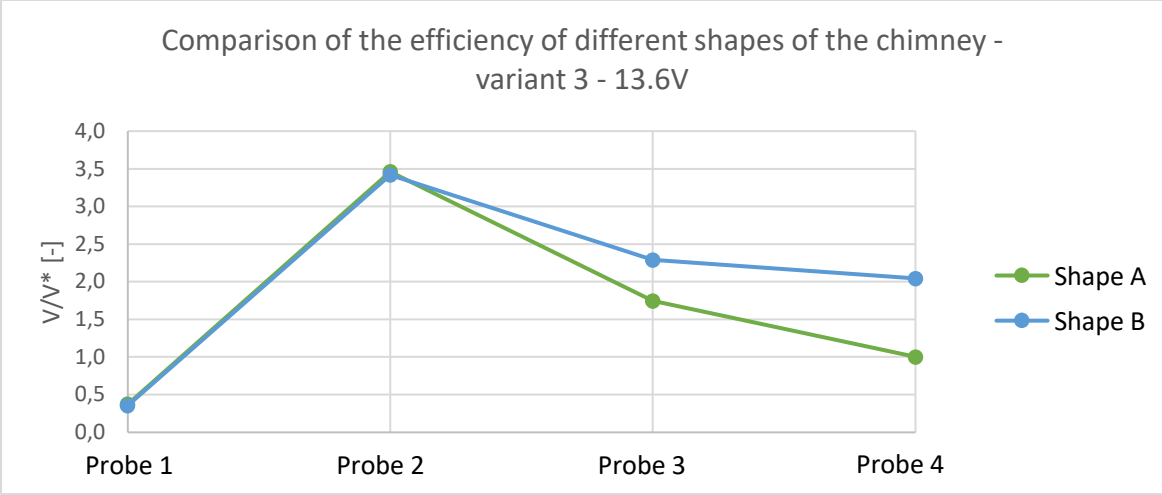

Fig. 8.63: Comparison of the efficiency of similar chimney variants for shape A and B - series V, variant 3, voltage 13.6 V

Fig. 8.64-8.69 show a comparison of dimensionless velocities for variants of chimneys A and B, obtained at different voltages applied to the fans for series IV. This allows us to determine the influence of the Reynolds number criterion on the studied phenomenon.

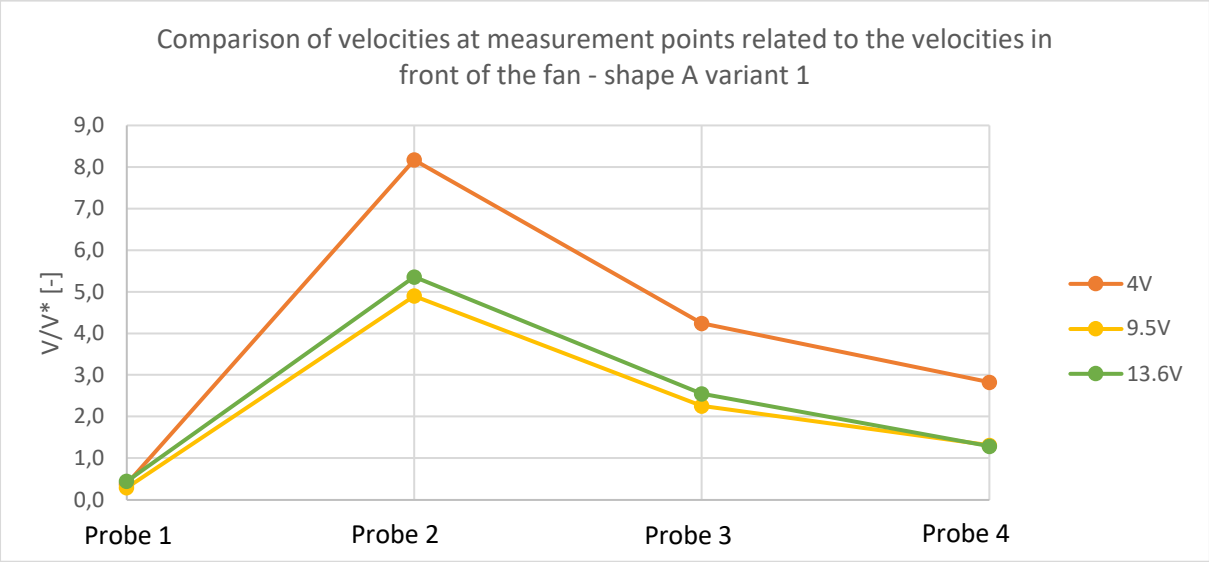

Fig. 8.64: Comparison of the stream velocity at various measurement points in relation to the velocity in front of the fan for various voltages supplying the system - V series, shape A, variant 1

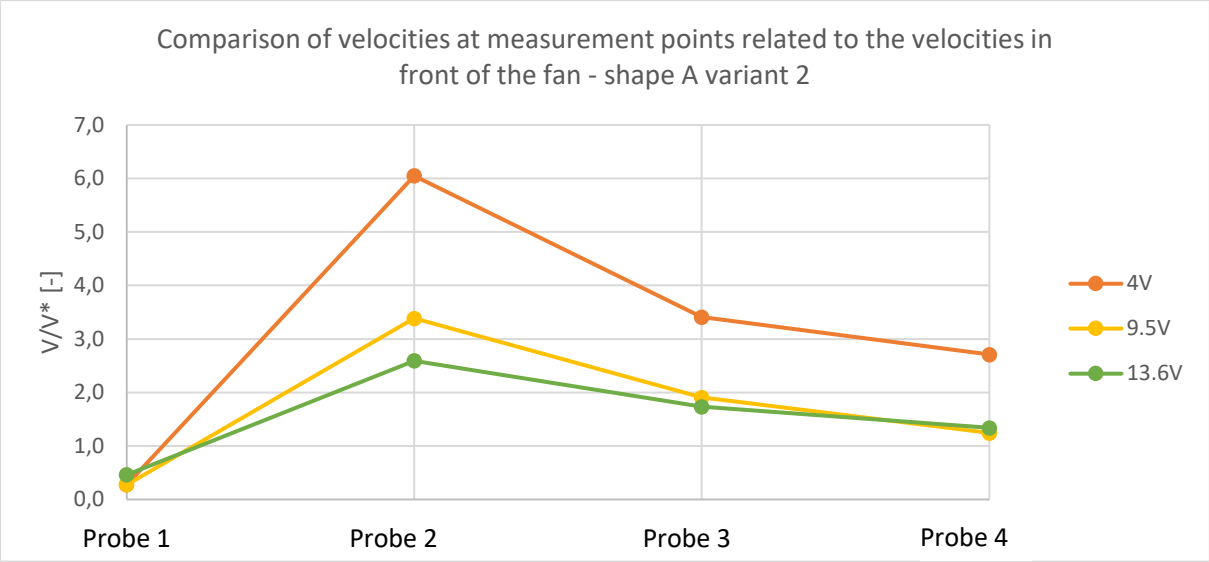

Fig. 8.65: Comparison of the stream velocity at various measurement points related to the velocity in front of the fan for various system supply voltages - V series, shape A, variant 2

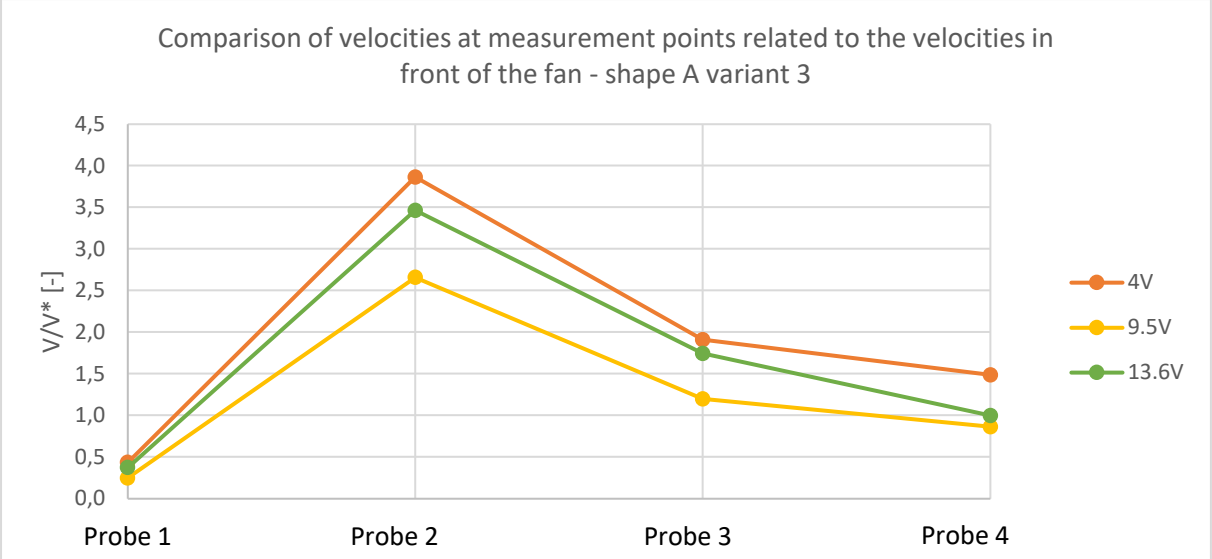

Fig. 8.66: Comparison of the stream velocity at various measurement points to the velocity in front of the fan for various voltages supplying the system - V series, shape A, variant 3

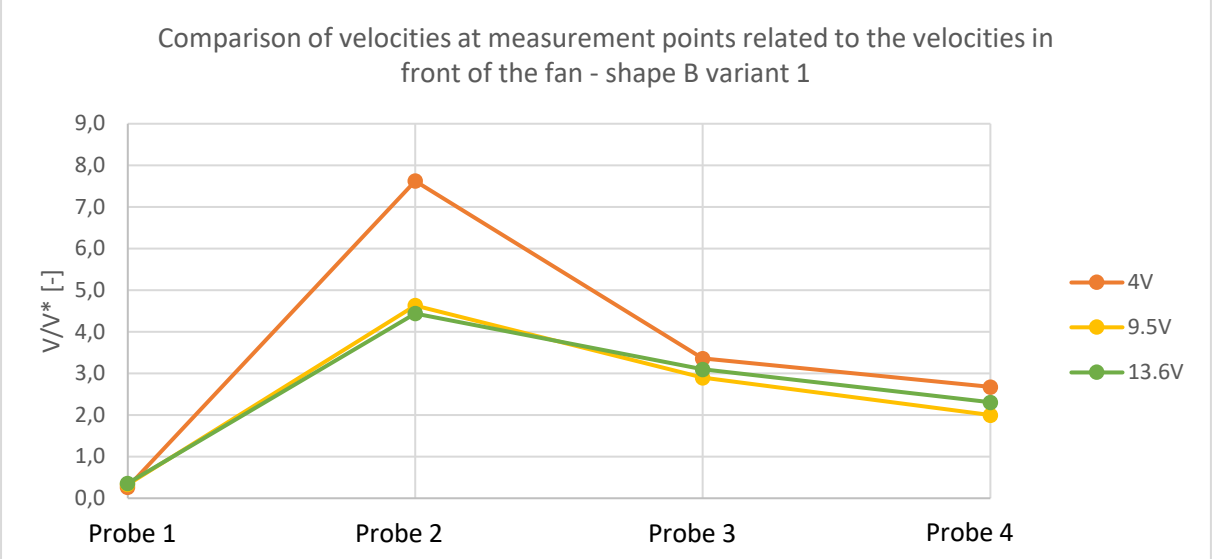

Fig. 8.67: Comparison of the stream velocity at various measurement points related to the velocity in front of the fan for various system supply voltages - V series, shape B, variant 1

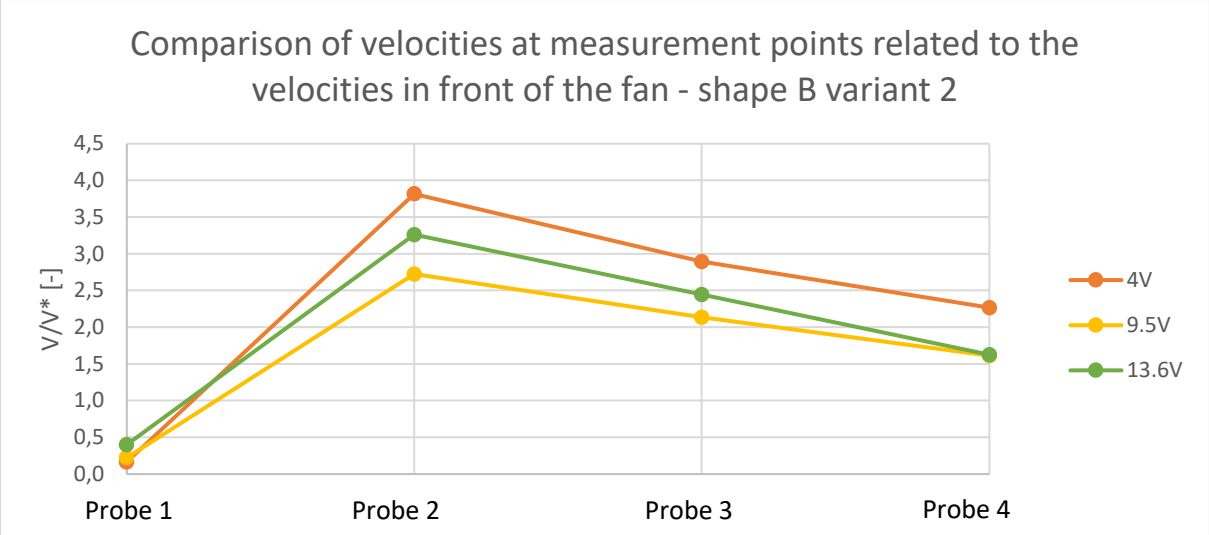

Fig. 8.68: Comparison of the stream velocity at various measurement points to the velocity in front of the fan for various voltages supplying the system - V series, shape B, variant 2

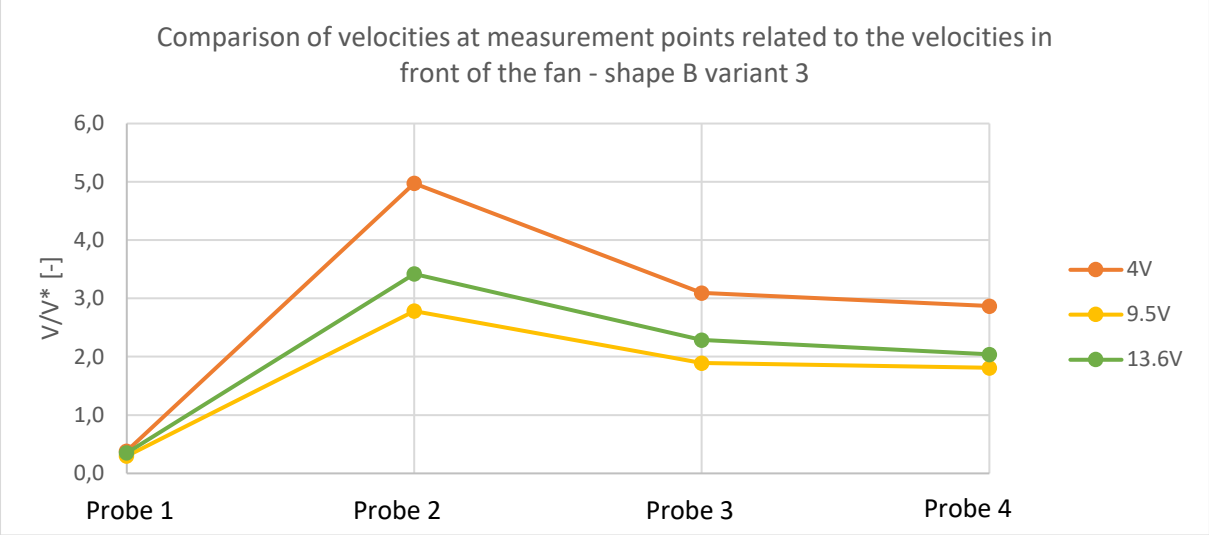

Fig. 8.69: Comparison of the stream velocity at various measurement points to the velocity in front of the fan for various voltages supplying the system - V series, shape B, variant 3

8.6. Analysis and conclusion for the results of the III stage (ventilation chimneys)

Series III

Probe 1 has been placed at a point where the air stream produced by the outer ring of fans disappears, but there is no significant draft from the stack inlet fan yet. Obtaining a velocity exceeding the background velocity at this point, therefore, means that there is an interference between the outer ring and the chimney inlet fans. This results in stream continuity within the system. The speed at this point is similar for each type of chimney.

The comparison of chimneys presented in Fig. 8.23-8.25 shows that the velocity over the chimney outlet (probe 2) is the highest in the case of shapes A and B, which results

directly from their similarity to the confusor. The velocity on probe 3, placed on the model under the inversion layer, is still clearly higher for these two types of chimneys. At probe 4 (placed at the height corresponding to 1 km above the ground surface, i.e. approximately the height of the temperature inversion layer of the atmosphere), similar values of dimensionless velocity are obtained for all shapes of chimneys. This is important primarily from the point of view of economics and the technology of implementing the solution on a real scale - the possibility of obtaining similar results in the absence of a ventilation chimney (shape D) would mean a significant reduction of costs and facilitate the feasibility of the solution.

For shape C of the chimney, results obtained for each probe were at a similar or worse level in relation to shape D, which practically disqualifies this shape for possible implementation in the project. In the case of shape D, it should be determined whether the vertical air stream formed above the chimney is formed in a similar way as in the case of shapes A and B, i.e. it is not too turbulent.

From the comparison of the same shapes of chimneys at different voltages (Fig. 8.26-8.29) it can be seen that while at higher velocities of the stream produced by fans (at voltages of 9.5 V and 13.6 V) the dimensionless velocities at individual points are similar, the graph for the lowest (4.0 V) differs significantly from them. This proves the influence of the Reynolds number on the phenomenon at lower values of the stream velocity. According to the graphs, in this case, the air velocity at the chimney inlet is relatively highest in relation to the velocity of the air stream generated in front of the fan, however, obtaining such efficiency would not be possible on a natural scale, where it would be necessary to produce higher speeds on the fans.

Series IV

Graphs comparing the shape of individual chimneys with the outer ring distance reduced from 150 cm to 120 cm (Fig. 8.30-8.32) are similar to the graphs obtained for series III. It is worth noting here that at higher speeds (voltages 9.5 V and 13.6 V supplied to the fans), the air velocity of the vertical air stream on probe 4 (inversion layer) is higher for chimney B in relation to other chimneys, which give similar results. Also, the comparison of the influence of the Reynolds number on the phenomenon (Fig. 8.33-8.36) gives similar results as those obtained in series III. For the voltage of 4.0 V, the dimensionless air velocities values differ from the values for the other voltages given on the fans. The graphs presented in Fig. 8.37-8.48 suggest that the influence of the external fan distance on the air stream continuity (measured by the air velocity on probe 1) is negligible. The air stream continuity is maintained for both series, and the air velocity on this probe has similar values for both series. For chimney B, the air velocities over the chimney outlet are lower at a closer distance to the outer ring. For shape D, however, the values on probe 4 are higher at a closer distance of the first ring of fans.

V series In series V of the tests, the shapes of chimneys A and B were taken into account with various variants of reducing the height. This would allow for easier and more cost-effective construction of chimneys in the case of the implementation of the project. Fig. 8.49-8.54 presents a comparison of shape variants A and B at different air velocities

resulting from the voltage applied to the fans. In the case of chimney A, the differences in the air stream velocity at the chimney outlet are significant and depend on the height of individual variants. On the other hand, the air velocities on probe 4 (corresponding to 1 km above ground level) for variants 1 and 2 are very similar, which suggests the possibility of using a lower chimney height for a similar final effect. The air velocities at the outlet of the chimney B for variants 2 and 3 are similar, while for variant 1 significantly higher values were obtained. On probe 4, similar values were obtained for the chimney shape B for all three variants and it is worth noting that the air values obtained for variant 3 (half-reduced) of the chimney are slightly higher than for the higher structure of variant 2.

Comparing the variants of the chimney A shape with the variants of the chimney shape B of a similar height (Fig. 8.65-8.63), it can be observed that the air velocity at the outlet reaches similar values for variants 1 and 3 for both shapes, while for variant 2 these velocities differ: for lower resulting from the voltage applied to the fans (4.0 V and 9.5 V), the air stream velocity at the chimney inlet is higher for chimney A but for a higher speed (13.6 V) this air velocity is higher for chimney B. Air velocities values on probe 4 are higher for chimney B. The biggest difference can be seen in the third variant of both shapes of the chimney. The effect of the Reynolds number on the test results in this series (Fig. 8.64-8.69) is similar to the two previous series. The relative air velocities values for individual measurement points are similar for the speed at 9.5 V and 13.6 V, but much higher at 4.0 V.

8.7. Fog visualization

As the last task in stage III, a smoke visualization of the operation of the ventilation system in a radial configuration was performed.

Many smoke visualizations of the examined phenomenon were made with various parameters (shapes of the chimney, distances from the outer ring of the fans to the chimney, and the inclination of the fans) to evaluate the phenomenon qualitatively. For the visualization, a heavy smoke generator using dry ice and steam was used to model and visualize a layer of polluted air/smog. After the initial introduction and even distribution and stabilization of the layer of smoke remaining low on the floor in the room, the fan system was started.
In addition to the shapes and variants of the chimneys described in point 7, a second variant of the shape D (inlet fans without a chimney) was also used, consisting in rebuilding the base and directing the inlet fans at an angle of 6º to the horizontal, which resulted in the location of the focal point of the fans about 1 m above the fans. In this configuration, the setting of the fan ring has also been changed - they have been directed upwards at an angle of 15º to the horizontal.

Fig. 8.70-8.73 shows examples of smoke visualization of systems with different types of chimneys. The photos show the situation after the room has been smoked without the system running, the system operation in the room with smoke, and the situation in the room after the system operation has ended.

a)

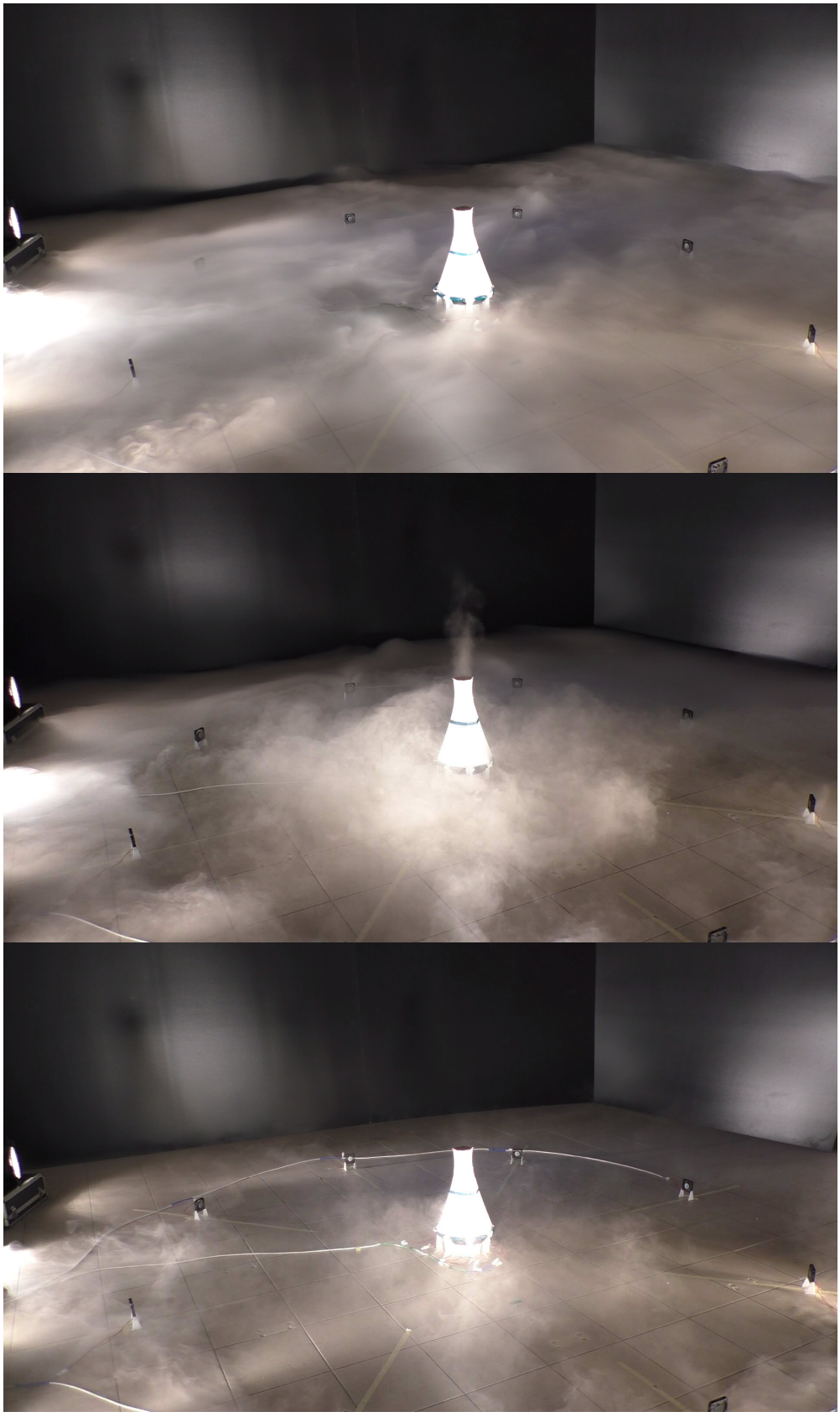

b)

c)

Fig. 8.70: Pictures of smoke visualization showing the qualitative effects of the system operation - chimney shape B variant 1: a) heavy smoke after distribution in the ground floor b) dynamic ventilation system with a chimney during operation c) system after ventilation is completed

a)

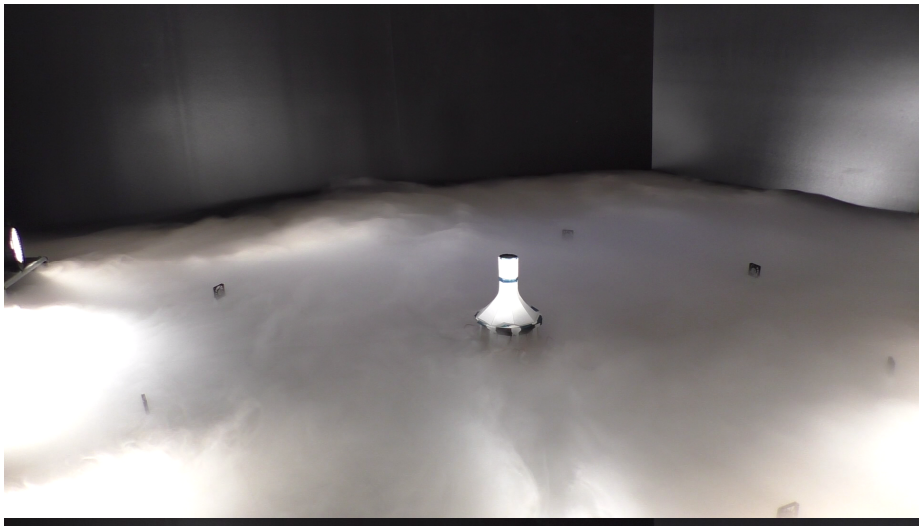

b)

c)

Fig. 8.71: Pictures of smoke visualization showing the qualitative effects of the system operation - chimney shape A variant 2: a) heavy smoke after distribution in the ground floor b) dynamic ventilation system with a chimney during operation c) unfavorable interference of streams from the outer ring fans with vortices forming at the chimney, causing disturbance of the efficiency of the system

a)

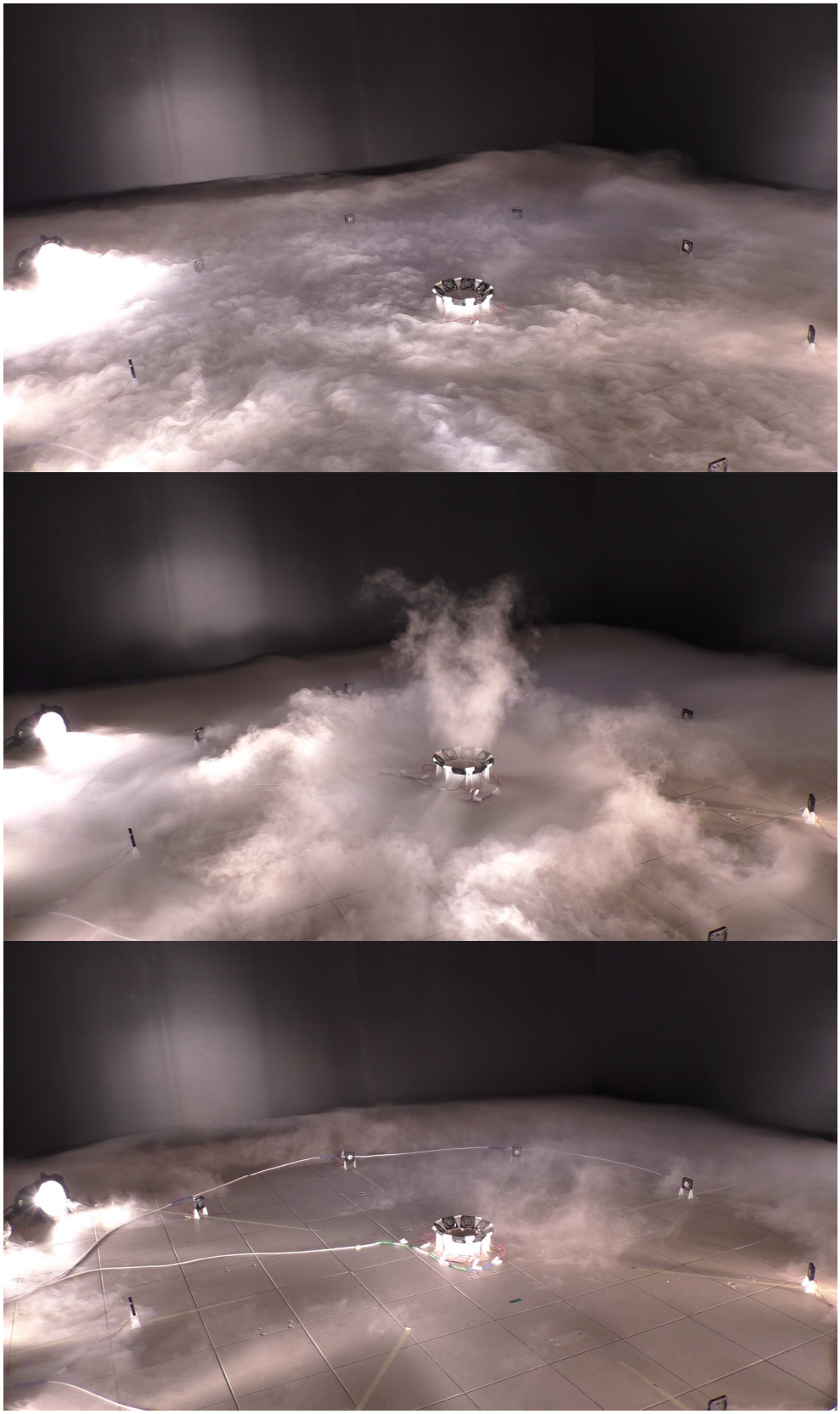

b)

c)

Fig. 8.72: Pictures of smoke visualization showing the qualitative effects of the system operation - chimney shape D variant 1: a) heavy smoke after distribution in the ground floor b) dynamic ventilation system with a chimney during operation c) system after ventilation is completed

a)

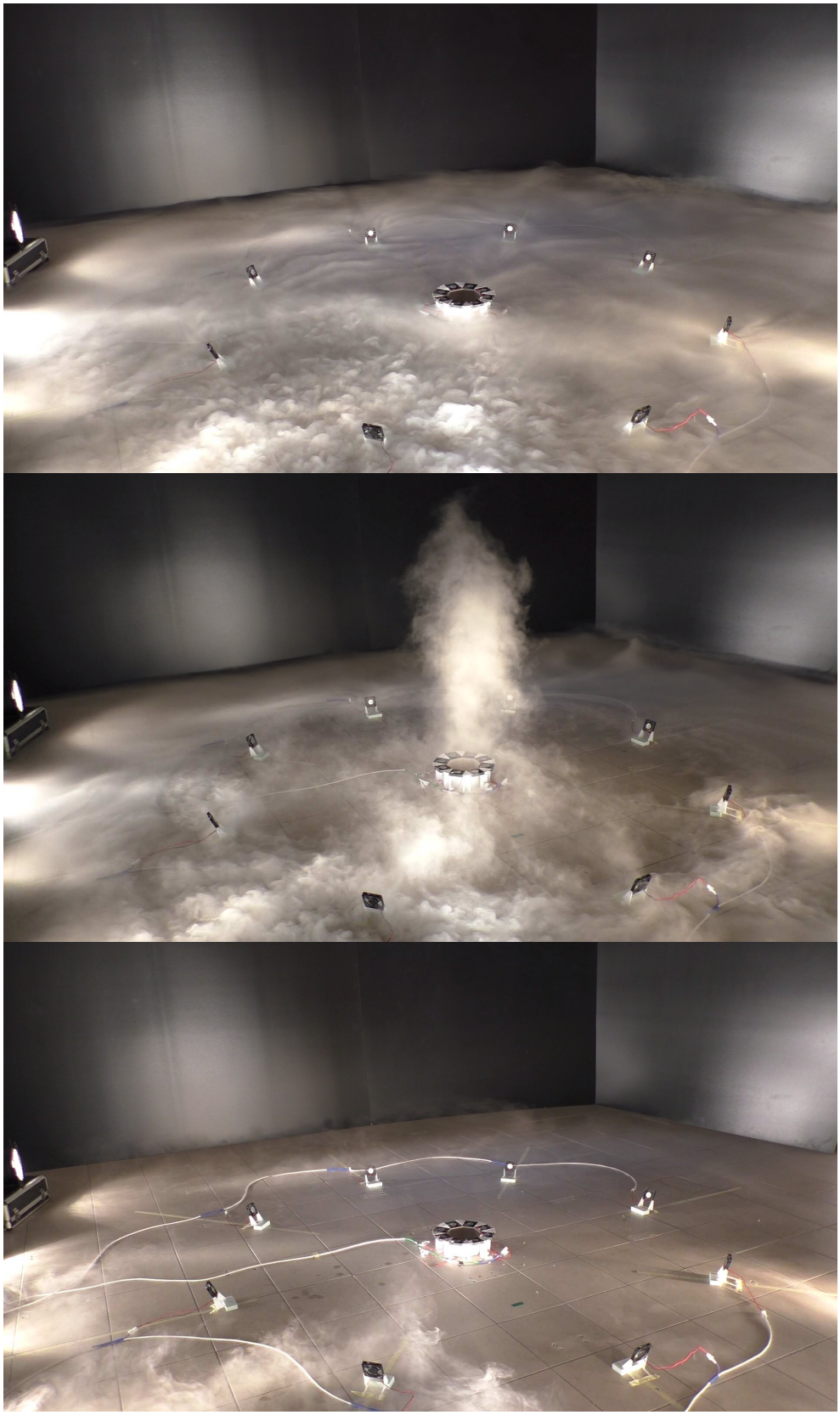

b)

c)

Fig. 8.73: Pictures of smoke visualization showing the qualitative effects of the system operation - chimney shape D variant 2: a) heavy smoke after distribution in the ground floor b) dynamic ventilation system with a chimney during operation c) system after ventilation is completed

8.8. Conclusion of fog visualization

During the smoke visualization, clear cooperation of the ventilation chimney with external ventilation towers was observed. In the first stage of ventilation, the chimney inlet fans move the masses of polluted air from its immediate surroundings in a vertical direction through the chimney, which results in the creation of a significant height clear air stream above the chimney. On the other hand the fans of the outer ring move masses of polluted air towards the chimney, effectively cleaning the space in front of them to a distance of several dozen centimeters and concentrating the polluted air in front of the chimney. In the next phase of the system work, the inlet fans introduce the supplied and accumulated around the chimney polluted air into the chimney, and then, they exhaust it by the outer ring fans upwards. The effect of this is the formation of a less distinct (polluted) air stream, which, however, persists for a longer time. Ultimately, the solutions result in ventilation of the affected area initially contaminated with heavy smoke.

In the case of variant 2 of the shape of the chimney A (Fig. 8.71), the formation of vortices can be observed (probably due to the shape of the outer shell of the chimney), which does not allow the inlet fans to effectively collect the air masses supplied by the outer ring fans. This causes the accumulation of polluted air masses around the chimney. In the case of variant 1 of the chimney D shape the air stream formed above the chimney is wide, but strongly turbulent. Locally formed eddies can be seen in its structure. This may result in a final reduction in the efficiency of this type of construction through excessive dispersion of the removed mass of polluted air. Therefore, variant 2 of the chimney shape D was proposed, which turned out to be the most effective from the point of view of creating a uniform stream cone with a large range and the time needed to ventilate the area.

9. TESTING THE POSSIBILITY OF PENETRATING THE INVERSION LAYER

In stage IV, the research focused on the possibility of penetrating the inversion layer and on the size and efficiency of the generated vertical air stream. The preparation of the measuring set up and model tests were entirely carried out by the author. Due to the complexity of the problem and the lack of scientific studies on the subject, the preparation of the research was preceded by establishing a physical model of the phenomenon and making numerous assumptions and simplifications.

9.1. Model of the inversion phenomenon

As mentioned earlier, the inversion layer can form at different times and for different reasons. In further consideration, it was assumed that the considered active ventilation system would operate during the most unfavorable smog episodes, i.e. wind calms lasting several days, in the inversion layer at the level of 300-500 m above ground level and especially in winter.

The first problem is the assumption of a model vertical temperature distribution. We have quite limited measurement data in which smog episodes and the occurrence of the inversion layer were described. In these data, it is difficult to distinguish which inversions were short-lived and which lasted several days, and what was the exact thickness and height of the inversion layer, temperature gradient, and wind speed. All these parameters are constantly changing over time, creating unique weather. Therefore, the temperature distribution proposed by the author should be treated as an idealized model assumption, which in the future may be the subject of separate meteorological research. For this thesis, due to limited resources, it was decided to adopt the probable temperature distribution proposed by the author. Another assumption is the invariance of the adopted distribution over time. Temperature, pressure, and humidity are always subject to daily oscillations, however, at this stage of research, we are unable to imitate these changes in a model scale.

An attempt to describe the physics of the phenomenon was preceded by considerations based on tracing the path of a certain volume of polluted air. Low emission is the main cause of air pollution in Krakow and sOutern Poland, therefore, further considerations focus only on low emission air pollution. When the fumes from the furnaces leave the chimney, they have a temperature much higher than the surroundings and a lower density, thanks to which a strong convection current is created and lifts them up. The fumes from low-quality household stoves contain a lot of dust, but also gases such as sulfur, nitrogen, and carbon oxides. When we consider a certain flue gas volume, we notice that the convection current acts with an upward force, which decreases as the height and temperature of the flue gases decrease and their density increases, see Fig. 9.1. Dust particles that are suspended in the considered volume rise upwards as long as the lifting force from the convection current is higher than the force of gravity acting on a single particle. Of course, the smaller the particles, the less force is needed to keep the particle in the air. Therefore, in the first place, the heaviest particles will stop at a certain height, and when the air cools down, and the force of gravity will be greater than the lifting force, they will fall right next to the chimney, creating a characteristic black tarry deposit. Further, depending on the weather conditions (we assume almost windless weather), smaller and smaller particles will stop as the altitude increases, creating a distribution of pollutant sizes from the largest and heaviest near the ground to finer and lighter at higher altitudes. From a certain size, the particles will not fall but will float in the air, creating the so-called suspended dust.

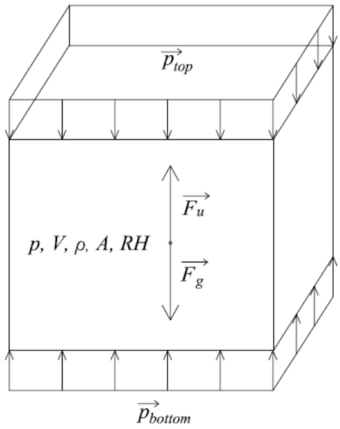

Fig. 9.1. The considered volume of air and the forces acting on it.

If the considered volume of air does not cool down quickly enough, it may rise to the height of the base of the inversion layer. Then, having a certain speed and at the same time inertia, it will begin to mix with it both through convection and diffusion, slightly breaking the inversion layer and creating a certain transition zone. If the inversion layer is sufficiently thin, it will be broken up by warm exhaust fumes which will rise further above it, successively dispersing in the air. However, if the layer is very thick, the flue gases will be trapped under the inversion layer. The buoyancy force of the exhaust gases will be balanced by the gravity force of the inversion layer (see Fig. 9.2.). In this way, the next portion of exhaust gas rising earlier will meet the retained exhaust gas without reaching the inversion layer at all and without exerting a major impact on it. So we can see that the pollutants will accumulate under the inversion layer going lower and lower until the ground level. At the same time, the heaviest particles of pollution will accumulate from the ground level up, accelerating the moment when all the air under the inversion layer will be saturated with exhaust gases. Then we have a serious smog episode. From the described mechanism, it can therefore be assumed that at a certain height above the terrain, there is a space that will be permanently polluted at the very end.

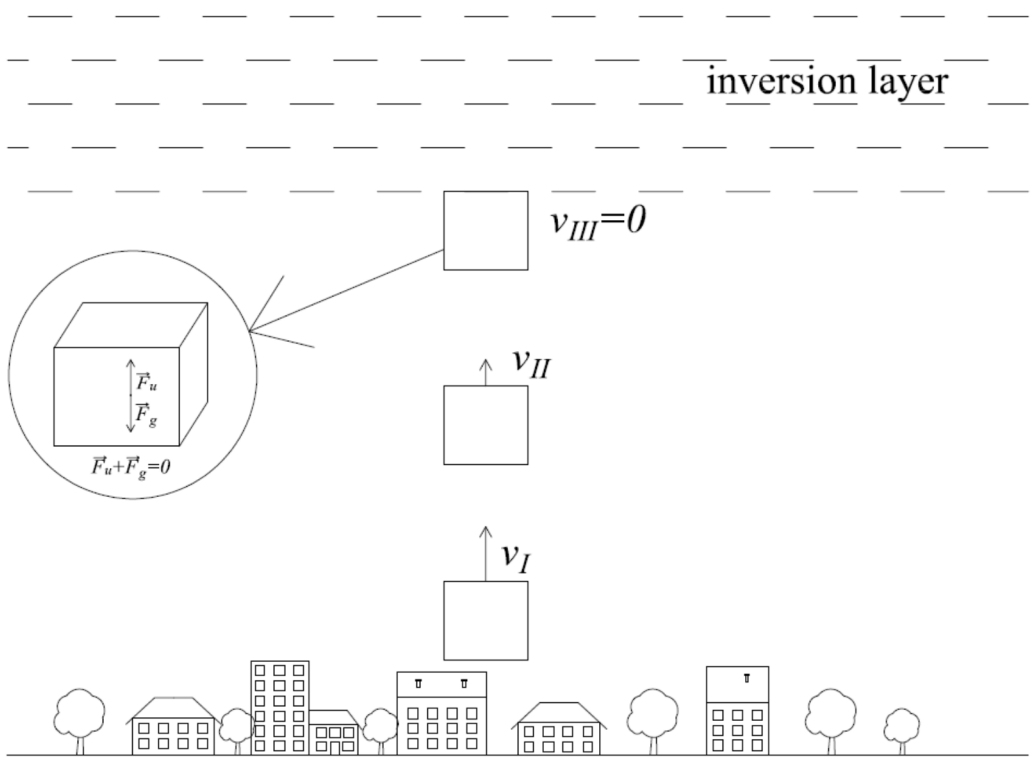

Fig. 9.2. The successive stages of rising of the considered air volume until it stops under the inversion layer.

The most important parameters that affect the movement of the considered air mass are:

- temperature, which should decrease with increasing altitude because heat will be released to the environment,

- density - depends on temperature, humidity, and pressure,

- the pressure depends on the height, but its change depends on the density of the layers above

- relative humidity - depends on temperature, pressure, and an initial amount of water vapor in the air. It should also be remembered that moist air has a lower density than dry air and that when relative humidity exceeds 100%, water vapor will condense in the form of fog. If during this time there are appropriate conditions for condensation and growth of large droplets, precipitation may occur and thus a sudden decrease in humidity - part of the water from the considered volume will be removed.

As can be seen, the above parameters are mutually dependent and it is impossible to isolate one of them without taking into account the influence of the others. Due to the lack of extensive measurement data of all four values depending on the height, the author attempted to construct a drone that could measure these data. The idea was to equip a small drone with measuring equipment that could simultaneously record temperature, pressure, density, and humidity. The measuring drone would rise to a height above the inversion layer, i.e. about 1000m, and then, gradually lowering the flight, collect measurement data from different heights. However, the idea was not implemented due to the lack of available humidity sensors that would be light enough and have a fast response time so that the measurements could be made in a reasonable time, taking into account the limited time the drone hovers in the air. An additional problem turned out to be

the regulations regarding permission to fly a drone at higher altitudes. The procedure of obtaining permission for a high flight takes several months, and it is not possible to predict the occurrence of inversions and smog episodes so far in advance. Therefore, it would be necessary to apply for several dozen permits covering various days on which smog and inversion may potentially occur. The subject of direct measurements of the physical parameters of smog and the inversion layer has been included in further development directions.

It also should be remembered about factors outside the considered system, such as wind and terrain. Locally, they can cause vertical air movements and change their speed. For this model, we assume their negligible influence as we are dealing with the case of nearly windless weather.

Assumptions and simplifications:

1. The model refers to a smog episode lasting several days, i.e. a fixed inversion layer at an altitude of 300-500m above sea level, wind speed < 2ms, and a smog layer at a height of 0-300m above ground level
2. In the layer above and below the inversion layer, the temperature gradient is 0.6°C/100m height (typical value for a humid-adiabatic gradient).
3. The layer from the ground to the inversion layer is treated as homogeneous air with evenly distributed pollutants - in nature, the distribution of pollutants is not uniform, heavier dust will accumulate closer to the ground, and at the same time, warm exhaust gases will rise upwards at first, creating convection microcurrents.
4. We ignore the electrostatic forces that may act on the particles of impurities.
5. The aerodynamic resistance of the inversion layer is represented by the resistance of the mesh.
6. The model describes the situation for the equilibrium state of the steady atmosphere, i.e. the moment just before turning on the ventilation system and at the beginning of its operation, i.e. the moment of breaking the inversion layer. In fact, when the inversion layer breaks through, the air forming it will be mixed and replaced by polluted air flowing vertically, and the balance will be disturbed. Thus, the resistance of the inversion layer will decrease. If we want to recreate this in laboratory conditions, we should remove the mesh at some point, which is difficult to do without disturbing the air flow. In addition, one would need to know the time parameter of how fast the grid would have to "disappear". Instead, it was decided to leave the nets. The nets, resisting at all times, work to the detriment of the ventilation system, so if we manage to demonstrate its operation anyway, we are on the safe side, additionally having a certain amount of power.
7. The air entering the ventilation tower from the horizontal system of ventilation towers has the same parameters as the air discharged vertically upwards through the ventilation chimney. We do not take into account that after some time, cleaner air with different parameters will begin to flow in.
8. In a situation of stable equilibrium of the atmosphere, convection is crucial, the resistance of the layer must be large enough to stop it.

9.1.1. Physical parameters of the model

Air temperature distribution

Starting from the ground level, the air temperature gradient remains constant or close to zero. This happens up to a height of a few or several meters due to the presence of heated buildings, concrete surfaces, street surfaces, and the emission of hot exhaust gases. Since the height of occurrence of the described anomaly is difficult to determine and strongly depends on the urbanization factor and local development, in the model we assume a typical and uniform temperature gradient of 0.6°C/100m from the ground level to the base of the inversion layer. At the contact point of the smog layer and the inversion layer, a certain transition layer is formed, it is the bigger the less the temperature gradient changes. In conditions of a strong inversion, i.e. a strong gradient change, the air of the inversion layer will strongly press against the smog layer below, limiting larger turbulent movements. Then, within the inversion layer, the temperature gradient decreases or even takes negative values, i.e. the higher it is, the warmer the air until it meets the layer of clean air above the inversion layer. Of course, there is also a transition layer at the contact point of the layers. In the layer of clean air, we assume the gradient is again 0.6°C/100m. Of course, in nature, the temperature never changes perfectly. A slight movement of air caused by local terrain, differences in surface color, the presence of water reservoirs, heat sources, etc. is enough to create convection currents, heat islands, and local turbulences disturbing the model temperature distribution.

Air density distribution

Due to the change in pressure, the density of air should decrease with increasing altitude, while in the ground zone, it may turn out to be higher. The heaviest particles of dust and various pollutants float close to the ground, especially if they were previously lifted, e.g. by traffic. In addition, it should be remembered that the density of moist air is lower than that of dry air. As the air rises, it cools, which increases its humidity and thus its density. The inversion layer is a layer with a slightly higher temperature that presses on the layer of smog below. From Archimedes' principle, it can be concluded that the air density in the inversion layer must be almost the same or greater than the density of the smog layer. Therefore, the angle of inclination of the straight line will change on the graph, analogously to the change in temperature. Of course, in reality, the density of the smog layer and the layer above the inversion layer will be different due to the difference in the chemical composition of the air and the presence of dust, and different humidity. In the adopted model, we ignore the differences.

Pressure distribution

The change of atmospheric pressure with height is a fairly well-known phenomenon and is described by various empirical formulas. It is known that the pressure, due to the decreasing mass of the atmosphere above, decreases with increasing altitude. Moreover, the pressure change is described exponentially. Since the density of the inversion layer varies differently from that of the other layers, the pressure gradient will also vary from layer to layer. In the figure below, the pressure distribution is schematically marked with a straight line, but the calculations were made using the so-called barometric altitude formula (9.1):

$$p_2 = p_1 \cdot exp\left[-\frac{g}{R_p T_m}(z_2 - z_1)\right] \tag{9.1}$$

where:

T_m – the average temperature of the layer thickness of $(z_2 - z_1)$,

z_2, z_1 – the pressure levels accordingly z_1 and z_2,

$g = 9.81 \left[\frac{\text{kg·m}}{\text{s}^2}\right]$ – the gravitational acceleration,

$R_p = 278{,}05 \frac{\text{J}}{\text{kg·K}}$ – the gas constant.

Humidity distribution

Relative humidity RH depends on the temperature and the amount of water vapor in a given volume of air. If the temperature decreases with increasing altitude, the relative humidity will increase. If the air reaches 100% humidity and conditions favoring condensation occurs, the excess will condense and remain suspended as mist (cloud) or it will freeze and fall as precipitation. Then the humidity drops sharply leaving the air relatively dry. Of course, in nature, humidity can change by mixing with other air masses, so the distribution of humidity should be treated as one of the possible ones and it should be in mind that this is the most difficult parameter to predict.

9.1.2. Model of the chimney

When analyzing the case of a ventilation chimney, we can distinguish three basic situations:

Situation I

Steady state just before activation of the active ventilation system. The smog layer extends from the ground level to the inversion layer. Windless weather, steady state equilibrium, Archimedean and inertial forces are decisive. For this situation, the aerodynamic drag of the inversion layer was determined. The transition layer occurring at the interface of the layers is not important because the whole system remains in equilibrium.

Situation II

The moment of activation of the ventilation chimney just before breaking through the inversion layer. A stream of air rises above the ventilation chimney and reaches the inversion layer. To break through it, it must overcome the resistance of the inversion layer, lifting it locally and causing violent mixing. The resistance of the inversion layer is modeled with grids. The viscosity of the air was neglected. The time parameter appears. The similarity scales for the considered model can be written:

Geometric similarity scales:

$$k_l = \frac{l'}{l} = \frac{1}{833.33} \tag{9.2}$$

Considering the required model parameters time similarity scales were adopted as:

$$k_t = \frac{t'}{t} = \frac{1}{833.33} \tag{9.3}$$

It means that 1 second on the model corresponds to 833.33s in nature scale (≈ 14min)

Then the air velocity similarity scale is:

$$k_v = \frac{v'}{v} = \frac{k_l}{k_t} = \frac{\frac{1}{833.33}}{\frac{1}{1833.33}} = 1 \tag{9.4}$$

Situation III

Stabilized state after breaking through the inversion layer. The ventilation chimney creates a strong stream of polluted air above the inversion layer. Over time, the polluted air will dilute, forcing the influx of clean air from further regions. It should be noted that in this state the inversion layer no longer resists as it has been broken, and it will probably be necessary to maintain only enough air stream force to prevent re-establishment of the inversion layer by closing the opening formed. In addition, the active operation of the chimney contributes to the systematic expansion of the opening due to the turbulent flow at the edges of the air stream, and thus the gradual mixing of the air mass from the inversion layer. The forces of inertia, drag and viscosity play a large role in this situation. This situation is not the subject of experimental research due to the complexity of the model, which would have to take into account viscous forces to correctly represent the turbulent motion.

The cases described above are schematically shown in Fig. 9.3-9.4.

a)

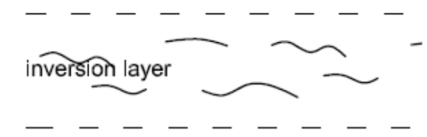

b)

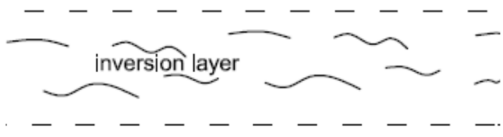

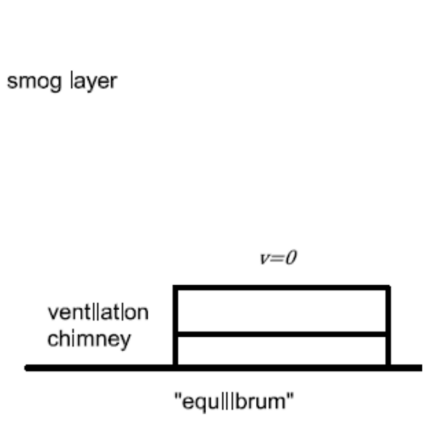

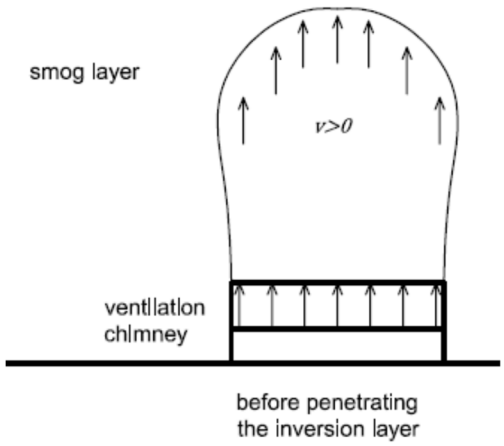

Fig. 9.4. Analyzed chimney operation situations, a) steady state just before turning on the system, b) state just before breaking through the inversion layer, c) stabilized state after breaking through the inversion layer.

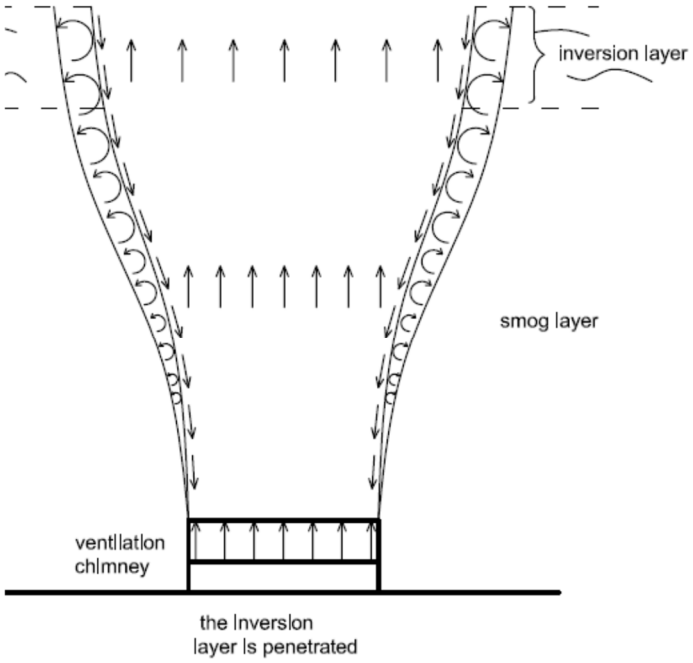

Fig. 9.4. Stabilized state after breaking through the inversion layer.

9.1.3. Estimation of the air velocities of the air stream

For the estimation of the air stream velocities and diameters on the considered levels, a theoretical model was created mainly by A. Flaga (Report 5).

1. Reference drawing

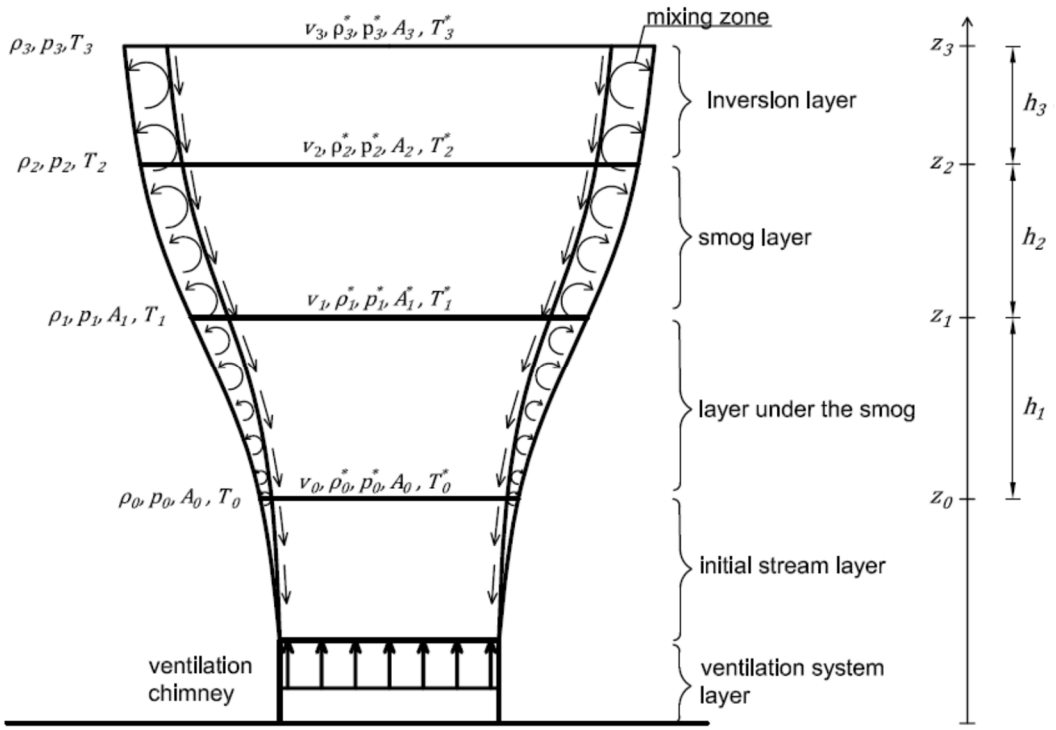

Fig. 9.5. Analyzed theoretical model of the ventilation chimney.

Where:

ρ_i – air density

p_i – air pressure

A_i –surface of the stream

T_i – air temperature

v_i – air velocity

2. Available/used problem equations

- State equations of the type:

$p_i = \rho_i R T_i; \quad i = 0,1,2,3$ (4 equations)

$p_i^* = \rho_i^* R T_i^*; \quad i = 0,1,2,3$ (4 equations)

Where:

R – the gas constant

- Continuity equations:
  $\rho_i^* A_i v_i = const; \ i = 0,1,2,3$ (3 równania)
- Energy equations of the type:

$$\frac{1}{2}\rho_i^* v_i^2 + p_i^* + \gamma_i^* z_i + \rho_i^* C_\Omega T_i^* = \frac{1}{2}\rho_{i+1}^* v_{i+1}^2 + p_{i+1} + \gamma_{i+1}^* z_{i+1} + \rho_{i+1}^* C_\Omega T_{i+1}^*;$$

$$i = 0,1,2,3$$

Where:

γ_i – the specific weight [N/m3]

C_Ω – the specific heat at constant volume [J/(kg*K)], for this case $C_\Omega = 716 \frac{m^2}{s^2 K}$

3. Simplifying assumptions

- Section 0 is far enough from the fan system that it can be assumed that:

$$p_0 = p_0^*$$

And similar:

$p_1 = p_1^*, p_2 = p_2^*, p_3 = p_3^*$

Then it will be (from the equation of state, assuming that: $R = R^* = const$):

$$\frac{p_i}{\rho_i R T_i} = \frac{p_i^*}{\rho_i^* R T_i^*}$$

That is:

$$\rho_i T_i = \rho_i^* T_i^*$$

4. Energy equations including kinetic, potential, and internal energy for an adiabatic process (without heat exchange with the environment).

$$\frac{1}{2}\rho_0 v_0^2 + p_0 + \rho_0 g z_0 + \rho_0 C_\Omega T_0 = \frac{1}{2}\rho_1 v_1^2 + p_1 + \rho_1 g z_1 + \rho_1 C_\Omega T_1 + \Delta p_1$$

$$\frac{1}{2}\rho_1 v_1^2 + p_1 + \rho_1 g z_1 + \rho_1 C_\Omega T_1 = \frac{1}{2}\rho_2 v_2^2 + p_2 + \rho_2 g z_2 + \rho_2 C_\Omega T_2 + \Delta p_2$$

$$\frac{1}{2}\rho_2 v_2^2 + p_2 + \rho_2 g z_2 + \rho_2 C_\Omega T_2 = \frac{1}{2}\rho_3 v_3^2 + p_3 + \rho_3 g z_3 + \rho_3 C_\Omega T_3 + \Delta p_3$$

Where:

Δp_i – pressure lost due to internal/viscous friction (tangential stresses at the jet boundaries)

$$\Delta p_j = \lambda_i(Re_{j-1}) \frac{h_j}{D_{j-1}} \frac{1}{2}\rho_{j-1} v_{i-1}^2;\ \ j = 1,2,3$$

Where:

λ_i –the loss coefficient

$$\frac{\pi D_{j-1}^2}{4} = A_{j-1}$$

D_j – the diameter of the stream

$$D_{j-1}^2 = 2\sqrt{\frac{A_{j-1}}{\pi}}$$

Re_i – the Reynolds number

$$Re_{j-1} = \frac{v_{i-1}D_{i-1}}{\nu}$$

ν – the kinematic viscosity of air

g – the gravitational acceleration

Let's consider the equilibrium state of the atmosphere when: $v_i = 0\frac{m}{s}$

4.1.The "equilibrium" part of the equation can be written as:

$$p_i + \rho_i g z_i + \rho_i C_\Omega T_i = p_{i+1} + \rho_{i+1} g z_{i+1} + \rho_{i+1} C_\Omega T_{i+1}; i = 0,1,2,3$$

Substituting:

$$p_i = \rho_i R T_i; \quad i = 0,1,2,3$$

we get:

$$\rho_i R T_i + \rho_i g z_i + \rho_i C_\Omega T_i = \rho_{i+1} R T_{i+1} + \rho_{i+1} g z_{i+1} + \rho_{i+1} C_\Omega T_{i+1}; i = 0,1,2,3$$

Assuming: $\rho_0, T_i, z_i, R, C_\Omega$ as constants, we get:

$$\rho_{i+1} = \rho_i \frac{R T_i + \rho_i g z_i + \rho_i C_\Omega T_i}{R T_{i+1} + \rho_{i+1} g z_{i+1} + \rho_{i+1} C_\Omega T_{i+1}}; i = 0,1,2,3$$

4.2.The state of slow stream movement in the vertical direction. Assumption: state of "quasi-equilibrium" means that apart from the kinetic energy and loss pressure - the other parts of the equation satisfy the equation of "equilibrium" of the atmosphere.

Then it will be:

$$\frac{1}{2}\rho_i v_i^2 = \frac{1}{2}\rho_{i+1} v_{i+1}^2 + \Delta p_{i+1}; i = 0,1,2,3$$

Hence:

$$v_{i+1} = \sqrt{\frac{\rho_i v_i^2 - 2\Delta p_i}{\rho_{i+1}}}; i = 0,1,2,3$$

Let us introduce the following dimensionless quantities:

$$\check{p}_i = \frac{p_i}{\frac{1}{2}\rho_0 v_0^2}; \quad i = 0,1,2,3$$

$$\check{g}_j = \frac{g(\rho_j z_j - \rho_{j-1} z_{j-1})}{\frac{1}{2}\rho_0 v_0^2}; \quad j = 1,2,3$$

$$\check{T}_j = \frac{C_\Omega(\rho_j T_j - \rho_{j-1} T_{j-1})}{\frac{1}{2}\rho_0 v_0^2};\ \ j = 1,2,3$$

$$\check{\rho}_i = \frac{\rho_i}{\rho_0};\ \ i = 0,1,2,3$$

$$\check{v}_i = \frac{v_i}{v_0};\ \ i = 0,1,2,3$$

$$\check{A}_i = \frac{A_i}{A_0};\ \ i = 0,1,2,3$$

Then the equations will take the form:

$$\check{\rho}_{i-1}\check{v}_{i-1}^2 = \check{\rho}_i\check{v}_i^2 + \Delta\check{p}_i; i = 1,2,3$$

They can be solved with respect to $\check{v}_i$ recursively:

$$\check{v}_1 = \sqrt{\frac{1 - \Delta\check{p}_1}{\check{\rho}_1}}$$

$$\check{v}_2 = \sqrt{\frac{1 - \Delta\check{p}_2}{\check{\rho}_2}}$$

$$\check{v}_3 = \sqrt{\frac{1 - \Delta\check{p}_3}{\check{\rho}_3}}$$

5. Continuity equations are written in the dimensionless form:

$$1 = \check{\rho}_1\check{A}_1\check{v}_1 = \check{\rho}_2\check{A}_2\check{v}_2 = \check{\rho}_3\check{A}_3\check{v}_3$$

From them, we determine the quantities $\check{A}_1, \check{A}_2, \check{A}_3$ when we know $\check{v}_1, \check{v}_2, \check{v}_3$.

6. Taking as input quantities v_0 and A_0

we determine A_1, A_2, A_3 and v_1, v_2, v_3,

further from the state equation:

$$\rho_i = \frac{p_i}{RT_i}; i = 0,1,2,3$$

We can eliminate, for example ρ_i.

In addition:

$$\check{\rho}_i = \frac{\rho_i}{\rho_0} = \frac{\frac{p_i}{RT_i}}{\frac{p_0}{RT_0}} = \frac{p_i}{p_0}\frac{T_0}{T_i}; i = 0,1,2,3$$

9.1.4.Estimation of the drag coefficient of the inversion layer

The drag coefficient is dimensionless, so it can be used to compare model tests with life-scale tests. The analysis of the available scientific literature did not provide an answer as to what the aerodynamic resistance of the inversion layer is, therefore the author attempted to estimate it.

To solve the problem of estimation of the aerodynamic drag coefficient of the inversion layer a theoretical model was created mainly by A. Flaga (Report 6).

1. Schematic drawing of the problem.

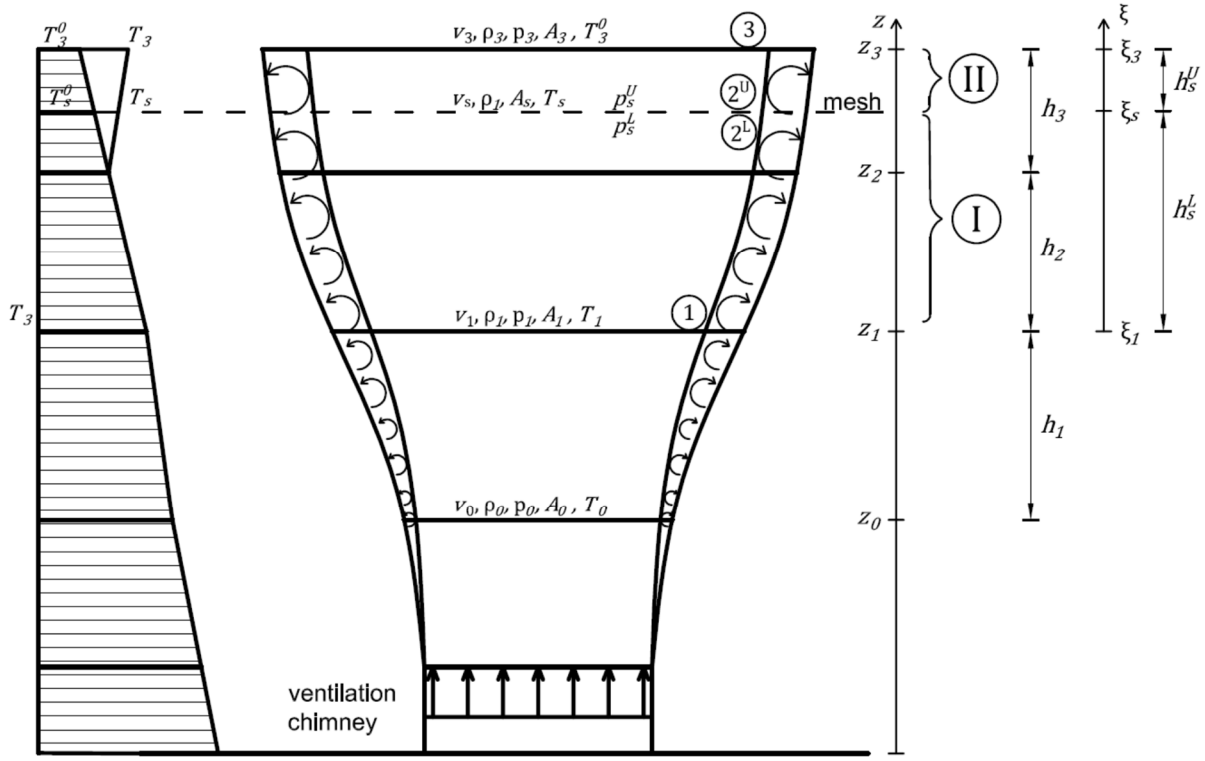

Fig. 9.6. Analyzed theoretical model of the ventilation chimney for the situation with the mesh replacing the inversion layer.

Notes and assumptions:

- We consider only two air streams I and II with thicknesses respectively h_s^L i h_s^U;
- There is no temperature inversion in the h_3 layer ($T_3 = T_3^0$);
- Instead of temperature inversion, we insert a resistance mesh with a resistance force coefficient C_s and area A_s;
- We assume that the data at levels 1 and 3 are as in the inversion problem, only instead of T_3 there will be T_3^0 and instead of T_s there will be T_s^0;
- On levels 2^L and 2^U there will be:

$$v_s^L = v_s^U = v_s,\ \rho_s^L = \rho_s^U = \rho_s,\ A_s^L = A_s^U = A_s,\ T_s^L = T_s^U = T_s,$$

$$p_s^L \neq p_s^U,\ p_s^L - p_s^U = \Delta p_s;$$

$p_s^L = p_s + \Delta p_s^L;\ p_s^U = p_s + \Delta p_s^U;$
$p_s^L - p_s^U = p_s + \Delta p_s^L - p_s + \Delta p_s^U = \Delta p_s^L + \Delta p_s^U;$

- Mesh drag force

$$F_s = \frac{1}{2}\rho_s v_s^2 C_s A_s$$

But from the momentum principle we have:

$$F_s = \rho_1 A_1 v_1^2 - \rho_3 A_3 v_3^2$$

Moreover, from the stream continuity equation we have:

$$\rho_1 A_1 v_1 = \rho_s A_s v_s = \rho_3 A_3 v_3$$

That is

$$F_s = \rho_s A_s v_s (v_1 - v_3)$$

Therefore:

$$\rho_s A_s v_s (v_1 - v_3) = \frac{1}{2}\rho_s v_s^2 C_s A_s$$

After reducing and rearranging, we get:

$$C_s = 2\frac{v_1 - v_3}{v_s} = 2(\breve{v}_{s1} - \breve{v}_{s3})$$

- Energy equations

$$\frac{1}{2}\rho_1 v_1^2 + p_1 + \gamma_1 z_1 + \rho_1 C_\Omega T_1 = \frac{1}{2}\rho_s v_s^2 + p_s^2 + \gamma_s z_s + \rho_s C_\Omega T_s^0 + \lambda_s(Re_1)\frac{h_s^L}{D_1}\frac{1}{2}\rho_1 v_1^2$$

$$\frac{1}{2}\rho_s v_s^2 + p_s^U + \gamma_s z_s + \rho_s C_\Omega T_s^0 = \frac{1}{2}\rho_3 v_3 + p_3 + \gamma_3 z_3 + \rho_3 C_\Omega T_3^0 + \lambda_s(Re_s)\frac{h_s^U}{D_s}\frac{1}{2}\rho_s v_s^2$$

- We derive dimensionless quantities by dividing the energy equations by $\frac{1}{2}\rho_s v_s^2$:

$\breve{\rho}_{s1} = \frac{\rho_1}{\rho_s}, \breve{\rho}_{s3} = \frac{\rho_3}{\rho_s};$

$\breve{v}_{s1} = \frac{v_1}{v_s}, \breve{v}_{s2} = \frac{v_s}{v_s} = 1, \breve{v}_{s3} = \frac{v_3}{v_s};$

$\breve{p}_{s1} = \frac{p_1}{\frac{1}{2}\rho_s v_s^2}, \breve{p}_s^L = \frac{p_s^L}{\frac{1}{2}\rho_s v_s^2}, \breve{p}_s^U = \frac{p_s^U}{\frac{1}{2}\rho_s v_s^2};$

$\breve{g}_{s1} = \frac{g(\rho_s z_s - \rho_1 z_1)}{\frac{1}{2}\rho_s v_s^2}, \breve{g}_{s2} = \frac{g(\rho_3 z_3 - \rho_s z_s)}{\frac{1}{2}\rho_s v_s^2};$

$\breve{T}_{s1} = \frac{C_\Omega(\rho_s T_s^0 - \rho_1 T_1)}{\frac{1}{2}\rho_s v_s^2}, \breve{T}_{s2} = \frac{C_\Omega(\rho_3 T_s^0 - \rho_s T_s^0)}{\frac{1}{2}\rho_s v_s^2};$

$\breve{h}_s^L = \frac{h_s^L}{D_1}, \breve{h}_s^U = \frac{h_s^U}{D_s};$

Then the energy equations in the dimensionless form will take the form:

$$\check{\rho}_{s1}\check{v}_{s1}^2 + \check{p}_{s1} = 1 + \check{p}_s^L + \check{g}_{s1} + \check{T}_{s1} + \lambda_s(Re_1)\,\check{h}_s^L\check{\rho}_{s1}\check{v}_{s1}^2$$

$$1 + \check{p}_s^U = \check{\rho}_{s3}\check{v}_{s3}^2 + \check{p}_{s3} + \check{g}_{s2} + \check{T}_{s2} + \lambda_s(Re_s)\,\check{h}_s^U$$

The solutions to these equations are as follows:

$$\check{p}_s^L = \check{\rho}_{s1}\check{v}_{s1}^2 + \check{p}_{s1} - \check{g}_{s1} - \check{T}_{s1} - \lambda_s(Re_1)\check{h}_s^L\check{\rho}_{s1}\check{v}_{s1}^2 - 1$$

$$\check{p}_s^L = \check{\rho}_{s1}\check{v}_{s1}^2\left(1 - \lambda_s(Re_1)\check{h}_s^L\right) + \check{p}_{s1} - \check{g}_{s1} - \check{T}_{s1} - 1$$

$$\check{p}_s^U = \check{\rho}_{s3}\check{v}_{s3}^2 + \check{p}_{s3} + \check{g}_{s2} + \check{T}_{s2} + \lambda_s(Re_s)\check{h}_s^U - 1$$

$$\Delta\check{p}_s = \check{p}_s^L - \check{p}_s^U = \Delta p_s =$$

$$\Delta\check{p}_s = \check{\rho}_{s1}\check{v}_{s1}^2\left(1 - \lambda_s(Re_1)\check{h}_s^L\right) - \check{\rho}_{s3}\check{v}_{s3}^2 + (\check{p}_{s1} - \check{p}_{s3}) - (\check{g}_{s1} - \check{g}_{s2}) - \left(\check{T}_{s1} - \check{T}_{s2}\right) - \lambda_s(Re_s)\check{h}_s^U$$

Because:

$$F_s = \Delta p_s A_s = \rho_s A_s v_s (v_1 - v_3)$$

Hence:

$$v_s = \frac{\Delta p_s}{\rho_s(v_1 - v_3)} = \frac{\Delta\check{p}_s\frac{1}{2}\rho_s v_s^2}{\rho_s(v_1 - v_3)} = \frac{\Delta\check{p}_s v_s^2}{2(v_1 - v_3)}$$

$v_s = \frac{2(v_1 - v_3)}{\Delta\check{p}_s}$

And finally:

$$C_s = 2\frac{v_1 - v_3}{v_s} = 2\frac{v_1 - v_3}{2(v_1 - v_3)}\Delta\check{p}_s = \Delta\check{p}_s$$

$C_s = \Delta\check{p}_s$

Assuming values similar to the nature scale model:

$v_0 = 2.0\frac{m}{s}, D_0 = 200m, z_0 = 190m, z_1 = 266m, z_s = 400m, z_3 = 500m, T_0 = 3.9°C, \lambda_1 = \lambda_2 = \lambda_3 = 1, p_0 = 97687.9Pa, R = 278{,}05\frac{\text{J}}{\text{kg·K}}$

And using the above formulas physical values were calculated:

$$v_1 = 15.58\frac{m}{s}, v_s = 1.00\frac{m}{s}, v_3 = 0.81\frac{m}{s}$$

$$D_1 = 225.4m, D_s = 282.6m, D_3 = 315.3m$$

Hence:

$$C_s = 1.53$$

9.2. Model of the inversion layer

The inversion layer was modeled as a system of steel meshes with mesh dimensions of 0.26 x 0.26 mm, made of 0.5 mm thick wire. The size of a single mesh was 100x100cm. To compensate for the bending and sagging of the mesh, they were stiffened with aluminum tubes glued on a square plan. The tubes were also the supporting structure of the net, which was suspended from thin steel lines attached to both the ceiling and the floor. The lines were stretched and fixed at an angle to eliminate swinging and displacement. The inversion layer was reconstructed using a system of 3 grids placed one above the other at a distance of 7.5 cm from each other, see Fig. 9.7. The test stand from stage III, i.e. a vertical ventilation chimney with a ring of ventilation towers, was used for the tests, see Fig. 9.8-9.10. The height of the first corresponds to the height of the base of the inversion layer of 300m and the last corresponds to the height of 500m. These heights were adopted by the author, based on data available in the literature.

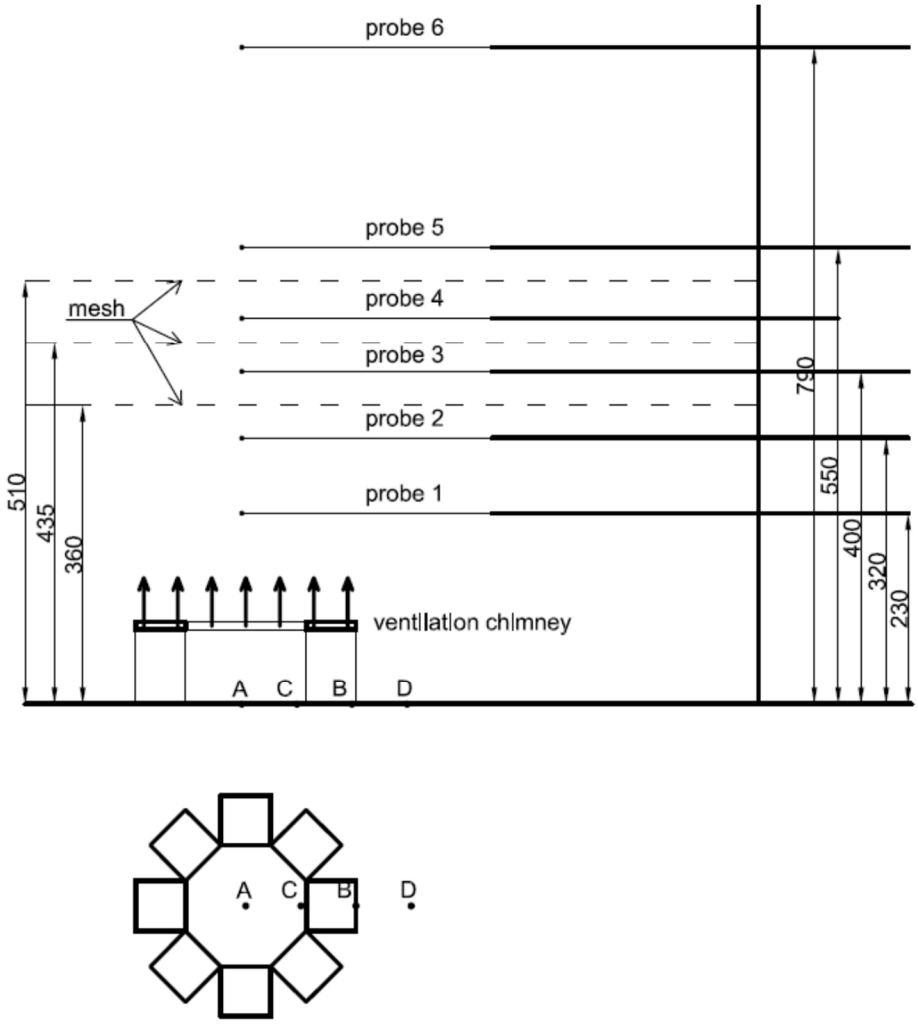

Fig. 9.7. A schematic view of the ventilation chimney model with an inversion layer and an outer ring of fans and 6 measuring probes, distances in mm.

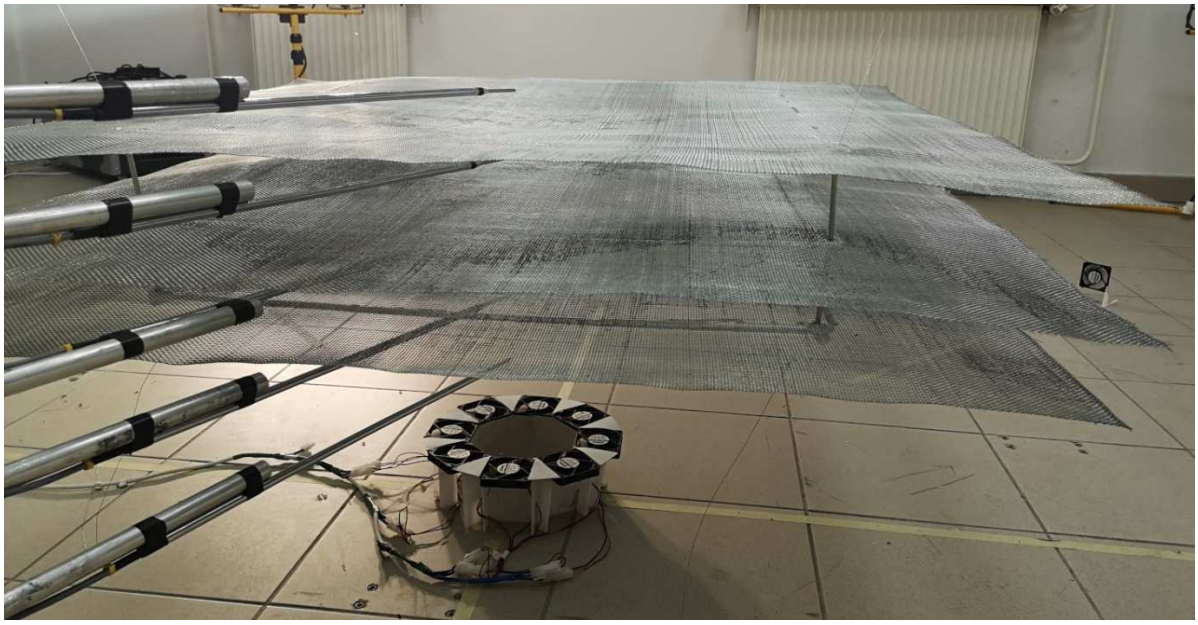

Fig. 9.8. A ventilation chimney with a base height of 90mm with an inversion layer modeled with 3 meshes.

Fig. 9.9. A ventilation chimney with an inversion layer and an outer ring of fans and 6 measuring probes.

Fig. 9.10 Top view of the ventilation chimney and measuring probes between the mesh.

9.3. Tests of the mesh

Before the tests of the inversion layer, the aerodynamic resistance of a single mesh was determined. For this purpose, a measuring station was built in the wind tunnel. The mesh was hung on an aerodynamic balance, and the tests were carried out at a range of air flow speeds close to the range generated by the fans, i.e. 1-3 m/s (see Fig. 9.11).

Fig. 9.11 The mesh in the test set up in the wind tunnel.

The force was measured using an aerodynamic balance. The aerodynamic scale was constructed based on a serial 6-component sensor by JR3. A strain gauge scale is a set of elastic elements on which strain gauges are glued, allowing to determine the stresses in the measuring elements based on the measured deformations, and thus to assess the aerodynamic forces and moments acting on the structure model. The aerodynamic scale is connected to a stepper motor that allows you to set the desired angle of the model relative to the wind.

A six-component aerodynamic balance allows the measurement of three component forces and three moments. The general view of the six-component aerodynamic balance is shown in Fig. 9.12. Tab. 9.1 presents the JR3 sensor data sheet with measurement ranges and accuracies.

Fig. 9.12. Six-component aerodynamic scale in the test setup (Fot. Ł. Flaga).

Table 9.1. Data sheet of the JR3 sensor, which is the main element of the aerodynamic scale

JR3 Multi-Axis Force-Torque Sensor Technical Specifications

Sensor Model: **Mechanical Load Rating:**	**45E15A4** **50 lb**
Diameter (in)	4.50
Thickness (in)	1.50
Material	AL 2024
Weight (lb)	1.75
Nominal Accuracy, all axes (% measuring range)	±0.25
Operating Temp. Range, non-condensing (°F)	-40 to +150
F_x, F_y	
Standard Measurement Range (lb)	±50
Digital Resolution (lb)	0.0063
Stiffness (lb/in)	0.056e6
Single-axis Overload (lb)	290
Multi-axis Overload Coefficient, a (lb)	290
Multi-axis Overload Coefficient, b (lb)	440
F_z	
Standard Measurement Range (lb)	±100
Digital Resolution (lb)	0.013
Stiffness (lb/in)	0.62e6
Single-axis Overload (lb)	1050
Multi-axis Overload Coefficient, c (lb)	1050
M_x, M_y	
Standard Measurement Range (in-lb)	±225
Digital Resolution (in-lb)	0.028
Stiffness (in-lb/rad)	1.1e6
Single-axis Overload (in-lb)	990
Multi-axis Overload Coefficient, d (in-lb)	990
M_z	
Standard Measurement Range (in-lb)	±225
Digital Resolution (in-lb)	0.028
Stiffness (in-lb/rad)	0.31e6
Single-axis Overload (in-lb)	860
Multi-axis Overload Coefficient, e (in-lb)	860

Fig. 9.13 Attachment of the mesh to the aerodynamic balance.

To simplify the measurement and construction of the measuring station, the mesh was attached to the balance only on the upper edge. With the increase in air speed, the mesh slightly deviated from the vertical, which was taken into account and corrected when determining the aerodynamic drag force. The resistance was determined with a uniform flow profile - the mesh was placed in the central part of the measurement space. Turbulence intensity $I_v = 2\%$ and after adding a turbulent grille $I_v = 7\%$. The values of the drag coefficient $C_x = 0.63$ without the grille and $C_x = 0.70$ with the grille were obtained. Thus, it can be seen that the introduction of turbulence increased the value of the coefficient by 10%. For further consideration, the coefficient $C_x = 0.70$ was assumed, expecting high turbulence in the vertical air stream generated by the ventilation tower. No significant effect of the Reynolds number was observed depending on the set air velocity.

A set of 3 identical meshes was used to model the inversion layer. The equivalent coefficient C_s of aerodynamic drag was calculated as:

$$C_{s,model} = 1.36$$

What is quite close to value:

$$C_{s,theory} = 1.53$$

Obtained from the theoretical model.

9.4. Inversion layer tests

The tests were carried out using 6 hot-wire anemometric probes placed one above the other. See Fig. 9.14. Different series of tests included different positioning of the set of probes relative to the center of the chimney (A, B, C, and D) to obtain a wider field of the velocity of the vertical stream generated by the tower. It was checked whether the outer ring of fans affects the velocity distribution of the vertical stream of the chimney. To optimize the investment in the future, the height of the entire ventilation tower was gradually lowered. This made it possible to estimate the

minimum height of the ventilation tower at which the generated air stream is still efficient. The base of the tower was gradually shortened by ¼ of the height, obtaining the height of the base of the tower: 90mm, 67mm, 45mm, and 22mm respectively. The influence of the number of fans on the size and power of the stream was also checked. All tests were performed for a ventilation tower with 1, 4, and 8 fans, see Fig. 9.14-9.15 and for 3 values of the voltage applied to the fan system: 4.0V, 9.5V, and 13.6V.

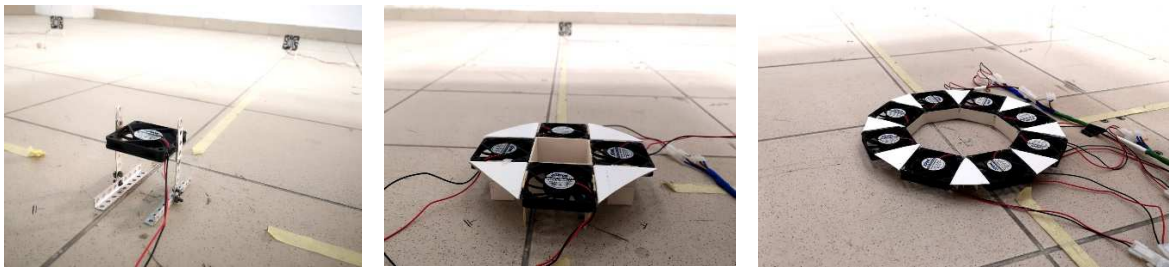

Fig. 9.14. Ventilation towers with 1, 4, and 8 fans.

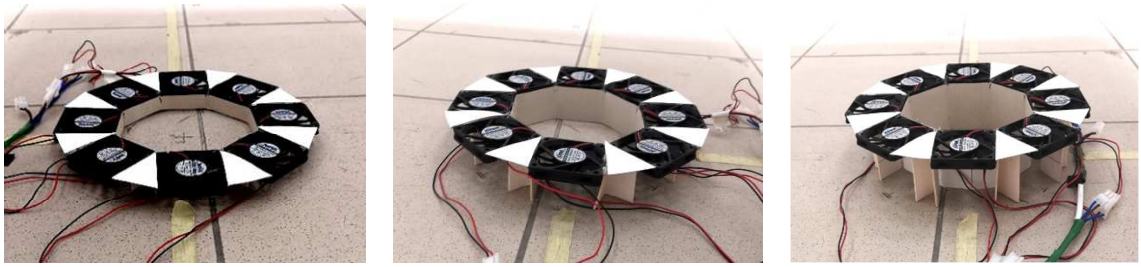

Fig. 9.15. Ventilation towers with base heights of 22mm, 45mm, and 67mm.

A summary of the series and parameters tested is shown in Tab. 9.2.

Tab. 9.2 Summary of a series of tests carried out in stage IV.

Parameter	**Series**
Voltage	4.0V, 9.5V, 13.6V
Probes location	A, B, C, D
Height of the tower base	90, 67, 45, 22mm
Number of fans	1, 4, 8 fans
Outer ring	on, off

9.5. Smoke Visualization of stage IV

During the tests, a smoke visualization was also made to better illustrate the spread of the stream and to check whether the stream is strong enough to break through the inversion layer. An author`s method was used consisting of a smoke hazer setting a fog close to the ground. The smoke was produced with propylene glycol and dry ice. After distributing the fog throughout the room and waiting for the larger air currents to stop, the ventilation system was turned on. The effects of the visualization are shown in Fig. 9.16.

a)

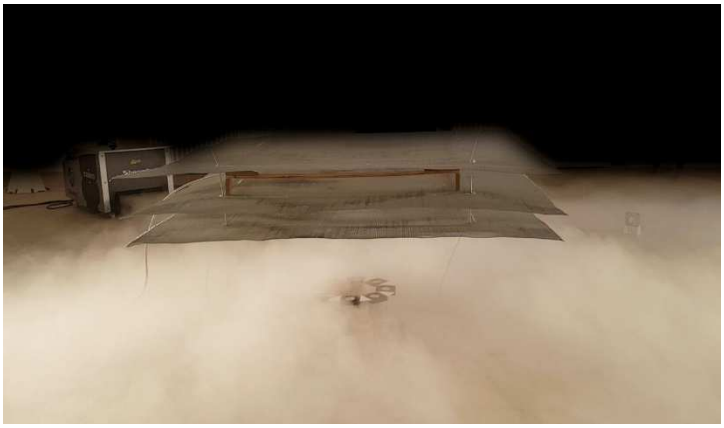

b)

c)

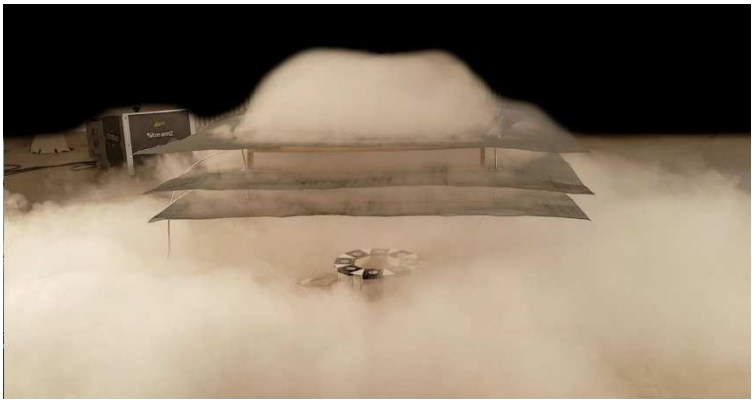

Fig. 9.16. Visualization in stage IV: a) moment before turning on the system, b) braking through the inversion layer, c) continuation of system operation (Fot. Ł. Flaga).

9.6. Test results and analysis

Due to the large number of graphs and a wide range of measurement results, the results are presented with a short analysis and the most interesting points are marked and descriptions of the figures are placed above them.

Fig. 9.6.1. Mean velocity for ventilation chimney with 8 fans, H=90mm, ***outer ring off***

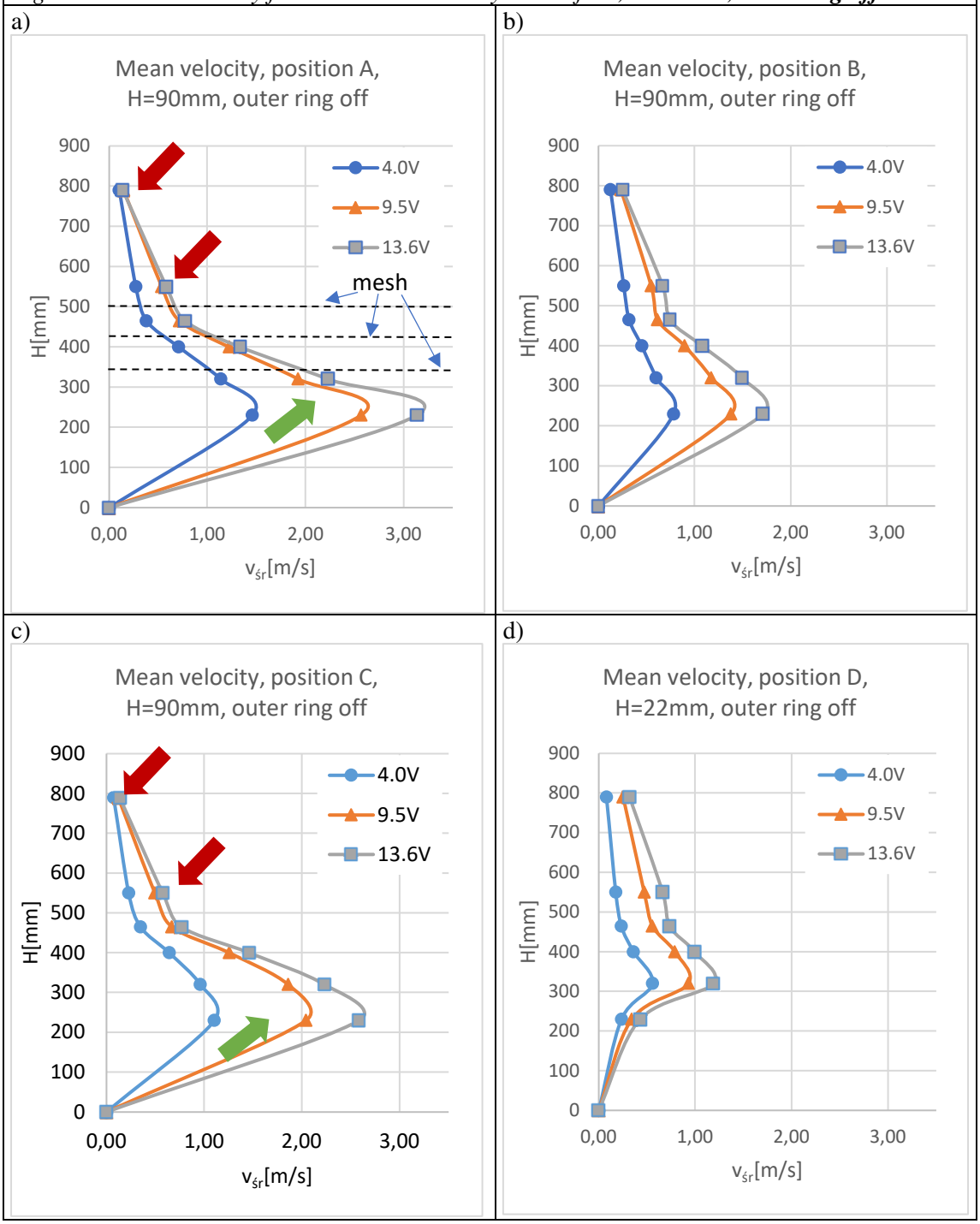

In the graphs above, there is a sudden drop in velocity just below the grid, especially for high velocities and points near the center of the stream (green arrows). For points A and C, there is almost no flux velocity difference above the inversion layer when the voltage is increased from 9.5V to 13.6V (red arrows).

Fig. 9.6.2. Mean velocity for ventilation chimney with 8 fans, H=90mm, ***outer ring on***

a)

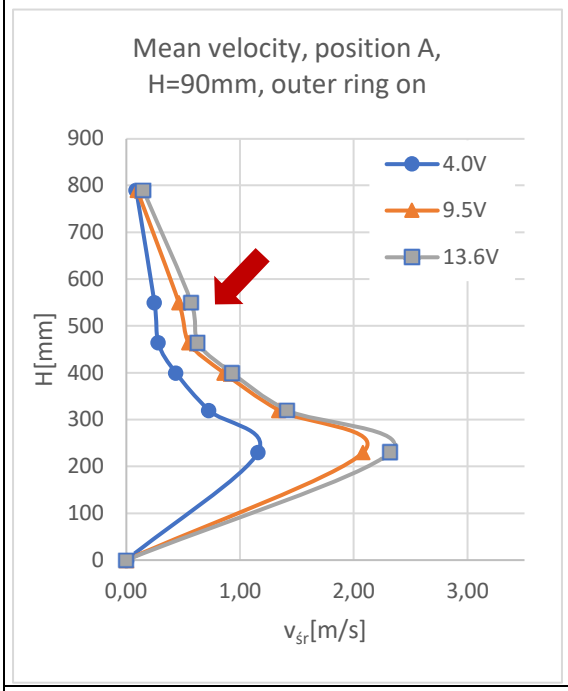

b)

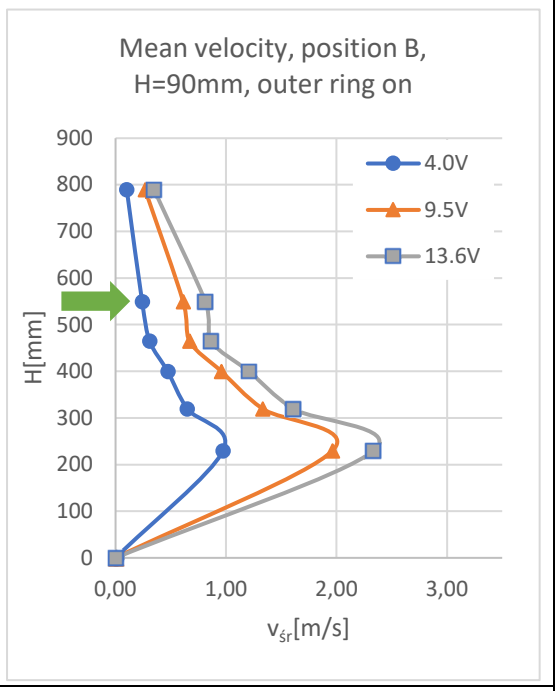

c)

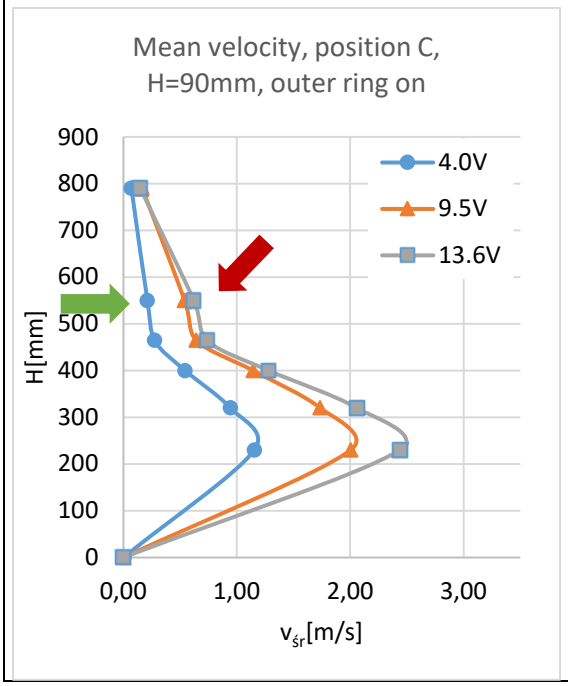

d)

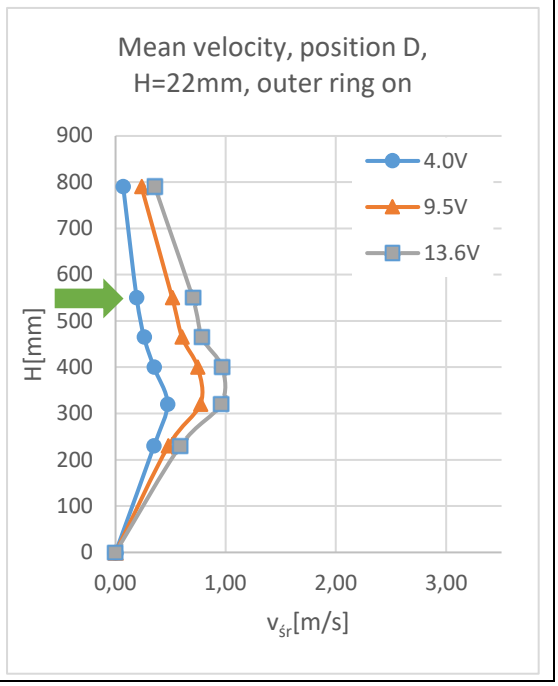

There is also no significant difference in air speed with the outer ring on when increasing the voltage from 9.5V to 13.6V (red arrows). In addition, for point C, it can be seen that the speed over the inversion layer for 4.0V is more than 2 times lower than for 9.5V (green arrows).

Fig. 9.6.3. Mean velocity for ventilation chimney with 8 fans, H=90mm

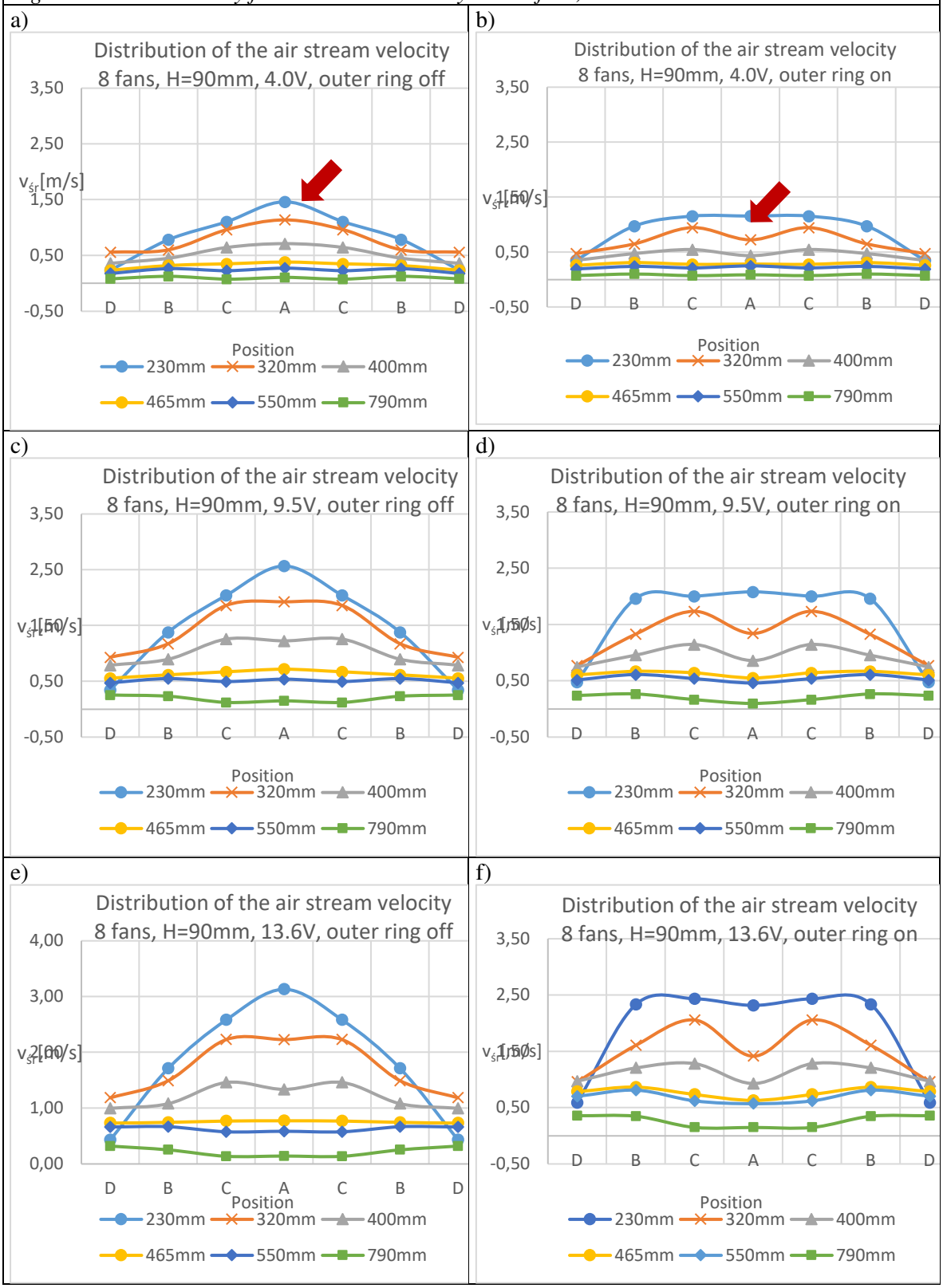

In the graphs above, it can be seen that in all cases, the activation of the outer ring resulted in a decrease in air velocity in the center of the air stream and an increase in velocity on the sides of the stream, increasing its diameter. The effect occurs weaker with height. Consideration should be given to turning on the ventilation chimney first to penetrate the inversion layer and then turning on the outer ring to ventilate the large area around it.

Fig. 9.6.4. Mean velocity for ventilation chimney with 4 fans, H=90mm, ***outer ring off***

a)

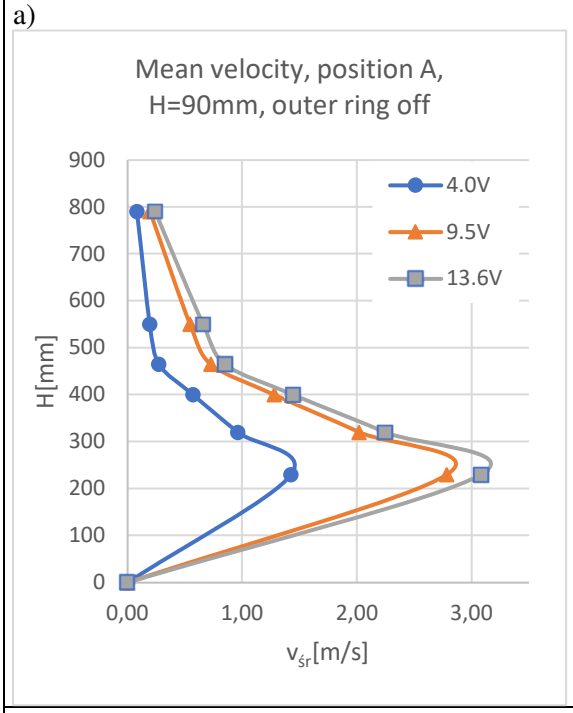

b)

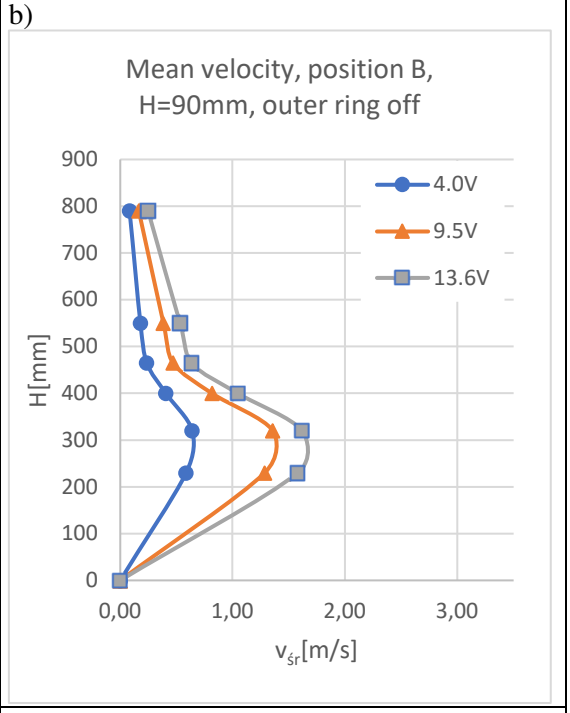

c)

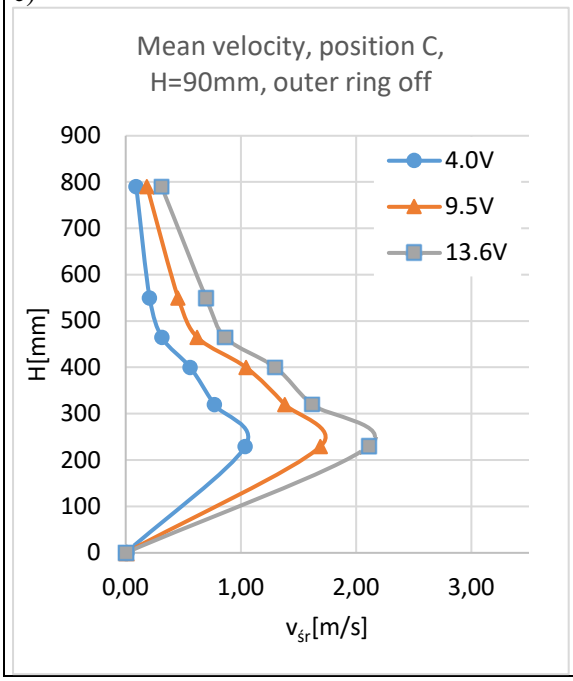

d)

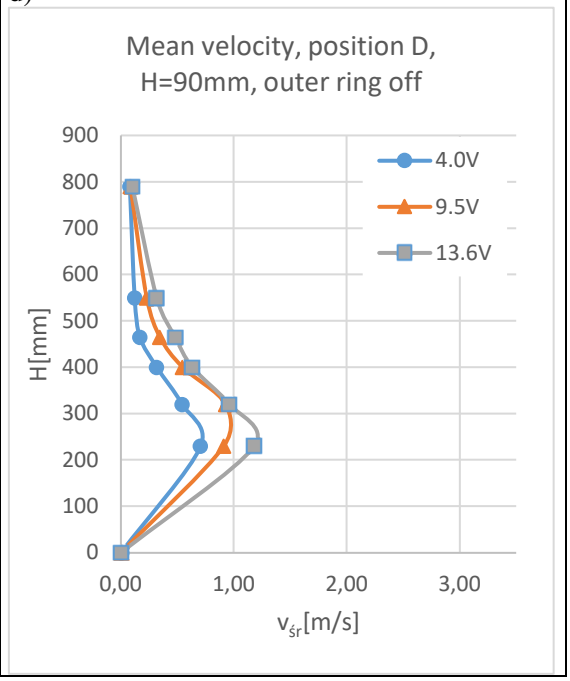

The shape of the air velocities graphs is similar to that with the 8 fans, at points A and B the values are almost identical.

Tab. 9.6.5. Mean velocity for ventilation chimney with 4 fans, H=90mm, ***outer ring on***

a)

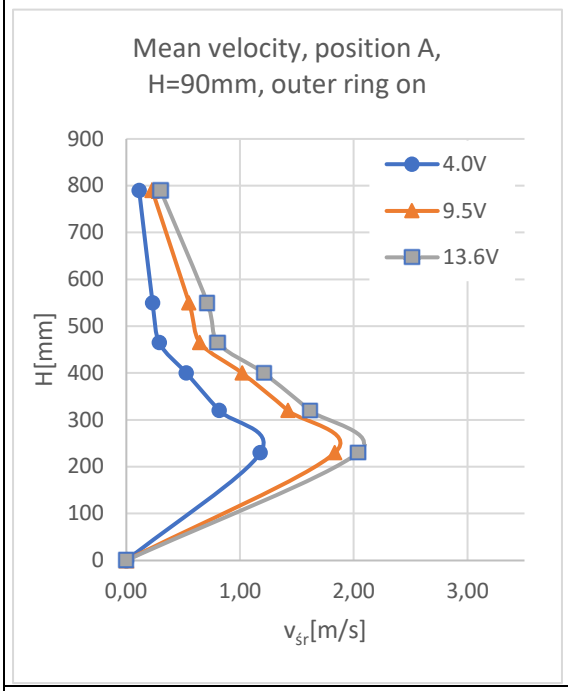

b)

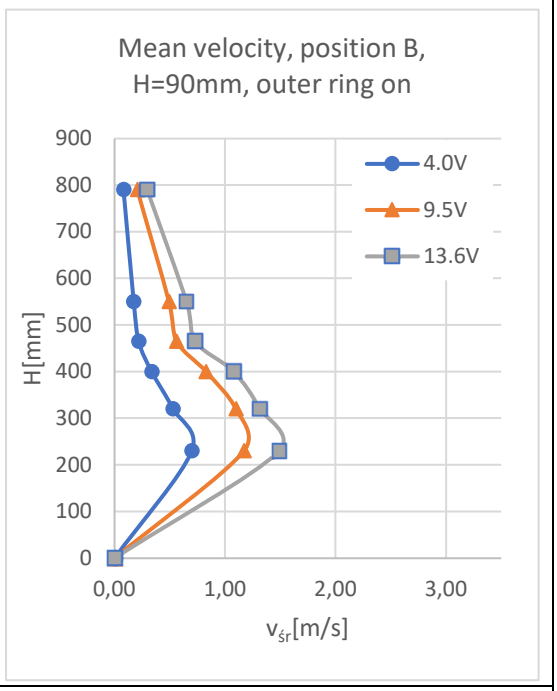

c)

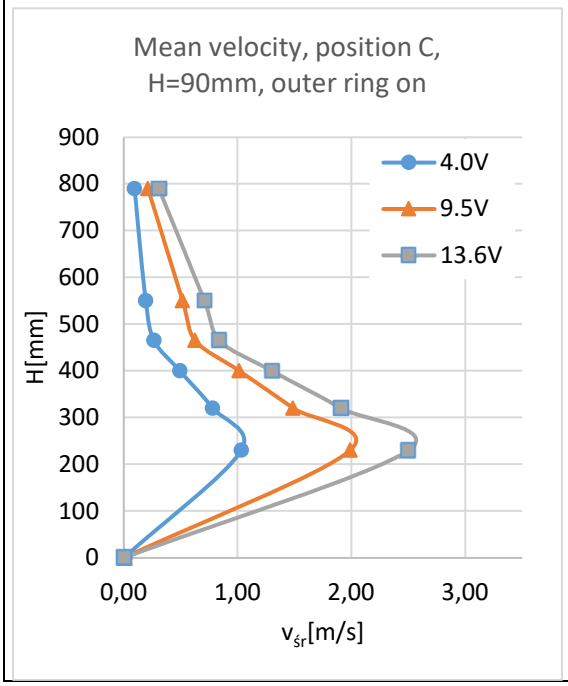

d)

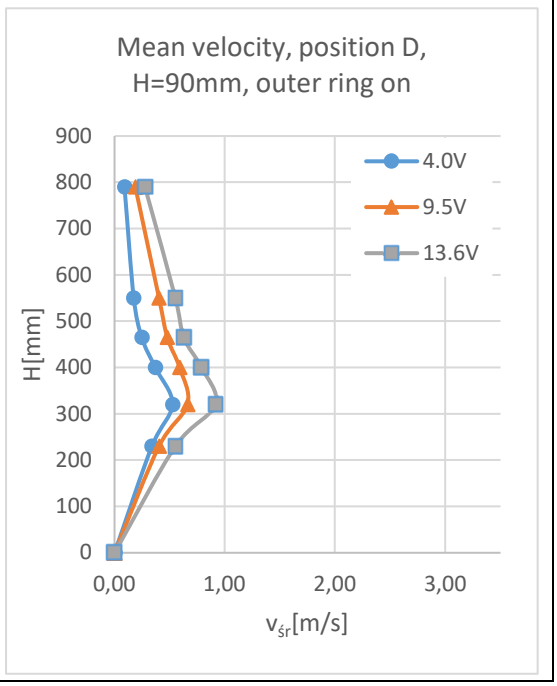

Fig. 9.6.6. Mean velocity for ventilation chimney with 4 fans, H=90mm

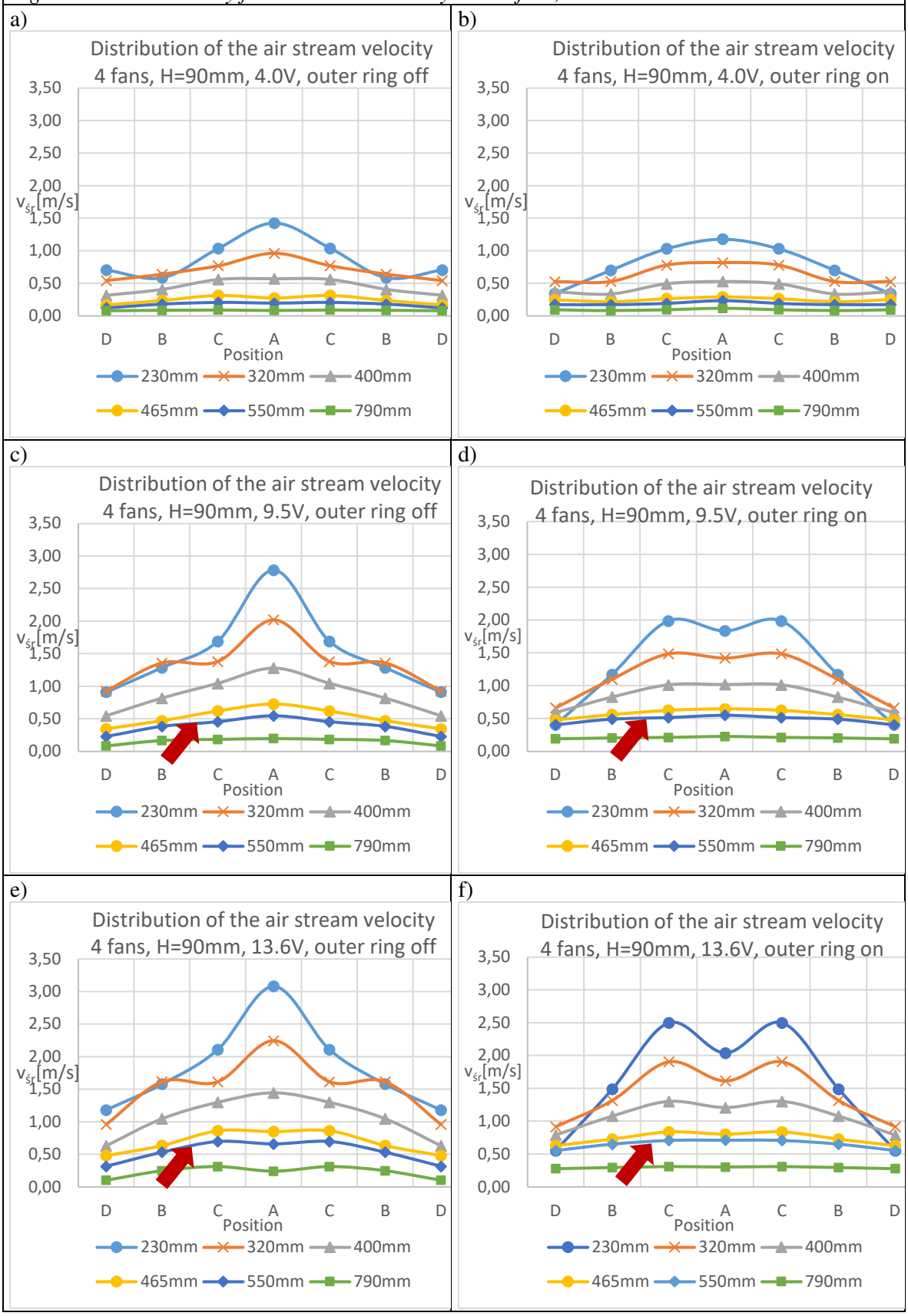

For the 4 fans ventilation tower, it can be seen the same effect of lowering the speed in the middle of the air stream, but not so much as for 8 fans. For the voltage of 13.6V and the outer ring on, the air velocity over the inversion layer was similar.

Fig. 9.6.7. Mean velocity for ventilation chimney with 1 fan, H=90mm, ***outer ring off***

a)

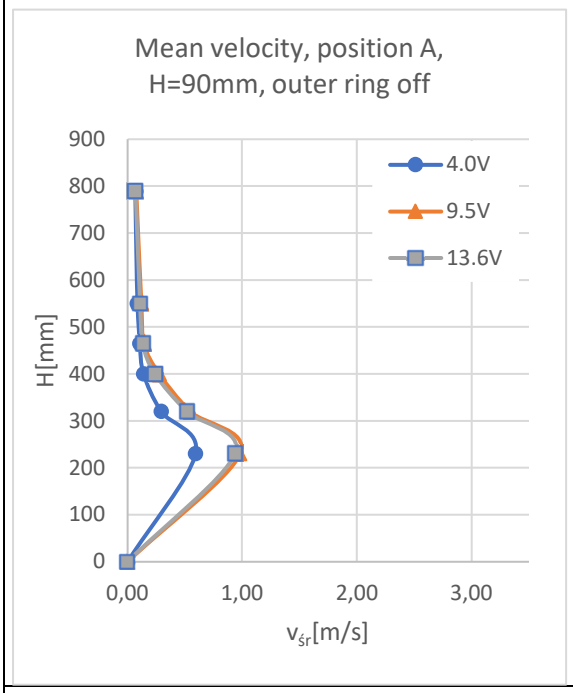

b)

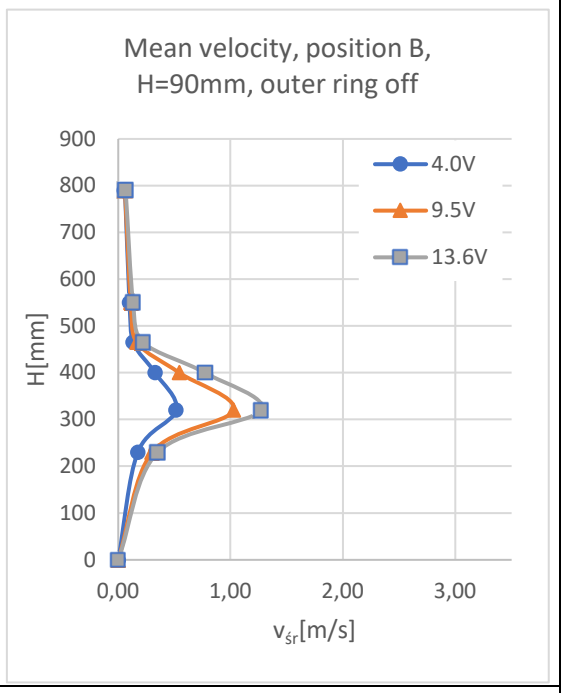

c)

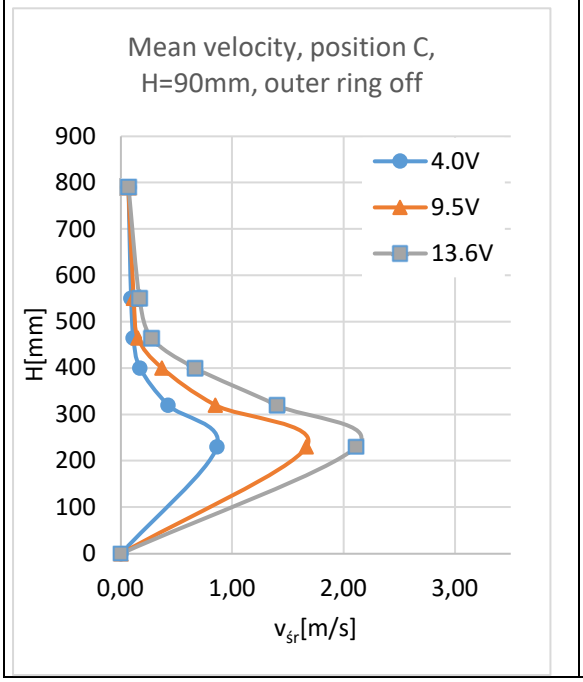

d)

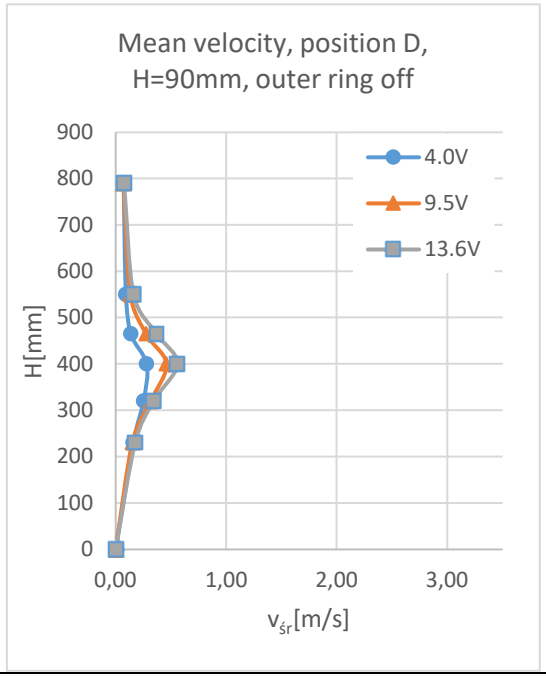

For the 1 fan ventilation chimney, the speed over the inversion layer is close to 0m/s. We can conclude that the air stream was not able to penetrate the layer. The air stream had very low velocity after passing through the first grid, which decreased to negligible value after the 2nd grid.

Fig. 9.6.8. Mean velocity for ventilation chimney with 1 fan, H=90mm, ***outer ring on***

a)

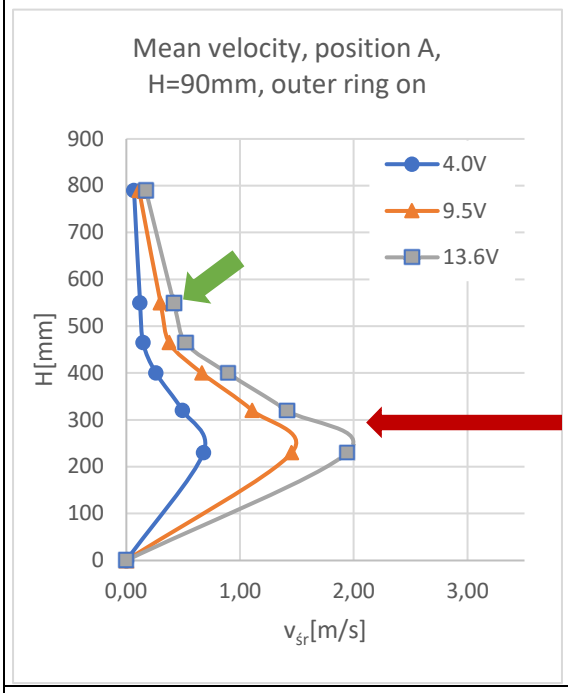

b)

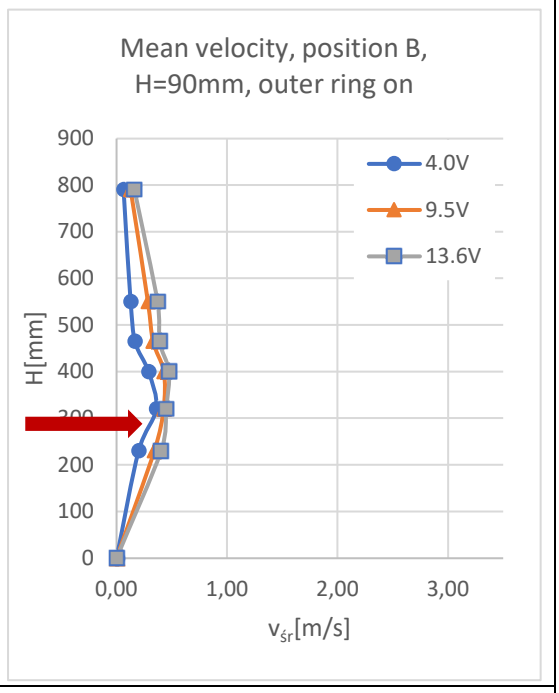

c)

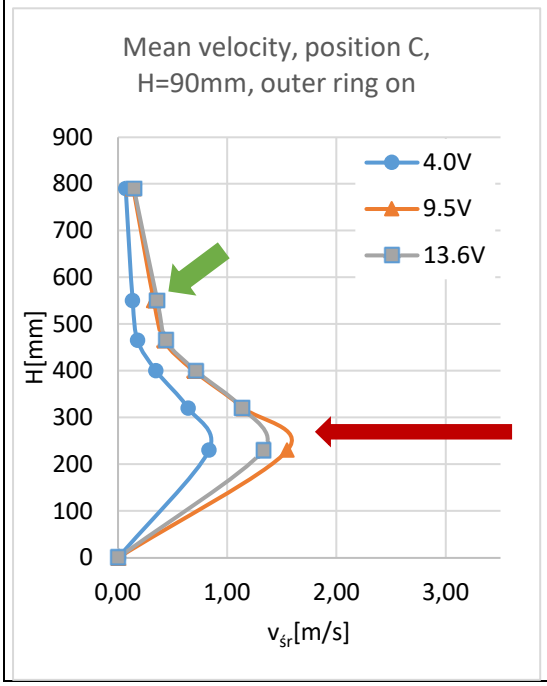

d)

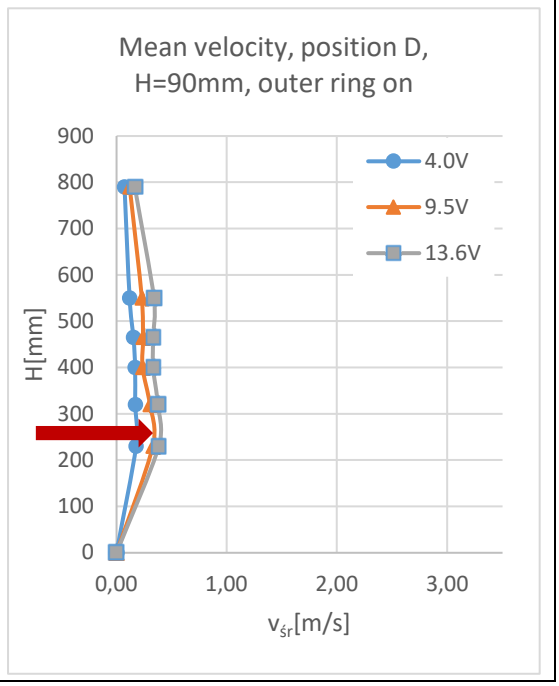

Comparing the situation after turning on the outer ring, it can be seen that turning it on caused a significant decrease in air stream speed under the mesh (red arrows).

With the outer ring on, the air stream penetrated through all 3 meshes (green arrows).

Fig. 9.6.9. Mean velocity for ventilation chimney with 1 fan, H=90mm

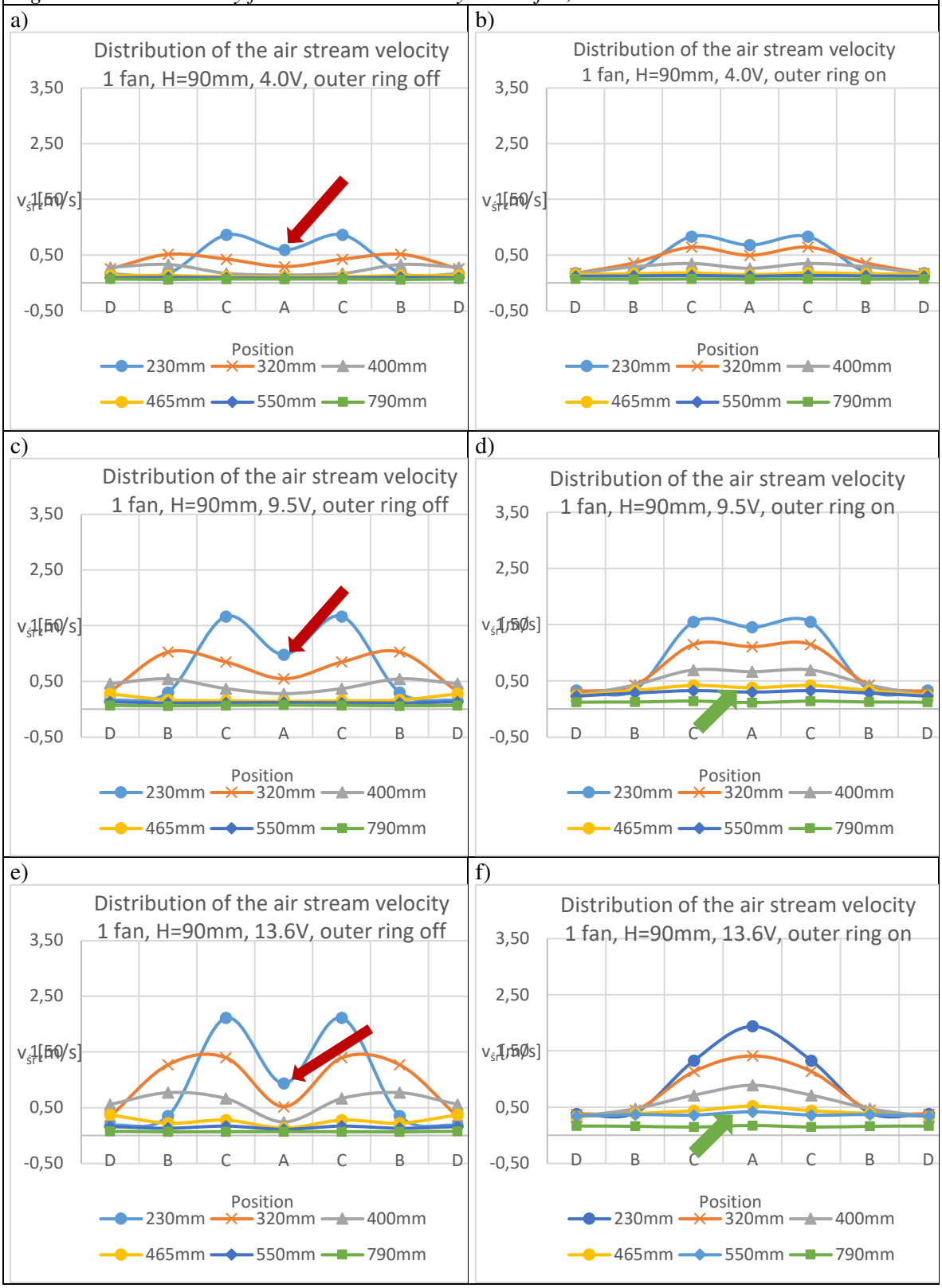

Very uneven distribution of velocities in the generated air stream occurs in this case (red arrows). This is probably due to the construction of the fan and its large, covered center. A similar effect was observed in stage I during the tests of a single fan.

In the case of an outer ring on, it can be seen the inversion breakdown at 9.5 V and 13.6 V (green arrows).

Fig. 9.6.10. Mean velocity for ventilation chimney with 8 fans, H=67mm, ***outer ring off***

a)

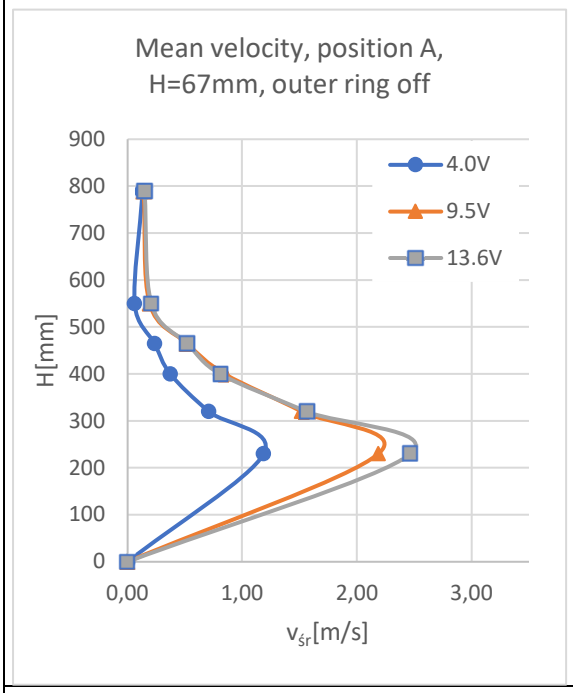

b)

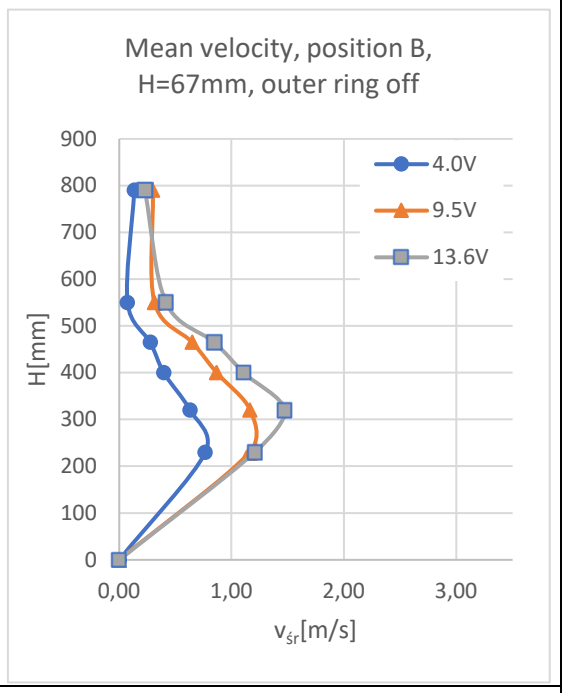

c)

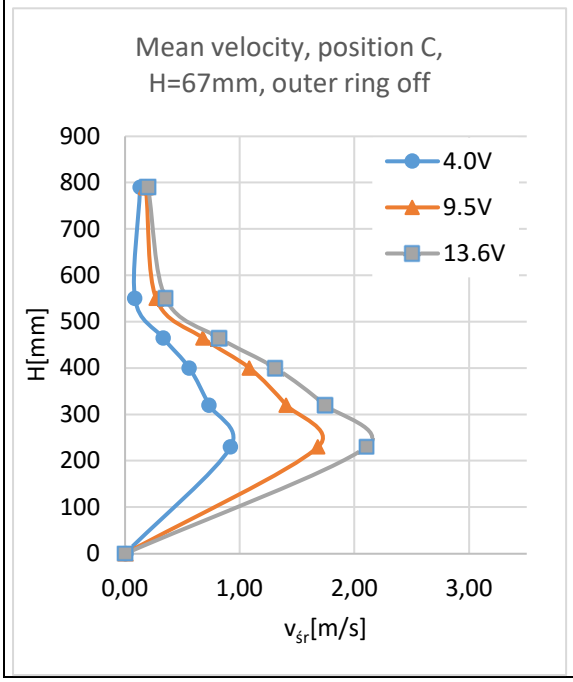

d)

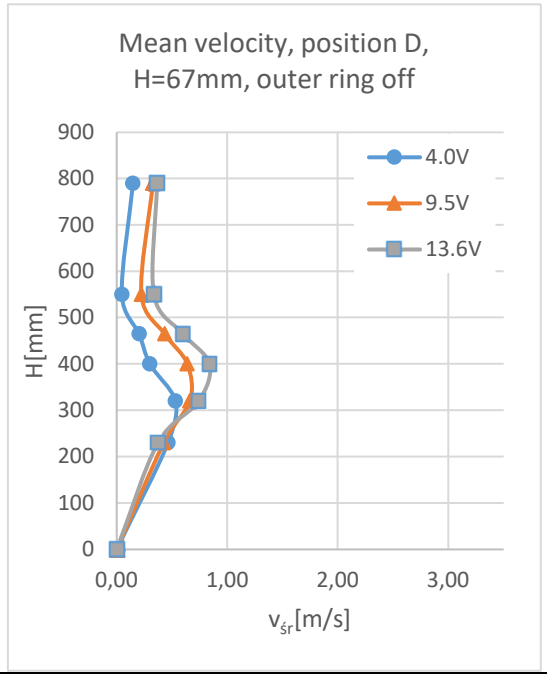

Fig. 9.6.11. Mean velocity for ventilation chimney with 8 fans, H=67mm, ***outer ring on***

a)

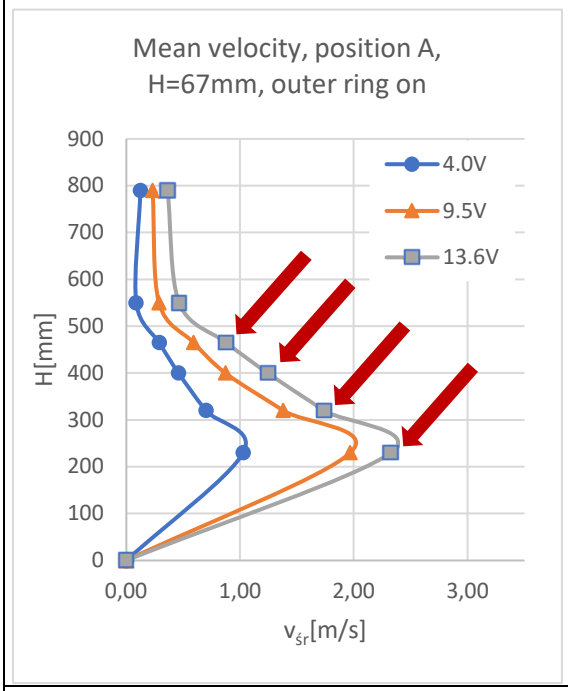

b)

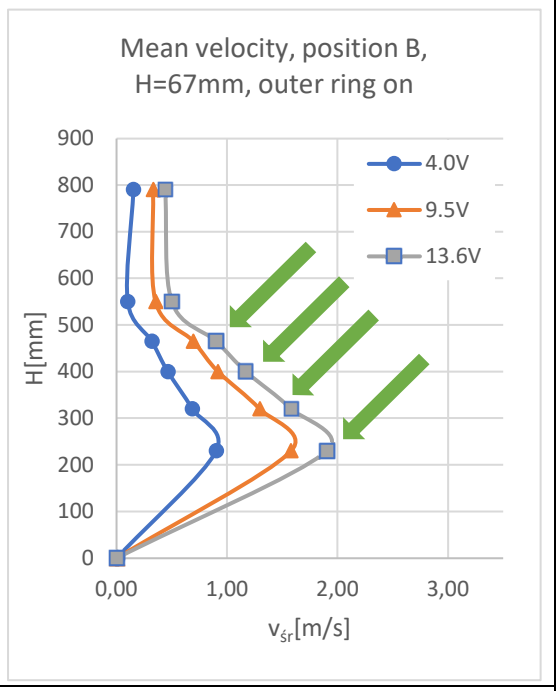

c)

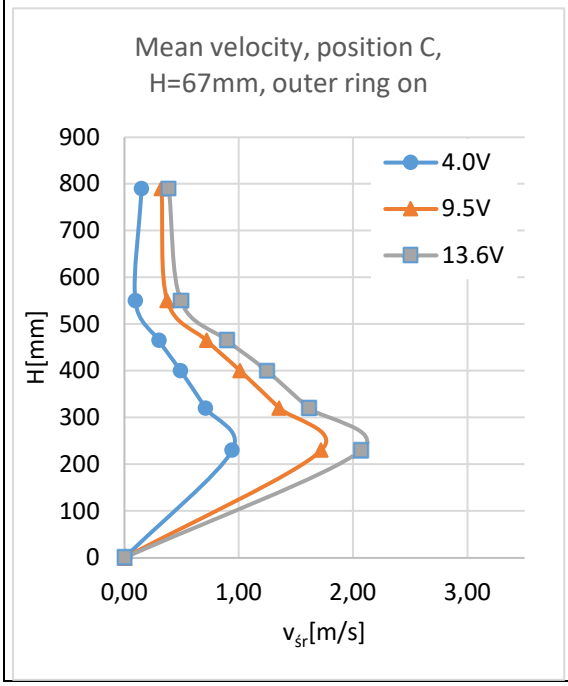

d)

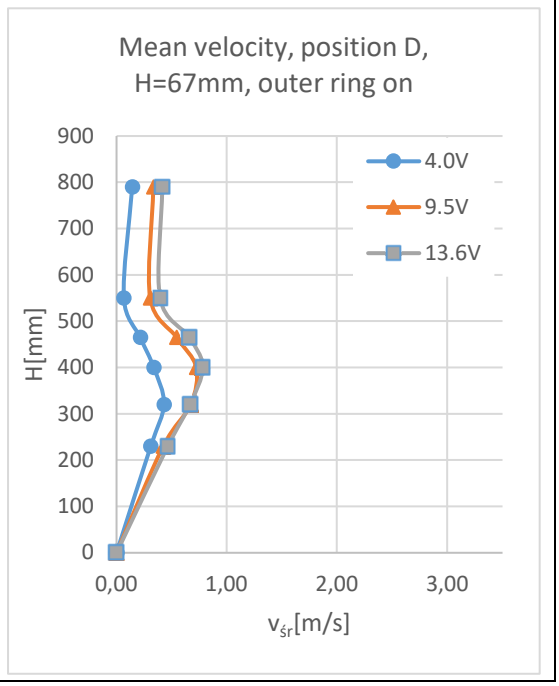

The values marked with red arrows are higher than for the ventilation chimney with a base height of 90mm but for position B the effect no longer exists (green arrows).

Fig. 9.6.12. Mean velocity for ventilation chimney with 8 fans, H=67mm

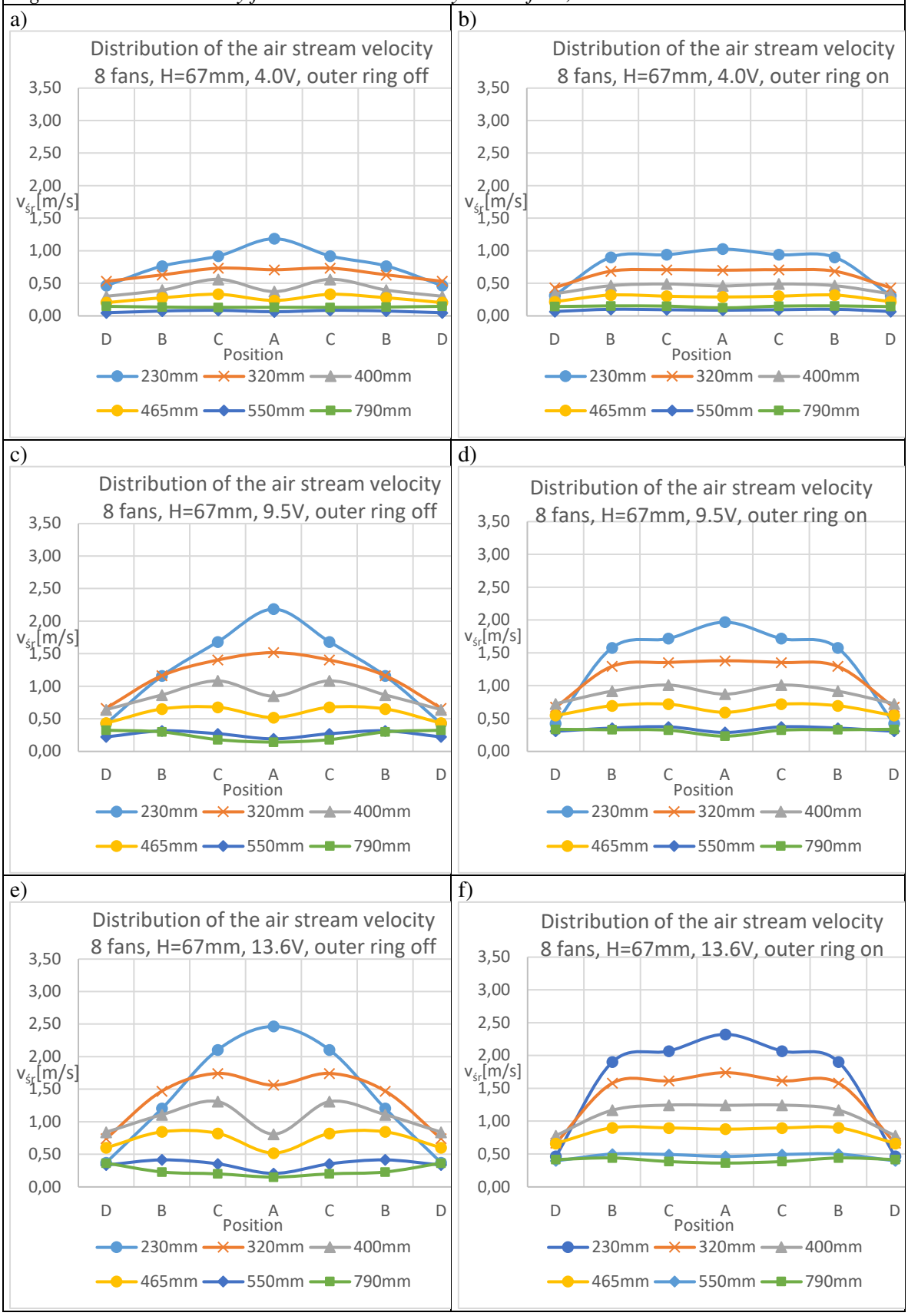

The shape of the graphs is almost the same as for a ventilation chimney with a base height of 90mm, but in each case, the values obtained are lower, especially above the inversion layer.

Fig. 9.6.13. Mean velocity for ventilation chimney with 4 fans, H=67mm, ***outer ring off***

a)

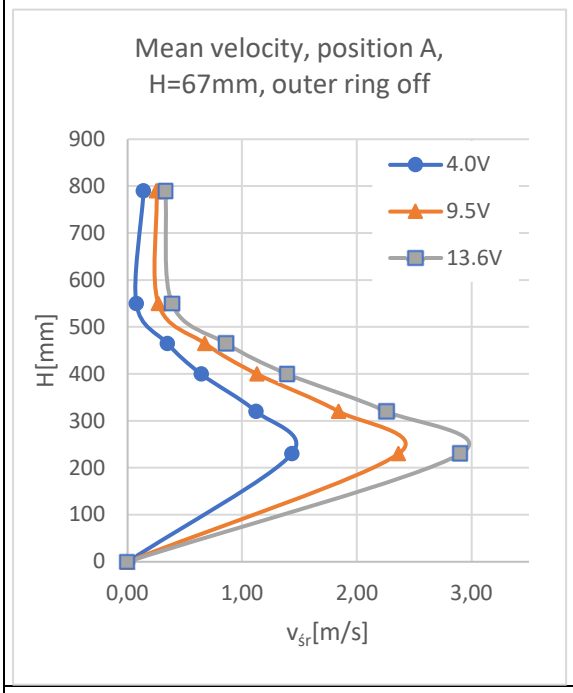

b)

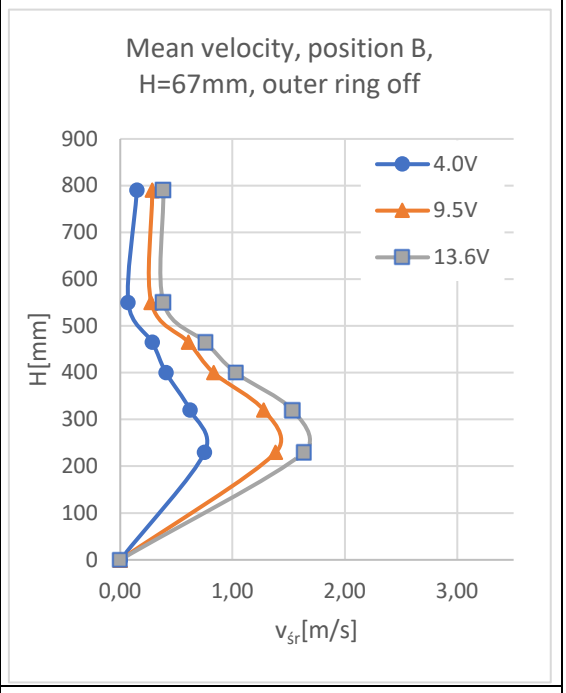

c)

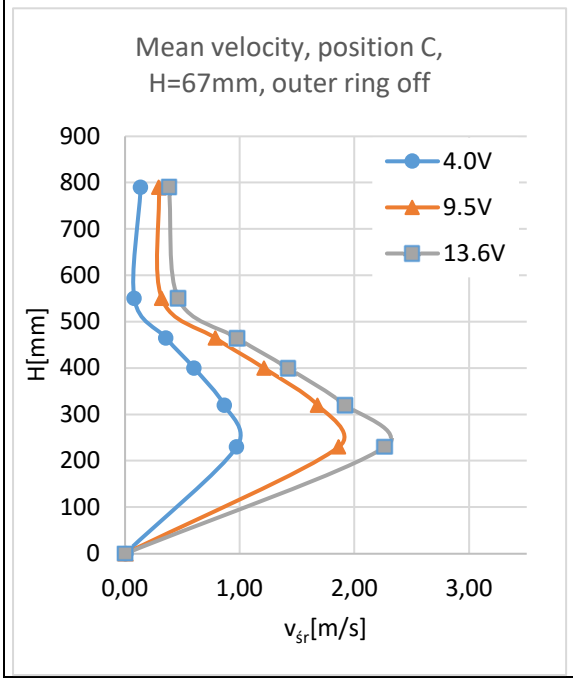

d)

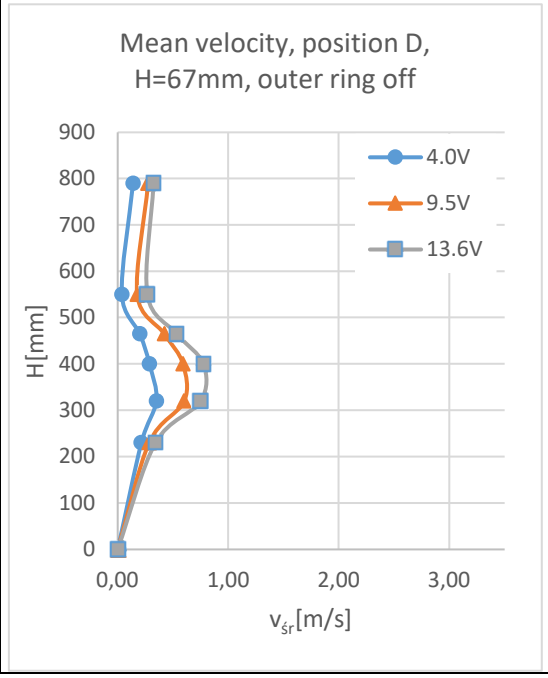

For points a, b, and c the values are the same or slightly higher than for the ventilation tower with 8 fans and the base height of 67mm.

Fig. 9.6.14. Mean velocity for ventilation chimney with 4 fans, H=67mm, ***outer ring on***

a)

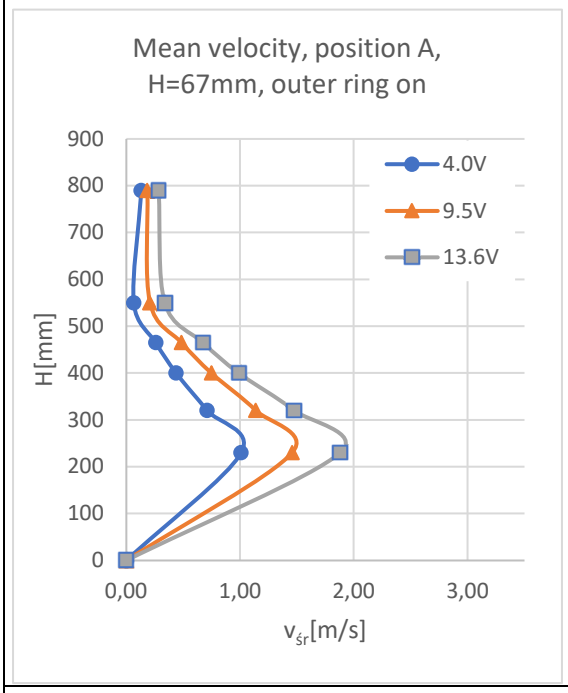

b)

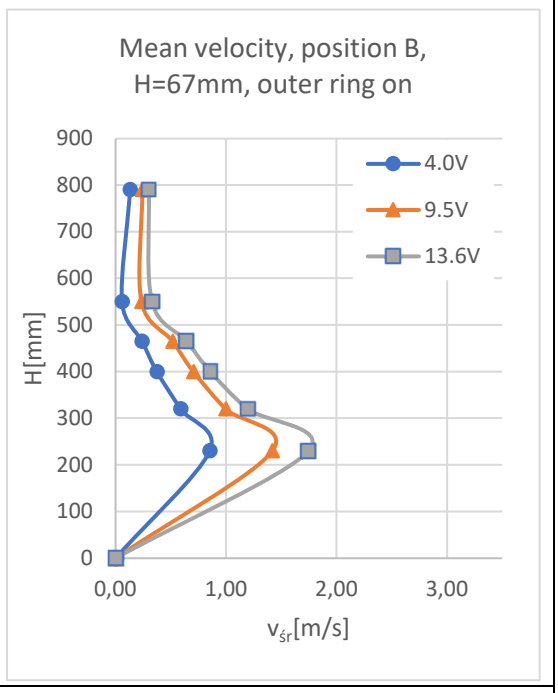

c)

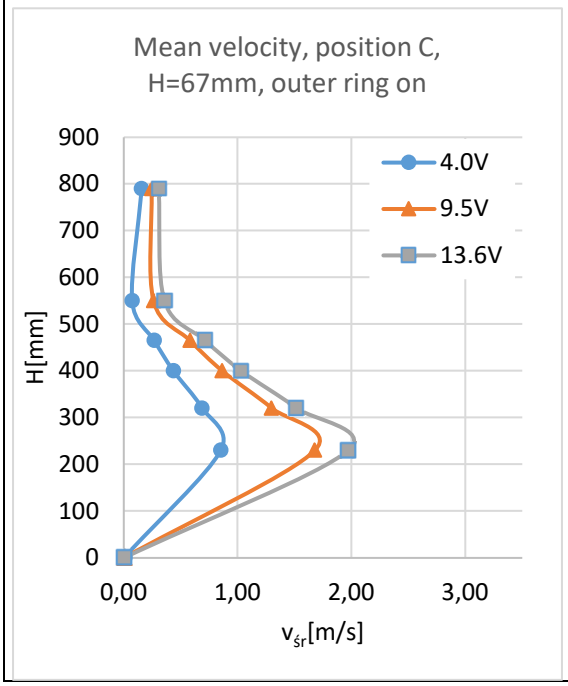

d)

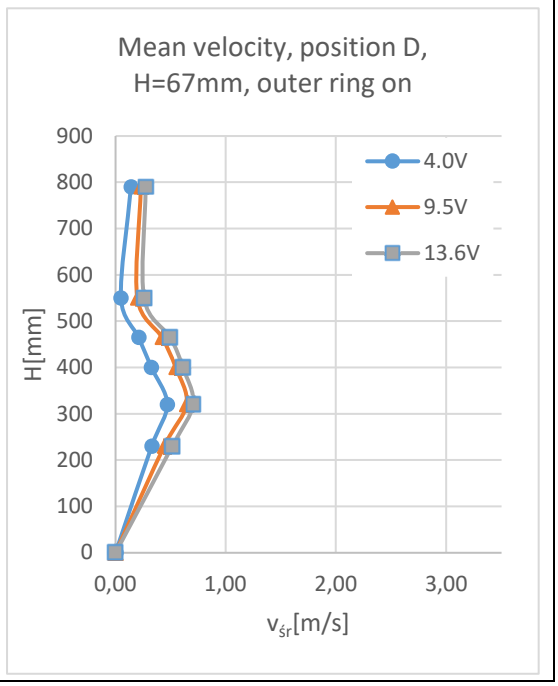

But after turning on the outer ring the values are lower than for the ventilation tower with 8 fans and the base height of 67mm.

Fig. 9.6.15. Mean velocity for ventilation chimney with 4 fans, H=67mm

a)

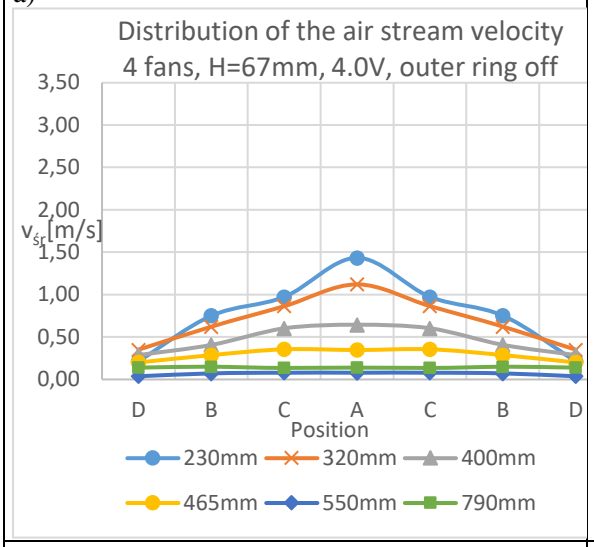

b)

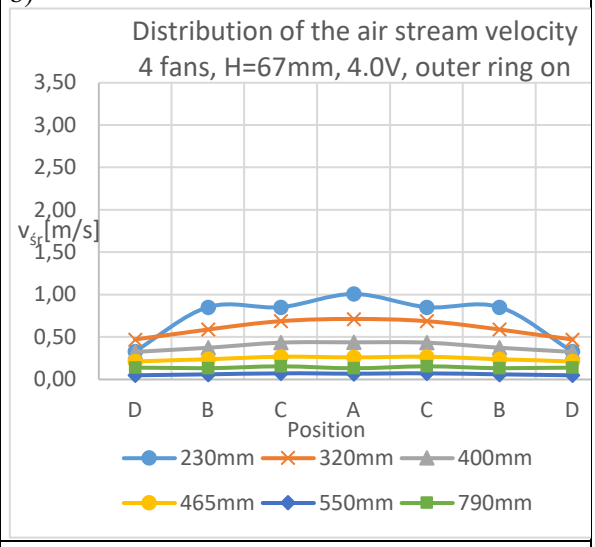

c)

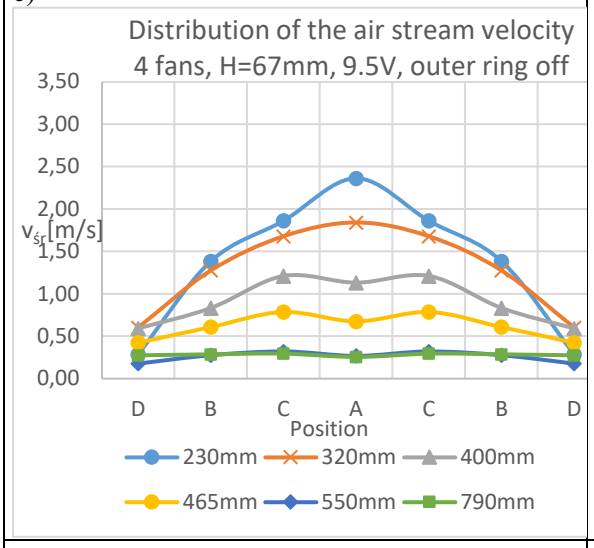

d)

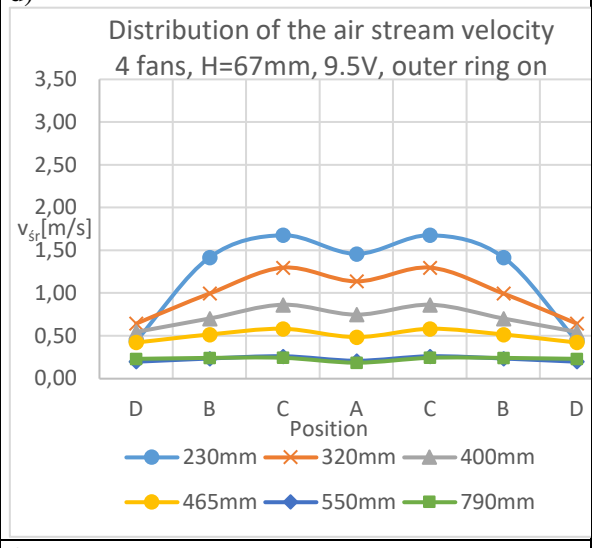

e)

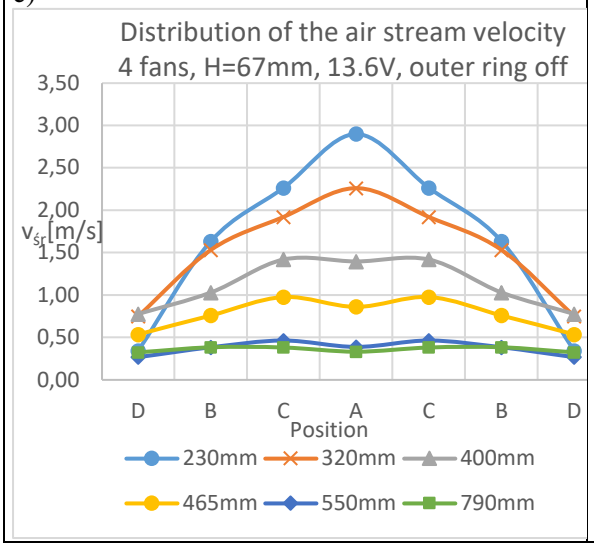

f)

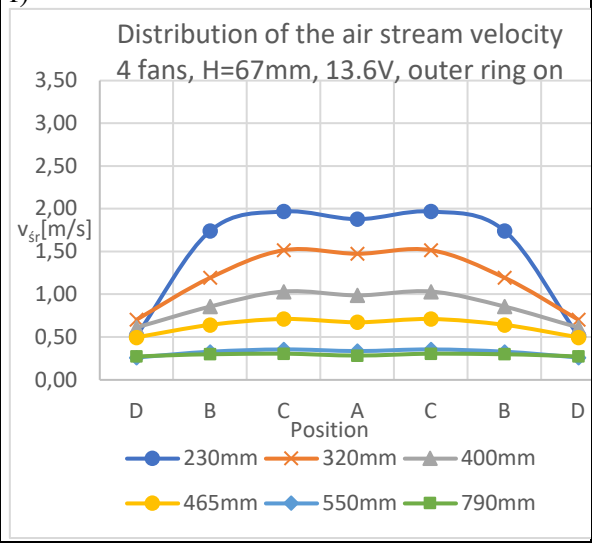

Compared to the ventilation tower with 4 fans and a base height of 90mm, the curves in the above graphs are less convex, i.e. the air flow is more evenly distributed. Comparing the values, the values for probe 5 (above the inversion layer) are much lower.

Fig. 9.6.16. Mean velocity for ventilation chimney with 1 fan, H=67mm, ***outer ring off***

a)

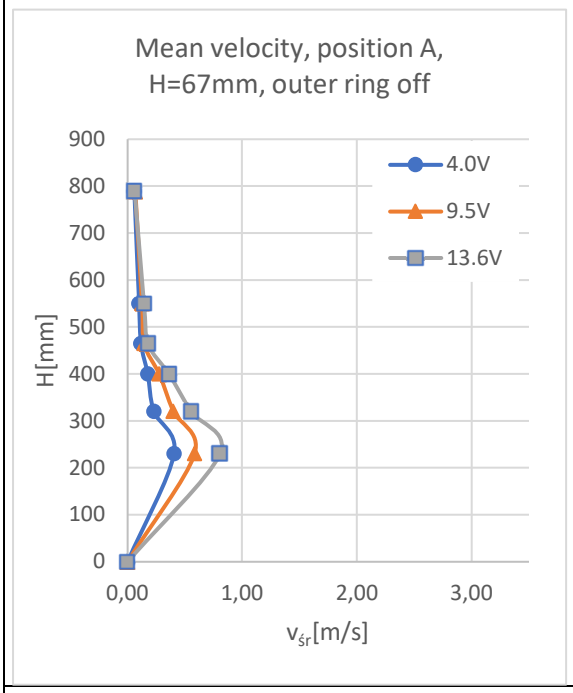

b)

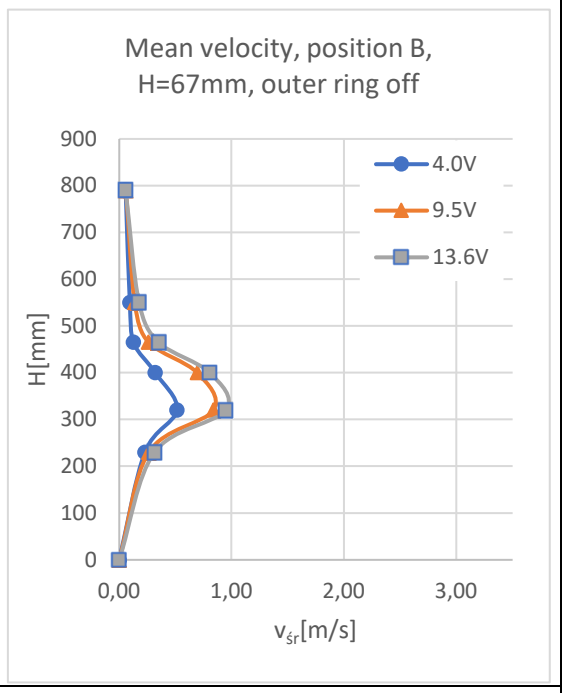

c)

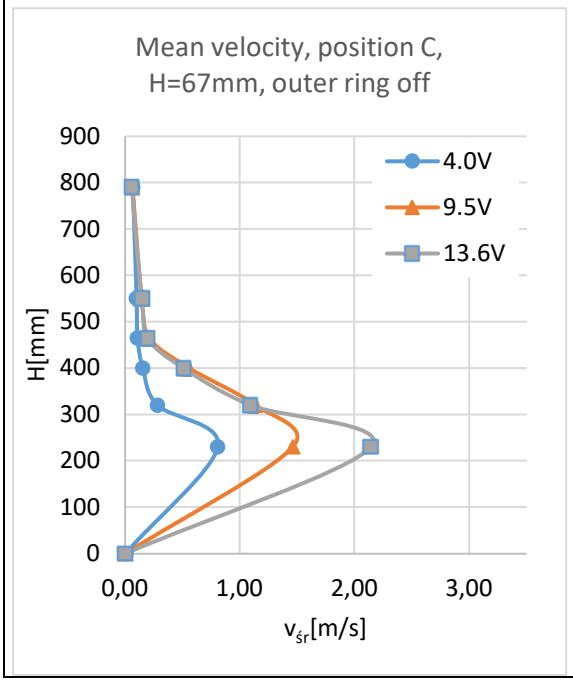

d)

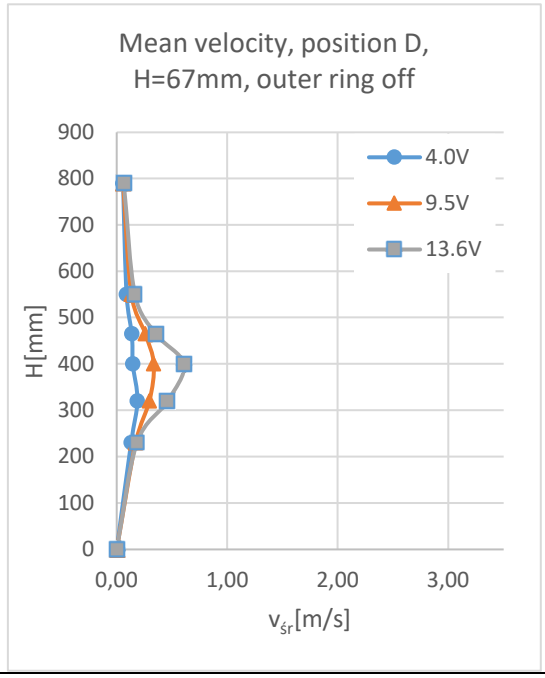

Obtained values are slightly lower than for 1 fan ventilation chimney and the base height of 90mm.

Fig. 9.6.17. Mean velocity for ventilation chimney with 1 fan, H=67mm, ***outer ring on***

a)

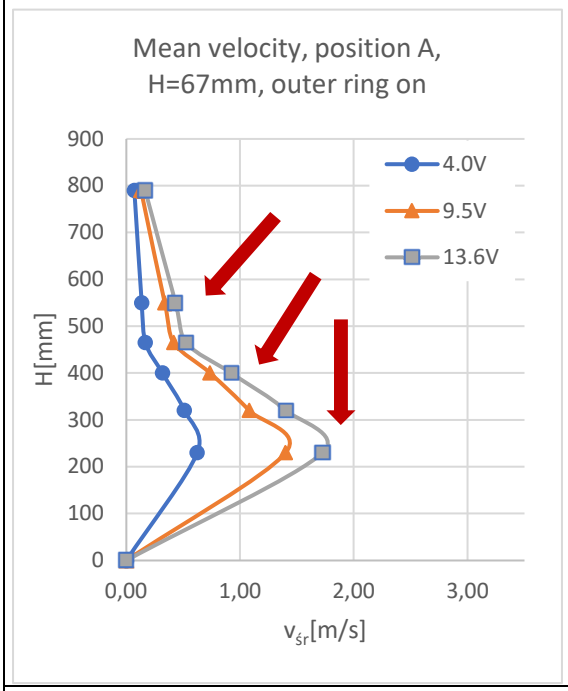

b)

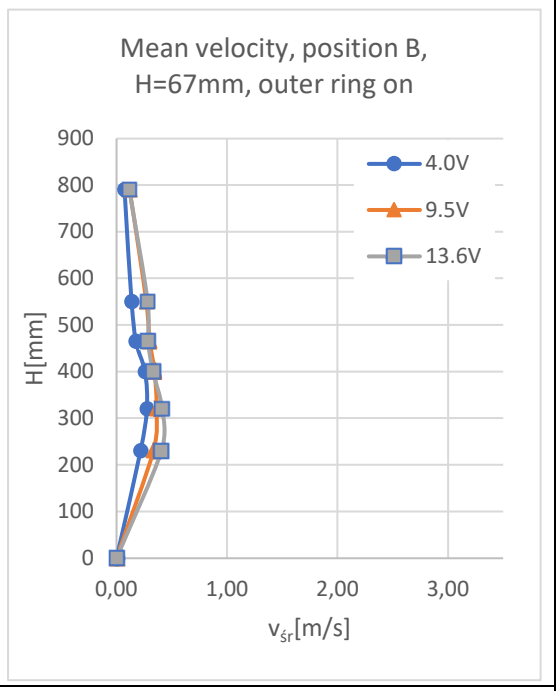

c)

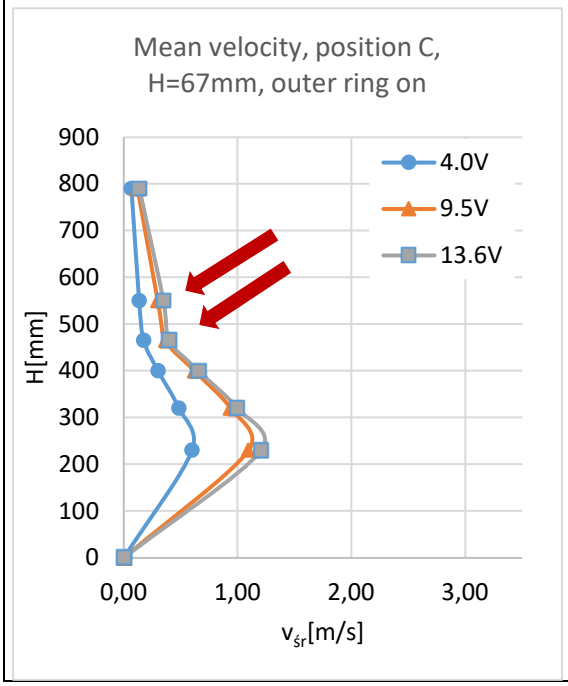

d)

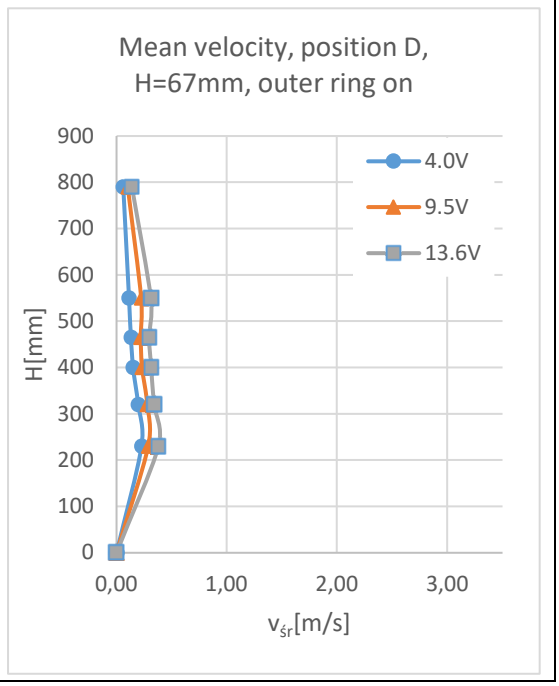

The red arrows show points with a strong increase in the air velocities after turning on the outer ring.

Fig. 9.6.18. Mean velocity for ventilation chimney with 1 fan, H=67mm

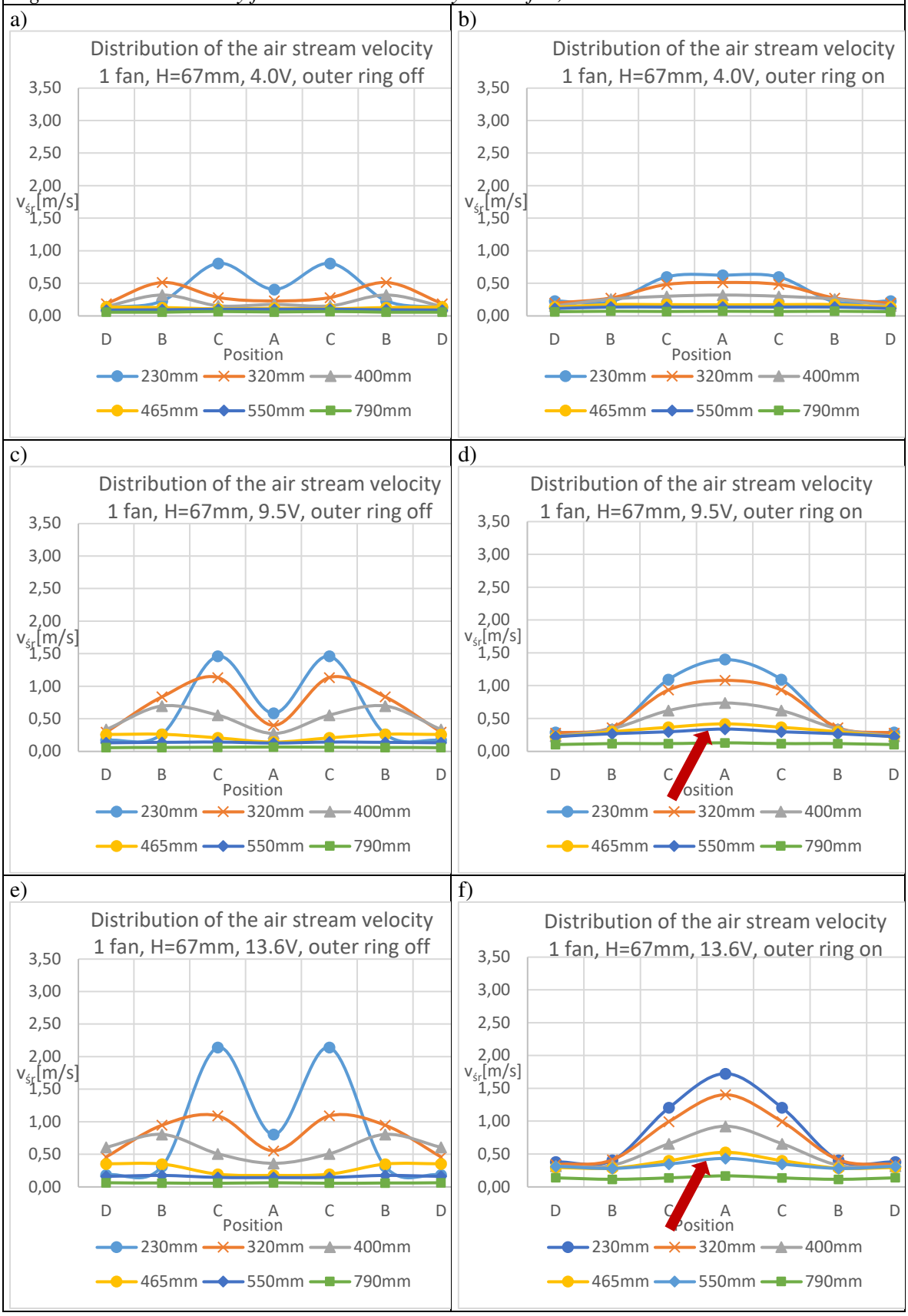

For the supply voltage of 9.5V and 13.6V and the outer ring turning on, it can be seen the breaking through the inversion layer (red arrows).

Fig. 9.6.19. Mean velocity for ventilation chimney with 8 fans, H=45mm, ***outer ring off***

a)

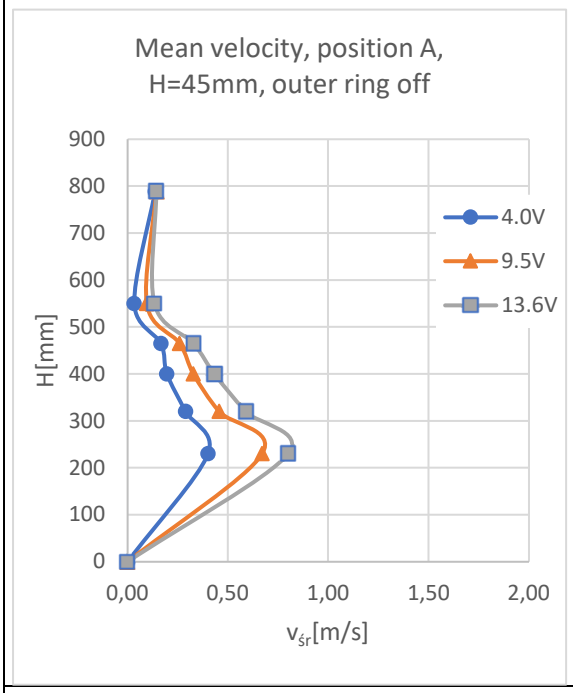

b)

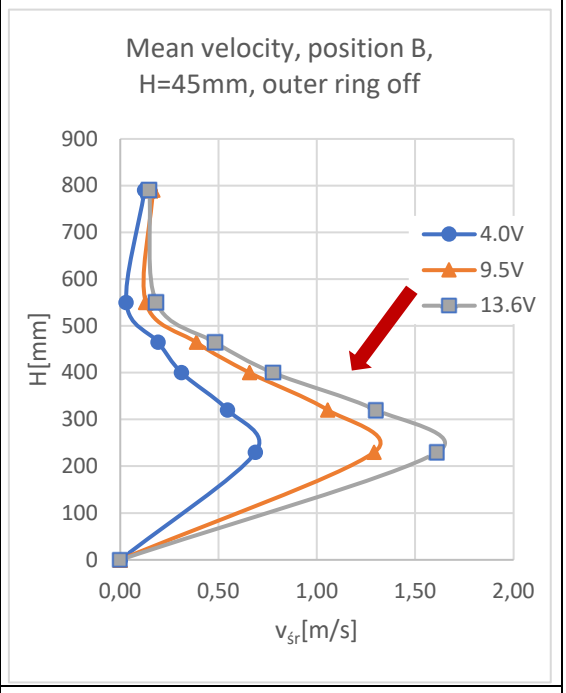

c)

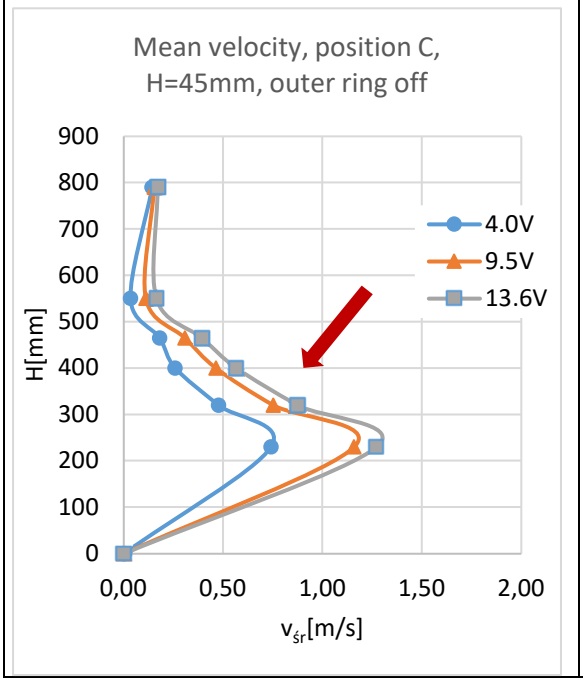

d)

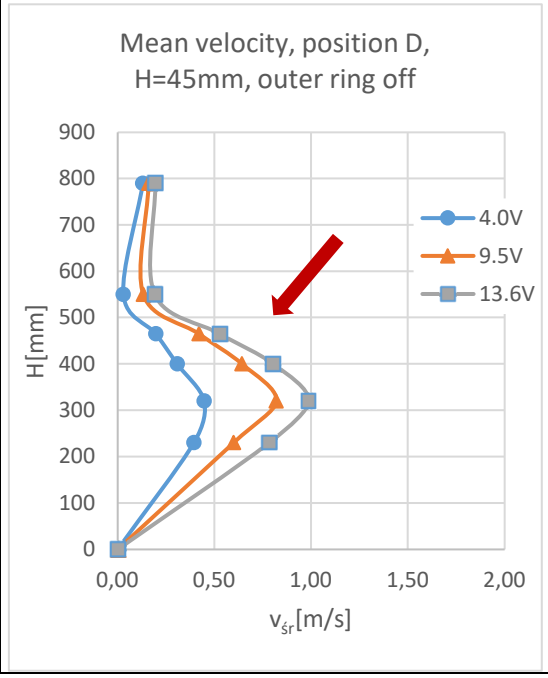

The graphs above show a sudden increase in air velocity on the sides of the air stream, i.e. at points B, C, and D (red arrows). However, the values obtained on probe 5 are smaller or comparable to those for a ventilation chimney with 8 fans and a base height of 67mm.

Fig. 9.6.20. Mean velocity for ventilation chimney with 8 fans, H=45mm, ***outer ring on***

a)

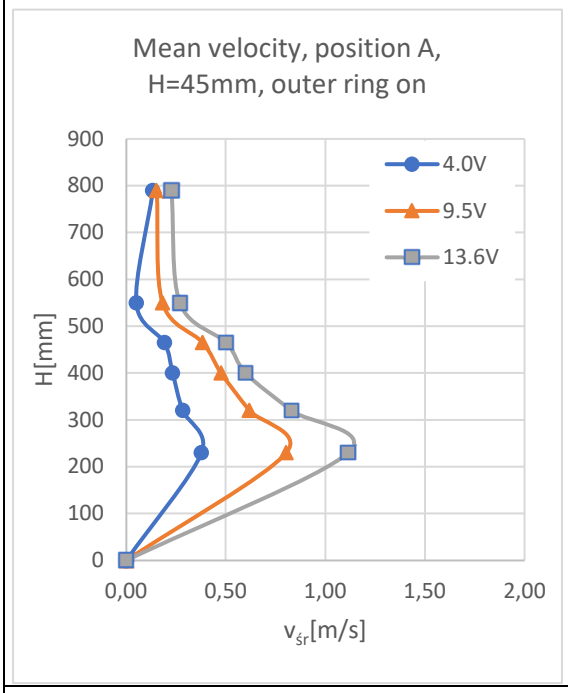

b)

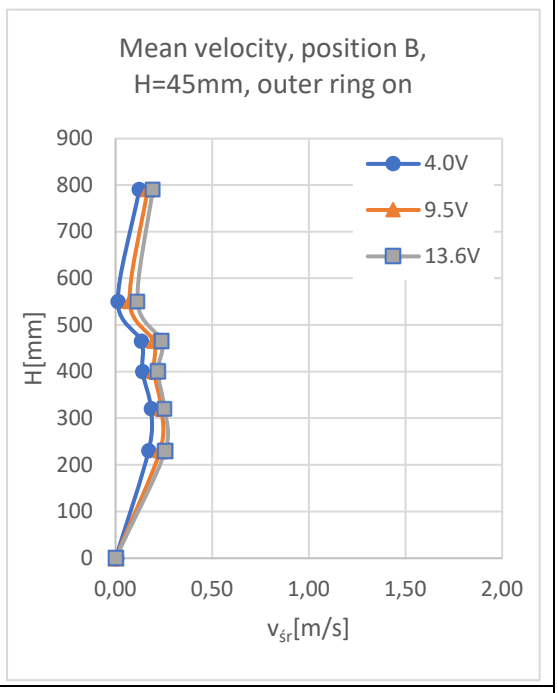

c)

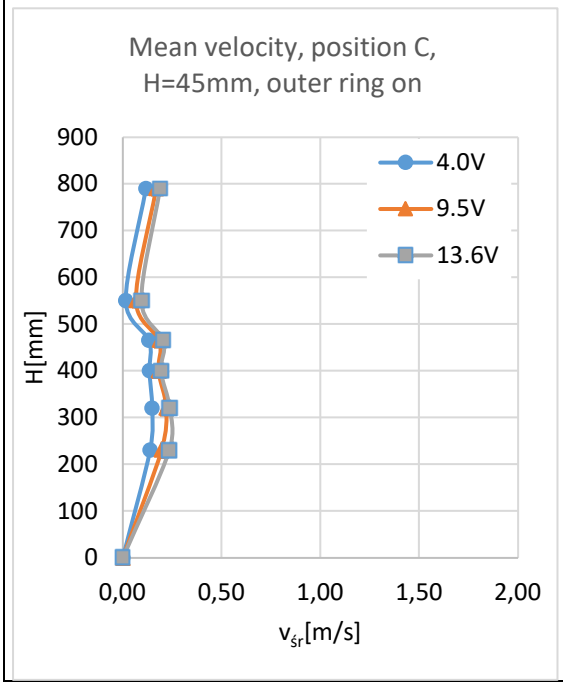

d)

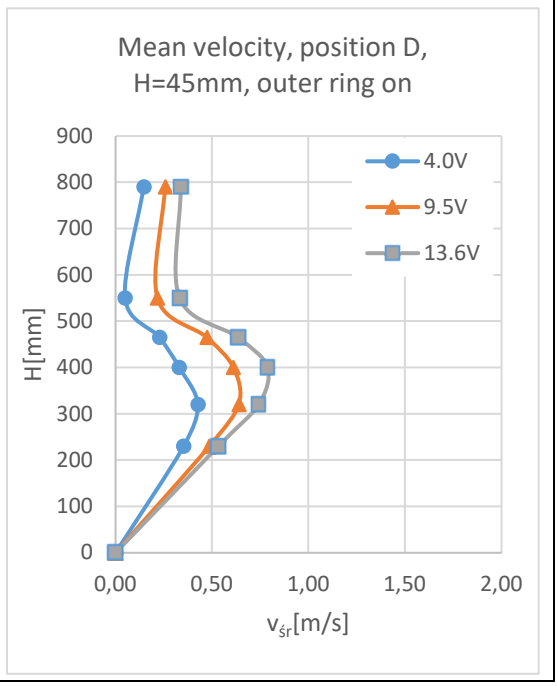

Fig. 9.6.21. Mean velocity for ventilation chimney with 8 fans, H=45mm

a)

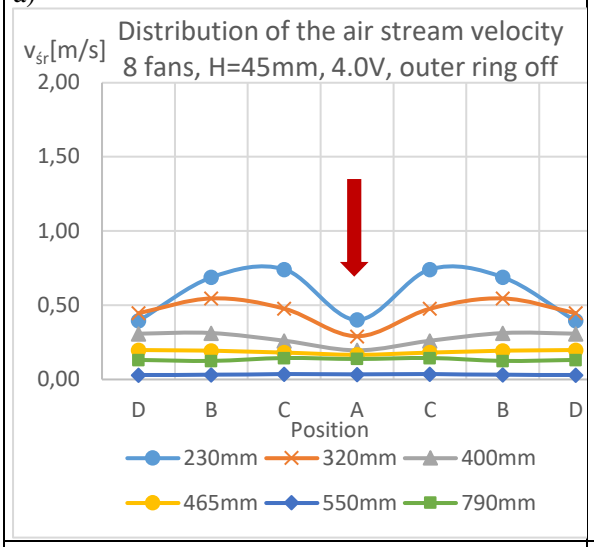

b)

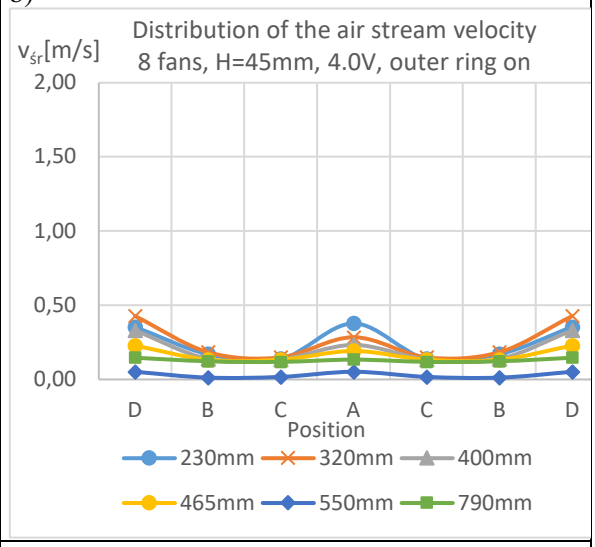

c)

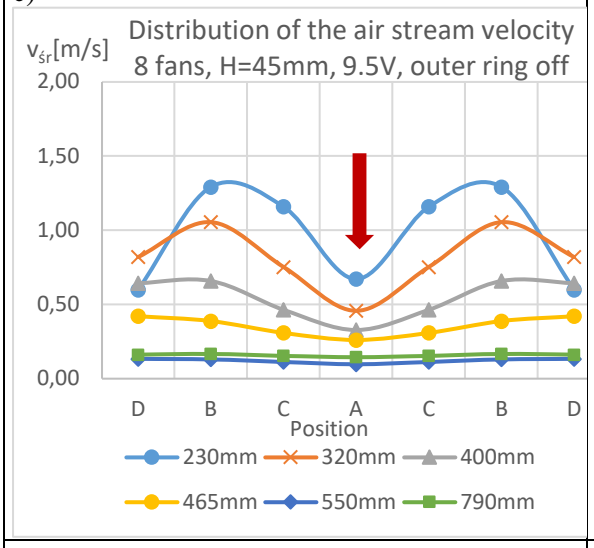

d)

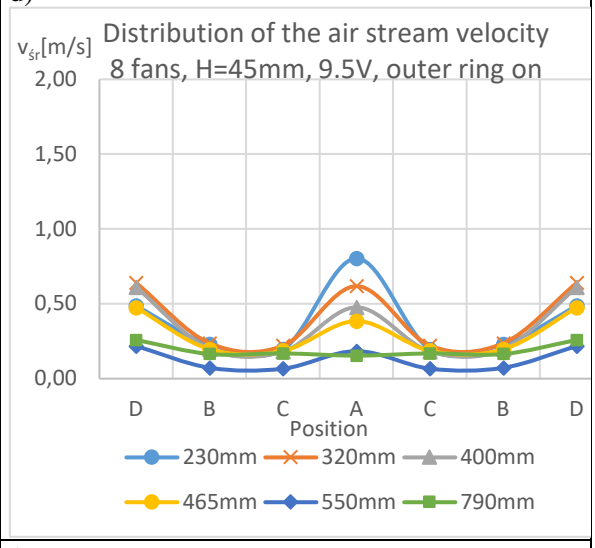

e)

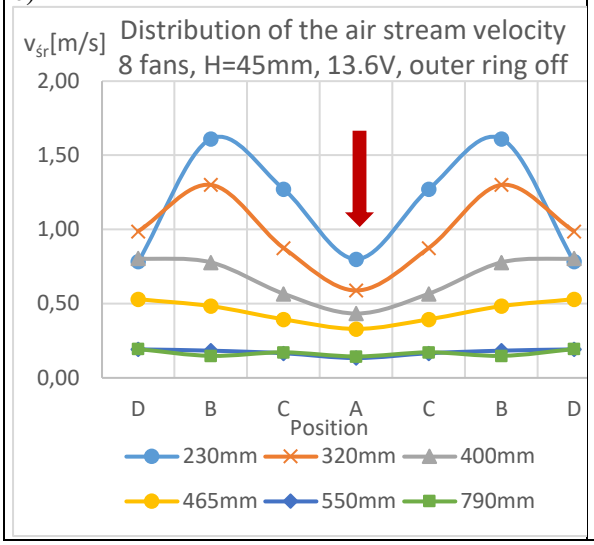

f)

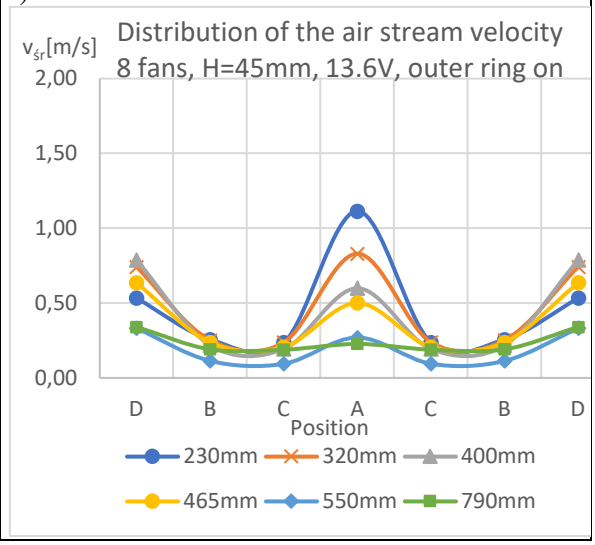

The graphs above show a decrease in air velocity in the center of the air stream when the outer ring is turned off, and the opposite effect when the outer ring is turned on. This is probably due to the formation of a vortex that is broken up when the outer ring is activated.

Fig. 9.6.22. Mean velocity for ventilation chimney with 4 fans, H=45mm, ***outer ring off***

a)

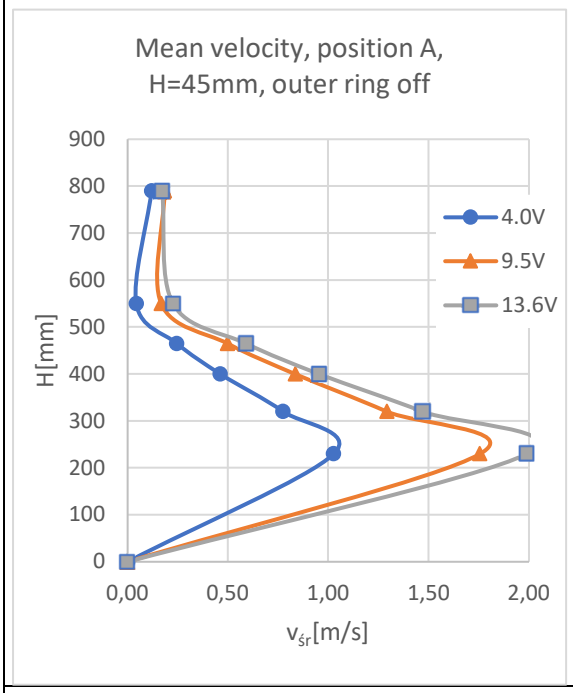

b)

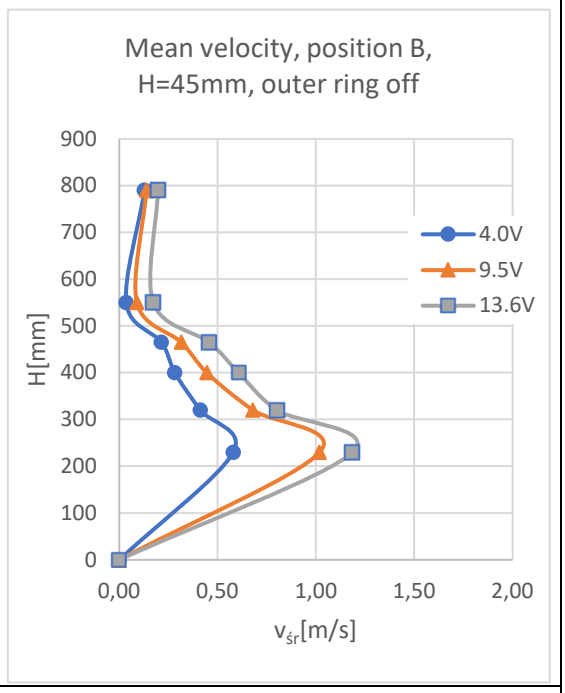

c)

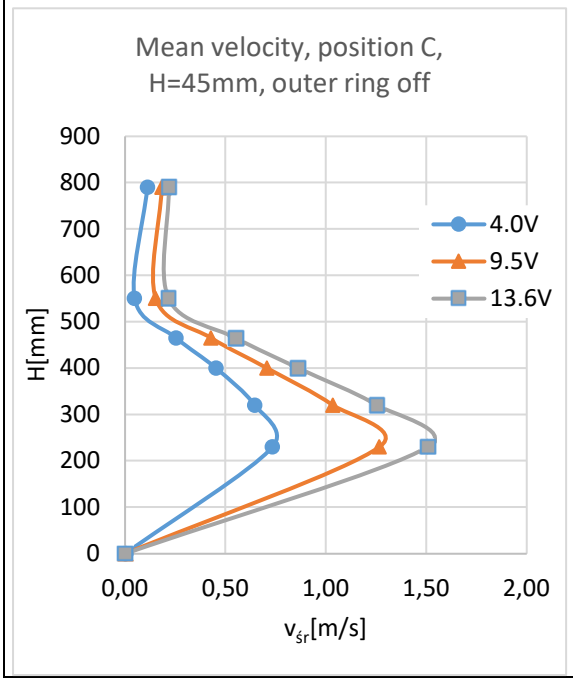

d)

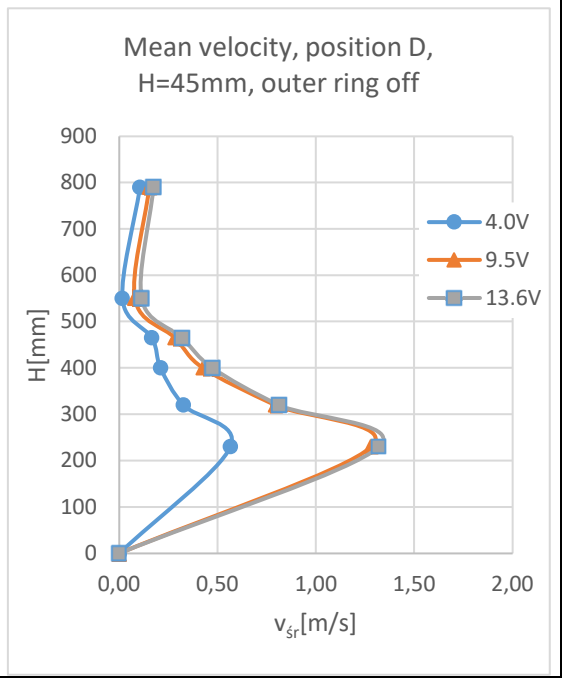

Fig. 9.6.23. Mean velocity for ventilation chimney with 4 fans, H=45mm, ***outer ring on***

a)

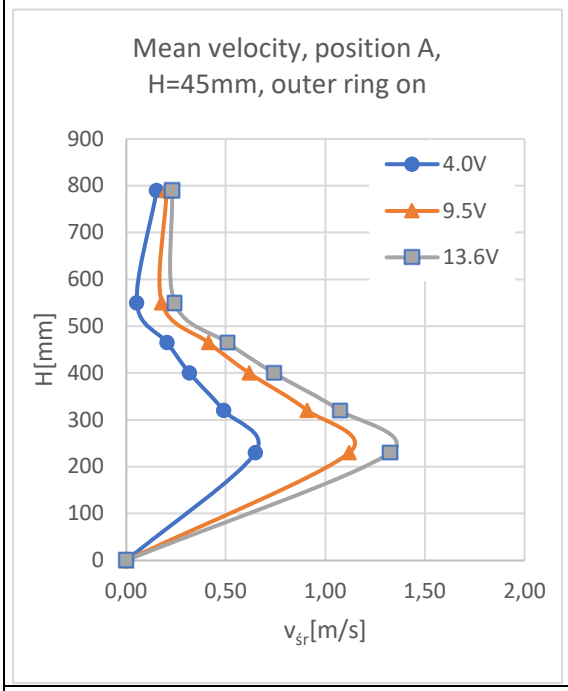

b)

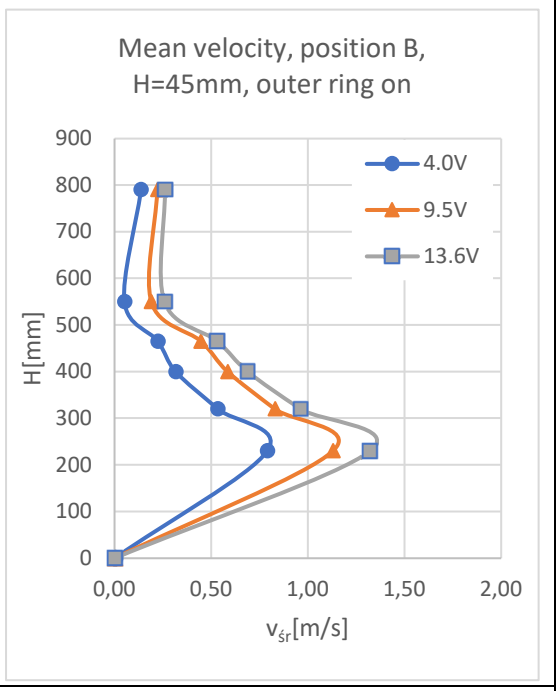

c)

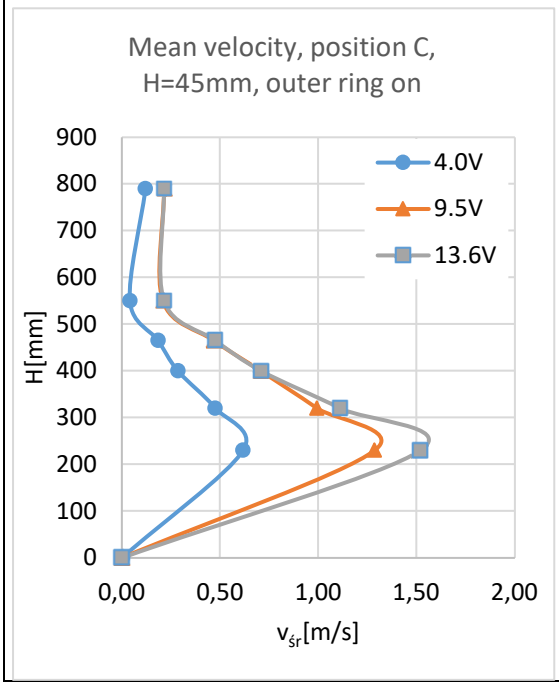

d)

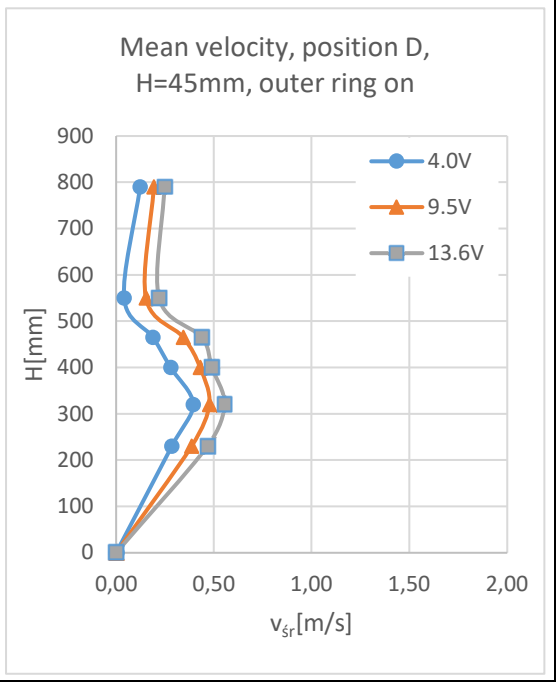

Fig. 9.6.24. Mean velocity for ventilation chimney with 4 fans, H=45mm

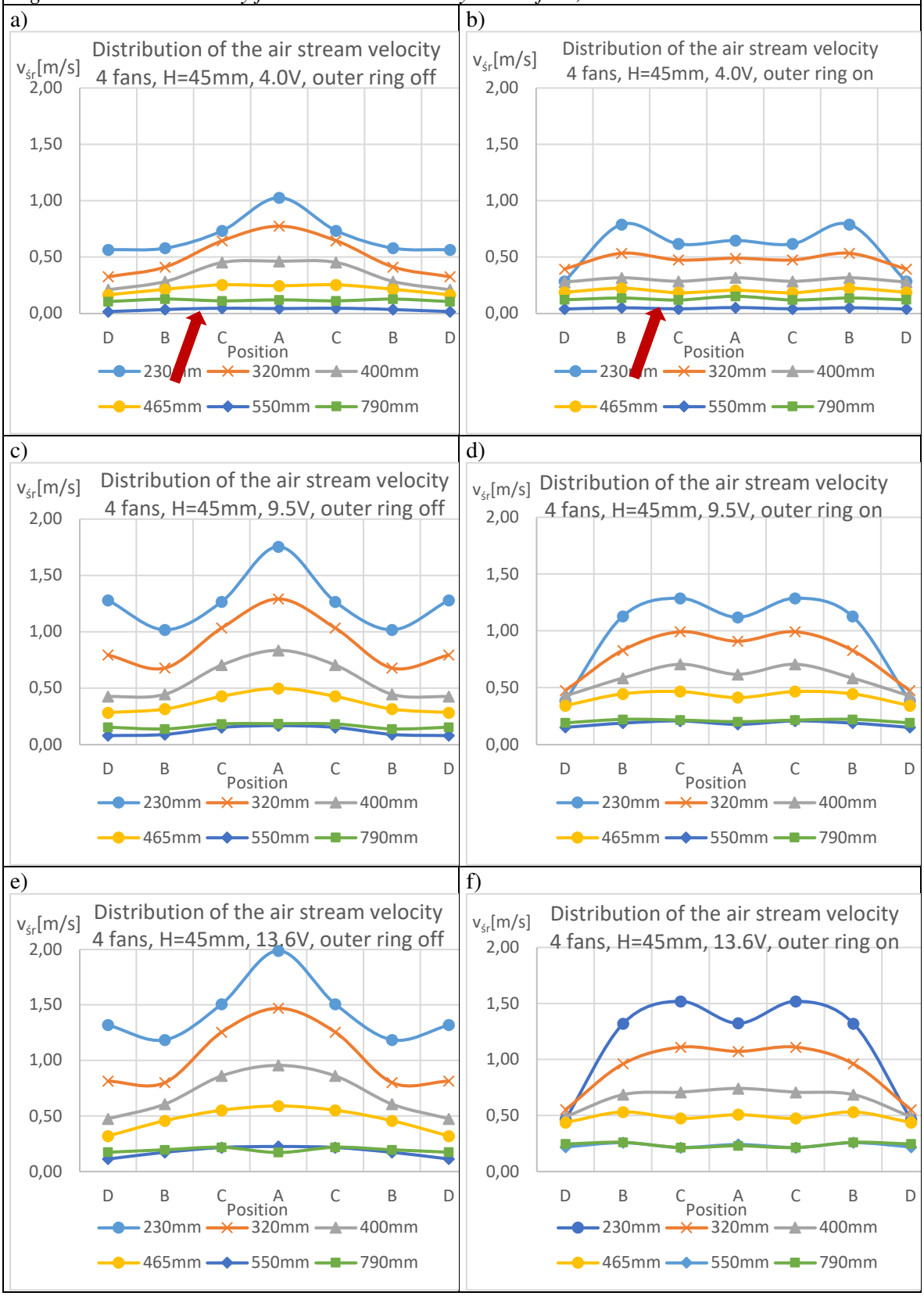

For the 4-fan tower and 45mm of the base height, the effect of reducing the air velocity in the middle of the air stream is no longer strongly noticeable. In all cases, the air velocities are higher than for the chimney with 8 fans and a base height of 45mm. The velocities at probe 5 are lower than for the chimney with 4 fans and base heights of 67mm and 90mm and at point A there is no breakthrough of the inversion layer (red arrows).

Fig. 9.6.25. Mean velocity for ventilation chimney with 1 fan, H=45mm, ***outer ring off***

a)

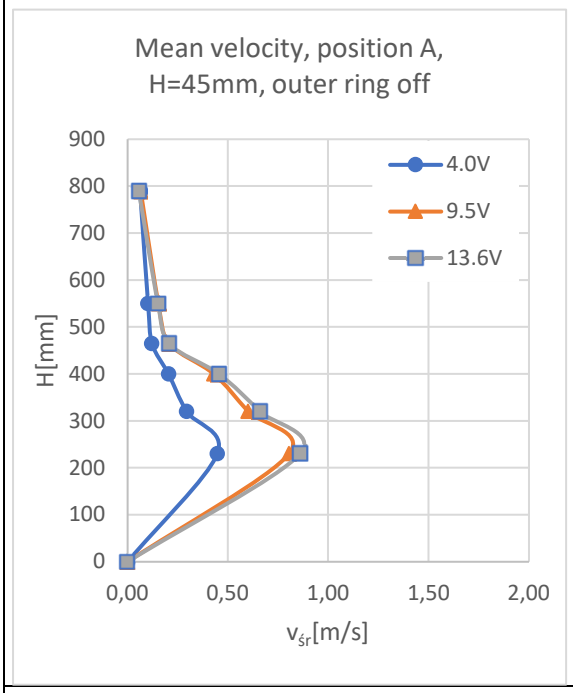

b)

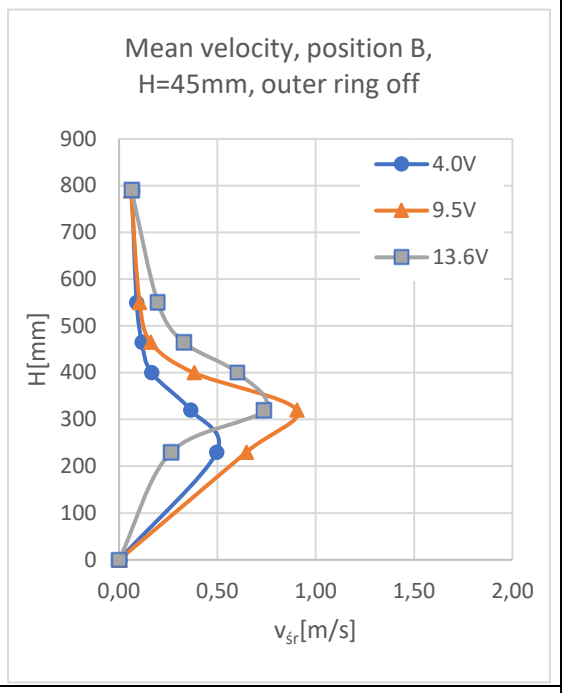

c)

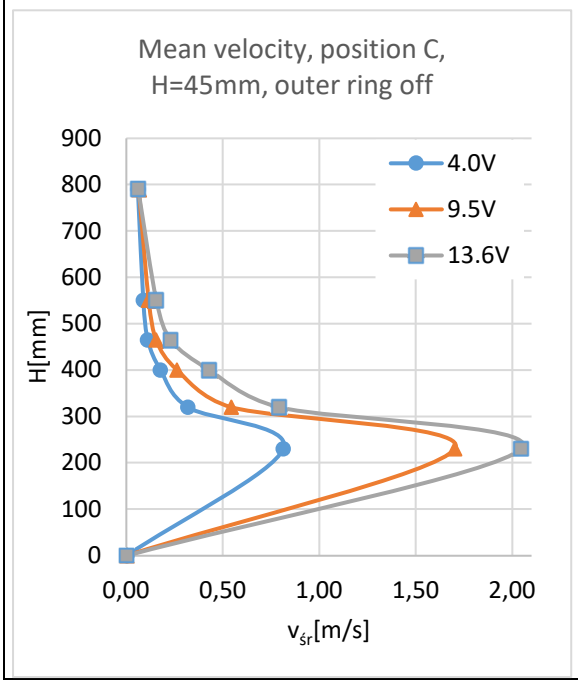

d)

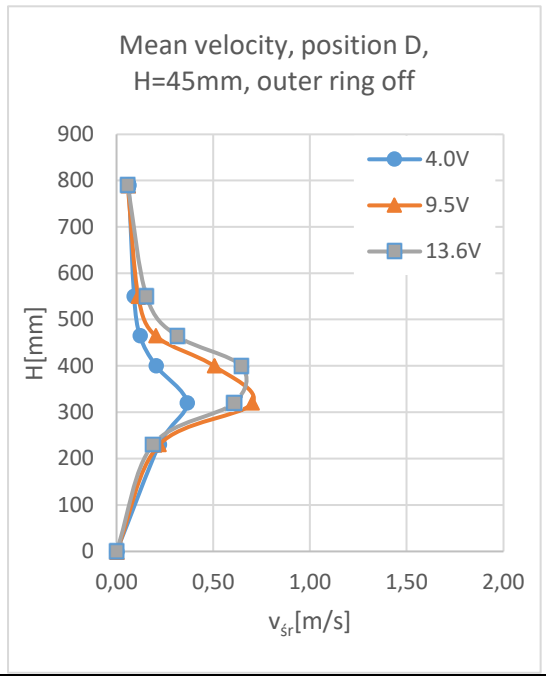

Fig. 9.6.25. Mean velocity for ventilation chimney with 1 fan, H=45mm, ***outer ring on***

a)

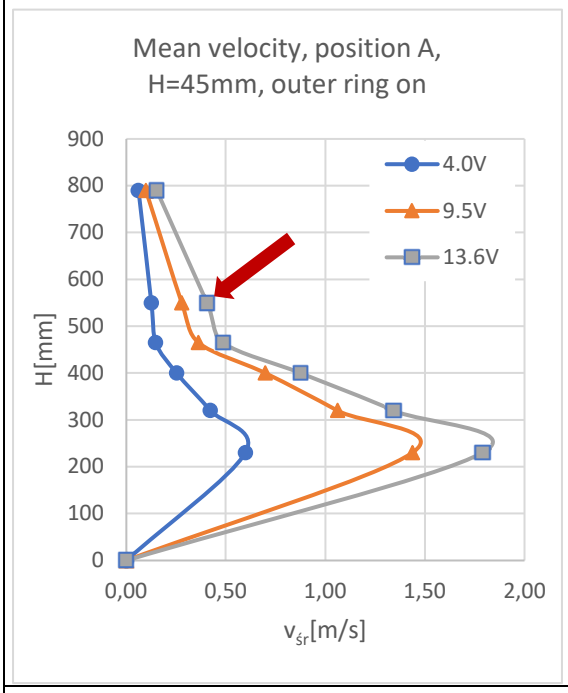

b)

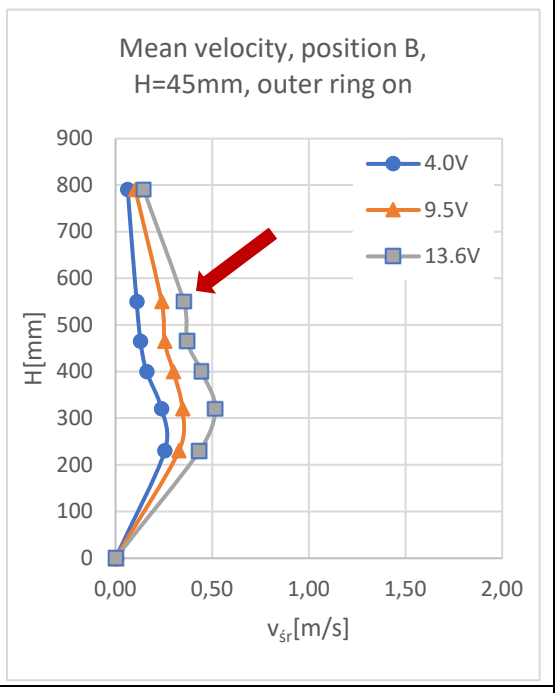

c)

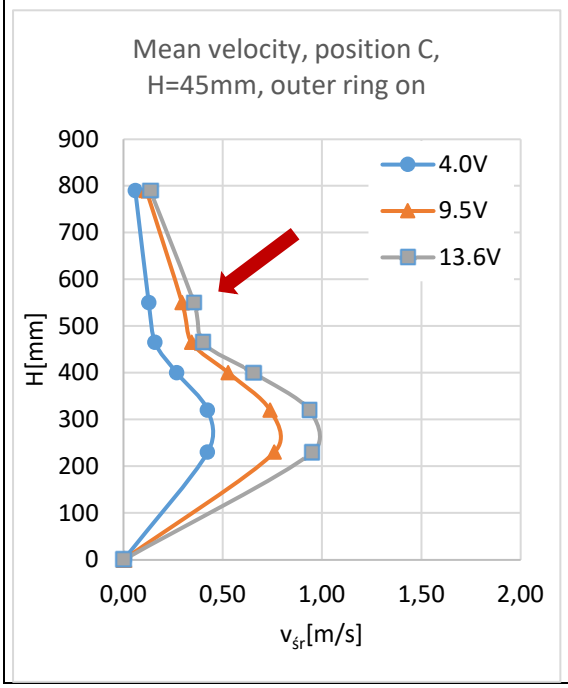

d)

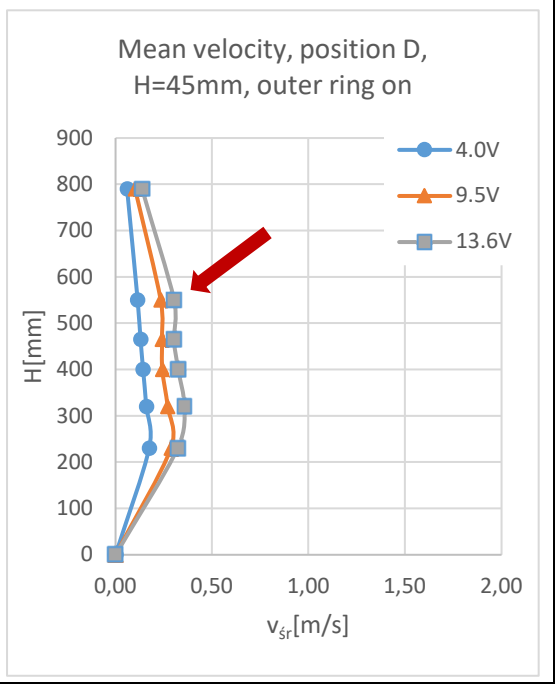

Turning on the outer ring significantly increase the air velocities above the inversion layer and allowed it to break through the layer.

Fig. 9.6.26. Mean velocity for ventilation chimney with 1 fan, H=45mm

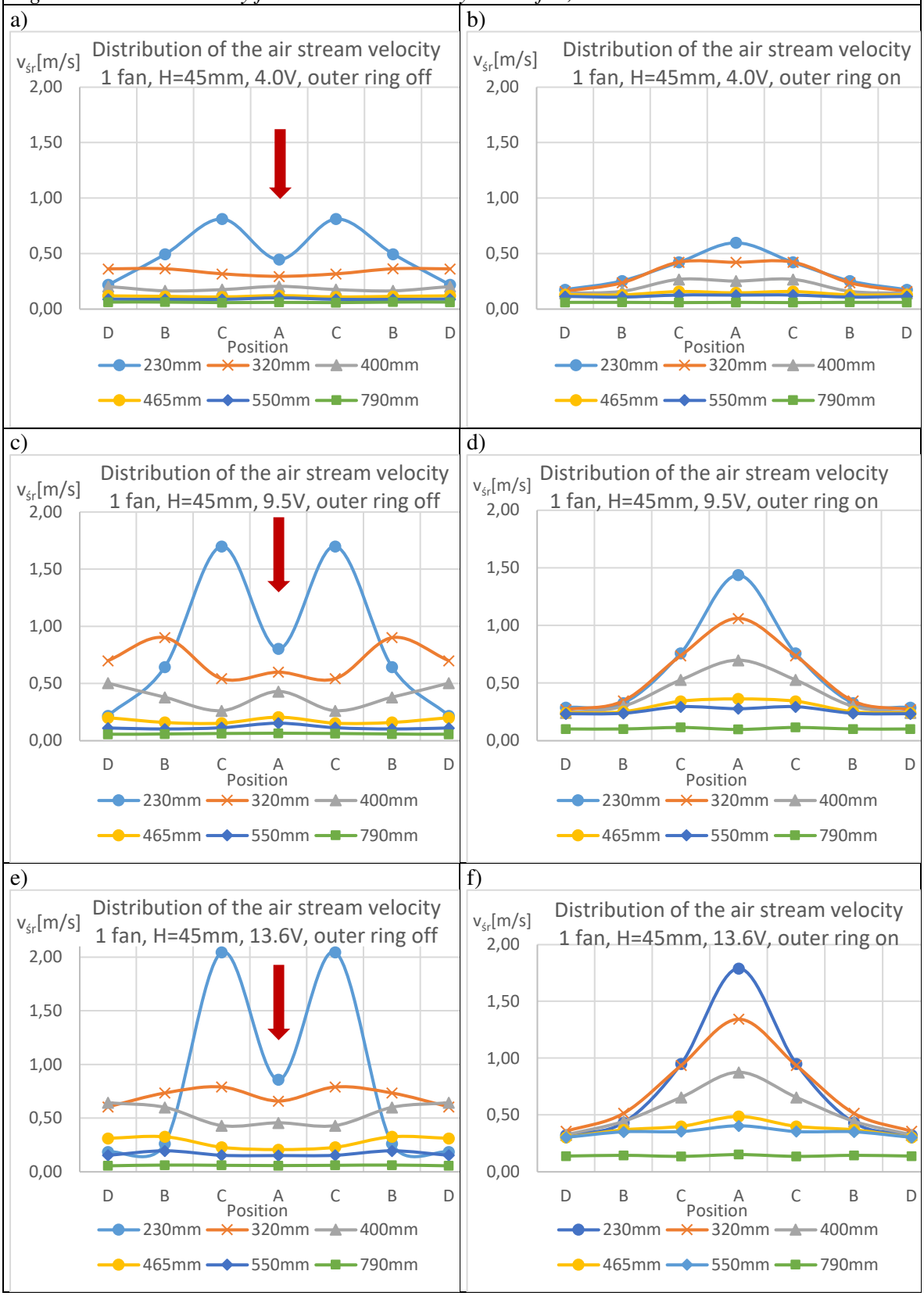

We can see again a decrease in air velocity at the center of the air stream. Penetration of the inversion layer occurred only for the voltage of 13.6V (in both cases) and 9.5V with the outer ring on.

Fig. 9.6.27. Mean velocity for ventilation chimney with 8 fans, H=22mm, ***outer ring off***

a)

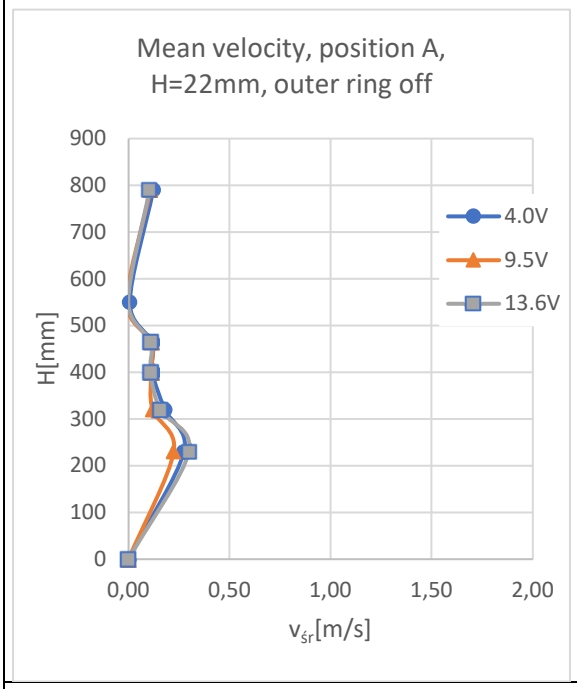

b)

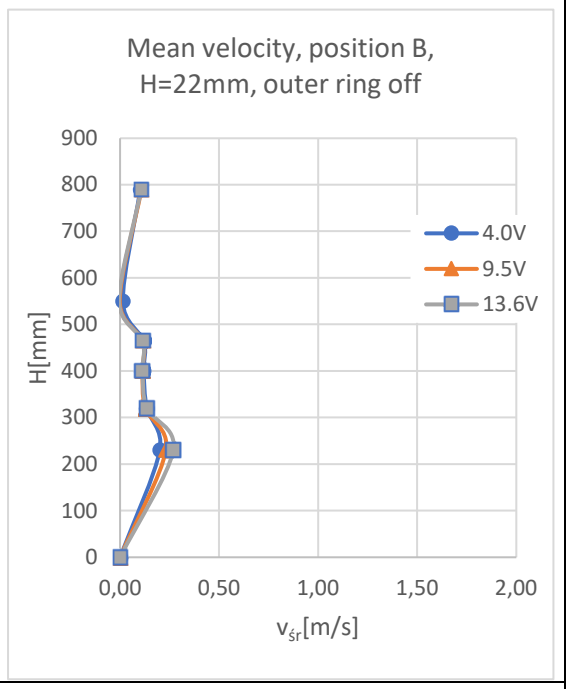

c)

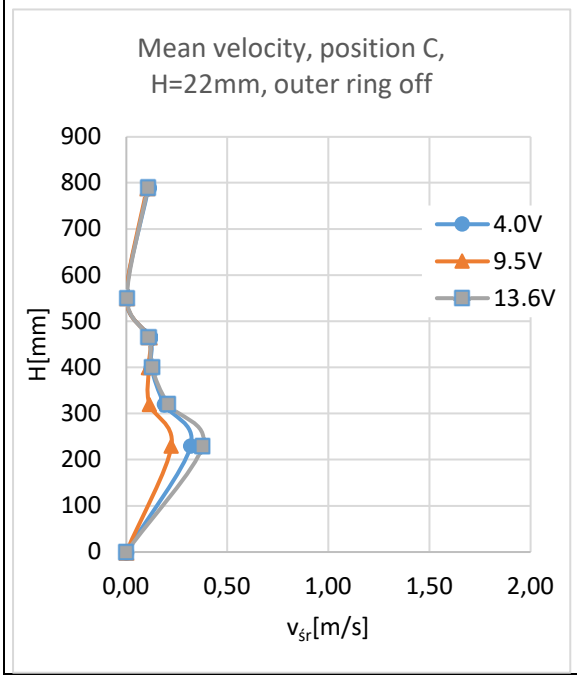

d)

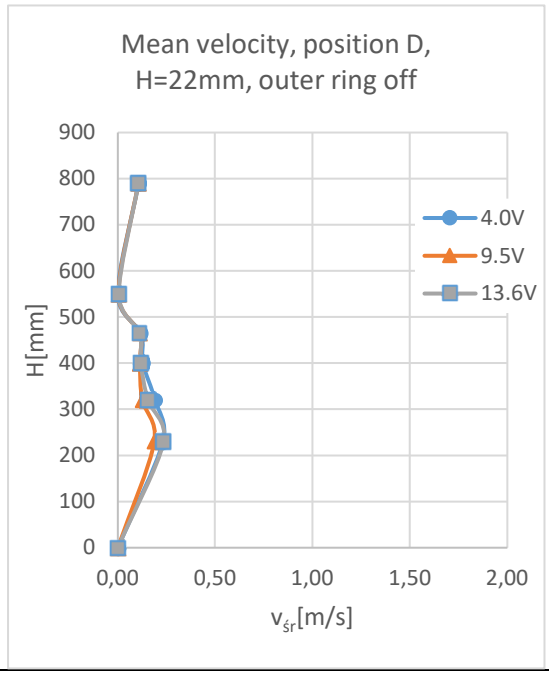

The air velocity in all the probes has dropped to almost zero. The ventilation system is no longer effective.

Fig. 9.6.28. Mean velocity for ventilation chimney with 8 fans, H=22mm, ***outer ring on***

a)

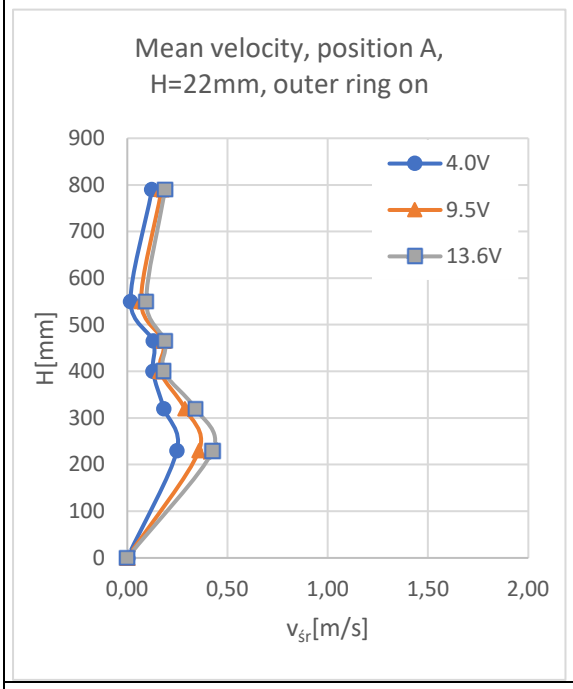

b)

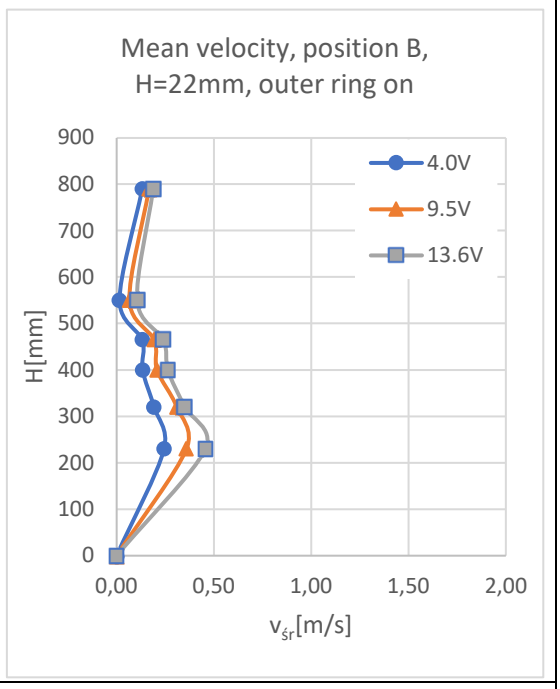

c)

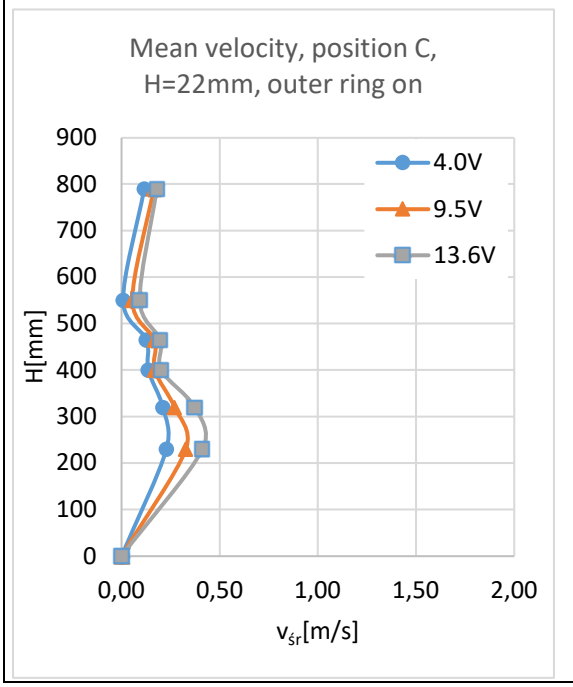

d)

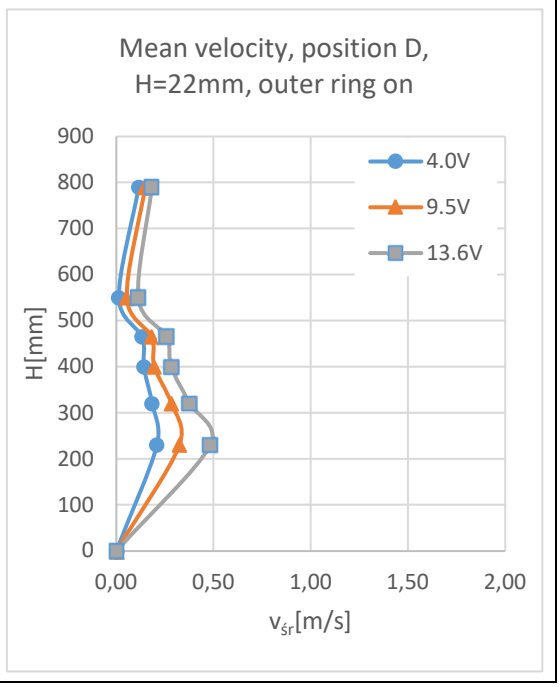

Fig. 9.6.29. Mean velocity for ventilation chimney with 8 fans, H=22mm

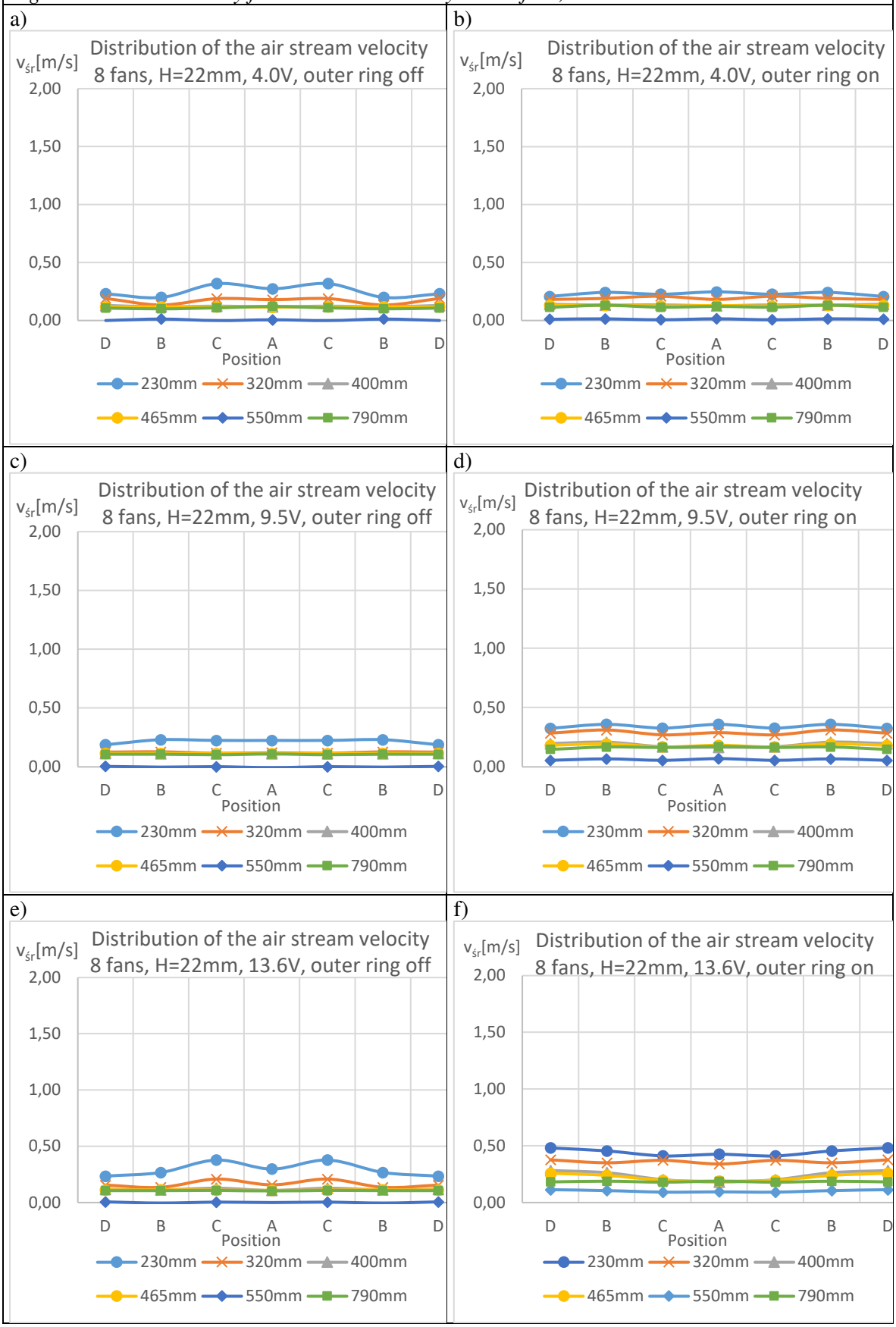

For this case and all cases below with the height of 22mm we can assume that the chimney does not generate any stream.

Fig. 9.6.30. Mean velocity for ventilation chimney with 4 fans, H=45mm, ***outer ring off***

a)

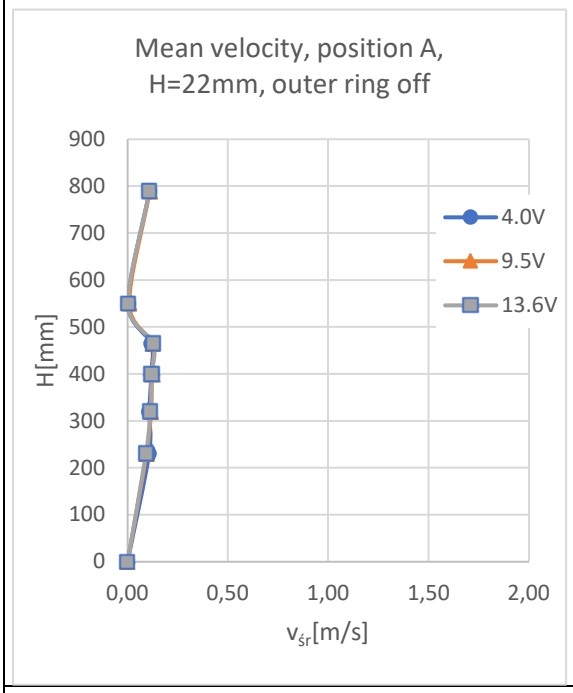

b)

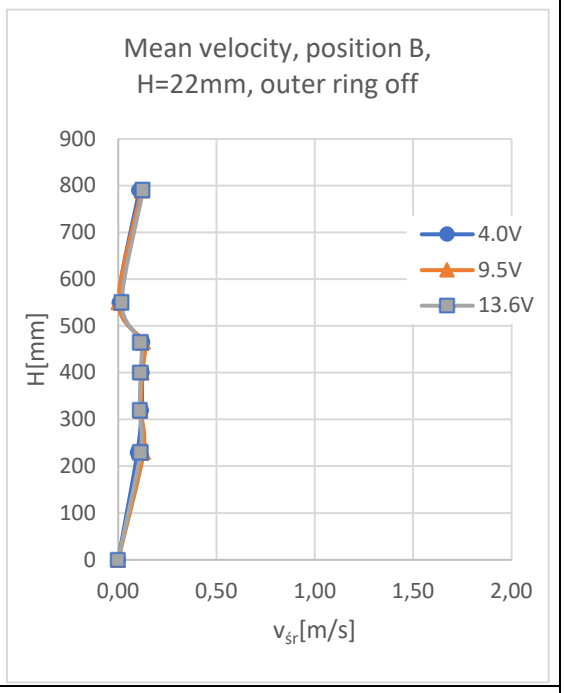

c)

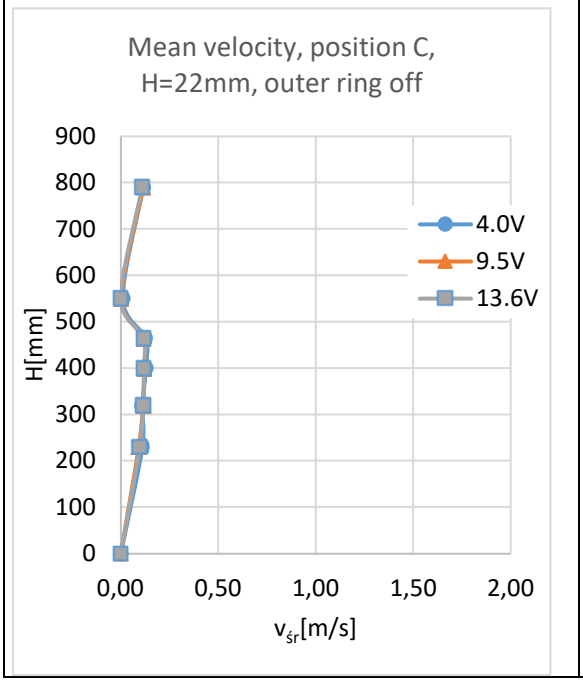

d)

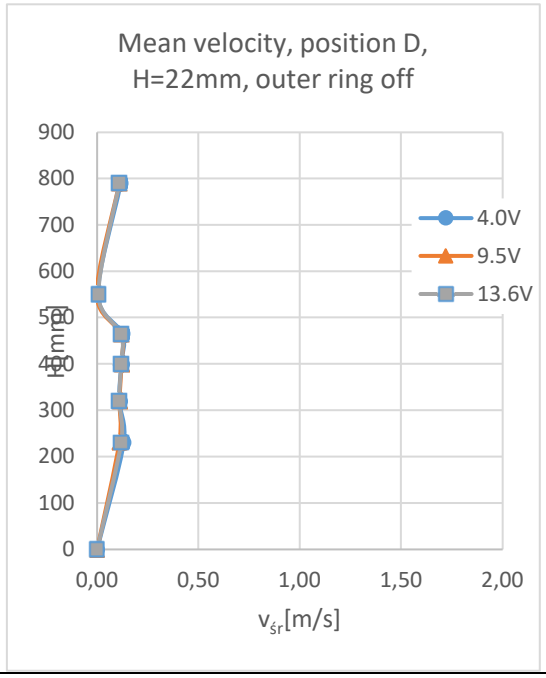

Fig. 9.6.31. Mean velocity for ventilation chimney with 4 fans, H=22mm, ***outer ring on***

a)

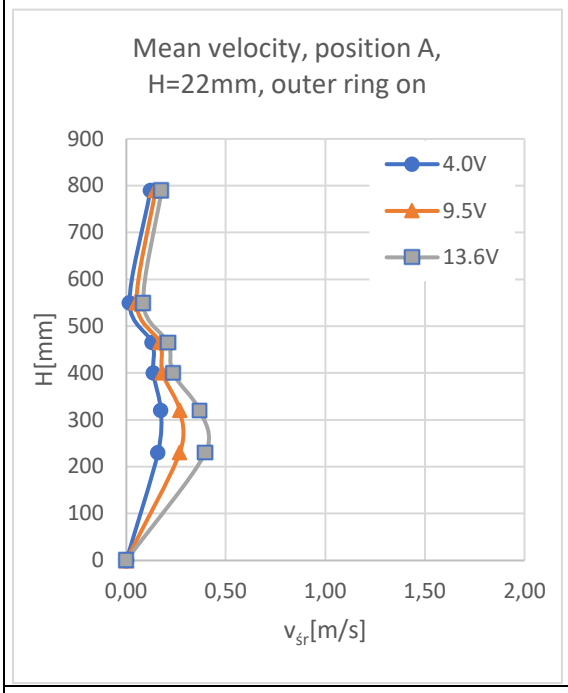

b)

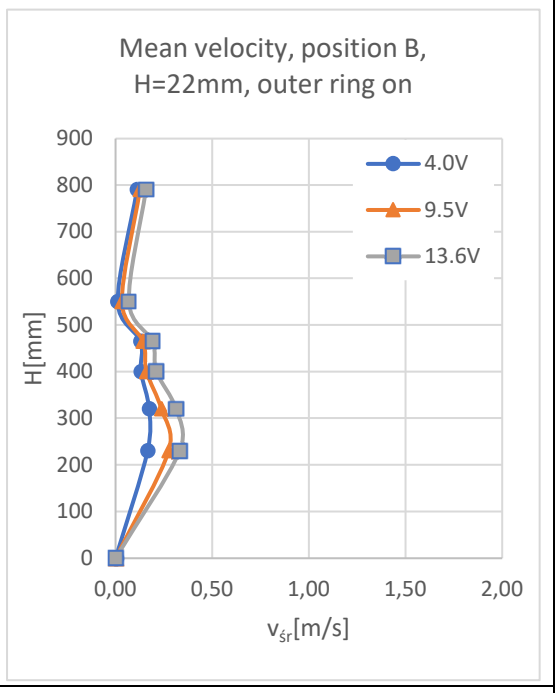

c)

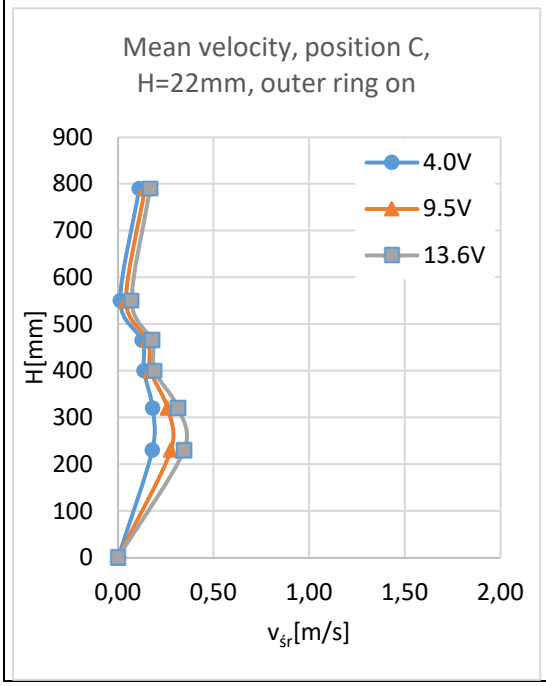

d)

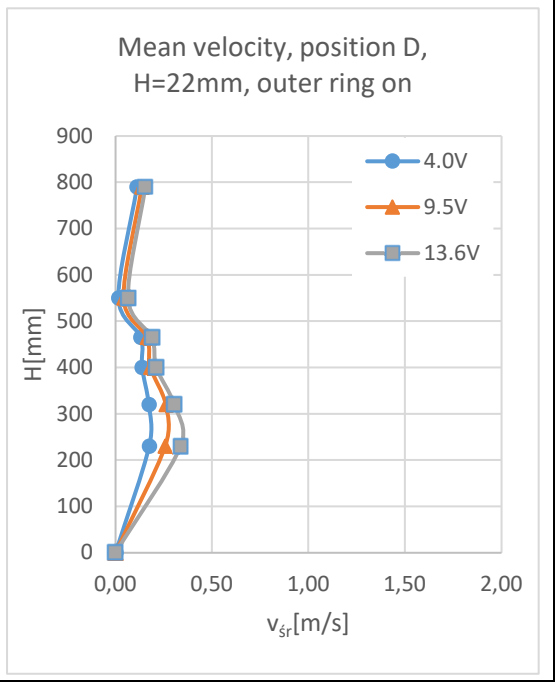

Fig. 9.6.32. Mean velocity for ventilation chimney with 4 fans, H=22mm

a)

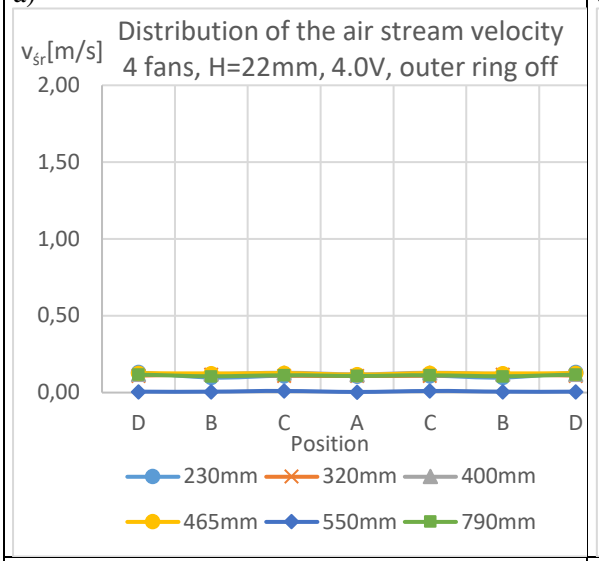

b)

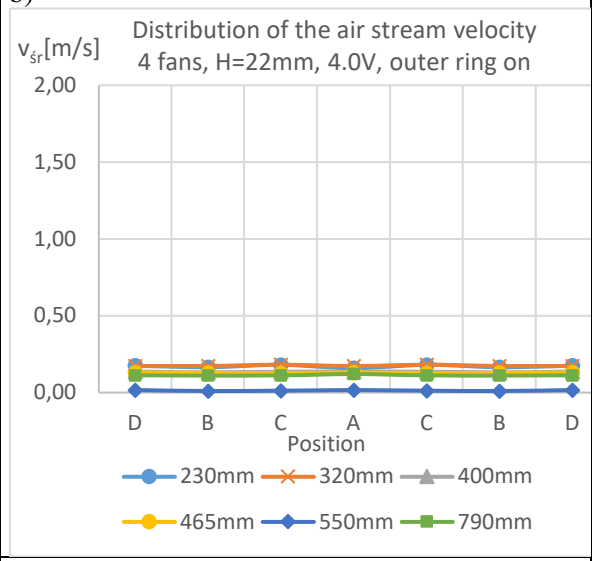

c)

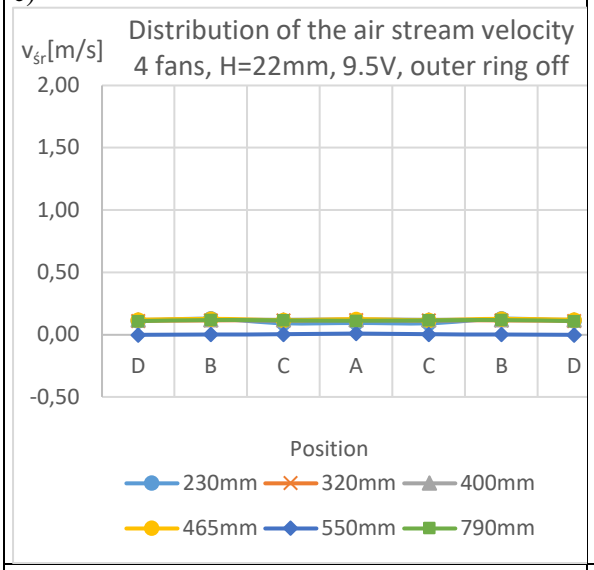

d)

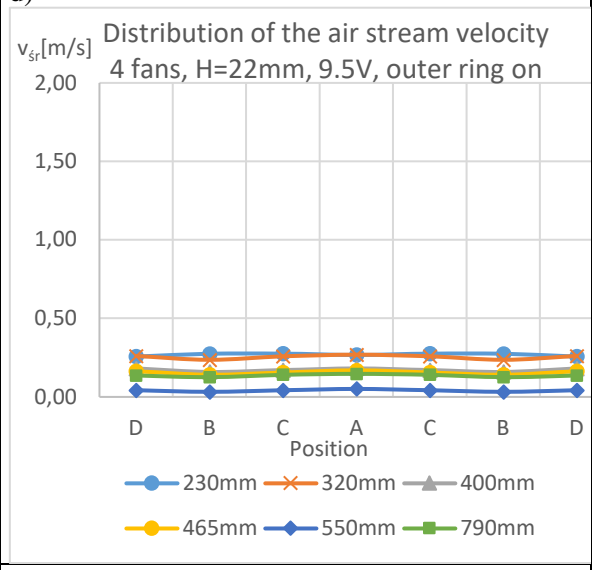

e)

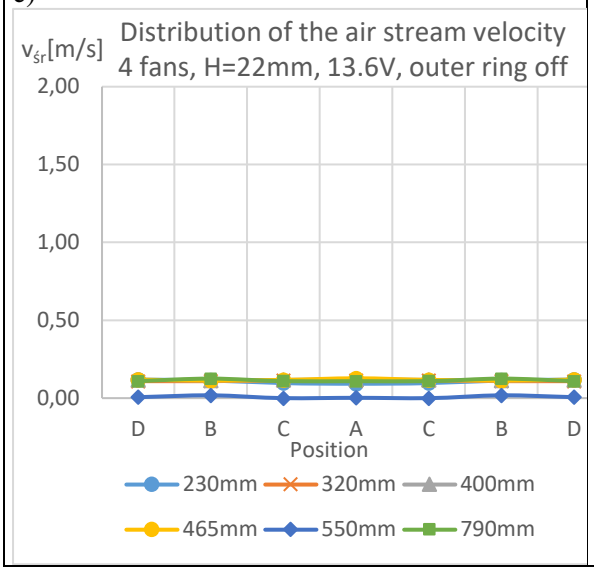

f)

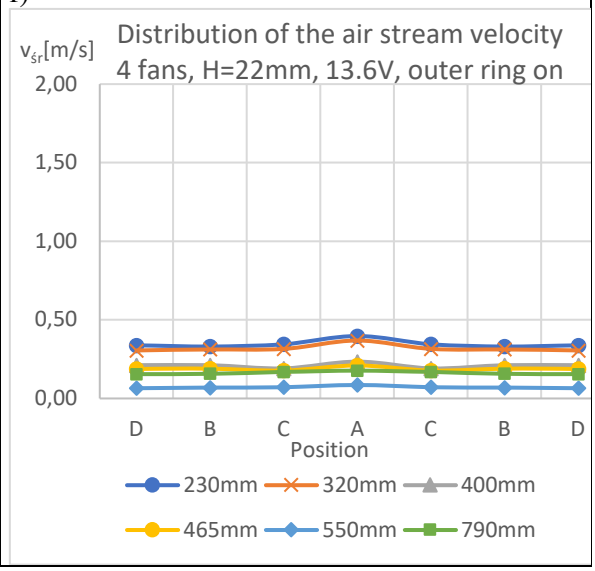

Fig. 9.6.33. Mean velocity for ventilation chimney with 1 fan, H=22mm, ***outer ring off***

a)

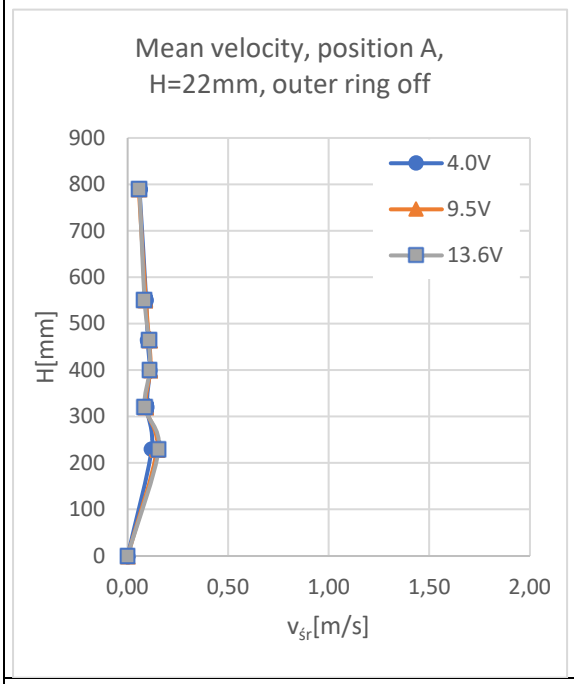

b)

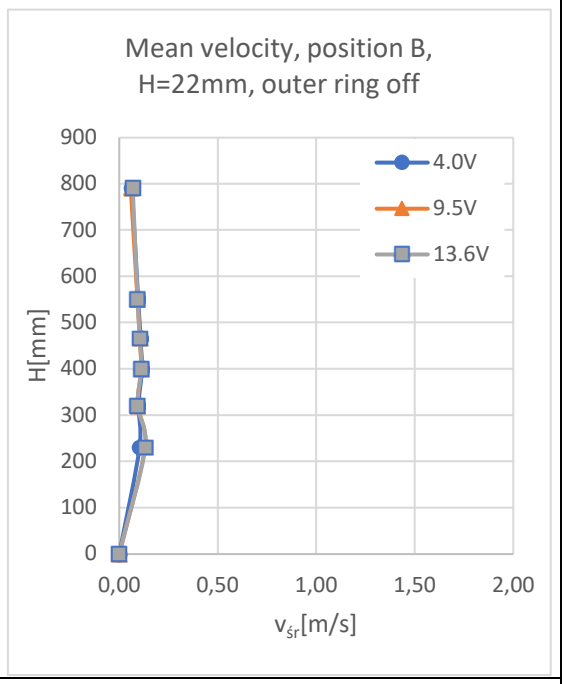

c)

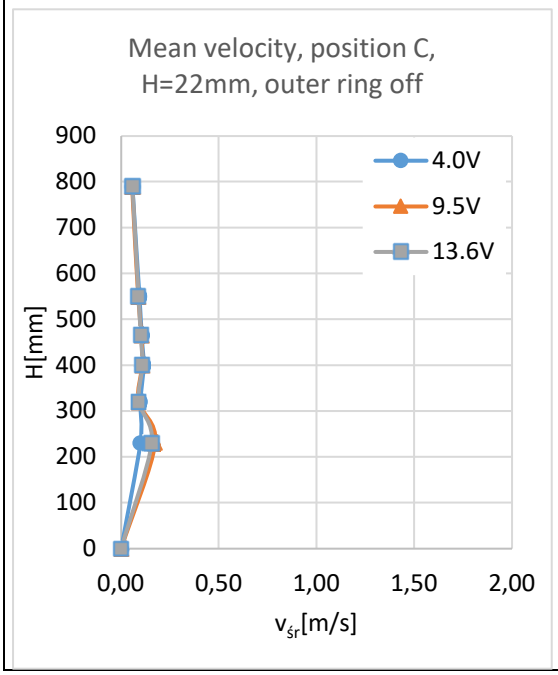

d)

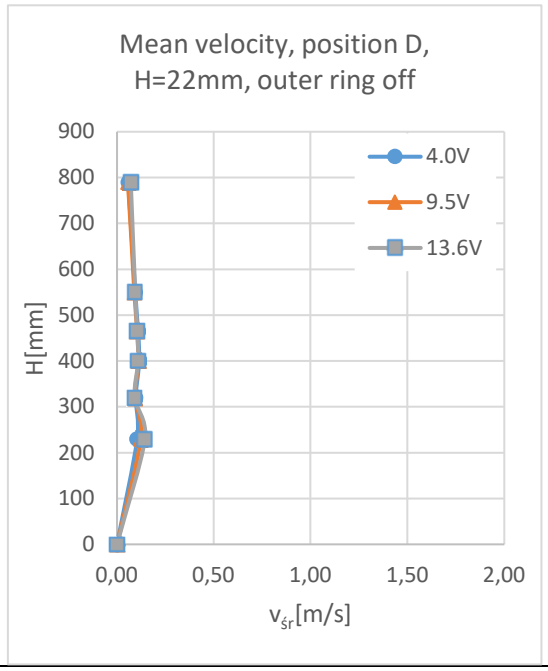

Fig. 9.6.34. Mean velocity for ventilation chimney with 1 fan, H=22mm, ***outer ring on***

a)

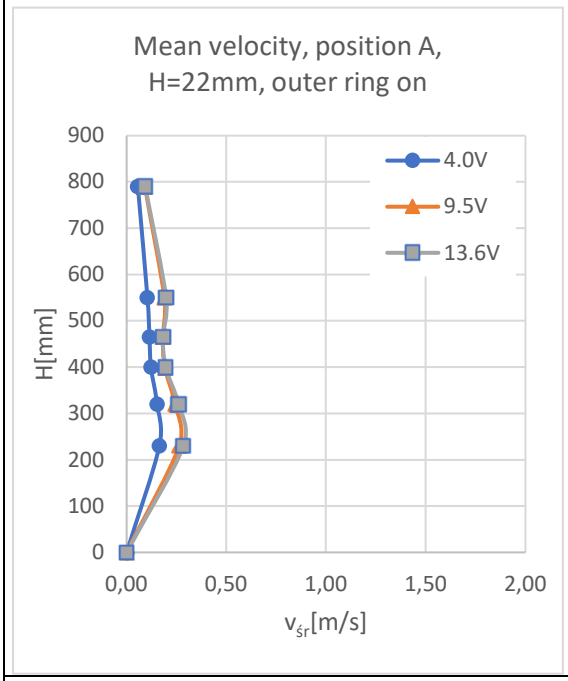

b)

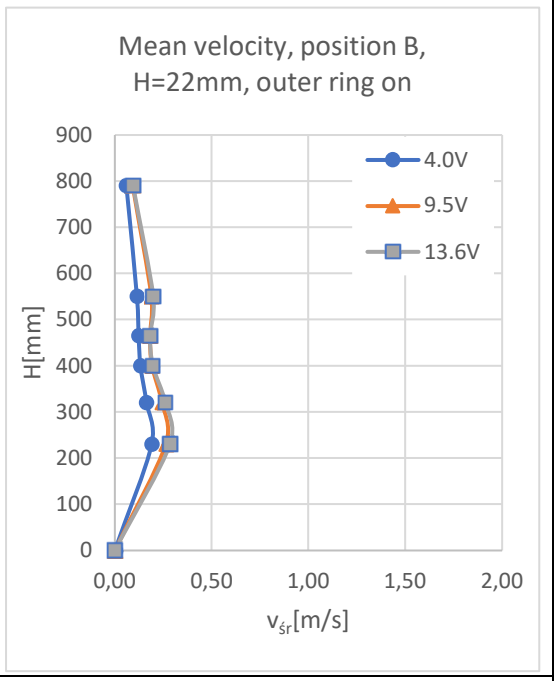

c)

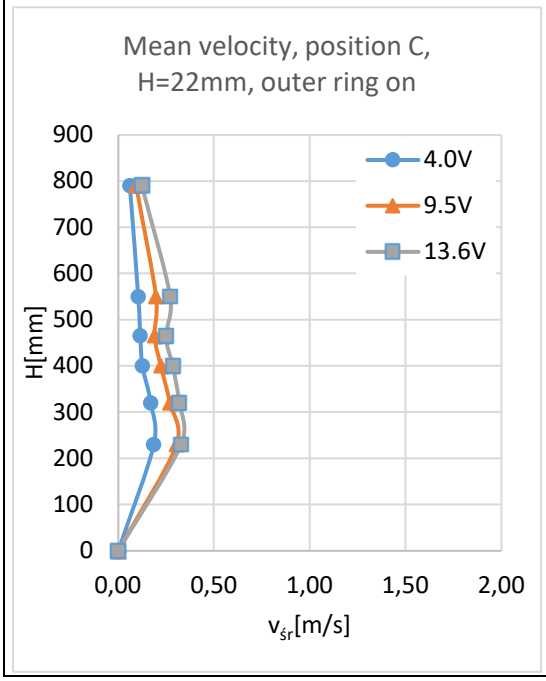

d)

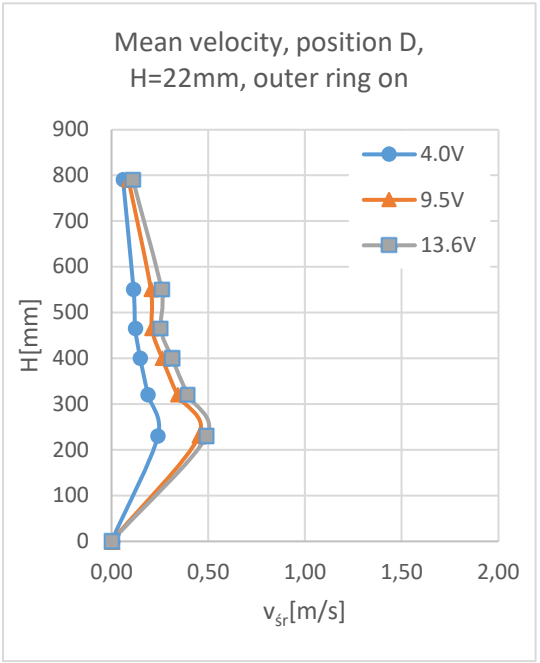

Fig. 9.6.35. Mean velocity for ventilation chimney with 1 fan, H=22mm

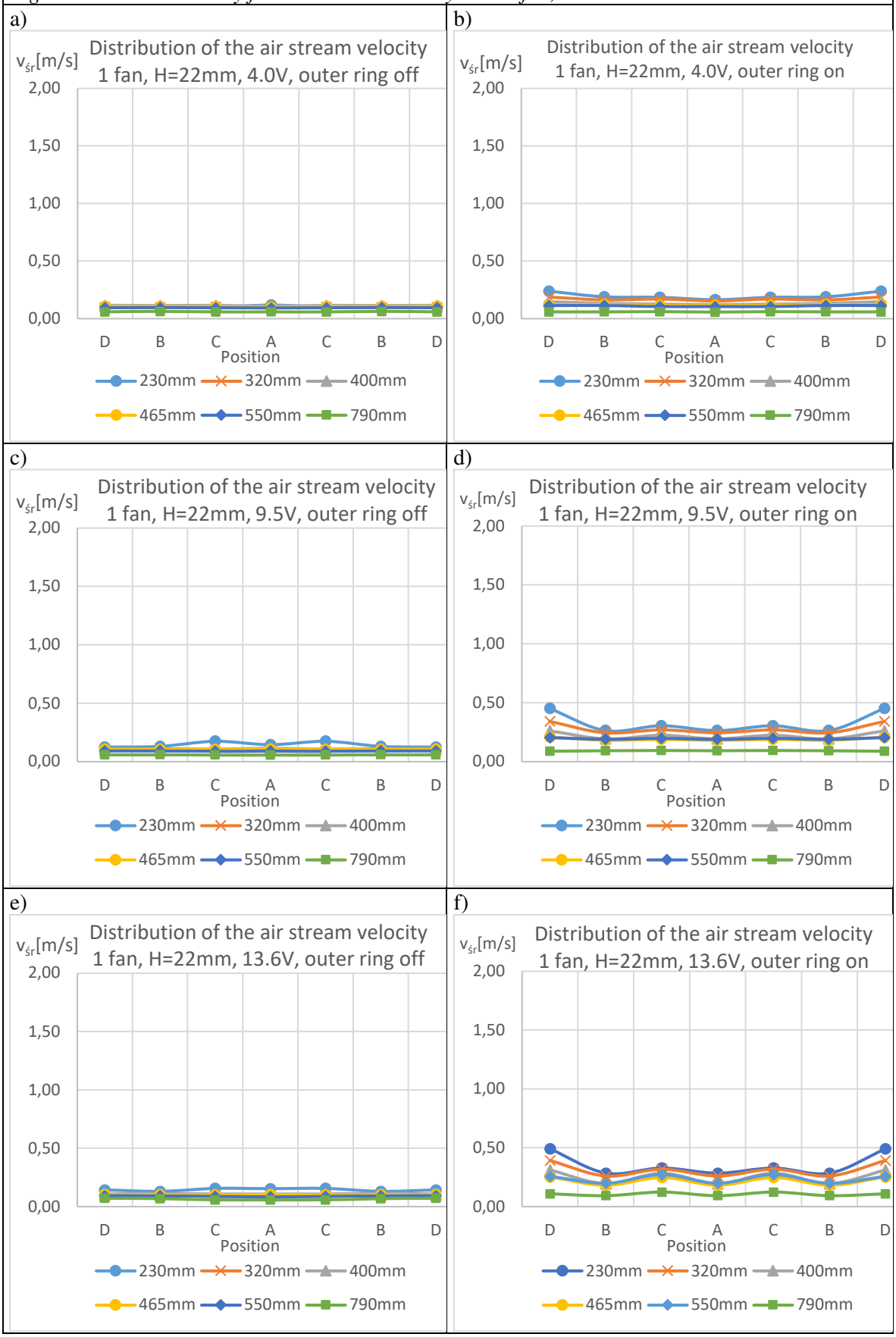

Fig. 9.6.38. Comparison of the mean velocity for 8 fans, ***different base levels*** *of the ventilation chimney, with outer ring on and off at different measurement points, supply voltage 13.6V.*

a)

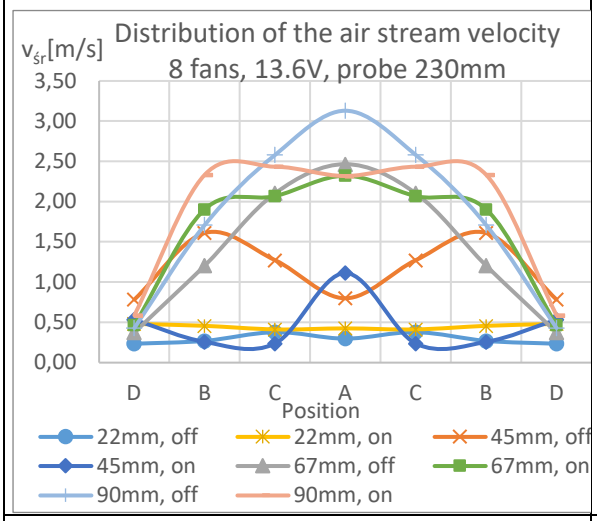

b)

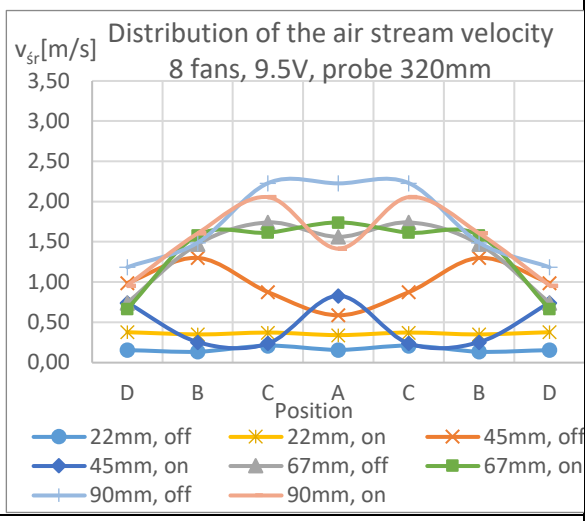

c)

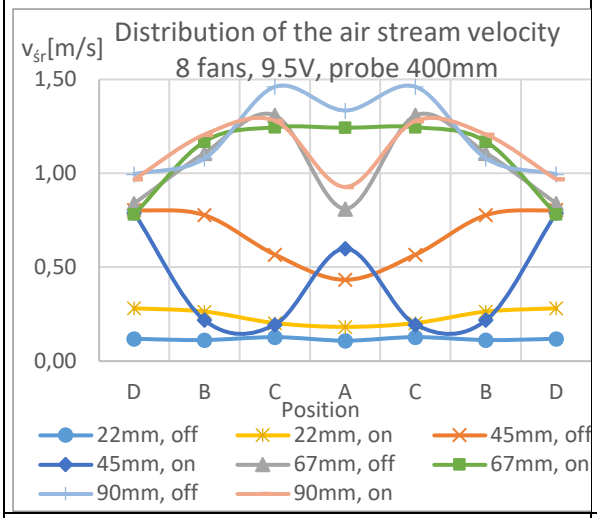

d)

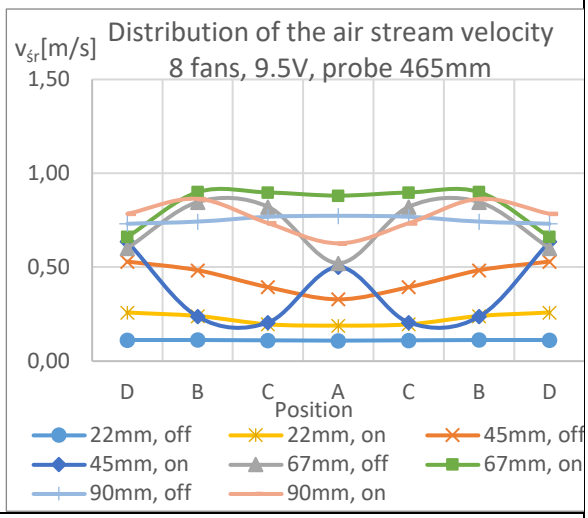

e)

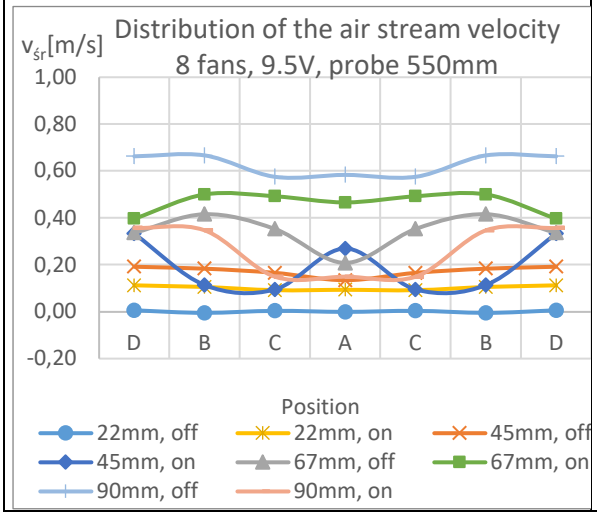

f)

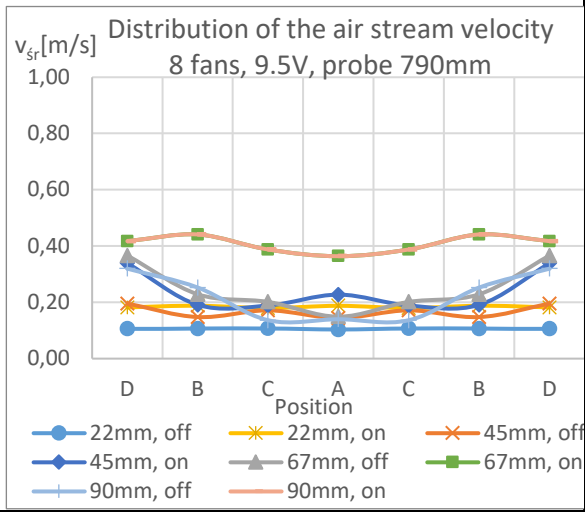

Fig. 9.6.38. Comparison of the mean velocity for 8 fans, different base levels of the ventilation chimney, with outer ring on and off at different measurement points, supply voltage 9.5V.

a)

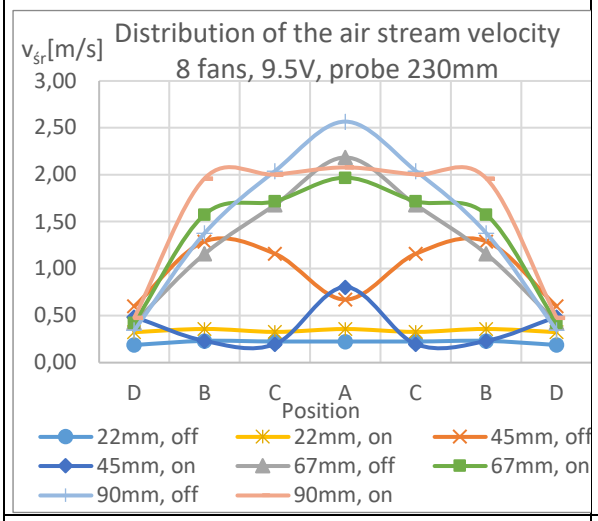

b)

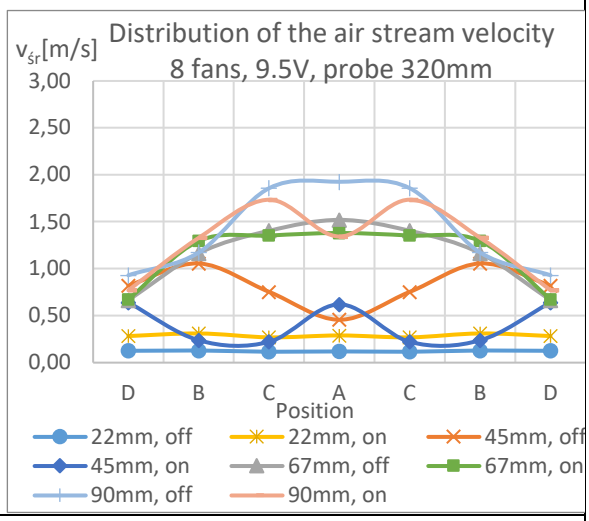

c)

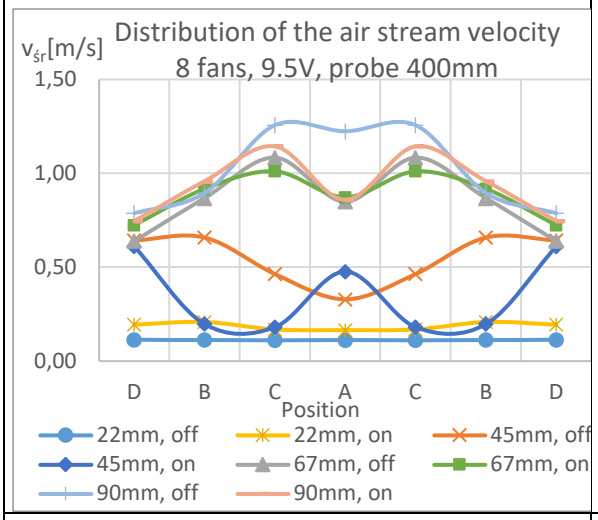

d)

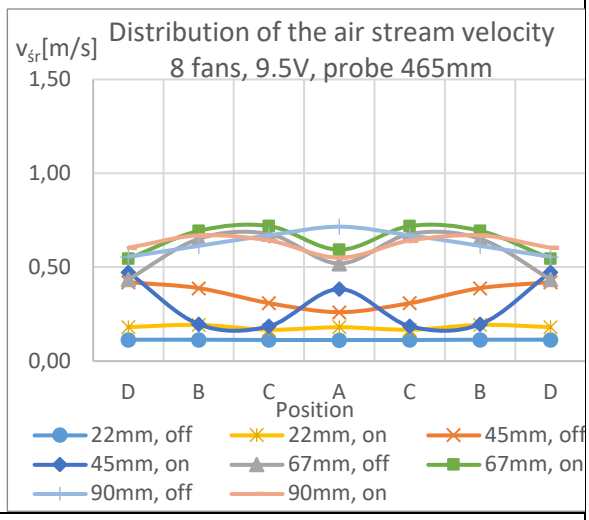

e)

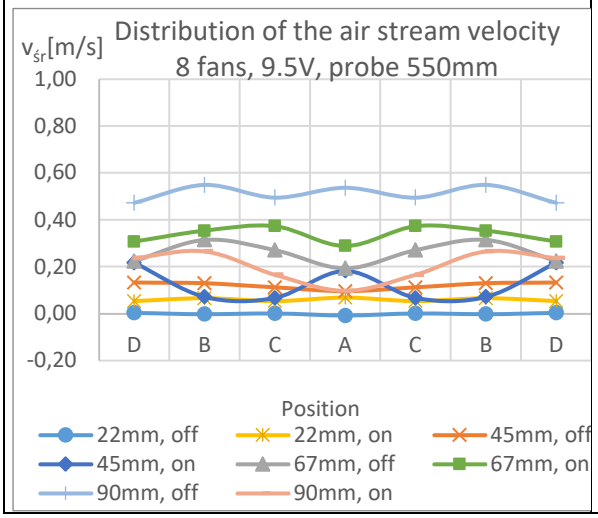

f)

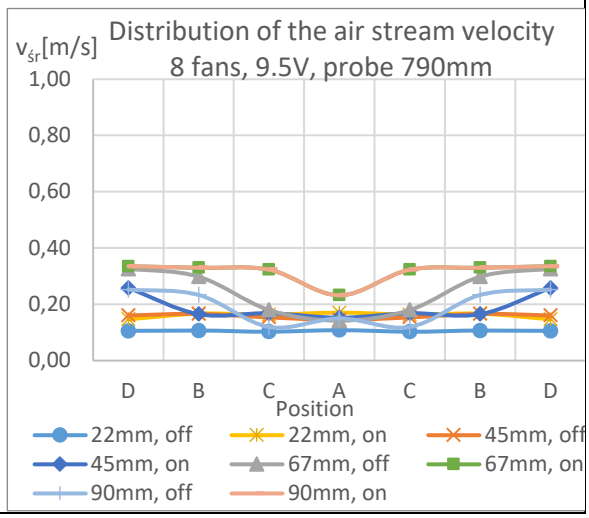

Fig. 9.6.38. Comparison of the mean velocity for 8 fans, different base levels of the ventilation chimney, with outer ring on and off at different measurement points, supply voltage 4.0V.

a)

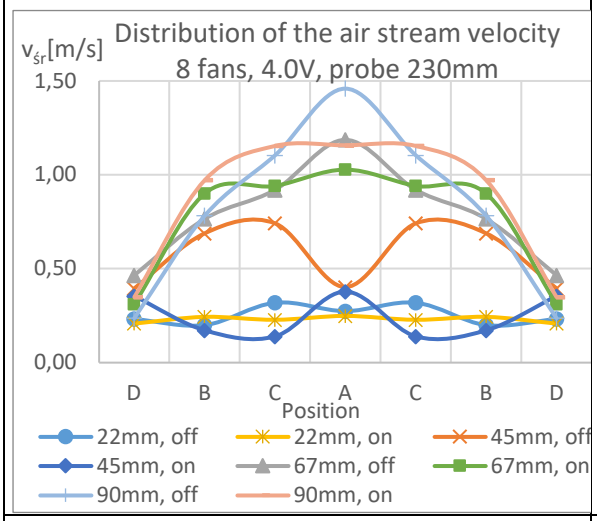

b)

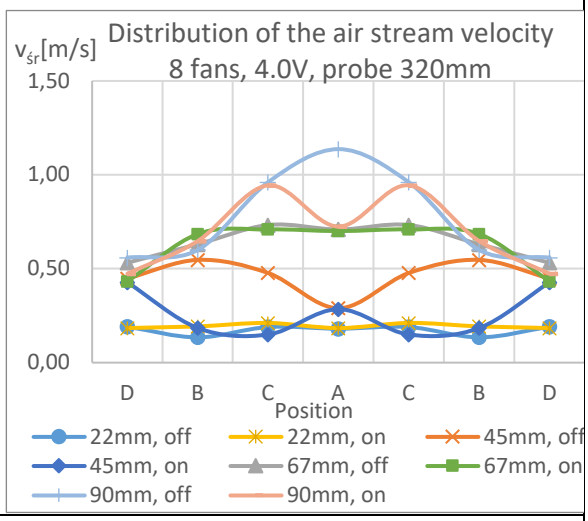

c)

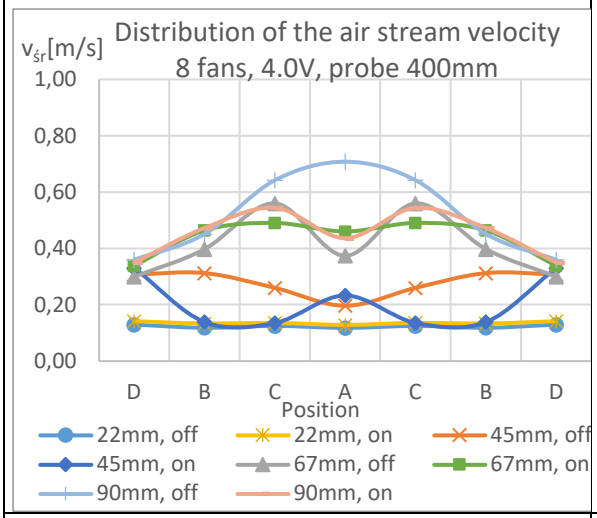

d)

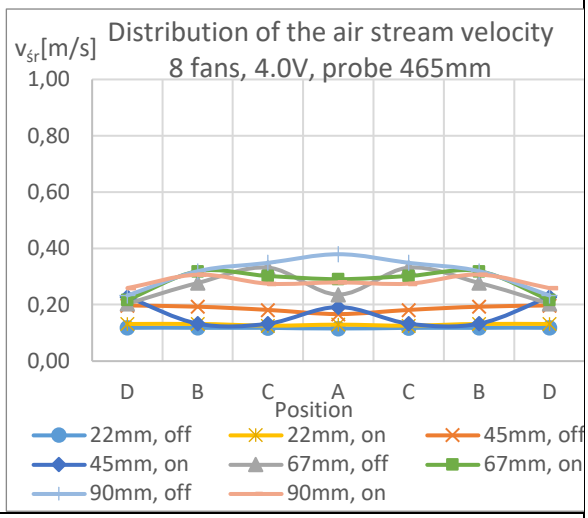

e)

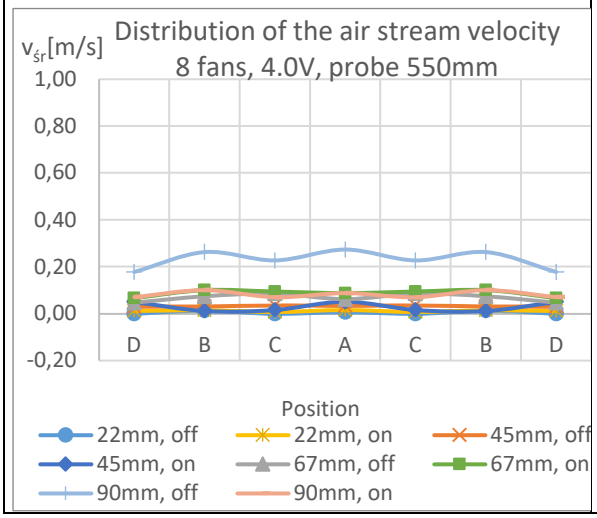

f)

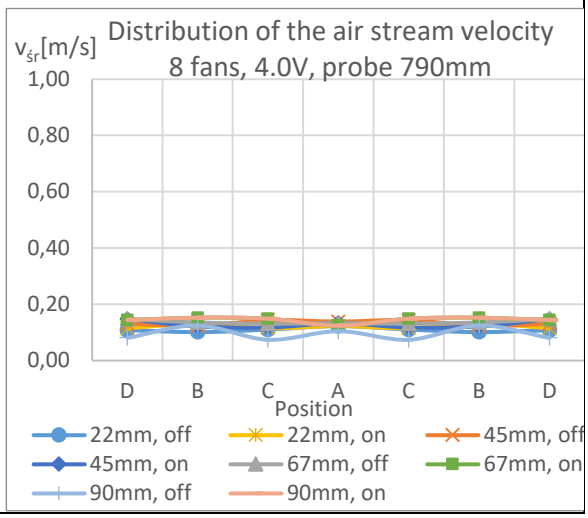

Fig. 9.6.38. Comparison of the mean velocity for 4 fans, different base levels of the ventilation chimney, with outer ring on and off at different measurement points, supply voltage 13.6V.

a)

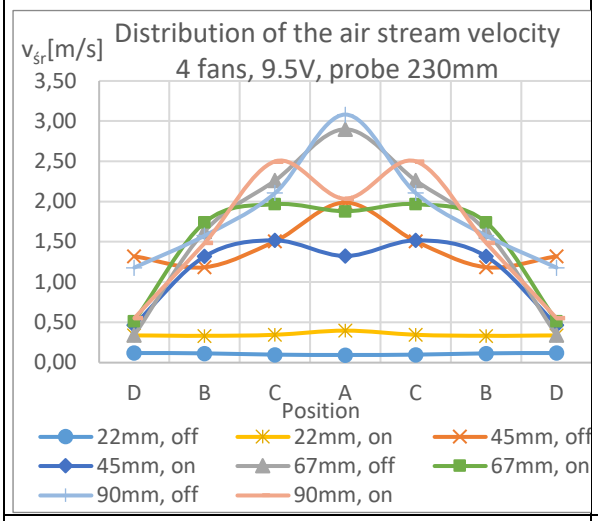

b)

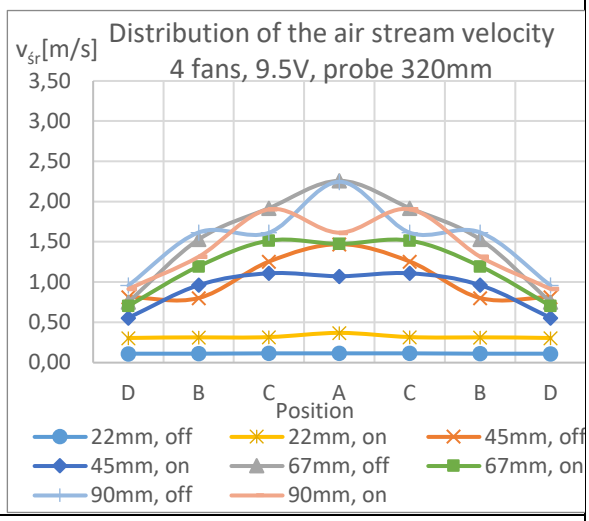

c)

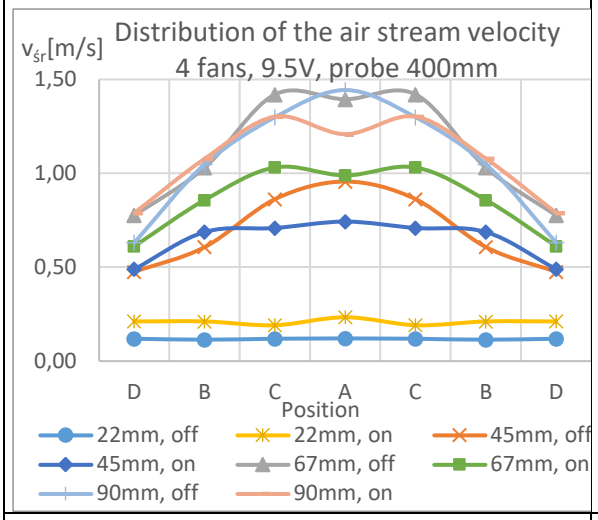

d)

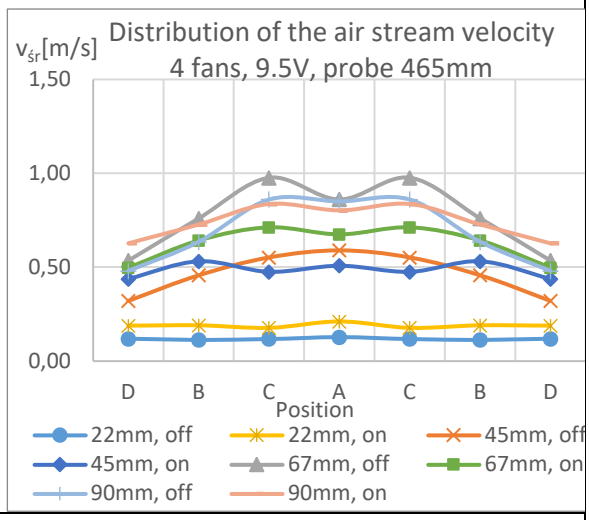

e)

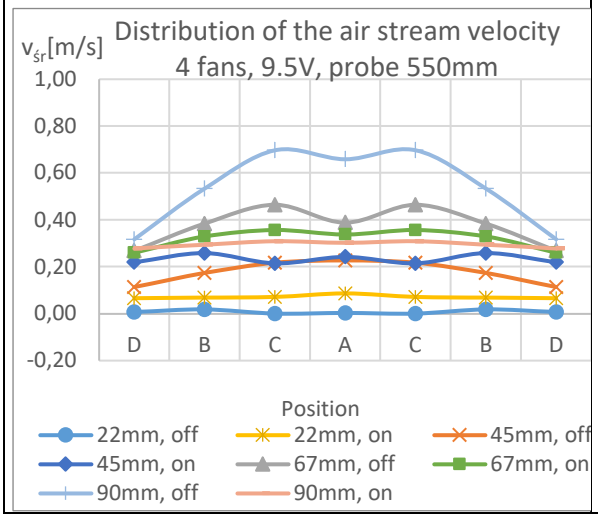

f)

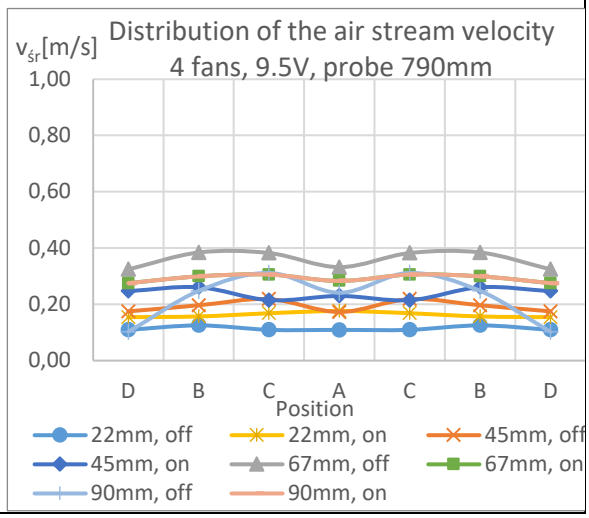

Fig. 9.6.38. Comparison of the mean velocity for 4 fans, different base levels of the ventilation chimney, with outer ring on and off at different measurement points, supply voltage 9.5V.

a)

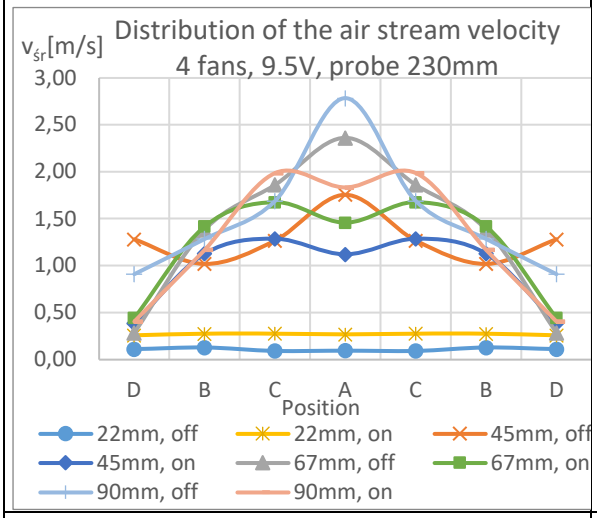

b)

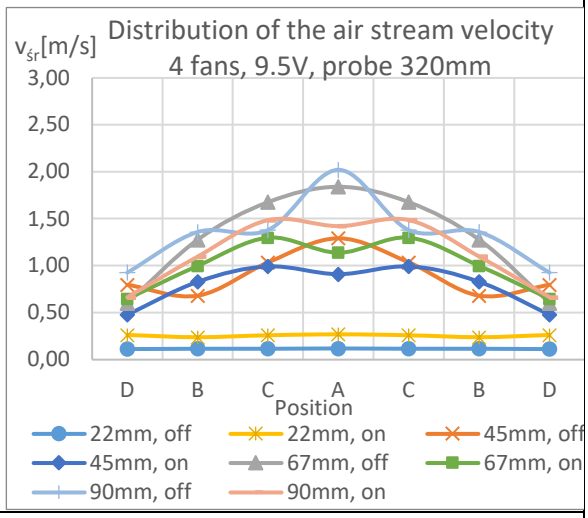

c)

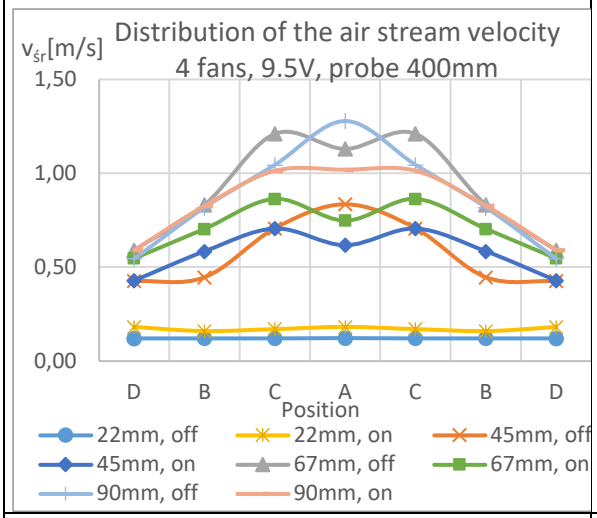

d)

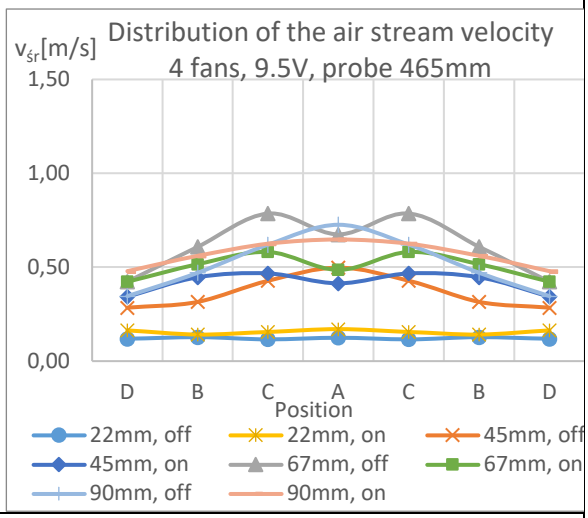

e)

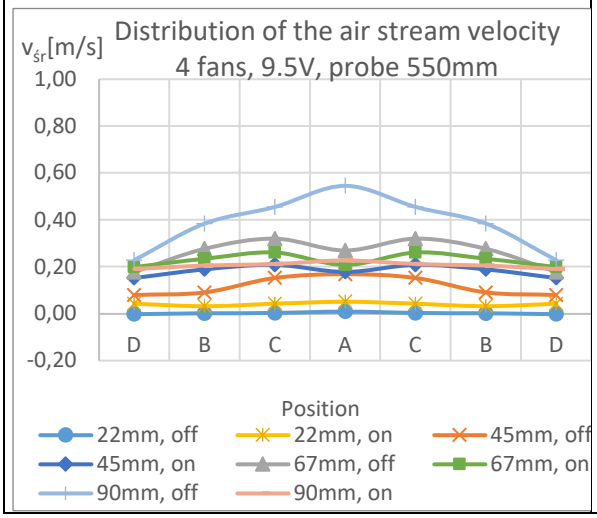

f)

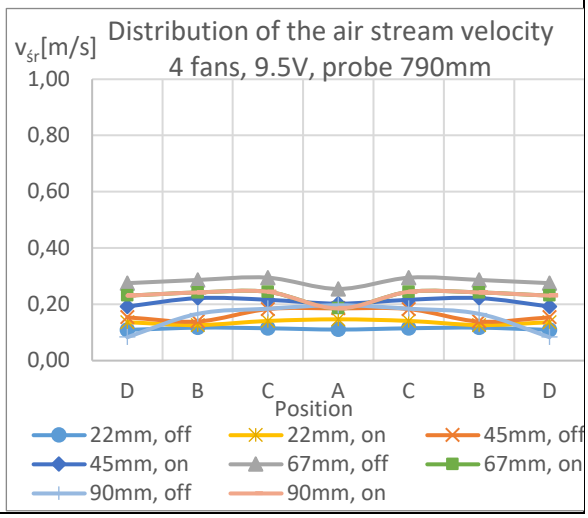

Fig. 9.6.38. Comparison of the mean velocity for 4 fans, different base levels of the ventilation chimney, with outer ring on and off at different measurement points, supply voltage 4.0V.

a)

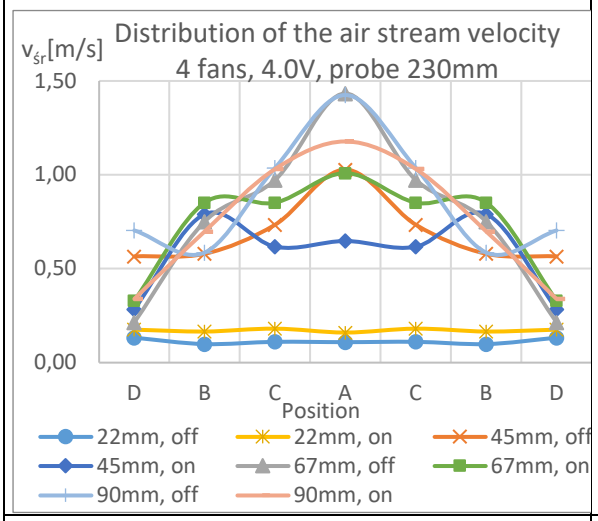

b)

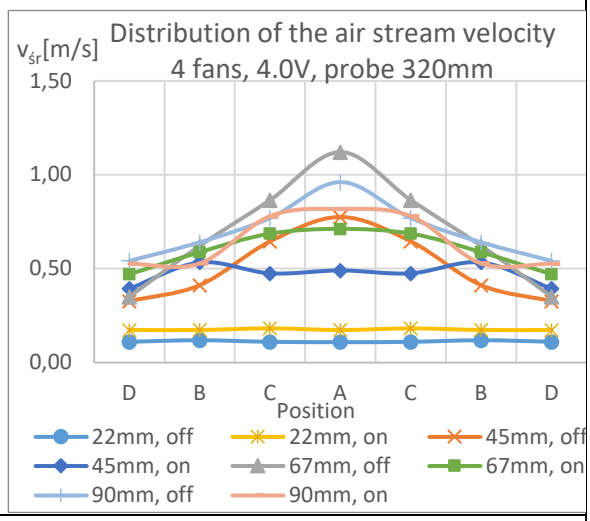

c)

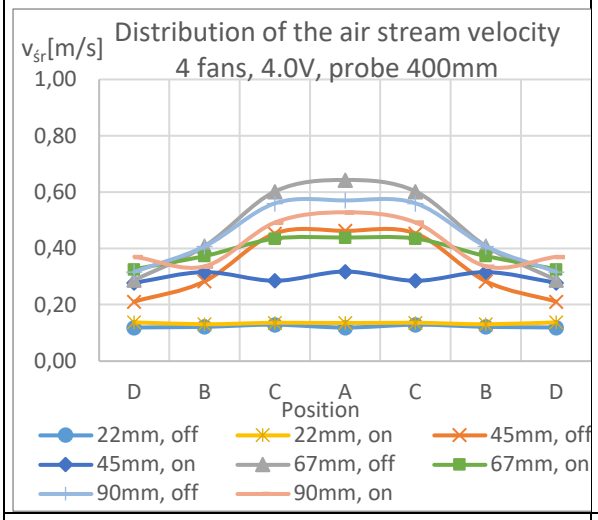

d)

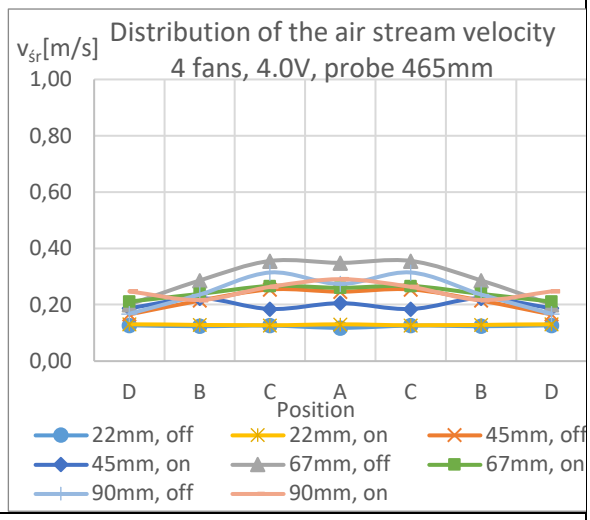

e)

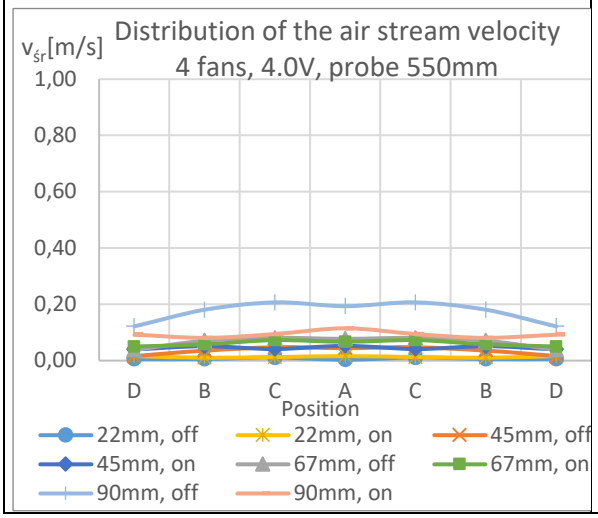

f)

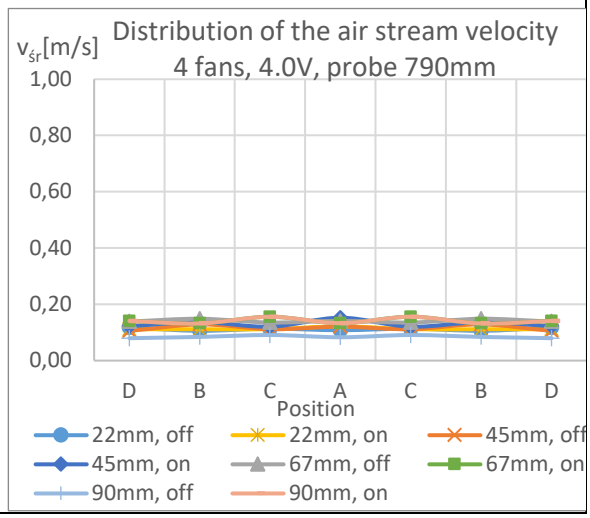

Fig. 9.6.38. Comparison of the mean velocity for 1 fan, different base levels of the ventilation chimney, with outer ring on and off at different measurement points, supply voltage 13.6V.

a)

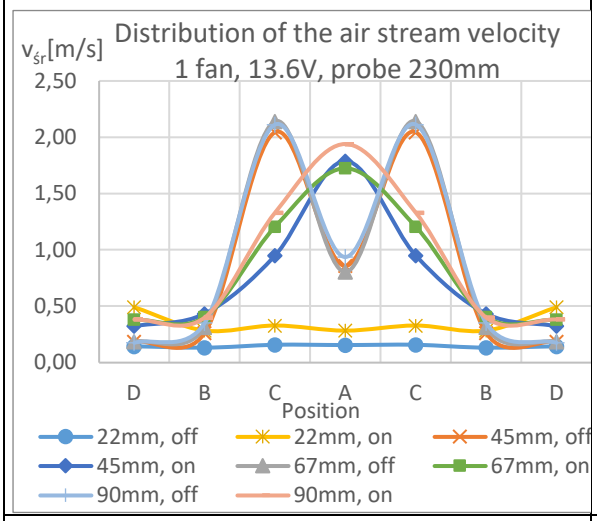

b)

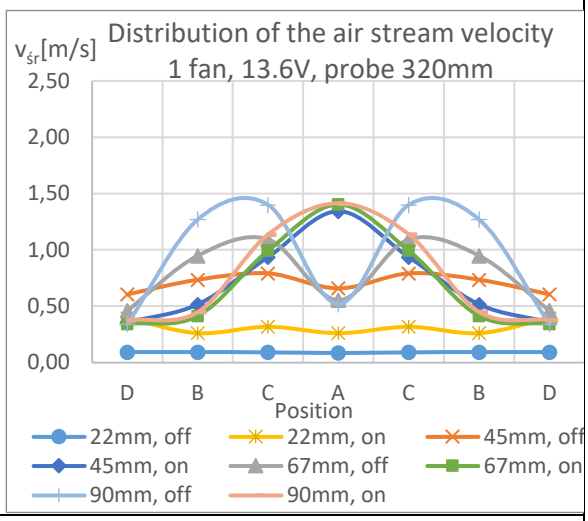

c)

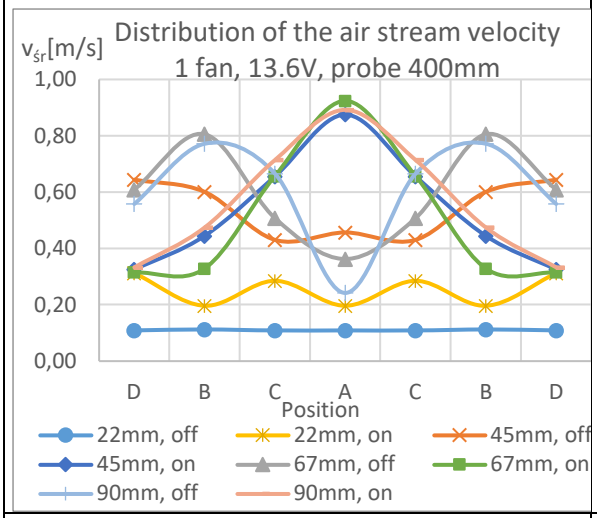

d)

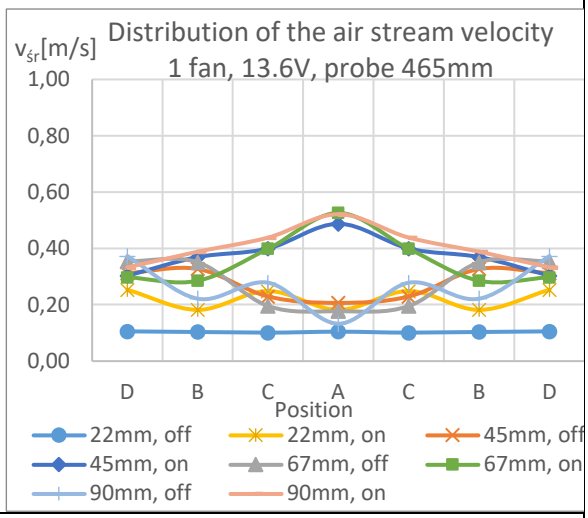

e)

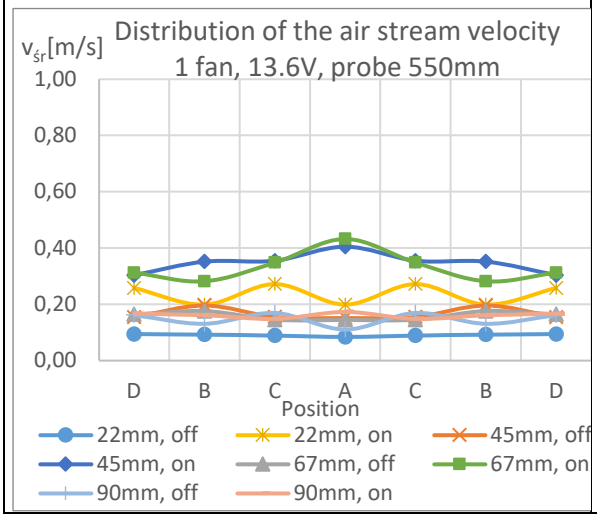

f)

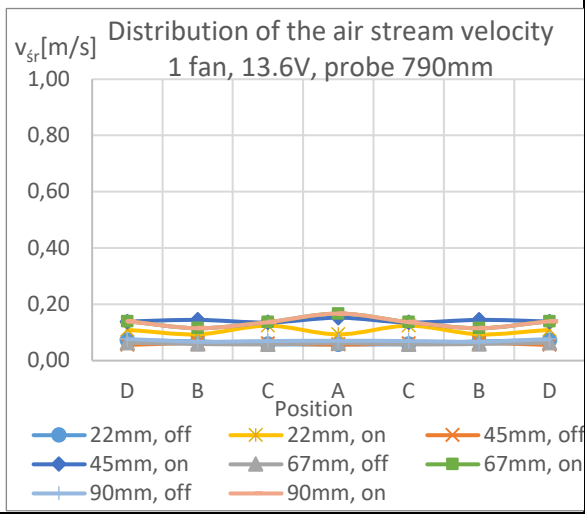

Fig. 9.6.38. Comparison of the mean velocity for 1 fan, different base levels of the ventilation chimney, with outer ring on and off at different measurement points, supply voltage 9.5V.

a)

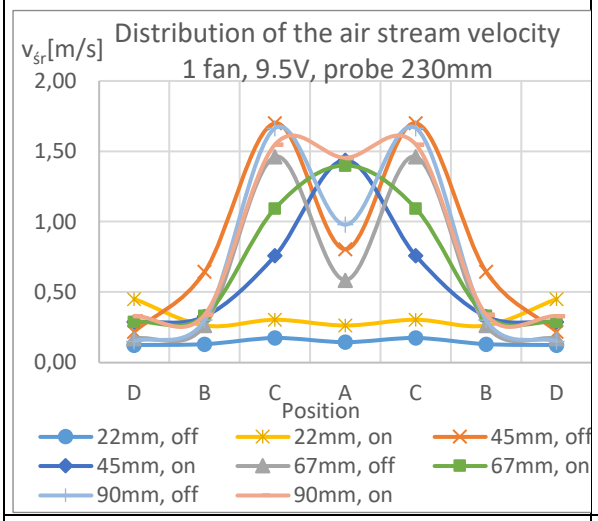

b)

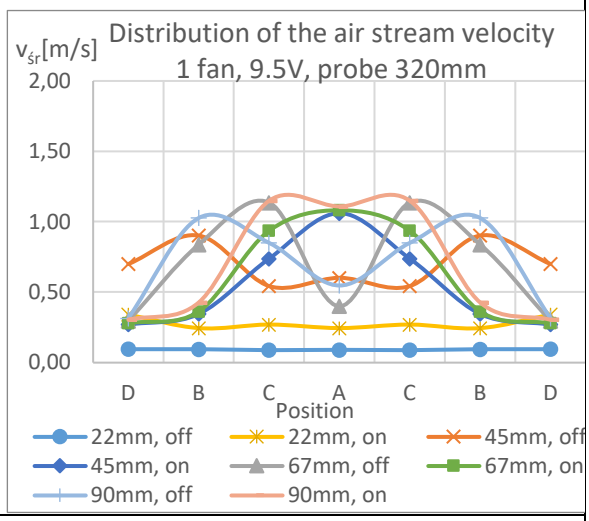

c)

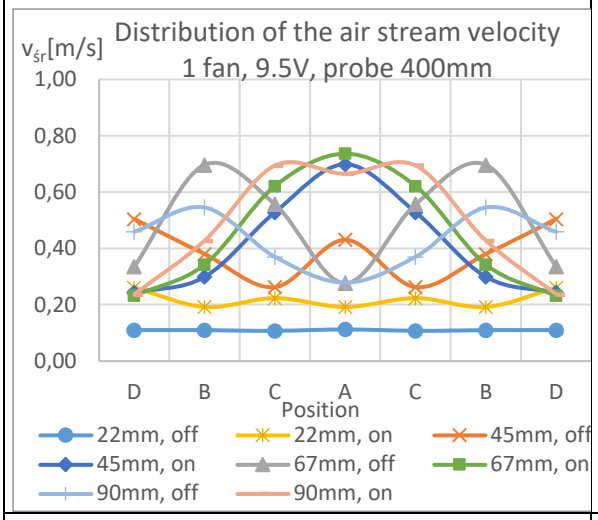

d)

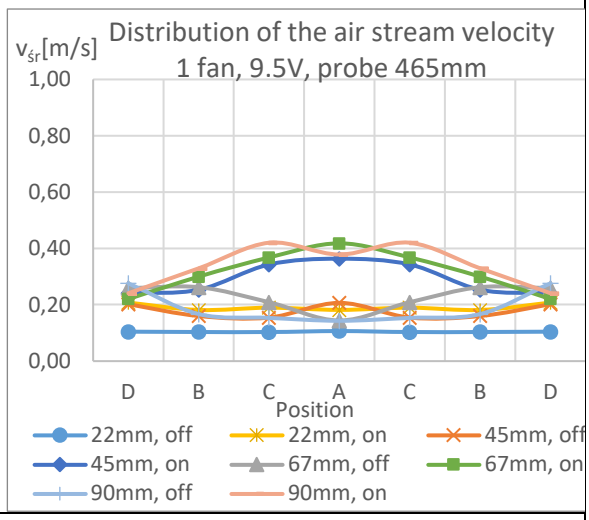

e)

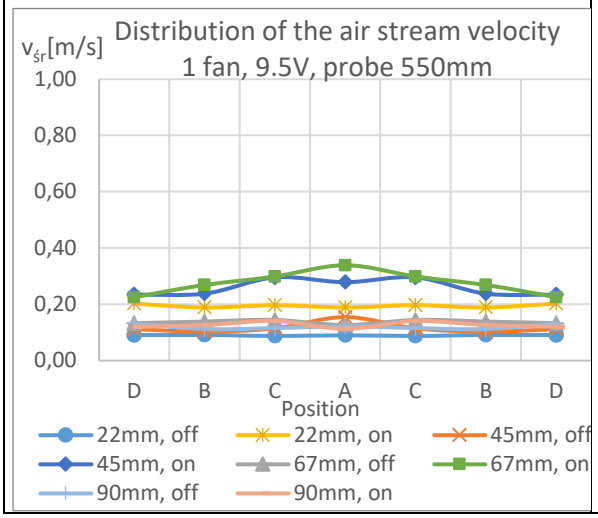

f)

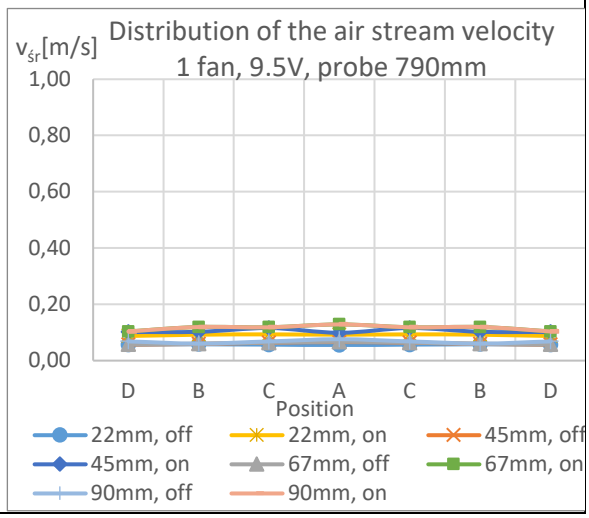

Fig. 9.6.38. Comparison of the mean velocity for 1 fan, different base levels of the ventilation chimney, with outer ring on and off at different measurement points, supply voltage 4.0V.

a)

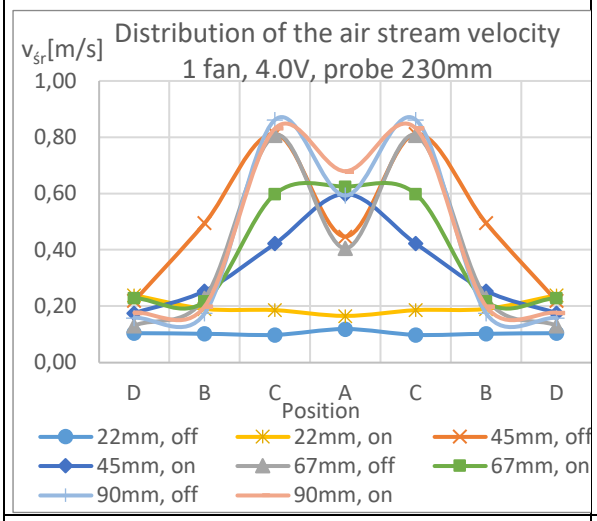

b)

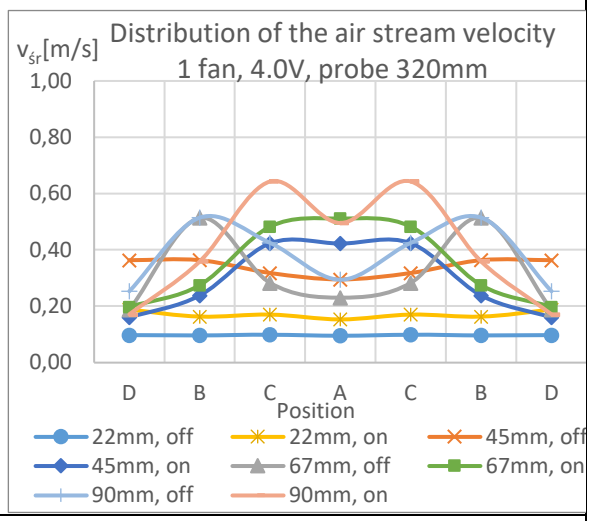

c)

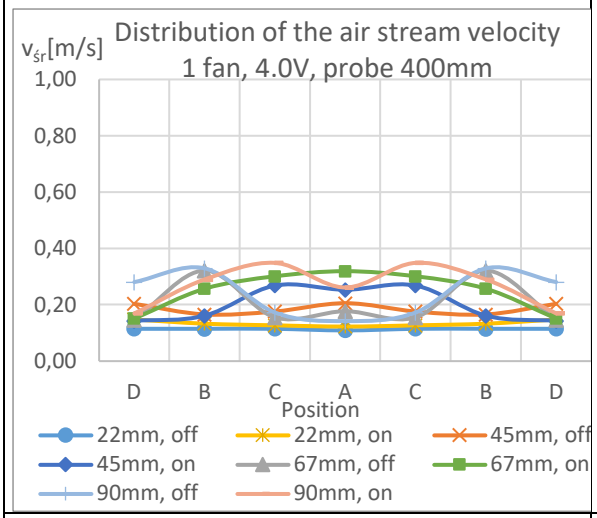

d)

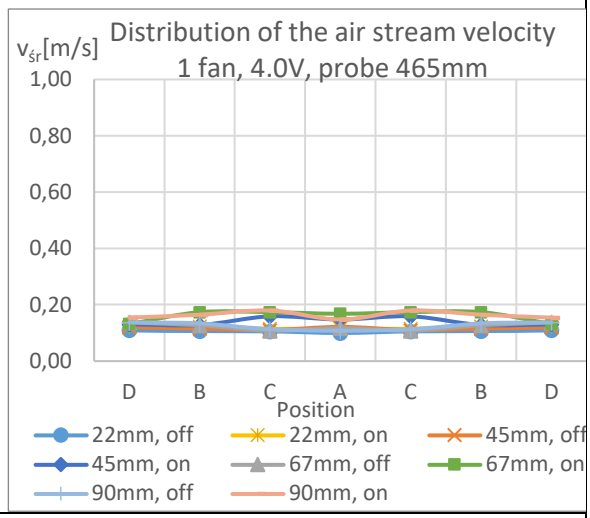

e)

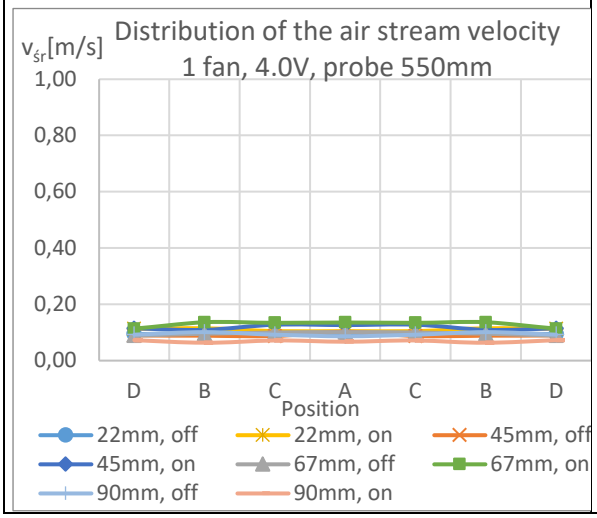

f)

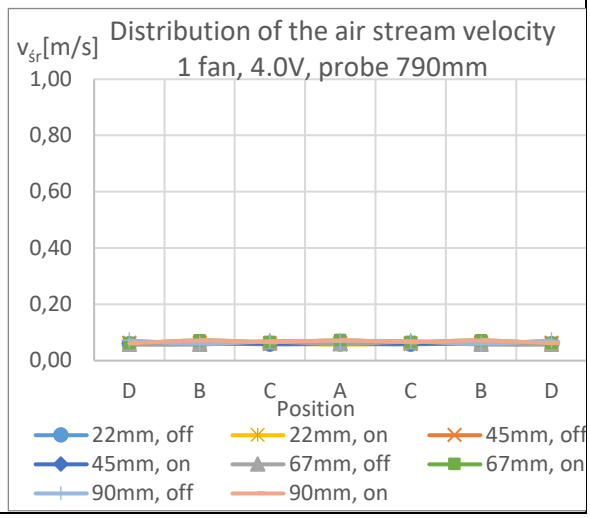

Fig. 9.6.36. Comparison of the mean velocity for ventilation chimneys with different numbers of fans, with outer ring on and off and different measurement points at supply voltage 4.0V, H=22mm.

a)

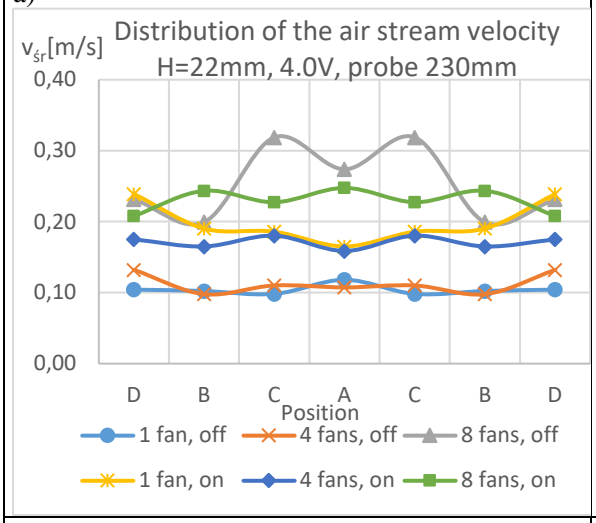

b)

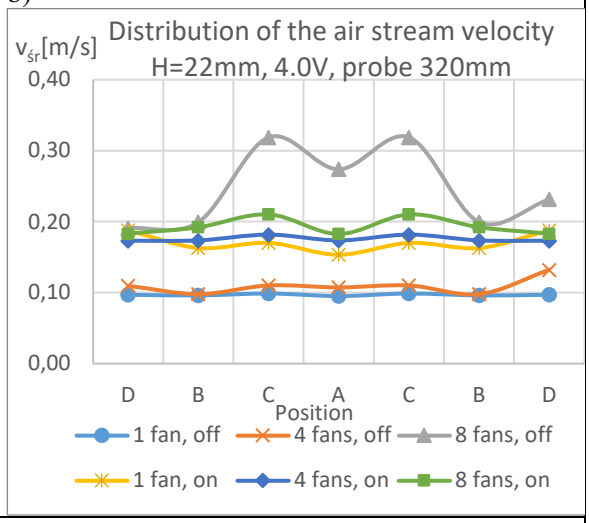

c)

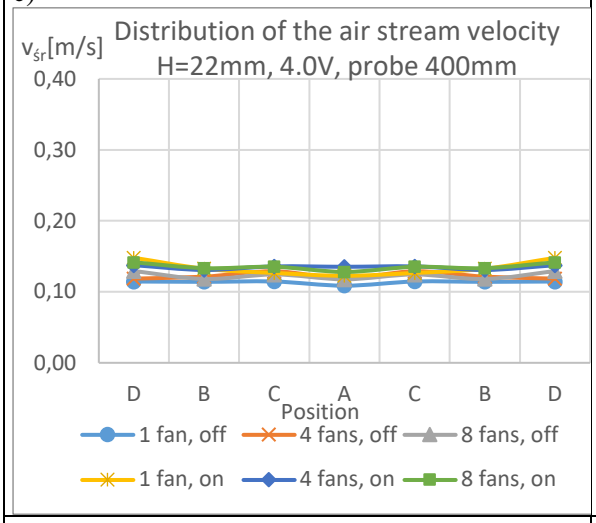

d)

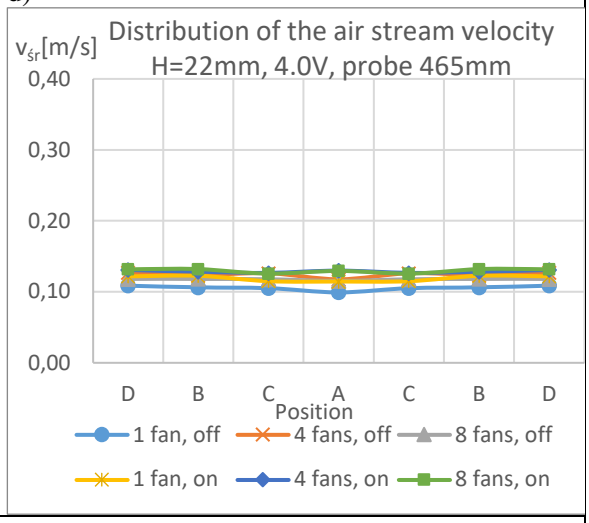

e)

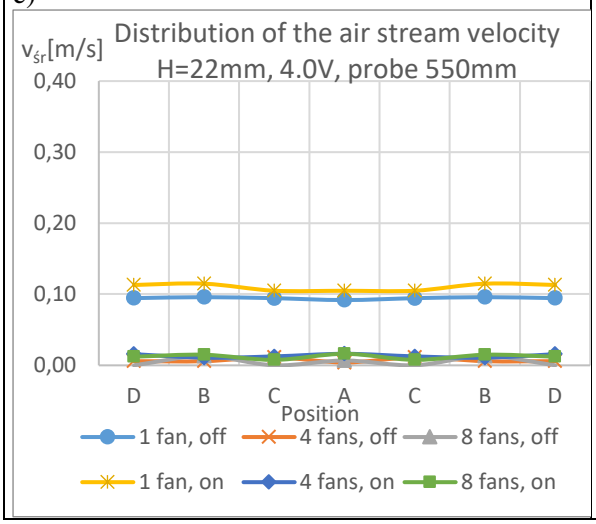

f)

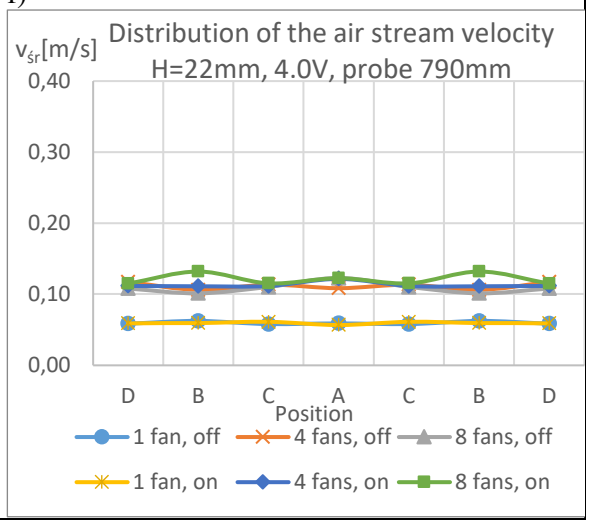

Fig. 9.6.37. Comparison of the mean velocity for ventilation chimneys with different numbers of fans, with outer ring on and off and different measurement points at supply voltage 9.5V, H=22mm.

a)

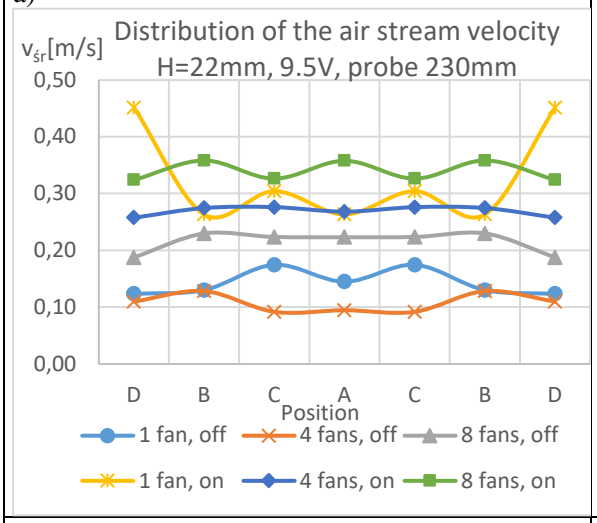

b)

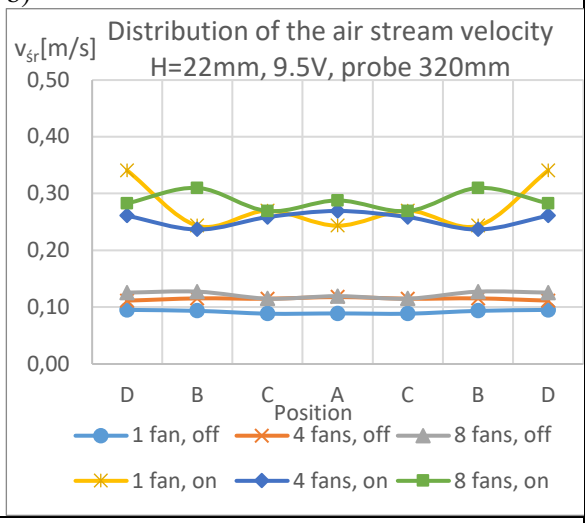

c)

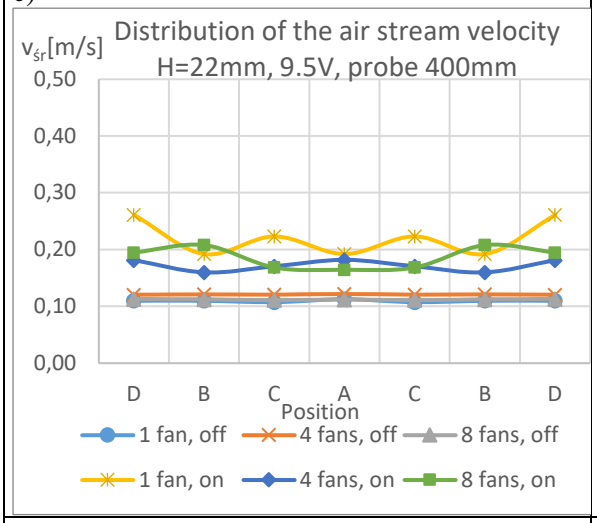

d)

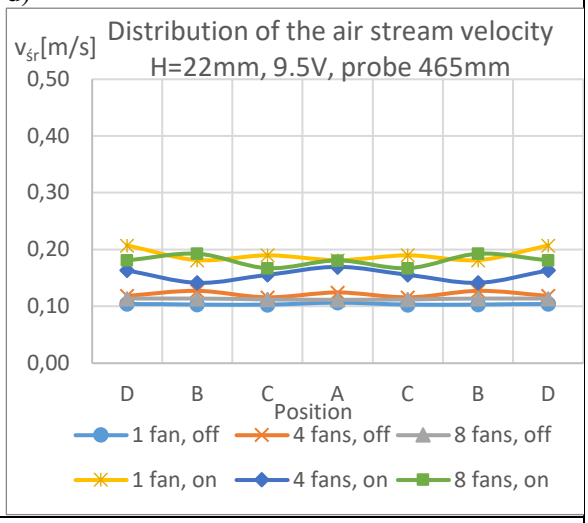

e)

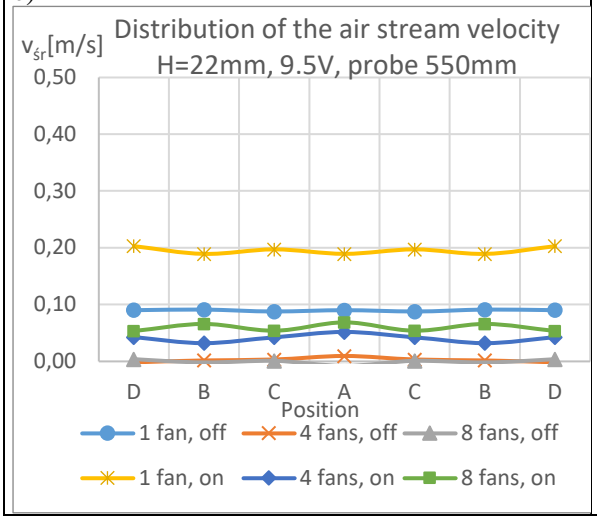

f)

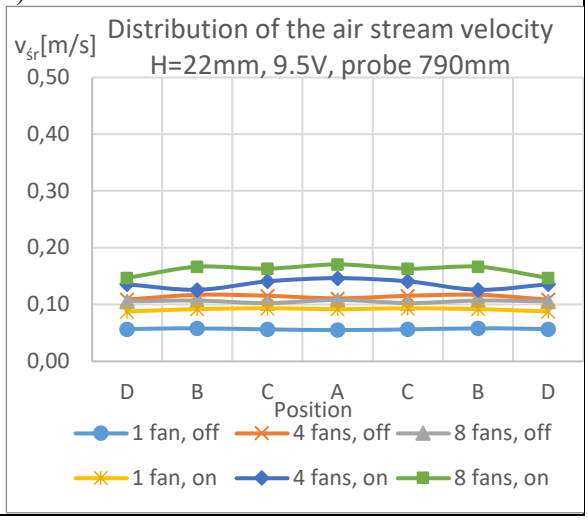

Fig. 9.6.38. Comparison of the mean velocity for ventilation chimneys with different numbers of fans, with outer ring on and off and different measurement points at supply voltage 13.6V, H=22mm.

a)

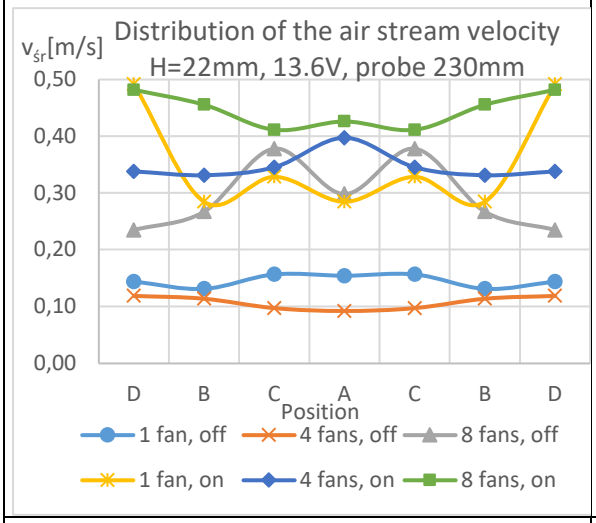

b)

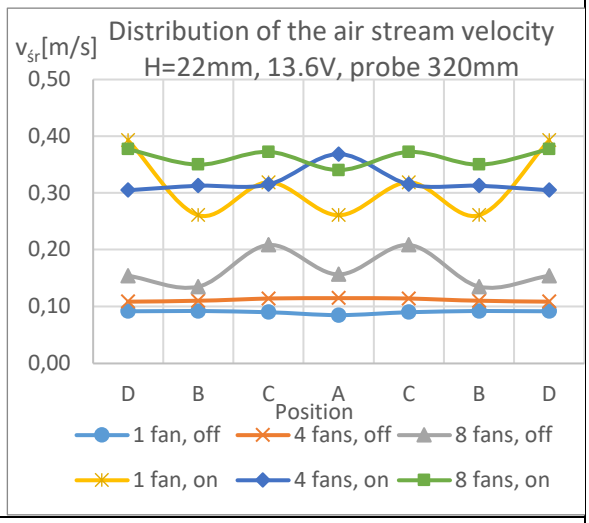

c)

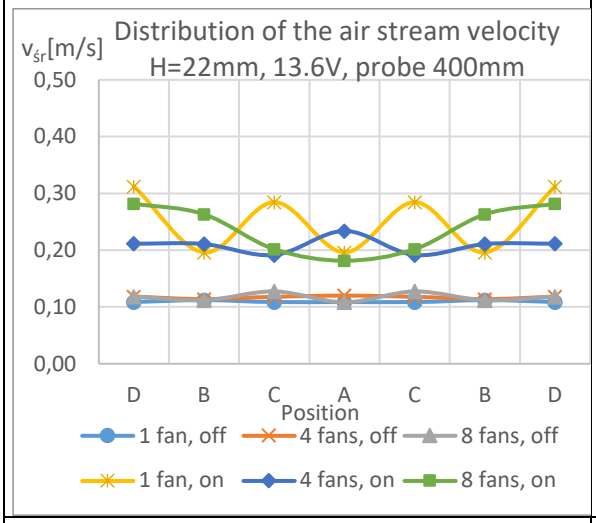

d)

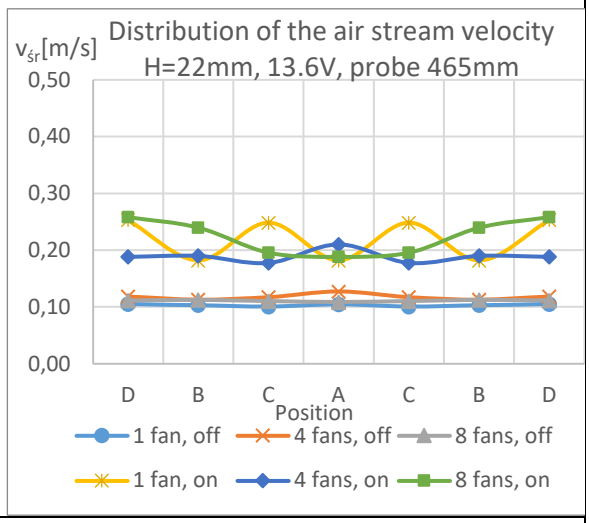

e)

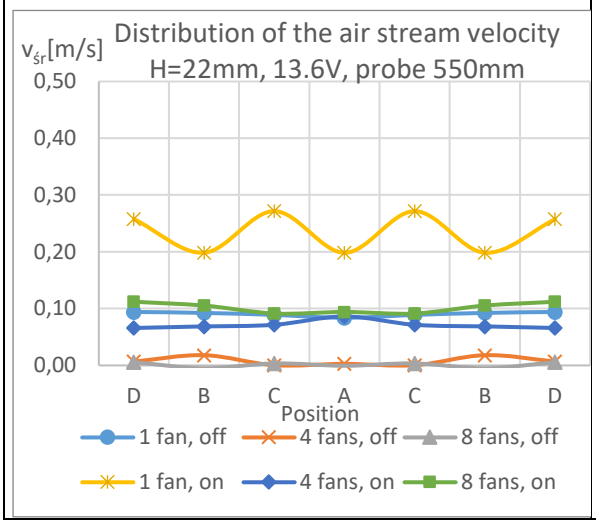

f)

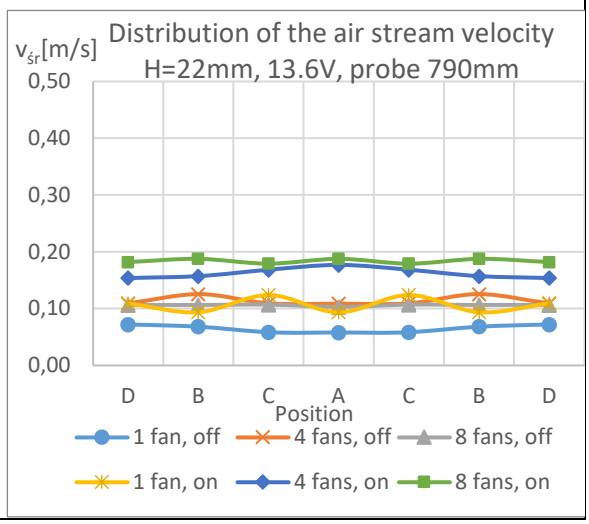

9.7. Analysis and conclusion for stage IV

The presented results show that with certain parameters it is possible to penetrate the inversion layer. A significant effect of the height of the ventilation chimney base was observed - the higher the height, the higher the stream velocity. It was also possible to observe the practical extinction of the air stream when lowering the base of the chimney to 1/4 of the initial height.

The outer fan ring has a visible effect primarily on the diameter of the vertical air stream - when it is turned on, the stream increases its diameter while equalizing the speed distribution in the air stream. With the outer ring turned off in the center of the vertical air stream, the velocity is significantly higher than on the sides - this phenomenon can be helpful until the inversion layer breaks through. After its initial breaking, the outer ring of fans should be turned on to increase the diameter of the penetration hole and the volume of ventilated air.

A significant effect of the number of fans in the base of the chimney was also observed, for 8 fans the penetration of the inversion layer was not a major problem, but with 4 it was only possible at the highest velocities. For a single fan, in most cases, there was no breakdown of the inversion layer.

Smoke visualization showed that the stream significantly expands with increasing height and in the case of the inversion layer laying at higher altitudes, the above model should be used with caution.

9.8. Power of the system and economic assessment

The presented system will require a large amount of electricity to operate. It is therefore necessary to estimate the order of magnitude of the electricity demand. The stream power for a given cross-section can be calculated from the formula:

$$P = pAv$$

Where:

p – the pressure

A – the area of the cross-section

v – the air stream velocity

Deriving the dependencies for the power similarity scale:

$$k_P = \frac{P_{model}}{P_{nature}} = k_p k_A k_v$$

Where:

The pressure scale $$k_p = \frac{p_{model}}{p_{nature}} = 1$$

The area scale $$k_A = \frac{A_{model}}{A_{nature}} = k_l^2 = \left(\frac{1}{833.33}\right)^2 \approx \frac{1}{694\,439}$$

Where: k_l- the length scale

Air stream velocity scale $k_v = \frac{v_{model}}{v_{nature}} = 1$

Hence we get:

$$k_P = 1 * \frac{1}{694\,439} * 1 = \frac{1}{694\,439}$$

Assuming, for example, 8 horizontal ventilation ducts consisting of 5 ventilation towers supplying air to a ventilation chimney with 8 fans in the base, we get 48 for one chimney system with outer rings. Knowing the power of a single fan in model tests for the voltage U=9.5V at the level

$$P = I * U = 0.17A * 9.5V = 1.615W$$

We get the estimated power of the chimney system with outer rings:

$$P_{system} = 1.615W * 48 = 77.52W$$

Which on a natural scale gives us:

$$P_{system,nature} = 77.52W * 694\,439 \approx 53.8MW$$

For Cracow, let's assume that we need 4 systems to improve anemological conditions, which gives us a power demand of:

$$53.8MW * 4 = 215.2MW$$

Assuming that the system would work, for example, 10 hours a day, we get:

$$215.2MW * 10h \approx 2.15GWh$$

In publicly available information, it is difficult to find exactly how much energy a given city consumes, while from statistical data we know that Poland's energy demand for 2022 was 173.5 TWh (wysokienapiecie.pl), dividing it by the number of inhabitants of 37750000 we get 4.64 MWh/person per year. The number of inhabitants of Krakow in 2022 was 802,800 (krakow.stat.gov.pl/), which gives Krakow's annual energy consumption at the level of 3.73TWh and an average of 10.2GWh per day. The above calculations are, of course, a very rough estimate. It is known that energy consumption is subject to both daily and annual cycles, in addition, urban residents consume more energy than rural residents, and the exact consumption also depends on the number of commercial buildings and production plants in a given area. The author aimed to check whether the presented concept is feasible at all.

Thus, we can see that the presented system needs an amount of electricity of the order of 21% of the mean daily demand of the city of Krakow. This is a high value, however, considering that the greatest problem with smog occurs at night when the energy demand is the lowest possible. Of course, it is also possible to decide to use only one system in the place where the concentration of pollutants is highest - economic optimization should be the subject of a separate study.

10. GENERAL CONCLUSION

This doctoral dissertation has shown that the concept of active ventilation of urban areas is real and feasible. It is obvious that the way to finalize the design and construction of the system on a full scale is long and many topics need to be better explored, but the first preliminary results are very promising and open the way for further research.

In the conducted experiments, it was possible to imitate, measure and visualize the penetration of the inversion layer, which is why the theses were put forward:

1. It is possible to dynamically act on the ground level layer of air in urbanized areas by using vertical ventilation systems cooperating with the radial horizontal system of ventilation ducts that effectively improve the aerosanitary conditions of these areas.

2. The model of vertical ventilation systems cooperating with the radial horizontal system used in wind model tests imitates this phenomenon with sufficient accuracy for engineering practice.

can be considered fulfilled.

11. DIRECTIONS FOR FURTHER RESEARCH

Directions for further research are proposed below:

1. The presented theoretical model contains many simplifying assumptions and the presented research should be treated as a basis for further, more detailed exploration of the active impact on the ground layer. When creating the model and describing the physical phenomenon, the biggest problem was the lack of measurement data of smog situations occurring within the inversion layer, which would contain distributions of temperature, humidity, pressure, and air density. The next step should be an attempt to build a drone or balloon system equipped with measuring instruments to collect the appropriate parameters at the same time. For this purpose, the research should cover a longer period, so that it is possible to isolate the most typical distributions during smog episodes.

2. Chimney efficiency tests can be extended to check the effect of a slight inclination of each fan around the axis of symmetry of the circle of the chimney base so that the stream created by the chimney twists upwards like a whirlwind. There is a high probability that such an arrangement will be more favorable. It is known that in many cases spiral flow is the most energetically favorable case, however, this phenomenon is poorly understood and difficult to model.

3. To optimize the structure, a numerical model of the tower and the ventilation chimney can be built together with the modeled inversion layer. The model should be scaled in relation to the tests carried out and then the parameters that were tested can be determined in more detail, such as: the number of fans, the power necessary to penetrate the inversion layer, the height of the tower base, the angle of inclination of the fans, etc.

4. The developed model could be used as a basis for building a broader numerical model mapping the area together with the terrain and the horizontal ventilation system. Having a properly calibrated numerical model, it would be possible to determine and check the best places for the location of towers and chimneys.

5. At least one model study on a larger scale of 1:100 should also be carried out. At such scale a temperature change with height becomes visible and it is possible to physically model the inversion layer as a mass of warmer air or even fog. In the current research, the author made such an attempt, however, due to the very small dimensions of the measuring station and thus technical difficulties, it was abandoned.

6. The next step would be to carefully design the structure of ventilation chimneys, the system of their distribution, transport, control, optimization of work, development of safety requirements, and determining the impact on the environment.

7. The final stage may be the construction of a small system on a natural scale. The optimal places for the first application of the ventilation system are small towns located in valleys, where the inversion layer is persisting due to being covered by mountain tops and is at a low level of 100-200 m. In such a situation, the ventilation chimney together with

the entire system can be smaller and the first start-up of the system can then be treated as a 1:2 scale test compared to the expected use in the ventilation of large cities and with the use of several chimneys and ventilation ducts.

12. Literature

Bharadwaj P., Graff Z. J., Mullins J. T., Neidelllast M.: *Early life exposure to the Great Smog of 1952 and the Development of Asthma*; American Journal of Respiratory and Critical Care Medicine. 194 (12): 1475–1482. doi:10.1164/rccm.201603-0451OC. PMC 5440984. PMID 27392261, 2016;

Blackman K., Perret L., Savory E., Piquet T.: *Field and wind tunnel modelling of an idealized street canyon flow*; Atmospheric Environment 106 p. 139-153, 2015;

Błażejczyk K., Degórska B.: *Możliwości poprawy jakości powietrza*; Red: Degórska B., Baścik M., Środowisko przyrodnicze Krakowa: Zasoby – Ochrona – Kształtowanie, IGiGP UJ, UMK, WGiK PW, Kraków, p. 190-192; 2013;

Błażejczyk. K.: S*ystem wymiany i regeneracji powietrza jako czynnik poprawy warunków aerosanitarnych i bioklimatycznych*; Red.: Degórska B., Baścik M., Środowisko przyrodnicze Krakowa: Zasoby – Ochrona – Kształtowanie, IGiGP UJ, UMK, WGiK PW, Kraków, p. 187-190, 2013

Buccolieri R., Salim S.M., Leo L. S., Di Sabatino S., Chan A., Ielpo P., de Gennaro G., Gromke Ch.: *Analysis of local scale tree – atmosphere interaction on pollutant concentration in idealized street canyons and application to a real urban junction*; Atmospheric Environment 45 p. 1702-1713, 2011;

Buccolieri R., Sandberg M., Di Sabatino S.: *City breathability and its link to pollutant concentration distribution within urban-like geometries*; Atmospheric Environment 44 p. 1894-1903, 2010;

Cao Z., Wang Y., Duan M., Zhu H.: *Study of the vortex principle for improving the efficiency of an exhaust ventilation system*; Energy and Buildings 142 p. 39-48, 2017;

Carpentieri M., Robins EnFlo A.G.: *Wind tunnel experiments of flow and dispersion in a real urban area*; The 7th International Conference on Urban Climate, Yokohama, Japan, 2009;

Chu A.K.M., Kwok R.C.W., Yu K.N: *Study of pollution dispersion in urban areas using Computational Fluid Dynamics (CFD) and Geographic Information System (GIS)*; Environmental Modelling & Software, 20 (2005) 273-277;

CN 101991999 A: *City air purifier;*

CN 203620447 U: *Device for preventing pollution of air suspended particles in urban industrial district*;

DE 3503138 A1: *Process for reducing smog by the chimney inversion/injector effect*;

en.wikipedia.org/wiki/Smog (23.01.2023);

Flaga A.: *Działanie dynamiczne na warstwę przyziemną powietrza jako efektywna metoda poprawy przewietrzania i redukcji smogu obszarów zurbanizowanych*: Dynamiczne przewietrzanie i redukcja smogu obszarów zurbanizowanych ze szczególnym uwzględnieniem miasta Krakowa, Politechnika Krakowska, Kraków 2019

Flaga A.: *Kryteria podobieństwa modelowego dla komina wentylacyjnego z promieniowym układem zastępczych wież wentylacyjnych*; Laboratorium Inżynierii Wiatrowej, Politechnika Krakowska, 2017;

Flaga A.: *Dynamic action on atmospheric boundary layer as an effective method of improving the urban areas ventilation with similarity criteria of the problem*; Environmental Effects on Buildings and People: Actions, Influences, Interactions, Discomfort, EEBP VIII, Cracow-Lublin 2018, Poland

Flaga Ł., Pistol A., Krajewski P., Flaga A.: *Model tests of dynamic action on the atmospheric boundary layer – linear configuration of ventilation towers on rough terrain*; Environmental Effects on Buildings and People: Actions, Influences, Interactions, Discomfort, EEBP VIII, Cracow-Lublin 2018, Poland

Godłowska J.: *Wpływ warunków meteorologicznych na jakość powietrza w Krakowie. Badania porównawcze i próba podejścia modelowego*; IMGW, Państwowy Instytut Badawczy, Warszawa 2019;

Godzik S., Hławiczka S., Poborski P.: *Smog – przyczyny – skutki – przeciwdziałania*; Państwowa Inspekcja Ochrony Środowiska, Warszawa 1995;

Hang J., Sandberg M., Li Y.: *Effect of urban morphology on wind condition in idealized city models*; Atmospheric Environment 43 p. 869-878, 2009;

Jiang Y., Alexander D., Jenkins H., Arthur R., Chen Q.: *Natural ventilation in buildings: measurement in a wind tunnel and numerical simulation with large-eddy simulation*; Journal of Wind Engineering and Industrial Aerodynamics 91 p. 331-353, 2003;

Karliński F.: *Pierwsze przypadki mierzenia chyżości wiatru w Krakowie*; Rozprawy i Sprawozdania z Posiedzień Wydział Matematyczno-Przyrodniczego Akademii Umiejętności, 4, Kraków, 1877;

Kożuchowski K. (red.): *Meteorologia i klimatologia*; Wydawnictwo Naukowe PWN, Warszawa 2005;

Krajewski P.: *Badania modelowe dynamicznego działania na warstwę przyziemną atmosfery*; Wpływy środowiskowe na budowle i ludzi; red. Ł. Flaga, R. Kłaput, Politechnika Krakowska, Kraków, 2022

Krajewski P., Pistol A., Flaga Ł., Flaga A.: *Badania modelowe dynamicznego działania na warstwę przyziemną atmosfery – efektywność różnych typów kominów wentylacyjnych*: Dynamiczne przewietrzanie i redukcja smogu obszarów zurbanizowanych, , Politechnika Krakowska, Kraków 2021.

Krajewski P., Pistol A., Flaga Ł., Flaga A.: *Model tests of dynamic action on the atmospheric boundary layer – vertical ventilation towers of urban areas*; Environmental Effects on Buildings and People: Actions, Influences, Interactions, Discomfort, EEBP VIII, Cracow-Lublin 2018, Poland

krakow.stat.gov.pl/

Kurt OK, Zhang J, Pinkerton KE.: *Pulmonary Health Effects of Air Pollution*; Current Opinion in Pulmonary Medicine. 22 (2): 138–143. doi:10.1097/MCP.0000000000000248. ISSN 1070-5287. PMC 4776742. PMID 26761628. 2016;

Lewińska J.: *Klimat miasta. Vademecum urbanisty*; Instytut Gospodarki Przestrzennej i Komunalnej, Oddział w Krakowie, p. 151,1991;

Lewińska J., Zgud K., Baścik J., Bartosik J., Czerwieniec M.:, *Wpływ miasta na klimat lokalny*; Instytut Kształtowania Środowiska, Warszawa, p. 106, 1982;

Marziali, Carl: *L.A.'s Environmental Success Story: Cleaner Air, Healthier Kids*; USC News. Retrieved 16 March 2015;

Matuszko D. (red.): *Klimat Krakowa w XX wieku*; IGGP UJ, Kraków, p. 250, 2007;

Mokoena KK., Ethan C., Yu Y., Shale K., Liu F.: *Ambient air pollution and respiratory mortality in Xi'an, China: a time-series analysis*; Respiratory Research. 20 (1): 139. doi:10.1186/s12931-019-1117-8. ISSN 1465-993X. PMC 6612149. PMID 31277656, 2019;

New Directions: *The future of European urban air quality monitoring*; Atmospheric Environment 87 p. 258-260, 2014;

Ng E.: *Policies and technical guidelines for urban planning of high-density cities – air ventilation assessment (AVA) of Hong Kong*; Building and Environment 44 p. 1478-1488, 2009;

Niedźwiedź T.: *Kalendarz typów cyrkulacji atmosfery dla Polski południowej – zbiór komputerowy*; Uniwersytet Śląski, Sosnowiec, online www.kk.wnoz.us.edu.pl/nauka/kalendarz-typow-cyrkulacji/ (12.12.2018) 2013;

Niedźwiedź T.:, *Sytuacje synoptyczne i ich wpływ na zróżnicowanie przestrzenne wybranych elementów klimatu w dorzeczu górnej Wisły*; Rozprawy Habilitacyjne, nr 58, Uniwersytet Jagielloński, Kraków, p. 165, 1981;

Oke T.R.: *Boundary layer climates*; Methuen, New York 1978;

Oleniacz R., Bogacki M., Rzeszutek M., Kot A.: *Meteorologiczne determinanty jakości powietrza w Krakowie – Meteorological factors affecting air quality in Krakow;* Ochrona powietrza w teorii i praktyce, T. 2 , red. Jana Konieczyński, Instytut Podstaw Inżynierii Środowiska Polskiej Akademii Nauk, Zabrze 2014;

Oleniacz R., Bogacki M., Szulecka A., Rzeszutek M., Mazur M.: *Assessing the impact of wind speed and mixing-layer height on air quality in Krakow (Poland) in the years 2014-2015*; Czasopismo Inżynierii Lądowej, Środowiska i Architektury, Oficyna Wydawnicza Politechniki Rzeszowskiej p. 327, 2016;

Olszewski K.: *Wpływ zjawisk meteorologicznych i warunków topograficznych na rozprzestrzenianie się zanieczyszczeń w atmosferze*; Ochrona powietrza przed zanieczyszczeniem, Dębe, 1991;

Omrani S., Garcia-Hansen V., Capra B., Drogemuller R.: *Natural ventilation in multi-storey buildings: Design process and review of evaluation tools*; Building and Environment 116 p. 182-194, 2017;

Ośródka L.: *Określenie warunków anemologicznych dla obszaru Krakowa na podstawie danych z sieci obserwacyjno pomiarowej IMGW*; IMGW w WARSZAWIE, Kraków 2010;

Parczewski W.: *Termiczno-dynamiczna równowaga pionowa powietrza w Polsce*; Prace IMGW nr 102. Warszawa, 1972;

Pasquill F.: *The Estimation of the Dispersion of Windburn Material*; Meteorological Magazine, 90, p. 33–49, 1961;

Pietras B.: *Czynniki meteorologiczne wpływające na koncentrację aerozoli w Krakowie oraz analiza cząstek aerozoli*; Prace Studenckiego Koła Naukowego Geografów Uniwersytetu Pedagogicznego w Krakowie vol. 2, Kraków 2013;

Pistol A., Krajewski P., Flaga Ł., Flaga A.: *Model tests of dynamic action on the atmospheric boundary layer – concentric configuration of ventilation towers witch central ventilation chimney*; Environmental Effects on Buildings and People: Actions, Influences, Interactions, Discomfort, EEBP VIII, Cracow-Lublin 2018, Poland

Ramponi R., Blocken B., de Coo L.B., Janssen W. D.: *CFD simulation of outdoor ventilation of generic urban configurations with different urban densities and equal and unequal street widths*; Building and Environment 92 p. 152-166, 2015;

Report 1: Flaga A., Flaga Ł., Krajewski P., Pistol A.: *Badania wstępne możliwości dynamicznego oddziaływania na warstwę przyziemną. Etap 1: Pomiar pola prędkości przepływu i zasięgu strumienia powietrza generowanego przez modele wentylatorów/wież wentylacyjnych w różnych wariantach ich konfiguracji*; Research Report, Wind Engineering Laboratory, Cracow University of Technology, Cracow 2017;

Report 2: Flaga A., Flaga Ł., Krajewski P., Pistol A.: *Badania wstępne możliwości dynamicznego oddziaływania na warstwę przyziemną. ETAP II – Badania w tunelu aerodynamicznym pola prędkości przepływu generowanego przez układ wentylatorów/wież wentylacyjnych w konfiguracji promienistej i specjalny membranowy komin wentylacyjny*; Research Report, Laboratorium Inżynierii Wiatrowej Politechniki Krakowskiej, Kraków 2017;

Report 3: Flaga A., Flaga Ł., Krajewski P., Pistol A.: *Badania wstępne możliwości dynamicznego oddziaływania na warstwę przyziemną. Etap III – Badania w tunelu aerodynamicznym wybranych zagadnień z Etapów I i II przy uwzględnieniu wpływu chropowatości podłoża (zabudowy miejskiej)*; , Laboratorium Inżynierii Wiatrowej Politechniki Krakowskiej, Kraków 2018;

Report 4: Flaga A., Krajewski P.: *Model of the ventilation chimney (vertical ventilation system)*: Research Report, Wind Engineering Laboratory, Cracow University of Technology 2023

Report 5: Flaga A.: *A proxy model for temperature inversion layer (vertical ventilation system)*: Research Report, Wind Engineering Laboratory, Cracow University of Technology 2023

Shi H., Wang Y., Chen J., Huisingh D.: *Preventing smog crises in China and globally*; Journal of Cleaner Production 112 p. 1261-1271, 2016;

Smog — Who Does It Hurt? What You Need to Know About Ozone and Your Health; (EPA-452/K-99-001) (Report), United States Environmental Protection Agency, 1999;

Sorbjan Z.: *Turbulencja i dyfuzja w dolnej atmosferze*; PWN, Warszawa 1983;

Spurr G.: *The penetration of atmospheric inversions by hot plumes*; Journal of Meteorology, vol. 16, 30-37, 1959;

Szczygłowski P.: Doctoral thesis - *Ocena przydatności wybranych modeli gaussowskich w obliczeniach stanu zanieczyszczenia powietrza*; Akademia Górniczo-Hutnicza, Kraków 2007;

US 20090308244 A1: *Method and Equipment for Filtering Air in an Urban Environment;*

US 4164256 A: *Cooling tower with forced ventilation and natural draft*;

US 5425413 A: *Method to hinder the formation and to break-up overhead atmospheric inversions, enhance ground level air circulation and improve urban air quality*;

Ustrnul Z.: *Zmienność cyrkulacji atmosfery na półkuli północnej w XX wieku*; Materiały Badawcze IMGW. Seria Meteorologia, 27, p. 47-80, 1997;

Walczewski J.: *Some data on the occurrence of the all-day inversions in the atmospheric boundary-layer in Cracow and on the factors stimulating this occurrence;* IMGW, Kraków 2009;

Watson, Traci: *EPA: Half of USA breathing illegal levels of smog*; USA Today. Washington, 2004;

Wielgosiński G., Zarzycki R., *Technologie I procesy ochrony powietrza*; PWN, Warszawa 2018;

Wingstedt E.M.M., Osnes A.N, Akerwik E., Eriksson D., Pettersson Reif B.A.: *Large-eddy simulation of dense gas dispersion over a simplified urban area*; Atmospheric Environment 152 p. 605-616, 2017;

WO 2010084385 A1: *Intake and filtering device for fine particulates present in the air;*

www.thoughtco.com/temperature-inversion-layers-1434435 (05.01.2023);

www.who.int/phe/health_topics/outdoorair/databases/cities/en/ (11.09.2017);

www.naturphilosophie.co.uk/temperature-inversions-city-pollution-defunct-jet-engines/ (30.09.2022);

Yang L., Li Y.: *Thermal conditions and ventilation in an ideal city model of Hong Kong*; Energy and Buildings 43 p.1139-1148, 2011;

Yang L., Qian F., Song D.X., Zheng K.J.: *Research on Urban Heat-island Effect*; Procedia Engineering 169 p. 11-18, 2016;

Zhai Z.J., Brannon B.: *Performance comparison of destratification fans for large spaces*; Procedia Engineering 146 p. 40-46, 2016;

Zhang J., Liu Y., Cui L., Liu S., Yin X., Li H.: *Ambient air pollution, smog episodes and mortality in Jinan, China*; Scientific Reports 7, Article number: 11209 doi:10.1038/s41598-017-11338-2, 2017;

Zwoździak J., Zwoździak A., Szczurek A.: *Meteorologia w ochronie atmosfery*; Wrocław, Oficyna Wydawnicza Politechniki Wrocławskiej, 1998;

wysokienapiecie.pl/81733-produkcja-energii-elektrycznej-w-polsce/